Eukaryotic elongation factor 2 kinase (eEF2K): its relation to cancer cell survival, autophagy and other cell signalling pathways

Roman Valeryevich Lenchine

BSc (Molecular Biology), BSc (Hons)

A thesis submitted to the University of Adelaide

For the degree of Doctor of Philosophy

December 2020



THE UNIVERSITY of ADELAIDE

Department of Molecular and Biomedical Science

School of Biological Sciences

Faculty of Sciences

The University of Adelaide

Table of Contents

List of Tables 5
List of Figures 5
Abstract 11
Declaration 13
Acknowledgements 14
Abbreviations 16
CHAPTER 1: INTRODUCTION 21
1.1 Structure of eEF2K 21
1.2 Regulation of eEF2K 26
1.3 eEF2K and cell survival 34
1.4 Autophagy 46
1.5 eEF2K and its relation to autophagy 51
1.6 eEF2K and its relation to other cell signalling pathways 54
1.7 Aims of the project 54
CHAPTER 2: MATERIALS AND METHODS 57
2.1 Chemicals and Reagents 57
2.2 Cell culture and treatments 63
2.2.1 Cell lines and maintenance 63
2.2.2 Cryopreservation of cells 64
2.2.3 Trypan Blue cell counts 65
2.2.4 Cell treatments and harvesting 65
2.3 Buffers and bacterial culture media 66
2.4 Molecular Biology Techniques 68
2.4.1 Making of Agar Plates for Bacterial Growth 68
2.4.2 Creation of chemically competent cells 68
2.4.3 Transformation 69
2.4.4 Plasmid DNA Purification 70
2.4.5 Agarose Gel Electrophoresis 70
2.5 Transfection 71
2.6 Wound-healing Assay 71
2.7 Transwell® migration and invasion assays 72
2.8 Adhesion Assay 73
2.9 Sodium dodecyl sulfate-polyacrylamide gel electrophoresis (SDS-PAGE) 74
2.9.1 Bradford Assay 74
2.9.2 SDS-PAGE gel preparation 75
2.9.3 SDS-PAGE gel running 75
2.9.4 Western blotting 76
2.10 Flow Cytometry 78
2.10.1 Cell Cycle (Propidium Iodide Staining) 78
2.10.2 Extracellular PD-L1 staining 78
2.11 RNA isolation using Trizol 79

2.12 RT-qPCR 79
2.13 96-well Plate Assays 81
2.13.1 Glucose Uptake-Glo™ Assay 81
2.13.2 Dual-Glo® Luciferase Assay 82
2.13.3 BrdU Cell Proliferation Assay 82
2.13.4 CellTox® Green Cytotoxicity Assay 83
2.13.5 Propidium Iodide/Calcein-AM assay 84
2.13.6 RealTime-Glo™ MT Cell Viability Assay 84
2.13.7 Caspase-Glo® 3/7, Caspase-Glo® 8 and CellTiter-Glo® 2.0 Assays 84
2.13.8 Magic Red™ Cathepsin L Assay 85
2.13.9 LysoTracker Red Assay 85
2.14 Generation of KO cells using CRISPR 86
2.14.1 CRISPR-Cas9 vector cloning 86
2.14.2 Nucleofection 89
2.14.3 Enrichment of CD4 expressing cells using Dynabeads 89
2.14.4 DNA Extraction with QuickExtract™ Solution 91
2.14.5 Polymerase Chain Reaction (PCR) 91
2.14.6 Solid Phase Reverse Immobilisation Clean-up 91
2.14.7 Restriction Endonuclease Digestion to check for positive clones 92
2.15 Isobaric tag for relative and absolute quantitation (iTRAQ) 93
2.15.1 Sample preparation 93
2.15.2 Mass-spectrometry analysis 93
2.16 Generation of Bafilomycin-A Resistant MDA-MB-231 cells 93
2.17 Dr. Sushma Rao's Proteomics Protocol 94
2.17.1 Label-free proteomics and phosphoproteomic analysis 94
2.17.2 LC-MS/MS and data acquisition 95
2.17.3 Data processing and analysis 95
2.18 Seahorse Assays 96
2.18.1 8-well Seahorse Assays 96
2.18.2 96-well Seahorse Assays 99
CHAPTER 3: eEF2K AND ITS LINK TO AUTOPHAGY 101
3.1 Introduction 101
3.1.1 eEF2K and autophagy 101
3.1.2 Aims of this Chapter 103
3.2 Results 105
3.2.1 eEF2K inhibition via JAN384 has no cytotoxic effect on breast cancer cells experiencing nutrient deprivation 105
3.2.2 Concurrent inhibition of eEF2K via JAN384 and autophagy via BafA leads to increased MDA-MB-231 and A549 cell cytotoxicity under nutrient deprivation. 113

3.2.3 Creation of eEF2K knock-out MDA-MB-231 and PC3 cells using CRISPR-Cas9 Genome Editing 129
3.2.4 A lack or inhibition of eEF2K and autophagy leads to increased cell death of MDA-MB-231 and A549 cells under nutrient deprivation. 147
3.2.5 A lack of eEF2K assists cell survival of PC3 cells under nutrient deprived conditions. 173
3.2.6 Caspase activity is increased in MDA-MB-231 and A549 cells that lack eEF2K. 185
3.2.7 An inhibition or lack of eEF2K lowers or increases cellular ATP depending on cell type. 193
3.2.8 Knocking out or silencing eEF2K does not significantly alter cell glycolysis or mitochondrial oxidation. 199
3.3 Discussion 219
CHAPTER 4: CREATION OF CELLS RESISTANT TO A LACK OF EEF2K, NUTRIENT DEPRIVATION AND INHIBITION OF AUTOPHAGY – A PROTEOMICS STUDY 223
4.1 Introduction 223
4.1.1 Creation of cells resistant to chemotherapy drugs 223
4.1.2 Aims of this chapter 224
4.2 Results 225
4.2.1 Creation of MDA-MB-231 WT and eEF2K-KO cells that are resistant to glucose deprivation and inhibition of autophagy 225
4.2.2 The resistance to nutrient deprivation and autophagy inhibition is lost over time 237
4.2.3 Protein abundance and phospho-proteomic analysis of 'resistant and sensitive' cells 245
4.3 Discussion 258
CHAPTER 5: Eef2K AND ITS RELATION TO OTHER CELL SIGNALLING PATHWAYS 265
5.1 Introduction 265
5.1.1 eEF2K and its role in cell migration and invasion 265
5.1.2 eEF2K and translation fidelity 266
5.1.3 eEF2K and hypoxia 268
5.1.4 eEF2K and Nrf2 270
5.1.5 eEF2K and PD-L1 272
5.1.6 eEF2K and IRS-1 273
5.2 Results 274
5.2.1 eEF2K positively regulates cell migration and invasion 274
5.2.2 eEF2K increases the accuracy of translation elongation 306
5.2.3 eEF2K activity is increased in hypoxic conditions in MDA-MB-231, A549 and HCT116 cells 311

5.2.4 Inhibition or knock-out/knock-down of eEF2K does not affect Nrf2 levels in MDA-MB-231 and A549 cells 314
5.2.5 eEF2K promotes PD-L1 expression and assists cancer cells to escape immune surveillance 317
5.2.6 eEF2K does not affect glucose uptake but may regulate IRS-1 levels 325
5.3 Discussion 337
Chapter 6: General Discussion 343
Appendices 353
References 354

LIST OF TABLES

Table 2.1 Solutions used to prepare SDS-PAGE gels. 75
Table 2.2 List of antibodies and their dilutions that were used in this study. 77
Table 2.3 Settings used on the StepOne Plus Real-Time PCR system to run the RT-qPCR reaction 80
Table 3.1 Summary of the changes in cellular processes under control conditions. 220
Table 3.2 Summary of the changes in cellular processes when autophagy was inhibited. 220
Table 4.1 Log_2 fold changes of select groups of proteins between resistant and non-resistant cells. 256
Table 4.2 Phosphorylation site changes between non-resistant and resistant cells. 257

LIST OF FIGURES

Figure 1.1 NRM structure of $eEF2K_{627-725}$. 25
Figure 1.2 Regulation of eEF2K by mTORC1, AMPK and ERK. 31
Figure 1.3 eEF2K regulation by Pro98 hydroxylation 33
Figure 1.4 Tumour adaptation under nutrient deprived conditions. 35
Figure 1.5 The autophagic process. 49
Figure 3.1 Schematic of the hypothesis. 104
Figure 3.2 eEF2K is successfully inhibited by JAN384. 108
Figure 3.3 eEF2K inhibition via JAN384 has no effect on breast cancer cell cytotoxicity under nutrient deprived conditions. 111
Figure 3.4 Bafilomycin A successfully inhibits autophagic flux in MDA-MB-231 cells. 114
Figure 3.5 Bafilomycin A successfully inhibits autophagic flux in A549 cells. 117

Figure 3.6	A combination of eEF2K and autophagy inhibition or silencing leads to increased cell death under nutrient deprived conditions than when either pathway is inhibited individually in MDA-MB-231 and A549 cells.	119
Figure 3.7	A combination of eEF2K and autophagy inhibition or silencing leads to increased cell death under nutrient deprived conditions than when either pathway is inhibited individually in MDA-MB-231 cells (CellTox Green images).	123
Figure 3.8	A combination of eEF2K and autophagy inhibition or silencing leads to increased cell death under nutrient deprived conditions than when either pathway is inhibited individually in A549 cells (CellTox Green images).	125
Figure 3.9	A combination of eEF2K and autophagy inhibition or silencing leads to decreased cell viability under nutrient deprived conditions than when either pathway is inhibited individually in MDA-MB-231 and A549 cells.	127
Figure 3.10	Creation of eEF2K-KO MDA-MB-231 and PC3 cells using CRISPR-Cas9.	130
Figure 3.11	Ligation of CRISPR-Cas9 CD vector with gRNA and possible eEF2K-KO clone digests.	133
Figure 3.12	Schematic of the isolation of possible eEF2K-KO clones.	135
Figure 3.13	Screening of potential eEF2K-KO clones.	137
Figure 3.14	Screening of potential eEF2K-KO clones.	138
Figure 3.15	Confirmation of MDA-MB-231 eEF2K-KO Clone #1.	140
Figure 3.16	Confirmation of MDA-MB-231 eEF2K-KO Clone #2.	141
Figure 3.17	Confirmation of the MDA-MB-231 eEF2K-KO Clones via Benchling.	143
Figure 3.18	Confirmation of PC3 eEF2K-KO Clone #2.	145
Figure 3.19	Confirmation of the eEF2K KO Clones via Benchling.	146
Figure 3.20	Bafilomycin A successfully inhibits autophagic flux in MDA-MB-231 WT and eEF2K-KO cells.	149
Figure 3.21	JAN384 and A484954 do not significantly alter cell survival of eEF2K-KO MDA-MB-231 cells; JAN384 increases p62 and LC3 II levels.	151
Figure 3.22	A combination of eEF2K inhibition or knock-out and autophagy inhibition leads to increased cell death under nutrient deprived conditions than when either pathway is inhibited individually in MDA-MB-231 cells.	155

Figure 3.23 A combination of eEF2K inhibition or knock-out and autophagy inhibition leads to increased cell death under nutrient deprived conditions than when either pathway is inhibited individually in MDA-MB-231 cells (CellTox Green images). 157
Figure 3.24 A combination of eEF2K inhibition or knock-out and autophagy inhibition leads to decreased cell viability under nutrient deprived conditions than when either pathway is inhibited individually in MDA-MB-231 cells. 159
Figure 3.25 A combination of eEF2K inhibition or knock-out and autophagy inhibition leads to decreased cell viability under nutrient deprived conditions than when either pathway is inhibited individually in MDA-MB-231 cells (Calcein-AM Images). 161
Figure 3.26 A combination of eEF2K inhibition or knock-down and autophagy inhibition leads to increased cell death under nutrient deprived conditions than when either pathway is inhibited individually in A549 cells. 165
Figure 3.27 A combination of eEF2K inhibition or knock-down and autophagy inhibition leads to increased cell death under nutrient deprived conditions than when either pathway is inhibited individually in A549 cells (CellTox Green images). 167
Figure 3.28 A combination of eEF2K inhibition or knock-down and autophagy inhibition leads to decreased cell viability under nutrient deprived conditions than when either pathway is inhibited individually in A549 cells. 169
Figure 3.29 A combination of eEF2K inhibition or knock-down and autophagy inhibition leads to decreased cell viability under nutrient deprived conditions than when either pathway is inhibited individually in A549 cells (Calcein-AM Images). 171
Figure 3.30 Bafilomycin A successfully inhibits autophagic flux in PC3 WT and eEF2K-KO cells. 175
Figure 3.31 A lack of eEF2K reduces cytotoxicity of PC3 cells under nutrient deprived conditions. 177
Figure 3.32 A lack of eEF2K reduces cytotoxicity of PC3 cells under nutrient deprived conditions (CellTox Green images). 179
Figure 3.33 A lack of eEF2K increases the viability of PC3 cells under nutrient deprived conditions. 181
Figure 3.34 A lack of eEF2K increases cell viability of PC3 cells under nutrient deprived conditions (Calcein-AM images). 183
Figure 3.35 Knocking out or silencing of eEF2K leads to an increase in caspase 3 and 7 activity. 189
Figure 3.36 Knocking out or silencing of eEF2K leads to an increase in caspase 8 activity. 191
Figure 3.37 A lack of or inhibition of eEF2K leads to a decrease in ATP levels in MDA-MB-231 and A549 cells. 195

Figure 3.38	Knocking out eEF2K leads to an increase in ATP levels in PC3 cells under –Gln conditions.	198
Figure 3.39	Knocking out eEF2K does not affect the metabolic potential of MDA-MB-231 cells.	201
Figure 3.40	Knocking out eEF2K does not affect the glycolysis of MDA-MB-231 cells.	203
Figure 3.41	Knocking out eEF2K does not affect the mitochondrial respiration of MDA-MB-231 cells.	207
Figure 3.42	Inhibition of eEF2K using JAN384 decreases MDA-MB-231 cell glycolysis but increases the glycolytic reserve.	209
Figure 3.43	Inhibition of eEF2K using A484954 increases MDA-MB-231 cell glycolytic reserve.	211
Figure 3.44	Knocking out eEF2K does not affect MDA-MB-231 cell glycolysis.	213
Figure 3.45	Silencing eEF2K does not affect A549 cell glycolysis.	214
Figure 3.46	Knocking out eEF2K does not affect PC3 cell glycolysis.	215
Figure 3.47	Knocking out eEF2K does not affect MDA-MB-231 cell mitochondrial respiration.	216
Figure 3.48	Silencing eEF2K does not affect A549 cell mitochondrial respiration.	217
Figure 3.49	Knocking out eEF2K does not affect PC3 cell mitochondrial respiration.	218
Figure 4.1	Schematic of the process used to create cells resistant to nutrient deprivation, lack of eEF2K and autophagy inhibition.	227
Figure 4.2	Resistant cells are partially resistant to cell death under nutrient deprived conditions and autophagy inhibition.	229
Figure 4.3	Chloroquine and Bafilomycin A successfully inhibit autophagy in WT and eEF2K KO MDA-MB-231 resistant cells.	231
Figure 4.4	eEF2K-WT resistant cells are partially resistant to cell death under nutrient deprived conditions and autophagy inhibition (Images).	233
Figure 4.5	eEF2K-KO #1 resistant cells are partially resistant to cell death under nutrient deprived conditions and autophagy inhibition.	234
Figure 4.6	eEF2K-KO #2 Resistant cells are partially resistant to cell death under nutrient deprived conditions and autophagy inhibition.	235
Figure 4.7	CQ and Baf A successfully inhibit autophagic flux. Resistant cells have higher levels of autophagic flux.	238
Figure 4.8	MDA-MB-231 WT Resistant cells lose their resistance to stress over time.	239
Figure 4.9	MDA-MB-231 eEF2K KO #1 Resistant cells lose their resistance to stress over time.	241
Figure 4.10	MDA-MB-231 eEF2K KO #2 Resistant cells lose their resistance to stress over time.	243
Figure 4.11	Heatmap of significantly altered proteins between MDA-MB-231 resistant and non-resistant cell lysates.	247

Figure 4.12	Fatty acid metabolism heatmap.	249
Figure 4.13	Protein changes in MDA-MB-231resistant cell lysates compared to non-resistant cell lysates followed the same trend as in the proteomics data.	251
Figure 5.1	Inhibiting eEF2K with JAN384 slows wound healing of MDA-MB-231 cells.	277
Figure 5.2	NH125 and A484954 successfully inhibit eEF2K in MDA-MB-231 cells.	279
Figure 5.3	Inhibiting eEF2K with A484954 or NH125 slows down healing of MDA-MB-231 cells.	281
Figure 5.4	Lack of eEF2K slows wound healing of MDA-MB-231 cells, with JAN384 slowing wound healing further.	283
Figure 5.5	Lack of eEF2K slows wound healing of MDA-MB-231 cells, with JAN384 slowing wound healing further.	285
Figure 5.6	Lack of eEF2K slows migration of MDA-MB-231 cells, with JAN384 slowing migration further.	287
Figure 5.7	Inhibition of eEF2K slows invasion of MDA-MB-231 cells through Matrigel.	291
Figure 5.8	Lack of eEF2K slows invasion of MDA-MB-231 cells, with JAN384 slowing invasion further.	293
Figure 5.9	Inhibition of eEF2K with NH125 decreases adhesion of MDA-MB-231 cells, while knocking it out has no effect.	295
Figure 5.10	Knocking out eEF2K in MDA-MB-231 cells has no effect on cell adhesion.	297
Figure 5.11	Overexpressing eEF2K accelerates wound-healing of MDA-MB-231 cells.	299
Figure 5.12	Partially silencing eEF2 accelerates wound-healing of MDA-MB-231 cells.	301
Figure 5.13	Knocking out eEF2K in MDA-MB-231 cells or silencing it in A549 cells does not affect cell proliferation.	303
Figure 5.14	Knocking out eEF2K in MDA-MB-231 cells does not affect the cell cycle.	304
Figure 5.15	Knocking out eEF2K in MDA-MB-231 cells does not affect the cell cycle.	305
Figure 5.16	eEF2K positively regulates translation fidelity.	308
Figure 5.17	eEF2K activity is increased under hypoxic conditions in MDA-MB-231, A549 and HCT116 cells.	313
Figure 5.18	Inhibition or knockdown of eEF2K does not alter Nrf2 levels in MDA-MB-231 or A549 cells.	315
Figure 5.19	Inhibition or knocking out of eEF2K does not alter Nrf2 levels in MDA-MB-231 cells.	316

Figure 5.20	Knocking out eEF2K decreases PD-L1 protein and mRNA levels in PC3 cells.	319
Figure 5.21	Knockdown or knock-out of eEF2K in A549 and MDA-MB-231 cells respectively does not change *PD-L1* mRNA level.	3.21
Figure 5.22	2-DG treatment quickly stimulates eEF2K activity.	327
Figure 5.23	Lack of eEF2K increases IRS-1 under control conditions and early after insulin treatment.	329
Figure 5.24	Lack of eEF2K in low pH medium does not significantly alter IRS-1 levels but may affect PKB signalling.	331
Figure 5.25	Knock out or knockdown of eEF2K does not affect glucose uptake in MDA-MB-231, A549 or PC3 cells.	335

Abstract

Eukaryotic elongation factor 2 kinase (eEF2K) is a calcium/calmodulin dependent alpha kinase that plays a central role in the regulation of one of the most important processes in cells – protein synthesis, specifically the elongation stage which consumes large amounts of energy (ATP/GTP) and amino acids. Disruptions in protein synthesis or in its regulation have been linked to various diseases and cancers. This makes eEF2K a prime target for study. eEF2K has been shown to assist cancer cell survival under nutrient-deprived conditions, allowing cells to reduce their rates of protein synthesis and thereby save energy. However, eEF2K's role in cancer cell survival appears to depend on the cancer cell type, with some cancer cells surviving for shorter times when eEF2K is disrupted, and *vice versa* for others. Therefore, it becomes important to test eEF2K's role in cancer cell survival in a variety of cell lines.

eEF2K has also been linked to autophagy, a process that allows cells to scavenge their own proteins for amino acids and energy. In this thesis, I have investigated these claims in breast, lung and prostate cancer cell lines. To more accurately assess the effects of eEF2K disruption, I created an eEF2K knock-out model via CRISPR-Cas9. Using this model, I found that autophagy and eEF2K act independently of each other in all the cell lines tested. In the case of lung and breast cancer cells, both processes act to help cells survive nutrient deprivation. In the case of prostate cancer cells, it was found that a lack of eEF2K assisted their survival, highlighting the need to study eEF2K in a range of cell lines. It was also found that eEF2K does not affect glycolysis or mitochondrial respiration.

Furthermore, to study how cancer cells gain resistance to nutrient deprivation and autophagy inhibition, I generated 'resistant' eEF2K wild-type and knock-out breast cancer cell lines.

Importantly, it was found that this resistance is reversible and is lost over time. These cell lines were analysed by proteomics and phospho-proteomics. A variety of proteins and cellular processes were affected in the resistant lines, including aminoacyl tRNA synthesis, translation factors, protein folding, lysosomal proteins, fatty acid metabolism among others. The phosphoproteomic analysis also revealed an overall decrease in phosphorylation of sites downstream of mTORC1 signalling in resistant cells, as well as potential new substrates for eEF2K.

This project also investigated the links that eEF2K has, or had been reported to have, to a variety of other signalling pathways, including cell migration/invasion, hypoxia, Nrf2 (nuclear factor erythroid 2-related factor), PD-L1 (programmed cell death 1 ligand 1) and glucose uptake.

Overall, this project helped to unravel the links between eEF2K and several other cellular processes. The finding that eEF2K and autophagy act together to assist cell survival under nutrient-deprived conditions could be important for potential therapies against certain cancers. Further supporting this finding, the analysis of resistant cell lines gives more insight into how cancer cells can gain resistance to certain adverse conditions and potential therapeutic agents.

Declaration

I certify that this work contains no material which has been accepted for the award of any other degree or diploma in my name, in any university or other tertiary institution and, to the best of my knowledge and belief, contains no material previously published or written by another person, except where due reference has been made in the text. In addition, I certify that no part of this work will, in the future, be used in a submission in my name, for any other degree or diploma in any university or other tertiary institution without the prior approval of the University of Adelaide and where applicable, any partner institution responsible for the joint-award of this degree.

I acknowledge that copyright of published works contained within this thesis resides with the copyright holder(s) of those works.

I also give permission for the digital version of my thesis to be made available on the web, via the University's digital research repository, the Library Search and also through web search engines, unless permission has been granted by the University to restrict access for a period of time.

I acknowledge the support I have received for my research through the provision of an Australian Government Research Training Program Scholarship.

Roman Valeryevich Lenchine Date

Acknowledgements

This PhD has been a long journey throughout which I was supported by a number of people, who I would like to thank.

First of all, I would like to thank Chris, whose supervision, wisdom and insight in this field guided me throughout my time in his lab. Your guidance and enthusiasm about our lab's work and my project taught me to never give up, persevere and this work was the great result. I also really appreciate your help in editing this massive document. I would also like to particularly thank Jianling for teaching me the various laboratory skills that were vital for my experiments and his friendship. I will think of our conversations fondly. My gratitude also goes out to other members of my lab – Kirk, with whose guidance my CRISPR cells were created much quicker than anticipated; as well as Min, Claire, Rui, Xuechan and Saman for their help in many aspects of the lab.

I also want to acknowledge the other students and colleagues in the lab for their camaraderie and support. James, Lauren, Wan Xian, Stuart, Shuye and Luis; your presence made the lab very entertaining to work in and I am grateful for you being there throughout my journey. Also, many thanks to Jodie, whose cheerfulness never failed to put a smile on my face.

I am very grateful to my close friends, David, Jacob and Laurence for all our conversations and fun days spent relaxing. Time spent with you always lifted my spirits.

I would also like to thank my close family for their support and love – Valeri, Tatiana, Valentin and Marina. My gratitude also goes to Violetta, Roumen, Desi and Maria who have been like another family for me here in Adelaide. Your hospitality always made me feel welcome. And last but not at all least, I am grateful to Maria. I am so glad to have met you

early on in this journey. Taking this road together, the many days working in the lab and the nights discussing it lightened the load off my shoulders. I am very grateful to have shared this journey side by side with you and every day of it was worth it.

Abbreviations

2-DG	2-Deoxy-D-Glucose
4E-BP1	eukaryotic translation initiation factor 4E-binding protein 1
AARS	alanyl tRNA ligase
ACADVL	mitochondrial very long-chain specific acyl-CoA dehydrogenase
ACAT2	cytosolic Acetyl-CoA-acetyltrasnferase
ACC	acetyl-CoA carboxylase
AD	Alzheimer's disease
ADH5	alcohol dehydrogenase 5
ALDH2	mitochondrial aldehyde dehydrogenase
AMP	adenosine monophosphate
AMPK	AMP-activate protein kinase
AP1B1	AP-1 complex subunit beta-1
APP	amyloid precursor protein
ATG4	cysteine protease ATG4
ATG5	autophagy protein 5
ATG7	ubiquitin-like modifier-activating enzyme ATG7
ATG12	ubiquitin-like protein ATG12
ATG13	autophagy-related protein 13
ATG16	autophagy protein 16
BafA	bafilomycin A1
BiP	endoplasmic reticulum chaperone BiP (HSPA5)
BSA	bovine serum albumin
CaM	calmodulin
Cas9	CRISPR-associate protein 9
cdc2	cell division control protein 2

cDNA	complementary DNA
CQ	chloroquine
CRISPR	clustered regularly interspaced short palindromic repeats
CTSD	cathepsin D
DAPI	4', 6-diamidine-2-phenylindole, dihydrochloride
DHCR7	7-dehydrocholesterol esterase
DLAT	mitochondrial dihydrolipoyllysine-residue acetyltransferase component of pyruvate dehydrogenase complex
DMEM	Dulbecco's modified Eagle's medium
DNAJB1	DnaJ homology subfamily b member1
DNAJC2	DnaJ homolog subfamily C member 2 (ZRF1)
ECAR	extracellular acidification rate
eEF2	eukaryotic elongation factor 2
eEF2K	eEF2 kinase
EGFR	epidermal growth factor receptor
eIF	eukaryotic initiation factor
ER	endoplasmic reticulum
ERK	extracellular signal-regulated kinase
ERO1L	ERO1-like protein alpha
FACS	fluorescence-assisted cell sorting
FASN	fatty acid synthase
FBS	foetal bovine serum
FLIP	cellular FLICE-like inhibitory protein long form
FOXM1	Forkhead box M1
GFPT1	glutamine-fructose-6-phosphate transaminase
Glc	glucose

Gln	glutamine
GSK3	glycogen synthase kinase 3
HAK	heart alpha kinase
HSPA4L	heat shock 70 kDa protein 4L
IFNγ	interferon gamma
IPTG	Isopropyl-β-D-thiogalactopyranoside
IRS-1	insulin receptor substrate 1
KO	knock-out
LAK	lymphocyte alpha kinase
LAMP2A	lysosomal-associated membrane protein 2A
LARS	leucyl tRNA synthetase
LC3	microtubule-associate protein 1A/1B light chain 3
LDHA	L-lactate dehydrogenase A chain
MAK	muscle alpha kinase
MAPK	mitogen-activated protein kinase
MCL1	induced myeloid leukemia cell differentiation protein Mcl-1
MEFs	mouse embryonic fibroblasts
MSCV	murine stem cell virus
mTORC1	mammalian target of rapamycin complex 1
NEB	New England Biolabs
NPC1	Niemann-Pick disease, type C1
NPM1	nucleophosmin 1
Nrf2	nuclear factor erythroid 2-related factor 2
OCR	oxygen consumption rate
p62	sequestrome 1 (SQSTM1)

PABPC1	polyadenylate-binding protein 1
PARP	poly-ADP-ribose polymerase
PBS	phosphate-buffered saline
PD-1	programmed cell death protein 1
PDK1	mitochondrial pyruvate dehydrogenase kinase isoenzyme 1
PD-L1	programmed cell death 1 ligand 1
PE	phosphatidylethanolamine
PFK1	ATP-dependent 6-phosphofructokinase 1
PFKFB3	6-phosphofructo-2-kinase
PGK	phosphoglycerate kinase 1
PI	propidium iodide
PI3K	phosphoinositide 3-kinase
PIP_2	phosphatidylinositol 3,4-bisphosphate
PKB	protein kinase B
PKM	pyruvate kinase PKM
PRAS40	proline-rich AKT1 substrate 1
PS1	presenilin 1
PTK2	focal adhesion kinase 1 (FAK)
Pyr	pyruvate
RAN	GTP-binding nuclear protein Ran
RANGAP	Ran GTPase-activating protein
RAPTOR	regulatory-associated protein of mTOR
ROS	reactive oxygen species
RPMI	Roswell Park Memorial Institute medium
RPS3	40S ribosomal protein S3

RPS6	ribosomal protein S6
RPS6K1	70 kDa ribosomal protein kinase 1
RPS8	40S ribosomal protein S8
SDS	sodium dodecyl sulphate
SDS-PAGE	SDS-polyacrylamide gel electrophoresis
SENP3	sentrin-specific protease 3
sgRNA	single-guide RNA
shRNA	short hairpin RNA
siRNA	small interfering RNA
TAE	tris-acetate EDTA
TARS	threonyl tRNA synthetase
TPI	triosephosphate isomerase
TRPM6/7	transient receptor potential cation channels subfamily M members 6 and 7
TSC1	hamartin
TSC2	tuberin
ULK1	serine/threonine-protein kinase ULK1
WARS	tryptophanyl tRNA synthetase
WT	wild-type
YARS	tyrosyl tRNA synthetase

1.1 Structure of eEF2K

Protein synthesis is a vital process that is required for all cellular functions. It requires a large amount of energy (~34% of cellular ATP supplies[1]) and therefore nutrients to function. The expression of many proteins is also regulated at the level of the translation of their mRNAs. For these reasons, protein synthesis carefully regulated by a complex network of intracellular signalling pathways[2]. These pathways respond to the availability of nutrients, hormones, growth factors, stress conditions and the presence of other cells, as well as to oxygen levels (normoxic/hypoxic conditions).

Defects in, or improper regulation of, these pathways can lead to a variety of diseases such as cancer, cardiovascular disease and neurological illnesses such as Alzheimer's and Huntington's diseases[3, 4].

Eukaryotic elongation factor 2 kinase (eEF2K) is one of the important proteins that regulates this vital process. eEF2K is a calcium/calmodulin (Ca/CaM) dependent kinase (initially discovered as CaM kinase III by Nairn *et al*.[5] in 1985) was identified as eEF2K in 1988 by Ryazanov *et al*.[6] It was found to phosphorylate its only known target – eukaryotic elongation factor 2 (eEF2) at Thr56 by Price *et al*.[7] in 1991. This phosphorylation event leads to a decrease in the ability of eEF2 to bind ribosomes, thereby inactivating it[8]. eEF2 promotes the GTP-dependent translocation of the nascent protein chain in the ribosome from the A to the P site and of the translating ribosome by one codon along the mRNA [9]. This means that when eEF2K phosphorylates and thus inactivates eEF2, the elongation phase is slowed down, inhibiting global protein synthesis.

eEF2K is 725 amino acid protein, with its catalytic domain lying towards its N-terminus. When eEF2K's cDNA was first cloned and expressed, it became clear that its sequence was different from typical protein kinases. The vast majority of protein kinases belong to the serine/threonine/tyrosine kinase superfamily (the other being the histidine kinase superfamily), which share a very similar structure of their catalytic domains, consisting of 12 conserved subdomains[10]. eEF2K was found to have no sequence homology to either of the kinase superfamilies.[10-13]. It soon became clear that eEF2K belonged to a group of six protein kinases in mice and humans called 'α-kinases', termed so for their preference for phosphorylating residues in the α-helices of proteins, rather than β-strands 'preferred' by typical kinases[12-14]. The other five alpha kinases are lymphocyte alpha kinase (LAK), heart alpha kinase (HAK), muscle alpha kinase (MAK), and transient receptor potential cation channels of subfamily M members 6 and 7 (TRPM6 and TRPM7). While the full-length eEF2K crystal structure is currently not available, it is known that it has significant sequence homology with TRPM7 and myosin-II heavy chain kinase A (MHCK A, a *Dictyostelium discoideum* α-kinase), for which structures are available[15, 16]. These two kinases also share structural similarities, particularly in the position of their catalytic residues.

Interestingly, the structure of TRPM7, despite having little sequence similarity with the main ('classical') kinase superfamily, has certain key features in the active site that were the same or similar. The catalytic domains of both classical and alpha kinases contain two lobes that bind nucleotides at their interface[16]. It was found that the N-terminal lobe of TRPM7 was similar to that of classical kinases. However, the structure of the C-terminal lobe had features that were akin to the lobes of ATP-grasp (adenosine tri-phosphate) metabolic enzymes[16]. These enzymes catalyse the ATP-assisted reaction of a nucleophile by forming an

acylphosphate intermediate[17]. It is of note that the structure of MHCK A showed an acyl-aspartate residue, suggesting an unusual substituted enzyme mechanism[15].

N-terminal to and very close to the catalytic domain of eEF2K is a region which binds the calcium-sensing protein calmodulin[18, 19]. The sequence of this CaM-binding motif is dissimilar to other calmodulin dependent kinase CaM-binding motifs, as well as having a different location. For example, the location of the CaM-binding domain in calcium/calmodulin dependent protein kinase types I, II and IV (CaMKs) is located C-terminal of their catalytic domains, not N-terminal like in eEF2K[20].

The C-terminal part of eEF2K contains four predicted SEL-1-like (tetratricopeptide repeats) α-helical motifs, which are typically involved in protein-protein interactions[21]. In 2016, a study by Will *et al.*[22] published the structure of this SEL-1 domain (residues 625-725) which was determined using soluble nuclear magnetic resonance (NMR). It was shown to be comprised of four helices with three rigid helices comprising a helical core (termed αII, αIII and α IV) and a flexible helix near the N-terminus (termed αI) as shown in **Figure 1.1**. This study also showed that mutating two highly conserved tyrosine residues in this region (Y712A/Y713A) led to the complete loss of eEF2K's ability to phosphorylate eEF2, confirming the result of another study by Pigott *et al*[23]. It suggests that this loss of eEF2K's ability to phosphorylate eEF2 is due to structural destabilisation, rather than the region being necessary for eEF2 binding. Consistent with this, a peptide that includes the 711-718 region of eEF2K or even the $eEF2K_{625-725}$ construct did not interfere with full length eEF2K's ability to phosphorylate eEF2. This study complements the findings of a study by Pigott *et al.*[23] in 2012 which showed that the deletion of the 711-725 region of eEF2K led to the loss of kinase activity against eEF2, but not against MH-1, a peptide substrate. Combined, these

studies showed that the extreme C-terminus end of eEF2K is necessary for eEF2 phosphorylation, but the last 99 amino acids do not provide a binding site for eEF2.

The catalytic and SEL-1 regions of eEF2K are connected by a region called the ‘linker’ that has little predicted structure but contains several residues that can be phosphorylated to regulate eEF2K activity.

Figure 1.1

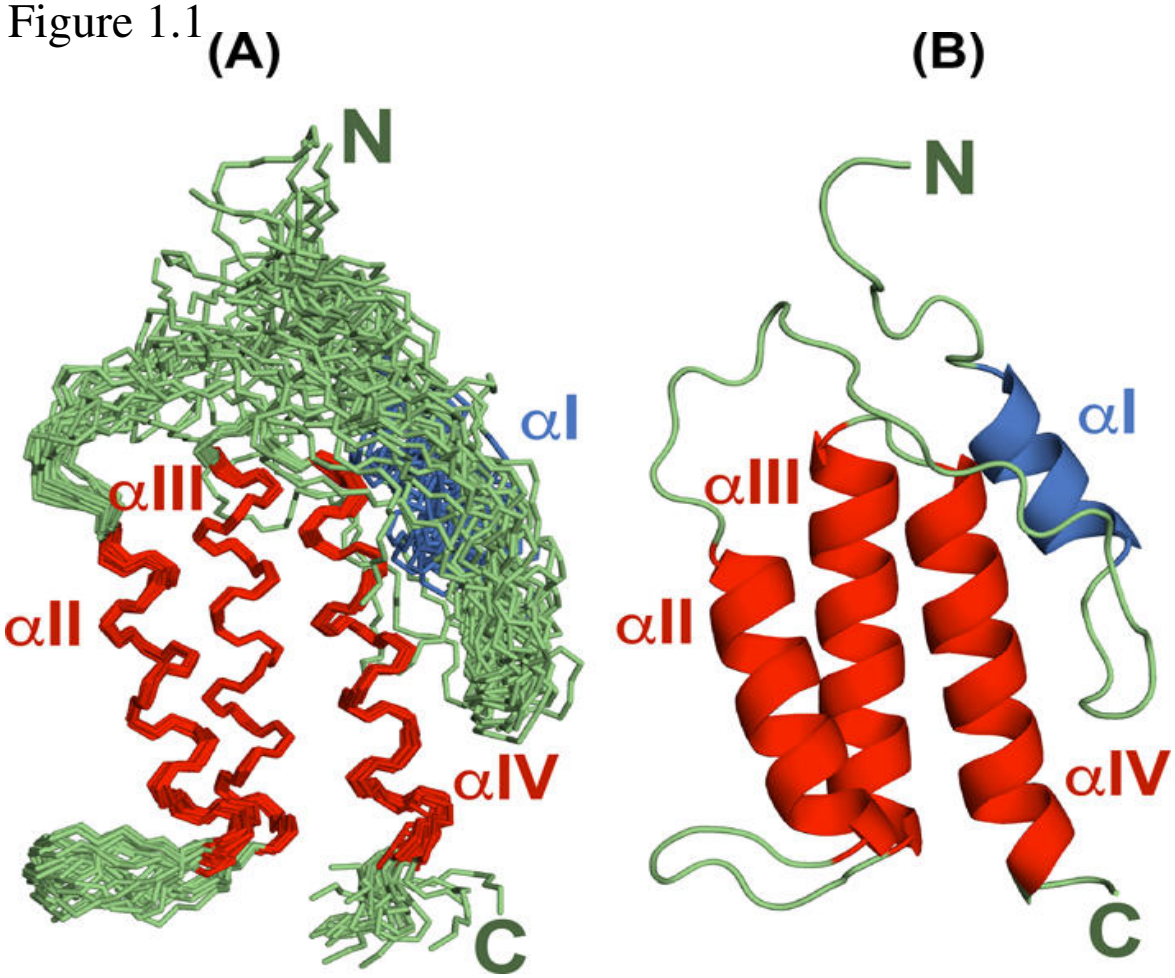


Figure 1.1: NMR structure of eEF2K$_{627-725}$. A: 20 lowest energy structures were overlaid on helices αII-αIV. **B:** A ribbon representation of the lowest energy structure that contains the four helices. The helical core, comprised of helices αII-αIV are marked in red, with the N-terminal helix αI is marked in blue. The loops are shown in green. This figure was taken from Will *et al.* 2016[22].

1.2 Regulation of eEF2K

eEF2K is activated by elevated calcium levels and calmodulin binding near its catalytic domain. This allows eEF2K to autophosphorylate at Thr348[24], which has been shown to increase its activity 2-3-fold[25, 26]. It is also of note that MHCK A is also able to autophosphorylate to become more active[27]. Calcium and calmodulin are necessary for eEF2K activity as they increase its ability to bind ATP, as well as stimulating its autophosphorylation. Besides being activated by Ca^{2+}/CaM, eEF2K is regulated by three other main pathways – mTORC1 (mammalian target of rapamycin complex 1), AMPK (adenosine monophosphate-activated protein kinase) and ERK (extracellular signal-regulated kinase).

mTORC1 is a major regulator of cell growth, through the regulation of protein synthesis and other anabolic processes such as ribosome biogenesis and lipid synthesis. It includes mTOR, a protein kinase and RAPTOR (regulatory-associated protein of mTOR), which is only found in mTORC1, not mTORC2, and serves to recruit substrates to mTORC1. mTORC1 is activated by growth factors and the availability of nutrients. mTORC2 contains Rictor in place of RAPTOR and phosphorylates distinct substrates. It is also regulated differently. mTORC2 can regulate mTORC1 through activation of PKB by phosphorylation of Ser473[28]. PKB in turn phosphorylates the TSC1/TSC2 (hamartin/tuberin) dimer. This inhibits TSC2 (by impairing its GTPase activating function), leading to the activation of Rheb (which needs GTP to be active). In its GTP-bound form, Rheb is able to bind RAPTOR, which leads to mTORC1 activation[29]. PKB can also phosphorylate PRAS40 (proline-rich AKT1 substrate 1), which dissociates PRAS40 from the mTORC1 complex, also leading to its activation[30].

mTORC1 can then phosphorylate 4E-BP1 (eukaryotic translation initiation factor 4E-binding protein 1), dissociating it from eIF4E (eukaryotic translation initiation factor 4E), allowing the eIF4F complex to form, which enables the initiation of mRNA translation[31, 32]. mTORC1 also phosphorylates and activates RPS6K1 (70 kDa ribosomal protein kinase 1), which in turn phosphorylates rps6 (ribosomal protein S6), leading to its activation, which has been suggested to assist in ribosome biogenesis[33, 34]. Disruption of the mTORC1 pathway and thus hyperactivation of protein synthesis can lead to cancer. Direct evidence of the abnormalities caused by the dysregulation of mTORC1 signalling is that tuberous sclerosis occurs when TSC1 or TSC2 is lost, causing hyperactivation of mTORC1 and benign tumour formation[35]. mTORC1 regulated signalling is often upregulated in cancer, such as the overexpression of Rheb in acute myeloid leukemia which promotes its progression[36, 37].

AMPK is a major regulator of cellular homeostasis, balancing energy supply and demand. AMPK is activated under conditions of nutrient stress, when the ATP bound to it at its regulatory γ site is displaced by either ADP or AMP (adenosine monophosphate), causing a conformational change that results in its activation[38]. Once active, AMPK switches on catabolic pathways, such as fatty acid oxidation and autophagy, while turning off energy-consuming anabolic pathways, such as protein and lipid synthesis and gluconeogenesis[38]. AMPK is also known to phosphorylate Raptor, a scaffolding protein necessary for mTORC1 assembly, which leads to protein 14-3-3 binding and inactivation of mTORC1[39]. As tumours are generally characterised by uncontrolled cell division, the ability of AMPK to inhibit protein synthesis and proliferation have marked it as a tumour suppressor[40]. However, there is also evidence that AMPK can promote tumour growth[41], suggesting that if tumours become established, AMPK may assist these tumours in surviving nutrient and other

stresses. Deletion of AMPK has been shown to lead to a reduction in the tumour size of lung cancer in mice[42].

ERK1/2 (also known as MAPK – mitogen-activated protein kinase) is part of the Ras, Raf, MEK and ERK pathway, which is activated by mitogens, growth factors (and other agents) and by mutations in some of its components which are common in human cancers, e.g., Ras. This leads to a signalling cascade that activates in sequence, Ras, Raf, MEK and ERK. ERK is known to phosphorylate TSC2, leading to mTORC1 activation. ERK can also activate RSK (a serine/threonine protein kinase, that phosphorylates some sites in S6), which can also phosphorylate TSC2, as well as PRAS40, leading to mTORC1 activation[43]. ERK is known to be important for cancer cells to adapt to stress, as well as chemo and radiotherapy[44]. It's also been known to promote immune-evasive phenotypes in a variety of cancer cells[44].

All of these pathways are vital for the control of cell functions. Their ability to directly or indirectly regulate eEF2K also suggests that eEF2K is important for normal cell function.

When cells are in optimal conditions with plenty of nutrients and oxygen, mTORC1 is active and phosphorylates eEF2K at three sites either directly or indirectly, which leads to the inhibition of eEF2K[45, 46]. In contrast, AMPK becomes active when cells are under nutrient or hypoxic stress. In these conditions, mTORC1 and ERK are inactivated and AMPK phosphorylates eEF2K at a different site leading to its activation[47, 48].

mTORC1 negatively regulates eEF2K through direct or indirect phosphorylation of three sites – Ser78, Ser359 and Ser366[46]. Ser78 is directly phosphorylated by mTORC1 and inhibits the binding of calmodulin to eEF2K[49]. Ser359 is phosphorylated by cdc2 (cell

division control protein 2)-cyclin B complexes which mTORC1 regulates, as well as ERK. Phosphorylation at this site reduces eEF2K activity at high calcium concentrations[50]. eEF2K phosphorylation at Ser366 is induced by mTORC1 through activating p70 ribosomal protein S6 kinase (p70 S6K). This site is also phosphorylated by ERK signalling through activation of ribosomal protein S6 kinase alpha 1 (RSK1). Phosphorylation of Ser366 reduces eEF2K's sensitivity to calcium/calmodulin binding[51], thereby impairing its activation. Ser377 has also been reported as a site of phosphorylation through ERK signalling[46]. Ser70, Ser392, Ser396 and Ser470 have also been found to be mTORC1 regulated eEF2K sites[46]. It was shown that the phosphorylation of Ser392 and Ser396 facilitates the phosphorylation of Ser70 and Ser78, pointing to possible conformational changes between the 'linker' region and the N-terminus. Ser392 is also known to be directly phosphorylated by GSK3 (glycogen synthase kinase 3), a kinase which regulates glycogen metabolism, cellular transport and a wide array of other signalling pathways[52]. Ser491 has also been reported as another site directly phosphorylated by AMPK, suggesting it is also important for its activation[53]. Furthermore, eEF2K can be phosphorylated at Ser499 by cAMP-dependent protein kinase A (PKA), providing it with calcium/calmodulin independent activity.

AMPK positively regulates eEF2K through direct phosphorylation of Ser398. When cellular ATP levels decrease, AMP levels increase very markedly, activating AMPK. When Ser398 is phosphorylated, eEF2K becomes active and undergoes a conformational change which allows it to bind and phosphorylate eEF2 at Thr56, inhibiting its activity[48]. This slows down translation elongation and thus global protein synthesis, reducing the consumption of ATP and GTP.

It is also important to note that eEF2K is regulated by proline hydroxylation, which is sensitive to oxygen concentration, as found by Moore *et al*. in 2015[54]. During normoxia, Pro98, which is immediately C-terminal of the CaM binding domain is hydroxylated, impairing CaM's ability to activate eEF2K. Under hypoxic conditions, prolyl hydroxylase activity is impaired, thus this hydroxylation does not take place. Since hydroxylation cannot be reversed[55], existing eEF2K remains inhibited. However, newly synthesised eEF2K will be able to function more actively, allowing cells to save energy during hypoxic conditions, through the inhibition of protein synthesis. A diagram of these regulatory pathways is shown in **Figure 1.2**, which is adapted from Wang *et al*. 2017[45]. A diagram representation of the effect of Pro98 hydroxylation of eEF2K is shown in **Figure 1.3**.

Figure 1.2

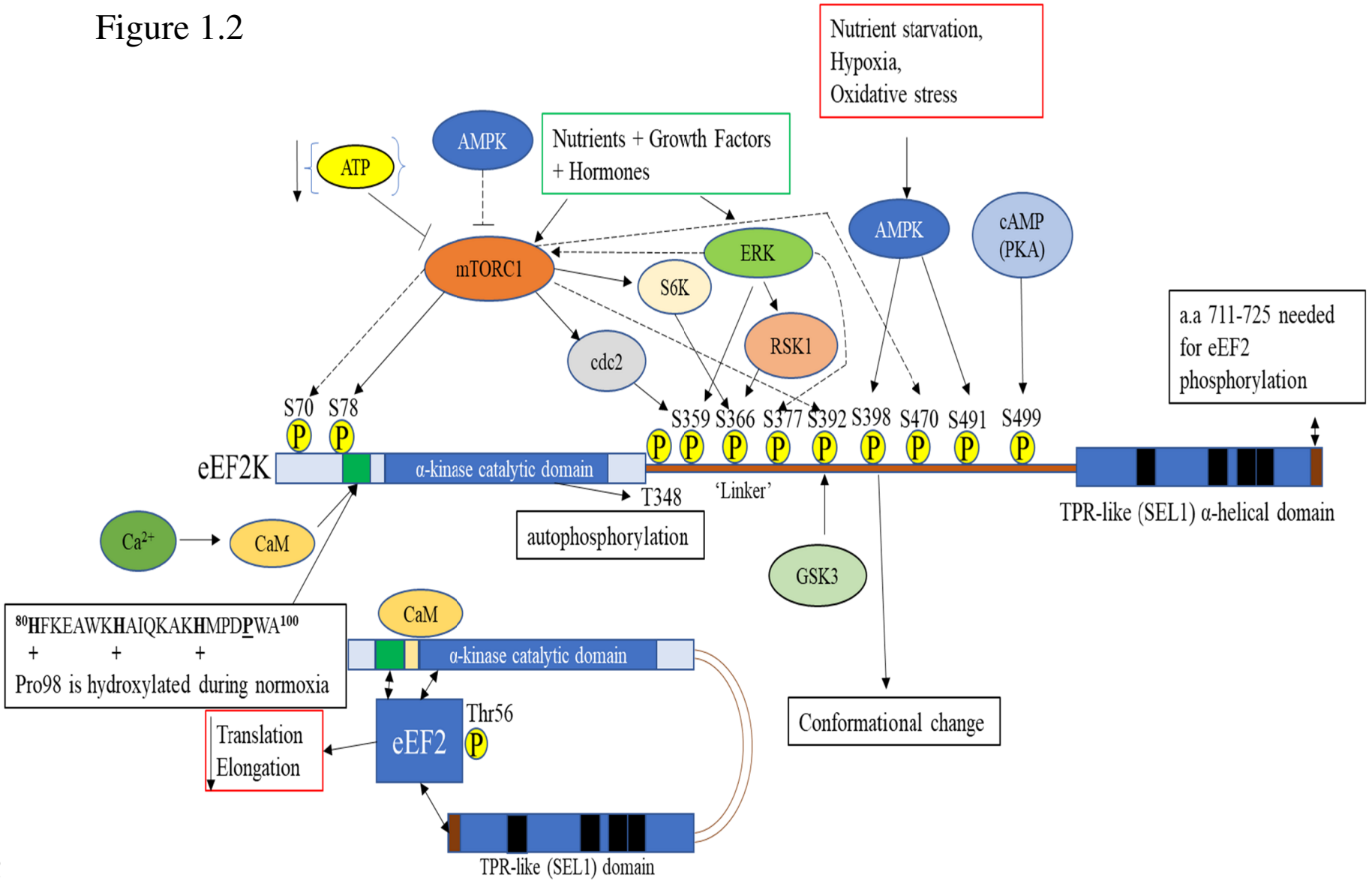

Nutrient starvation,
Hypoxia,
Oxidative stress
AMPK
ATP
Nutrients + Growth Factors
+ Hormones
AMPK
cAMP
(PKA)
mTORC1
ERK
S6K
RSK1
cdc2
a.a 711-725 needed
for eEF2
phosphorylation
S70 S78
S359 S366 S377 S392 S398 S470 S491 S499
eEF2K
α-kinase catalytic domain
T348
'Linker'
TPR-like (SEL1) α-helical domain
autophosphorylation
Ca2+
CaM
GSK3
80HFKEAWKHAIQKAKHMPDPWA100
+ + +
Pro98 is hydroxylated during normoxia
CaM
α-kinase catalytic domain
Thr56
eEF2
Translation
Elongation
Conformational change
TPR-like (SEL1) domain

Figure 1.2: Regulation of eEF2K by mTORC1, AMPK and ERK. Under normal conditions, mTORC1 is active and either directly or indirectly phosphorylates eEF2K at Ser78, Ser 359 (also phosphorylated by ERK) and Ser 366 which all lead to its inactivation. When cells undergo nutrient or hypoxic stress, mTORC1 is deactivated while AMPK becomes active. AMPK phosphorylates eEF2K at Ser398, allowing eEF2K to phosphorylate itself at Thr348. This leads to a conformational change, allowing eEF2K to bind eEF2 and phosphorylate it at Thr56, thus inhibiting translation elongation. During normoxic conditions, Pro98 is hydroxylated (underlined), inhibiting calmodulin's ability to activate eEF2K. The histidines in the CaM-binding domain are shown in bold, with the '+' indicating that their protonation aids in CaM binding under acidic conditions. Dotted lines indicate indirect regulation, while solid lines indicate direct phosphorylation. This diagram has been adapted from Wang, *et al*. 2017[45].

Figure 1.3

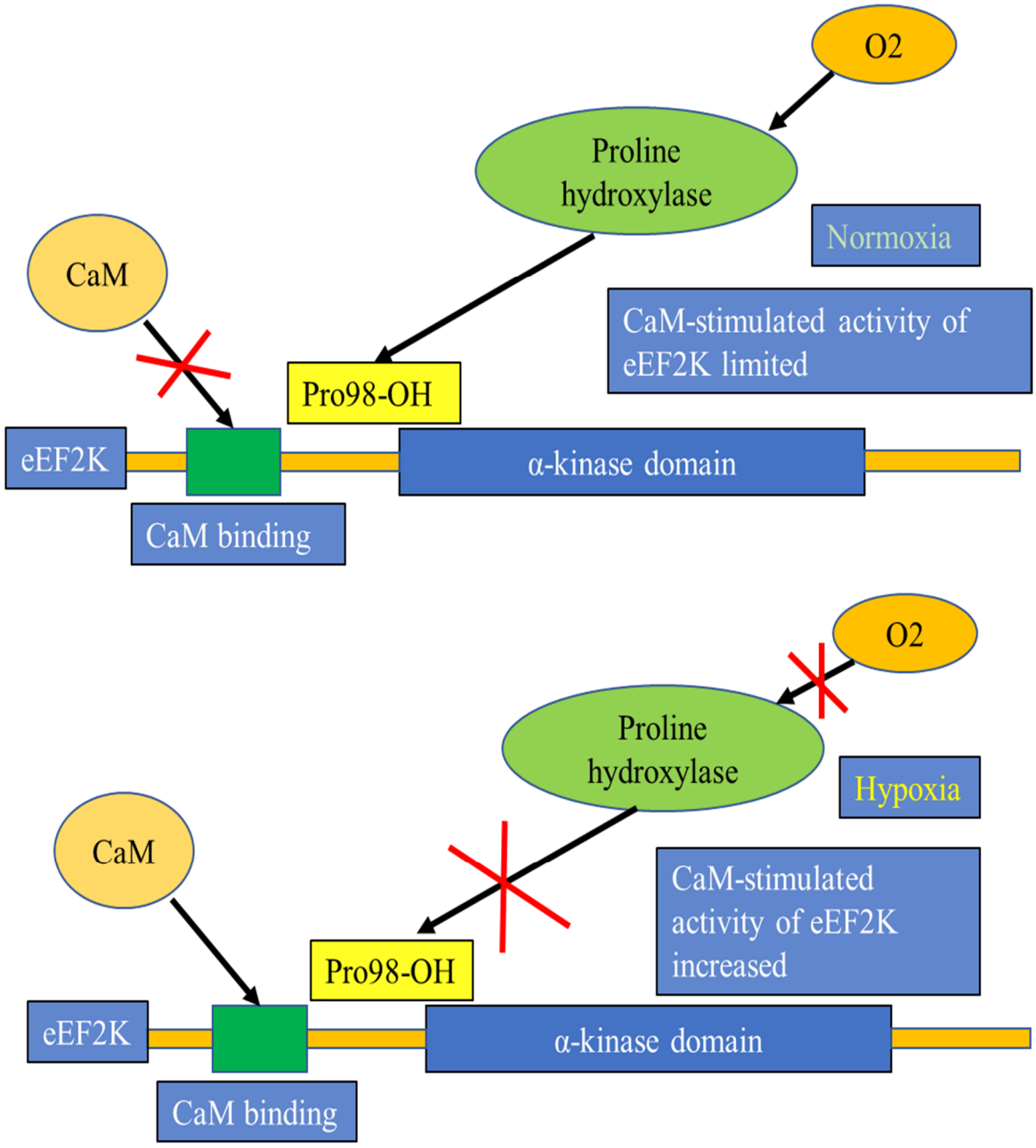


Figure 1.3: eEF2K regulation by Pro98 hydroxylation. Under normoxic conditions, enough oxygen is present to activate proline hydroxylases which hydroxylate eEF2K at Pro98, reducing calmodulin's (CaM's) ability to bind and activate eEF2K. Under hypoxic conditions, proline hydroxylases are inactive, thus Pro98 remains unhydroxylated and CaM can bind eEF2K unhindered, helping its activation to allow cells to regulate translation elongation.

1.3 eEF2K and cell survival

Disruptions in protein synthesis can lead to disease, and eEF2K has been linked to a variety of illnesses and cancers[56], such as glioblastoma, breast and colon cancer. Typically, the area inside solid tumours has poor vascularisation, leading to hypoxic conditions for the cancer cells, especially those that are in the centre of the tumour, as the oxygen cannot reach them. As cancer cells proliferate almost continuously, they a good deal of nutrients, energy and oxygen, and thus need to be able to cope with nutrient deficiency and hypoxia in the centre of the tumour. Proliferating cancer cells tend to have even higher rates of protein synthesis than normal cells due to mutations in oncogenes such as Ras/Raf, which can in turn inactivate eEF2K through ERK, as well as activating other steps in protein synthesis. If cancer cells continue to synthesise proteins and proliferate uncontrollably, they would eventually starve and die. Therefore, some cancers have adapted to use eEF2K to slow down protein synthesis and hence reduce their energy consumption, allowing them to survive for longer periods of time. A schematic of this adaptation is shown in **Figure 1.4**. In such cases, it would be interesting to investigate a combination therapy approach of inhibiting eEF2K and angiogenesis (such as with VEGF antagonists) at the same time. This could cut off the cancer cell's oxygen supply and force them to use up their energy on protein synthesis, unrestricted by eEF2K, thus starving themselves.

Figure 1.4

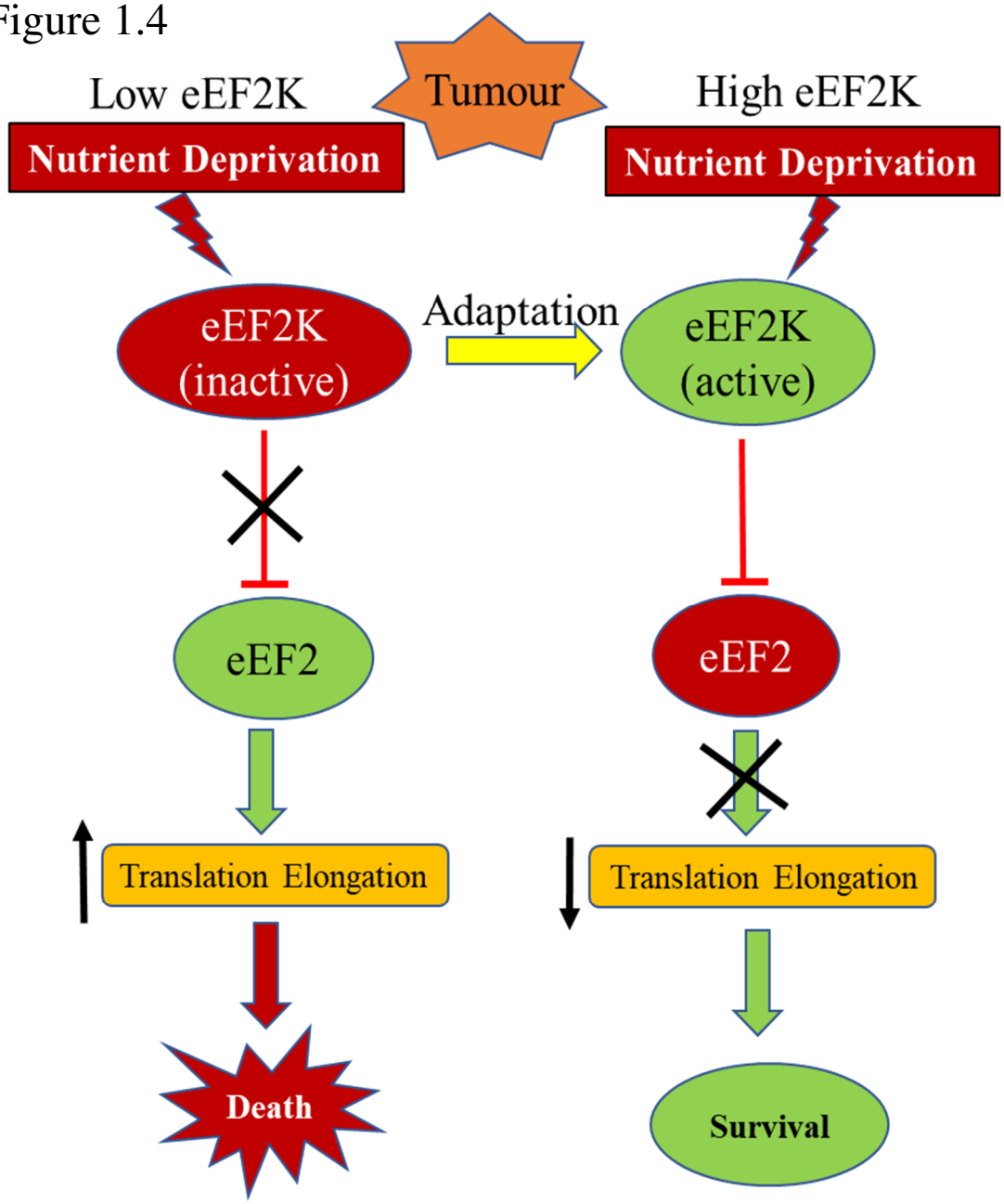


Figure 1.4: Tumour adaptation under nutrient deprived conditions. Tumours that experience nutrient deprivation and have low levels of eEF2K cannot slow down their translation elongation, using up their energy and nutrients quickly and perishing. Tumours that adapt to have high levels of eEF2K are able to inhibit eEF2, thus slowing down translation elongation and saving their energy to prolong their survival. This diagram has been adapted from Leprivier *et al*. 2013[57].

Several studies have previously shown that inhibiting eEF2K impairs cell survival or tumour growth[57-60] while, unexpectedly, a few others showed the opposite[61, 62]. An important study by Leprivier *et al*.[57] in 2013 showed that eEF2K is essential in protecting transformed (by activated K-Ras^{V12} and ETV6-NTRK3 chimeric tyrosine kinase) cells from nutrient deprivation and thus helps tumours adapt to metabolic stress. Both mutations lead to the activation of the Ras-ERK and PI3K-PKB (phosphoinositide 3-kinase, protein kinase B) pathways[63]. Importantly, NIH 3T3 MSCV (murine stem cell virus) fibroblasts that were transformed in this way showed almost a 3-fold increase in cell death compared to non-transformed cells under nutrient-deprived (ND) conditions. eEF2 phosphorylation was also blunted in these transformed cells, while the inhibitory phosphorylation of eEF2K at Ser366 was retained, showing that eEF2K is not very active in these cells. Importantly, mTORC1 signalling was inhibited in all three cell lines under ND, while AMPK signalling (as assessed by AMPK Thr172 and acetyl CoA carboxylase [ACC] Ser 79 phosphorylation) was also reduced. Transformed cells also exhibited elevated ATP levels. Elevated adenosine diphosphate (ADP):ATP and AMP:ATP ratios are associated with AMPK activation[64]. While control cells were able to raise these ratios, they remained unchanged in transformed cells. This further suggests an energy defect in these cells in which they maintain high ATP levels and unable to activate AMPK. Blocking ATP production with 2-deoxyglucose (2-DG – a glucose analogue that cannot be metabolised) and rotenone (a mitochondrial complex I inhibitor) increased AMPK activity, as well as p-eEF2 levels. Taken together, these data show that transformation of cells sensitises them to ND with defects in AMPK signalling and its regulation of eEF2.

The study then introduced these transformed cells to prolonged cycles of ND, followed with nutrient re-supplementation, eventually leading to the selection of cells that can survive

prolonged exposure to ND even after multiple passages. As with non-selected cells, mTORC1 signalling was inhibited but AMPK signalling was increased, suggesting that these cells had reacquired the ability to activate AMPK under ND. The phosphorylation of eEF2 was also greatly increased. After blocking ATP production, it was observed that these cells were able to raise their AMP:ATP and ADP:ATP ratios, which can be interpreted as suggesting that the cells were now able to adapt to ND by activating AMPK and eEF2.

Looking at the effects of ND on translation initiation, it was found that in both control and transformed cells, sub-polysomal fractions (40S, 60S and 80S-mRNA complexes, separated on a sucrose gradient) were increased, indicating a block in translation initiation. This was also confirmed by a loss of phosphorylation of 4E-BP1 (eukaryotic elongation initiation factor 4E binding protein 1), which is indicative of a block in cap-dependent translation, as hypophosphorylyaed 4E-BP1 associates with the cap-binding initiation factor eIF4E, inhibiting it[65]. Under ND, the ratio of polysomal to sub-polysomal (P/S) fractions was not significantly affected in non-transformed cells (approximately 4% reduction) but was greatly decreased in EN and Ras^{V12} transformed cells (82% and 91% reductions respectively). This suggested that transformed cells were continuously translating mRNAs. It was observed in mouse embryonic fibroblasts (MEFs) with WT eEF2K ($eEF2K^{+/+}$) and those lacking eEF2K ($eEF2K^{-/-}$) that the P/S ratios were reduced far more strongly in $eEF2K^{-/-}$ cells under ND (89% compared to 49% in $eEF2K^{+/+}$ cells). $eEF2K^{-/-}$ cells also lacked eEF2 phosphorylation, as expected. Hence, these data indicated that under ND, cells that lack eEF2K sustained translation elongation.

Next, the study investigated the effects of silencing or knocking out eEF2K on cell survival under ND. $eEF2K^{-/-}$ MEF cells were approximately 2.5-fold more sensitive to ND than

eEF2K$^{+/+}$ cells (according to measurements of caspase 3 activity). Conversely, when partial eEF2 knockdown was performed in eEF2K$^{-/-}$ cells, these cells had approximately half of the caspase 3 activity of siRNA control eEF2K$^{-/-}$ cells under ND, suggesting less cell death in these cells. This result confirms that eEF2K assists cell survival by acting to inhibit eEF2, thus slowing down protein synthesis and its usage of the cell's energy resources.

The effect of co-knockdown of eEF2K and eEF2 was then tested in NIH 3T3 MSCV cells. Knockdown of eEF2K in these cells with two independent siRNAs led to increased cell death under ND. This sensitisation was then completely rescued when eEF2 was knocked down at the same time as eEF2K. This once more confirms that eEF2K assists cell survival under ND through its effect on eEF2. Furthermore, overexpressing eEF2K in EN and Ras^{V12} transformed cells led to increased eEF2 phosphorylation and enhanced cell survival under ND. There was no increase in cell survival in these cells when kinase-dead eEF2K was overexpressed, further confirming that eEF2 phosphorylation and thus, presumably, inhibition of elongation is important for cell survival under ND. This was also confirmed by testing the role of eEF2K in the adaptive response to ND of transformed NIH 3T3 cells, which had high levels of p-eEF2. Indeed, when eEF2K was knocked down in these cells, the cells became susceptible to ND once again. eEF2K$^{-/-}$ and eEF2K$^{+/+}$ MEF cells also underwent the adaptation to ND procedure. However, eEF2K$^{-/-}$ MEFs had a reduced capability to adapt to ND compared to eEF2K$^{+/+}$ MEFs. This demonstrates that eEF2K was a crucial factor in cells adapting to ND.

These findings were then extended to HeLa and MG63 osteosarcoma cells. HeLa cells showed a much lower level of p-eEF2 compared to MG63 cells, as well as lower AMPK activity under ND, as previously reported[66]. HeLa cells were far more sensitive to ND over

a period of 48 h compared to MG63 cells which showed no significant increase in cell death over the same period. Partially silencing eEF2 in HeLa cells significantly reduced their sensitivity to ND. Moreover, overexpressing eEF2K in HeLa cells reduced their sensitivity to ND by almost half. Knocking down eEF2K in MG63 cells made the cells sensitive to ND. The AMPK catalytic subunits α1 and α2 were also knocked down in MG63 cells, which sensitised cells to ND, similar to what eEF2K knock down did.

To test these findings *in* vivo, EN and Ras^{V12} transformed NIH 3T3 MSCV cells were subcutaneously implanted into *nu/nu* immunocompromised mice. The mice were fed either an ad libitum (AL) standard diet or a caloric restriction diet (CR) that consisted of 60% of the caloric intake of the AL diet prior to tumour development. Tumour sizes of the transformed cells were reduced by approximately 50% in mice on the CR diet. Tumours that overexpressed eEF2K had smaller sizes under the AL diet, likely due to lower levels of translation elongation. However, the sizes of eEF2K overexpressing tumours were not affected by CR. These tumours eventually outgrew the tumours with normal levels of eEF2K once the mice were put back onto AL diets from CR. Morphologically, transformed tumours that overexpressed eEF2K did not exhibit any apparent necrosis, unlike control tumours. Furthermore, transformed tumours that had normal levels of eEF2K had higher levels of cleaved caspase 3, indicated higher levels of apoptosis in these cells compared to tumours that overexpressed eEF2K. The phosphorylation of eEF2 was induced poorly in control transformed cells under CR. In contrast, p-eEF2 was very pronounced in transformed cells overexpressing eEF2K under both AL and CR, with CR causing a further increase in p-eEF2. Tumours created by $eEF2K^{-/-}$ MEF cells reduced in size further than tumours created by $eEF2K^{+/+}$ MEFs. Finally, CR led to significantly increased necrosis and apoptosis in $eEF2K^{-/-}$ MEF tumours compared to $eEF2K^{+/+}$ tumours.

The authors then looked at available data from medulloblastoma (MB) and glioblastoma (GBM) patients. MB and GBM are the most common brain tumours in children and adults respectively[67]. High *EEF2K* transcript levels were associated with the most metastatic MB tumours, called group 3 tumours (n=286). High *EEF2K* expression was also correlated with decreased survival in all subtypes of MB, including the aggressive non-WNT/non-SHH subtypes. Looking at GBM, *EEF2K* expression was increased approximately 2.5-fold compared to normal human brain tissue. Specifically, *EEF2K* expression was higher in classical and mesenchymal subtypes of GBM which are associated with poorer survival[68]. Furthermore, high *EEF2K* expression correlated with poorer survival in all types of gliomas, including GBM. This suggests that eEF2K (or *EEF2K*) could be used as a marker of more aggressive cancers.

Using an MB mouse model[69], it was found that both primary and the secondary metastasising tumours had high eEF2 phosphorylation, while the surrounding normal tissue had no p-eEF2 staining. The same pattern was observed in primary human MB tissue. Furthermore, it was found that the human medulloblastoma d283 cell line was highly resistant to ND. However, the cells exhibited higher cell death when eEF2K was knocked down.

The role of eEF2K ortholog *efk-1* was then examined in the nematode worm *Caenorhabditis elegans*. The survival of the *efk-1* (*ok3609*) *C. elegans* mutant which completely lacks EFK1 activity (as assessed by p-eEF2 levels)[70] was compared to the survival of WT (N2) worms under nutrient rich and ND conditions. While, the survival of *efk-1* (*ok3609*) worms was not affected in nutrient rich conditions, there was a significant decrease in survival under ND compared to N2 worms. The mean lifespan of N2 worms under ND was 13.1 days, compared

to 7.4 days survival for *efk-1* (*ok3609*) worms. Furthermore, *efk-1* transcripts were highly induced under ND in N2 worms.

Overall, this important study showed how a variety of cell lines and tumours depend on eEF2K to survive nutrient-deprived conditions through its inhibition of translation elongation.

While Leprivier *et al.*'s[57] study pointed towards the importance of eEF2K for cells experience nutrient deprivation, it is not the only condition during which eEF2K activity comes into play. A study by Dr. Jianling Xie *et al.*[59] from our group showed a protective role of eEF2K in cells experiencing acidosis. Solid tumours are typically in an environment of low extracellular pH, ranging from as low as 6.2 to 6.9, due to their poor vascularisation and high metabolic demand leading to hypoxic conditions. Since anaerobic glycolysis is largely used to meet those demands, there is a build-up of lactic acid, and thus a decrease in pH. This acidity can drive cancer cell invasion, as well as promoting angiogenesis and impeding the immune response, allowing the cancer to spread[71, 72]. While this acidity is toxic to normal tissues, cancer cells manage to survive these conditions in ways still not understood[73]. This study shows that eEF2K is activated under conditions of acidosis (similar to an older study by Dovorkob *et al.* [74] that showed eEF2K being significantly more active at a pH of 6.6), slowing down protein synthesis and helping cancer cells survive the pH stress, identifying eEF2K as one such mechanism.

Firstly, HEK293 cells were treated for 30 min in medium with a range of pH from 6 to 7.8 It was clearly shown that p-eEF2 was quickly induced at pH 6 and was inversely related to the pH of the medium. The same trend was seen over a period of 7 h, with p-eEF2 being

higher in acidic conditions (pH 6.6) compared to optimal pH (7.4). Interestingly, eEF2K mRNA levels decreased after 5 h in acidic medium, further decreasing at 7 h. eEF2K protein was also reduced after 3 h in acidosis. However, despite the decrease in eEF2K mRNA and protein, p-eEF2 remained higher at pH 6.6 than pH 7.4, indicating eEF2K is more active at low pH. Furthermore, when the eEF2K kinase dead K170M vector was transfected into cells, it remained stable at low pH, clearly showing that eEF2K activity is required for its degradation. Importantly, acidosis also decreased the phosphorylation of AMPK and its substrate ACC, meaning eEF2K's activity under these conditions is not dependent on its activation by AMPK. Supporting this, p-eEF2 levels were still increased under acidosis in $AMPK^{-/-}$ MEFs.

It was also found that mTORC1 inhibition did not affect the phosphorylation of eEF2K at Ser359 in acidic conditions, suggesting mTORC1 is not responsible for activating eEF2K in these conditions. $TSC2^{-/-}$ MEFs (where mTORC1 is hyperactive) were still able to phosphorylate eEF2 under acidosis, even though these cells had lower levels of eEF2K. Inhibiting mTORC1 in these cells increased eEF2K levels, suggesting that hyperactivity of mTORC1 negatively regulates eEF2K protein levels (the treatment was performed for 1 h which is long enough for eEF2K to become active but should not be so long as for it to start degrading due to its activity). This was supported by overexpression of Rheb in HEK293 cells (leading to constitutively active mTORC1) which showed a decrease in eEF2K protein at pH 7.4 (physiological pH). Furthermore, mTORC1 activity was decreased at pH 6.6 (assessed by looking at phosphorylation of S6K1 at Thr389). In contrast, immunoprecipitated eEF2K activity was increased at pH 7.4 when mTORC1 was inhibited with AZD8055 and even further at pH 6.9. These data show that acidosis directly inhibits mTORC1 activity while promoting eEF2K activation.

The study then looked into whether histidine residues within eEF2K could be important for its activation, as histidines are the only residues to undergo protonation in the shift from physiological to acidotic pH. Interestingly, the study also found that the conserved histidine residues (H80, H87 and H94) within the CaM-binding domain of eEF2K, as well as within the ATP-binding site (H227 and H230) are necessary for its activation under acidosis. When all of the histidine residues within the CaM binding domain were mutated to alanines, eEF2K's activation at acidic pH was greatly blunted. Conversely, mutating these residues to lysines, which are charged at both physiological and acidic pH, eEF2K activity was enhanced at both pH 6.9 and 7.4. Furthermore, a synthetic peptide of residues 78-100 of eEF2K had reduced CaM binding affinity when all three histidine residues were changed to alanines, while its CaM binding affinity was increased when they were altered to lysines. This suggests that the residues were important for binding of CaM to eEF2K and thus its activation. Mutating the H227 and H230 residues within the ATP-binding site to alanines showed that the eEF2K peptide could still strongly bind ATP, but showed reduced activity at pH 6.9, suggesting that the sites are required for eEF2K activation and not simply ATP-binding. Mutating the sole histidine residue on calmodulin (H108) to a lysine still allowed the calmodulin to bind to the eEF2K peptide but was unable to activate it, suggesting that this residue likely also contributes to eEF2K activation.

The study then tested the effects of eEF2K knockdown under acidic conditions in two lung carcinoma cell lines – A549 and HCT116. The cells were cultured at pH 6.4, 6.8 and 7.4. p-eEF2 increased at low pH values up to 40 h, after which it decreased. Interestingly, eEF2K levels decreased at low pH, even though p-eEF2 remained high, further suggesting that eEF2K activity is highly increased at low pH. Knockdown of eEF2K with shRNA in both

cell lines led to a greater decrease in ATP levels under acidosis compared to control cells. The CellTox Green cytotoxicity assay showed an increase in cell death at pH 6.2, 6.4 and 6.6 in eEF2K knock-down cells. This was confirmed by flow cytometry, with an increase in sub-G1 populations at the same pH levels. While this shows that eEF2K assists cell survival under acidosis, solid tumours can survive acidic conditions for months. To test whether eEF2K plays a role in this, the same cells were cultured in pH 6.7 (cells denoted pH 6.7EXT, = extended [time]) for 3 months and compared to cells grown in pH 7.4 (cells denoted 6.7EXT and 7.4EXT respectively) for the same amount of time. Surprisingly, p-eEF2 and eEF2K levels were lower in 6.7EXT cells, correlating with increased sub-G1 populations in these cells, suggesting that the impairment of eEF2K activity leads to increased cell death after chronic acidosis. 6.7EXT HCT116 cells showed increased mTORC1 signalling, suggesting these cells were adapting to chronic acidosis by using mTORC1 to maintain cell growth and proliferation. Importantly, knocking down eEF2K with shRNA further increased the chronic cell death induced by acidosis in both cell lines.

The final part of the study showed that eEF2K inhibits protein synthesis under acidosis. Using [^{35}S] methionine incorporation to measure protein synthesis, it was found that eEF2K knockdown increased incorporation of label into A549 cells, with the effect being large at lower pH levels. Furthermore, acidosis increased the amount of active polysomes with a concomitant decrease in translationally inactive monosomal fractions. eEF2K knockdown also led to a substantial increase in the subpolysomal fraction under acidosis, presumably because the faster translation elongation rate in cells deficient in eEF2K leads to ribosomal runoff in these cells. The increase in protein synthesis in eEF2K knockdown cells could explain the lower ATP levels and cell viability compared to control cells.

Overall, this study showed that eEF2K becomes highly active under acidic conditions, slows down the elongation stage of protein synthesis and assists cell survival.

Another condition that cancer cells have to contend with is hypoxia. Solid tumours are typically not just surrounded by a low pH environment, but also that of low oxygen. A lack of oxygen means that cells cannot undergo aerobic respiration, decreasing their ATP production[75]. Previous studies have shown that eEF2 phosphorylation increases under hypoxia in cardiomyocytes and breast cancer cells and contributes to cell survival[76, 77]. However, it remained unclear whether eEF2K was activated in hypoxia. As stated in section **1.2**, a study by Moore *et al*.[78] in 2015 showed that hypoxia did indeed activate eEF2K, through the inhibition of prolyl hydroxylases. An important part of the study showed that following hypoxia, primary cortical neurons from eEF2K$^{-/-}$ mice had lower levels of ATP and greater cleavage of poly-ADP-ribose polymerase (PARP), a marker of apoptotic cell death, compared to WT cells. This indicated that eEF2K protects primary neuronal cells under hypoxic conditions. These data were in line with previous findings that used carbimazole to inhibit protein synthesis in primary neuronal cultures. This induced p-eEF2, as well as preventing cell damage and drops in ATP levels[79].

To test whether the increase in p-eEF2 resulted in the inhibition of protein synthesis, and due to limitations of the study, DMOG (a prolyl hydroxylase inhibitor) was used instead of hypoxia in TSC2$^{-/-}$ MEFs to avoid effects on mTORC1. Indeed, treatment with DMOG significantly reduced protein synthesis in these cells, as judged by [^{35}S]-methionine incorporation. Importantly, this study implies that eEF2K acts to phosphorylate eEF2, inhibit protein synthesis and thus restrict ATP consumption during hypoxia in primary cortical neurons. Further discussion of this study is located in section **5.1.3**.

1.4 Autophagy

Autophagy is an essential pathway through which cells are able to degrade proteins, organelles and foreign bodies into their constituent building blocks[80-82]. These molecules can then be recycled for use during starvation, e.g., for energy production or synthesis of essential macromolecules[83]. There are three different types of autophagy: macroautophagy, microautophagy and chaperone-mediated autophagy[84, 85]. All three of these pathways end up with cell components being degraded by the lysosome. Macroautophagy involves the formation of the autophagosome – a double membrane structure to which cell components that are marked for degradation are brought. Once the autophagosome closes around the components, it fuses with the lysosome, whose digestive enzymes degrade the contents of the autophagosome. On the other hand, microautophagy involves the cellular components that are to be degraded directly engulfed by the lysosome through invagination of its membrane. Chaperone-mediated autophagy complexes targeted proteins with chaperone proteins, such as Hsc-70, which is recognised by lysosomal-associated membrane protein 2A (LAMP2A)[86, 87]. The proteins are then unfolded and degraded. This thesis will be discussing macroautophagy, hereafter referred to as autophagy.

To start the autophagic process, cysteine protease ATG4 cleaves pro-microtubule-associated protein 1 light chain 3 (pro-LC3) to form LC3-I. LC3 then becomes conjugated to phosphatidylethanolamine (PE) by ubiquitin-like modifier-activating enzyme ATG7, becoming LC3-II[80, 82, 83]. This then is recruited to the forming autophagosomal membrane to help its elongation. ATG7 is also involved in the formation of the ATG5-ATG12-ATG16 (autophagy protein 5, ubiquitin-like protein ATG12, autophagy protein 16) complex

formation which is necessary for autophagosome formation. Ubiquitinated proteins are bound by p62/SQSTM1 (Sequestrome-1) and are brought to the forming autophagosome membrane, by binding to LC3-II. Once the autophagosome membrane closes around the bound proteins, the autophagosome fuses with the lysosome, where the said proteins are degraded. LC3-II and p62 are then degraded at the end of the process and are commonly used as markers of autophagic flux[88]. This is schematized in **Figure 1.5**[89].

Autophagy has contrasting roles in cancer. On the one hand, it is thought to prevent cell death and tissue damage which can result in cancer formation[90]. On the other hand, autophagy is known to assist cancer cell survival, as shown by multiple studies. A 2003 study by Briceno *et* al.[91] showed that chloroquine (CQ), an autophagy inhibitor, improved the anti-tumour effect of antineoplastic treatment on patients with glioblastoma. In 2007, Amaravadi *et al*.[92] showed that inhibiting autophagy by using chloroquine or shRNA against ATG5, in combination with alkylating drug therapy, induced more cell death in a Myc-induced model of lymphoma than drug treatment alone. Several studies published in 2013 showed that genetic knockdown of autophagy-related genes resulted in decreased pancreatic and lung tumour growth *in vivo*[93-95]. Karsli-Uzunbas *et* al.[96] showed that conditional deletion of *Atg7* in mice compromises lung tumorigenesis in 2014. In the same year, multiple groups published clinical studies using hydroxychloroquine (HCQ) to inhibit autophagy in cancer patients and improved outcomes for patients with solid tumours when used in combination with other therapies[97-100].

In 2017, a study Mulcahy Levy *et al*.[101] looked at the effect of autophagy inhibition in brain tumours with the $BRAF^{V600E}$ (serine/threonine-protein-kinase B-Raf) mutations. These mutations occur in more than 50% of metastatic melanomas[102], which are therefore a prime

target for BRAF inhibitors (BRAFi). As is typical of cancer cells, these tumours eventually develop BRAFi resistance. A study in 2010 by Fan *et al*.[103] showed that autophagy inhibition in combination with dual PI3K-mTOR inhibitors improved response in $BRAF^{WT}$ gliomas that were resistant to PKB-PI3K-mTOR inhibition. In 2014, it was shown that autophagy inhibition overcame the BRAFi resistance in melanoma cell lines[104]. The 2017 study showed that metastatic glioblastoma patients (with the $BRAF^{V600E}$ mutation) treated with chloroquine in addition to vemurafenib had positive responses, showing reduced tumour growth.

Autophagy is regulated by mTORC1, PI3K, serine/threonine protein kinase ULK1 (ULK1) and PKB[105-109]. It has been shown that inhibition of mTORC1 via rapamycin leads to the induction of autophagy in glioma cells[110]. Using inhibitors of PI3K and PKB in the same cells also led to the stimulation of autophagy[110]. mTORC1 is known to inhibit autophagy through an inhibitory phosphorylation site on autophagy-related protein 13 (ATG13), which then reduces the activity of ULK1, leading to a reduction in the rate of autophagosome formation[108, 109]. AMPK is known to positively regulated ULK1 through direct phosphorylation of multiple sites. This leads to the recruitment of ATG proteins to the membrane domains in which autophagosome formation occurs[111]. mTORC1 has also recently been found to be able to reciprocally inhibit AMPK through phosphorylation of its catalytic α-subunits[112].

Considering mTORC1's and AMPK's role in regulating eEF2K and all of the evidence that autophagy plays a key role in survival of a variety of cancer cells, it was conceivable that autophagy and eEF2K are linked.

Figure 1.5

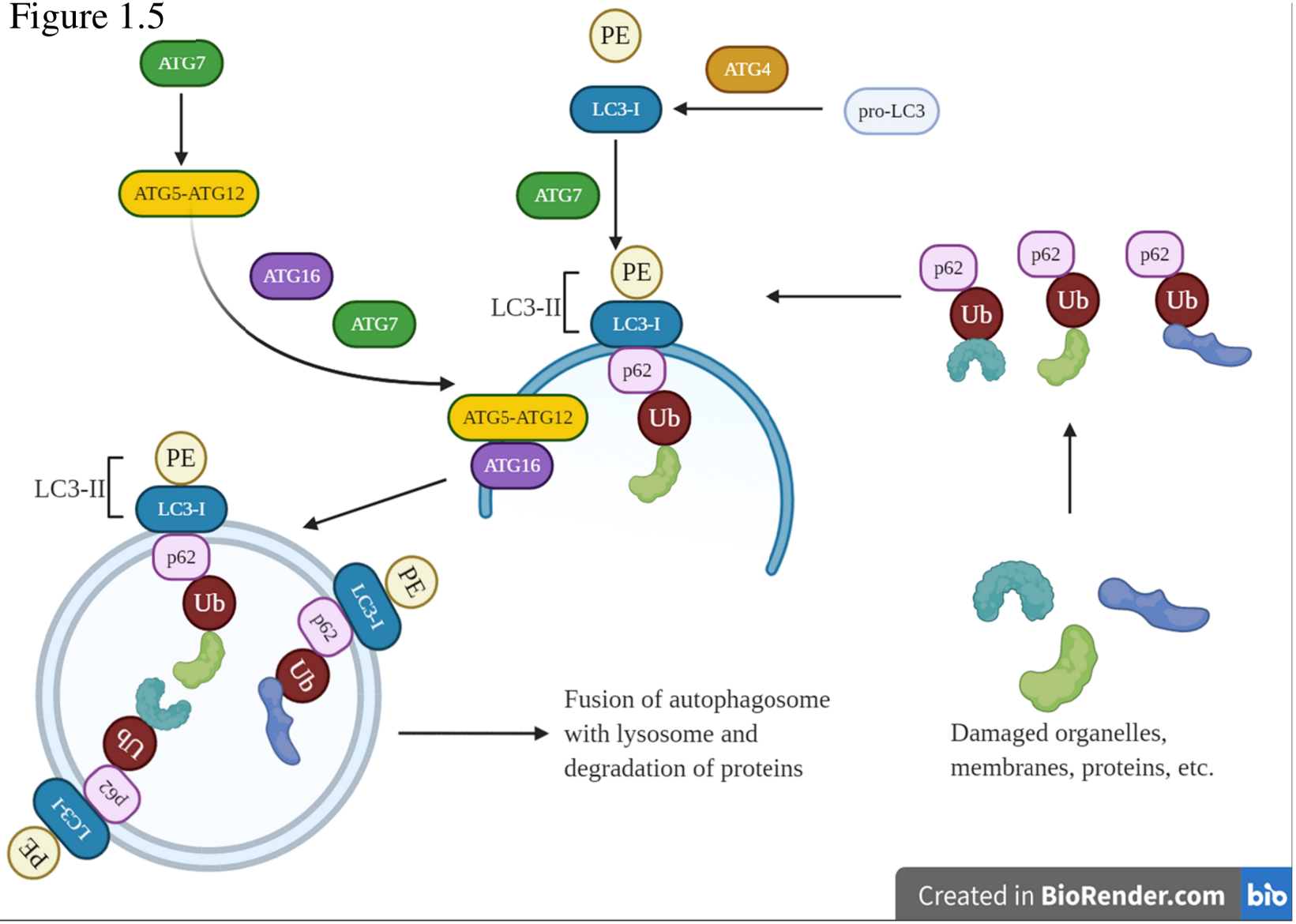

ATG7
ATG5-ATG12
ATG16
ATG7
PE
ATG4
LC3-I
pro-LC3
ATG7
PE
LC3-II
LC3-I
p62
Ub
ATG5-ATG12
ATG16
p62
Ub
p62
Ub
p62
Ub
PE
LC3-II
LC3-I
p62
Ub
Fusion of autophagosome with lysosome and degradation of proteins
Damaged organelles, membranes, proteins, etc.
Created in BioRender.com
bio

Figure 1.5: The autophagic process. ATG4 cleaves pro-LC3, which forms LC3-I. LC3-I is bound to PE by ATG7, creating LC3-II. ATG7 is also necessary for ATG5-ATG12-ATG16 complex formation, which is needed alongside LC3-II to form the autophagosome. Proteins and organelles marked with ubiquitin bind to p62/SQSTM1 and are brought to LC3-II which is bound to the forming autophagosome membrane. ATG7 is also involved in the formation of the ATG5-ATG12-ATG16 complex that is required for autophagosome formation. The autophagosome then fully forms around the proteins, binds to the lysosome and the proteins are degraded. This diagram was created using BioRender and was adapted from the Novus Biologicals website[89].

1.5 eEF2K and its relation to autophagy

There have a been a number of studies examining the possible links between eEF2K and autophagy but there is currently no clear picture. Several studies have suggested that eEF2K positively regulates autophagy[113-118].

A study by Wu *et al.*[114] in 2006 looked at the effects of eEF2K knockdown on autophagy in glioblastoma cells. eEF2K knockdown was performed in T98G, U138G and LN229 glioblastoma cell lines, following which, LC3-II levels were reported to decrease, implying a reduction in the autophagic flux. This was also evident in the human breast cancer cell line MCF7, as well as in eEF2K-KO MEFs. This decrease in LC3-II in eEF2K-KO MEFs was also seen by Py *et al.*[115] in 2009. It was also shown via electron microscopy that autophagosomes were rarely present in eEF2K silenced T98G cells. Furthermore, the effect of eEF2K knockdown on LC3-II levels was still evident in cells experiencing nutrient deprivation. It was then shown that eEF2K knockdown led to increased cell death under nutrient-deprived conditions in T98G cells. In another study by Wu *et al.*[113] in 2009, it was reported that 2-DG induced autophagy, while the silencing of eEF2K blunted this induction (assessed by LC3-II levels). Silencing of eEF2K in cells treated with 2-DG also led to increased cell death. The study concluded that silencing of eEF2K leads to sensitisation of glioma cells to 2-DG through the blunting of autophagy.

A study by Cheng *et al.*[118] in 2010 investigated the effects of eEF2K inhibition on autophagy in MCF7 and MDA-MB-468 breast cancer cell lines. The study showed significant decreases in LC3-II levels in these cell lines upon eEF2K silencing, as well as a sensitisation of cells

to epidermal growth factor receptor (EGFR) tyrosine kinase inhibitors gefitinib and lapatinib. These inhibitors were shown to increase LC3-II levels in a dose-dependent manner, suggesting the cells activate autophagy as a response to these inhibitors. The sensitisation of cells to these inhibitors upon eEF2K knockdown suggests that eEF2K protects these cells by inducing autophagy. Cheng *et al*.[117] also investigated T98G and LN229 cells and the effect of the PKB inhibitor MK-2206 on autophagy in 2011. It was found that MK-2206 induced LC3-II levels. Once again, the study reported decreased LC3-II levels in these cells upon eEF2K silencing, even when cells were also treated with MK-2206. Furthermore, it was shown that MK-2206 induced apoptosis in tumour xenografts, with the cells being further sensitised to MK-2206 upon silencing of eEF2K.

In 2014, Xie *et al*.[119] showed a different result in the colon cancer cells HT29 and HCT116. This study found that silencing of eEF2K in these cells led to the increase of LC3-II protein levels and LC3-II puncta. The study showed increased cell survival upon eEF2K silencing, with the converse decrease in cell survival upon its overexpression, linking it to eEF2K's negative regulation of autophagy. This shows that eEF2K's effect on cell survival has to be evaluated on a cell line by cell line basis.

An issue with most of these studies is the use of LC3-II as the main readout of autophagy. Considering that LC3-II is an intermediate in the process, which is degraded at the end, changes in its protein levels could be taken as a change in autophagic flux in either direction, increase or decrease. For example, an increase in LC3-II could mean an increase in autophagic flux, or it could mean its inhibition, as LC3-II builds up and cannot be broken down – this build up is commonly used as a marker that autophagic inhibitors are functioning, but should not be relied upon as the sole indicator of autophagic flux[89].

A contrasting study by Moore *et al*.[58] in 2016 examined autophagy and eEF2K in HCT116, A549 and MEF cells. This study showed that silencing eEF2K in A549 cells or knock-out of eEF2K in MEF cells did not lead to any changes in LC3-II protein levels, thus suggesting that eEF2K does not regulate autophagy in these cell lines. It is important to note that this study also used an mCherry-EGFP-LC3B vector to quantify autophagosome and lysosome fusion through the loss of GFP fluorescence. When using this reporter, the GFP signal is quenched upon protonation due to the decrease in lysosomal pH, while the mCherry signal is not. Thus, the ratio of fluorescence at the two wavelengths changes as this fusion protein enters lysosomes. This is a more direct way of measuring autophagic flux, thus providing a far better quantification of changes in autophagy than just a mesasurement of LC3-II levels. Following eEF2K knockdown in A549 cells, there was no significant change in the Green/Red signal ratio compared to control cells, further showing that eEF2K does not regulate autophagy in these cells.

These contradicting conclusions concerning the role that eEF2K plays in relation to autophagy make it difficult to determine eEF2K's function in this pathway. It is thus important to test eEF2K's effect on autophagy in more cell lines and using multiple and informative read-outs of autophagic activity.

1.6 eEF2K and its relation to other cell signalling pathways

eEF2K has also been linked to a variety of cellular processes and proteins which are worth investigation, such as cell migration/invasion/adhesion, hypoxic response, glucose uptake,

Programmed Cell Death 1 Ligand 1 (PD-L1) and Nrf2. These processes are discussed in detail in the Introduction section of **Chapter 5**.

1.7 Aims of the project

This thesis project focused on the roles of eEF2K and autophagy in cancer cell survival under nutrient-deprived conditions. The initial aim was to test the effects of concurrent eEF2K and autophagy inhibition on MDA-MB-231 breast cancer cell survival under nutrient stress.

The second aim of the project was to develop MDA-MB-231 eEF2K-KO cells and eventually PC3 eEF2K-KO cells (created by Danielle Fang following the same method used for MDA-MB-231 cells) to ensure the effects of eEF2K inhibition was not due to off-target effects of the inhibitors used.

The third aim was to examine the effects of combined nutrient deprivation, eEF2K and autophagy inhibition on cell survival of eEF2K-KO and knock-down MDA-MB-231, PC3 and A549 cells respectively.

The fourth aim was to examine the mechanisms that cells use to become resistant to combined nutrient deprivation and autophagy inhibition in MDA-MB-231 cells by generating resistant cells and performing proteomic analysis. As a part of this, non-resistant cells would be used for phospho-proteomic analysis to search for additional substrates of eEF2K.

The final aim of this thesis was to investigate eEF2K's possible link to a variety of cellular pathways and proteins – cell migration/invasion/adhesion, hypoxic response, glucose uptake, PD-L1 and Nrf2.

2.1 Chemicals and Reagents

Item	Company	Catalogue Number
1 kb DNA Ladder	New England Biolabs	N3232S
100 bp DNA Ladder	New England Biolabs	N3231S
10X CutSmart Buffer	New England Biolabs	B7200
10X T4 DNA Ligase Reaction Buffer	New England Biolabs	B0202
10x Tris/Glycine	Bio-Rad	1610771
10x Tris/Glycine/SDS	Bio-Rad	1610772
2% bis-acrylamide solution	Bio-Rad	1610143
2-Deoxyglucose	Sigma-Aldrich	D8375-1G
40% acrylamide	Bio-Rad	1610140
6X Purple Gel Loading Dye	New England Biolabs	B7024S
A484954	Sigma Aldrich	SML0861-5mg
Acetic Acid	Sigma Aldrich	320099
Agar	Thermo Fisher	FSBBP1423-500
Agarose	Thermo Fisher	FSBBP160-500
Ammonium Persulfate	Sigma Aldrich	A3678
AxyPrep MAG PCR Clean-up Kit	Fisher Biotech	MAG-PCR-CL-5
*Bae*I	New England Biolabs	B7200
Bafilomycin A1	Assay Matrix	A8627-1mg
β-glycerophosphate disodium salt hydrate	Sigma-Aldrich	G9422
Bovine Serum Albumin	Sigma-Aldrich	A9647-100G

Item	Company	Catalogue Number
*Bpm*I	New England Biolabs	R0613
BrdU Cell Proliferation Assay Kit	Cell Signaling Technology	6813S
Calcein-AM	Thermo Fisher	C3099
Calcium chloride dihydrate	Sigma Aldrich	C3306
Carbenicillin disodium salt	Sigma Aldrich	C1389-5g
Caspase-Glo® 3/7 Assay	Promega	G8090
Caspase-Glo® 8 Assay	Promega	G8200
Cell Line 4D nucleofector kit with SE buffer	Lonza	V4XC-1024-SE
Cell Line 4D nucleofector kit with SF buffer	Lonza	V4XC-2012
CellTox™ Green Assay Kit	Promega	G8741
CellTiter-Glo® 2.0 Assay	Promega	G9241
Chloroform	Sigma Aldrich	C7559
Corning® Matrigel®, Growth Factor Reduced	Corning	354230
D-Glucose	Sigma-Aldrich	G8270
Dimethyl sulfoxide	Sigma-Aldrich	D2650-100mL
DMEM – high glucose	Life Technologies	11995065
DMEM – no glucose, no pyruvate	Life Technologies	11966025
DMEM – no glutamine, no glucose, no pyruvate	Life Technologies	A1443001
Dual-Luciferase® Reporter Assay System	Promega	1395908

Item	Company	Catalogue Number
Dynabeads™ CD4 Positive Isolation Kit – 5mL	Life Technologies	11331D
*Eco*RI-HF	New England Biolabs	R3101
EDTA	Sigma Aldrich	E9884
eEF2 siRNA	Sigma Aldrich	EHU047821
EGTA	Sigma Aldrich	E3889
Ethanol	Thermo-Fisher	AJA214-20LPL
Fast SYBR™ Master Mix	Thermo Fisher	4385618
FBS	Life Technologies	10099141
Formaldehyde solution	Sigma-Aldrich	F8775-500ML
GelRed®	Jomar Life Research	41003
GeneArt™ CRISPR Nuclease CD4 Enrichment Kit	Thermo Fisher	A21175
GeneJet Gel Extraction Kit	Thermo Fisher	K0691
Glucose Uptake-Glo™ Assay	Promega	J1341
Glycerol	Sigma Aldrich	G5546
GoTaq Hot Start Green Master Mix	Promega	M5122
Hoechst 33342	BioRad	639
Hydrogen peroxide solution	Sigma-Aldrich	H1009-100ML
IPTG	Sigma-Aldrich	I6758-1G
JAN384	Janssen Pharmaceutica	N/A
JAN452	Janssen Pharmaceutica	N/A
JAN978	Janssen Pharmaceutica	N/A

Item	Company	Catalogue Number
Kanamycin sulfate	Sigma Aldrich	K1377
Lipofectamine 3000	Life Technologies	L3000015
Luria Broth Base	Life Technologies	12795084
LysoTracker Red DND-99	Thermo Fisher	L7528
Magic Red Cathepsin L Kit	Bio-Rad	ICT941
Manganese chloride tetrahydrate	Sigma Aldrich	203734
Methanol	Thermo Fisher	M/4000/17
MG-132	Sigma Aldrich	M8699
Mitomycin C	Sigma-Aldrich	10107409001
MOPS	Sigma Aldrich	M1254
NEBuffer 3.1	New England Biolabs	B7203
Nitrocellulose	Bio-Rad	1620115
NucleoBond Xtra Midi	Scientifix Life	740410.5
NucleoSpin Plasmid DNA Prep Kit	Scientifix Life	740588.250
One*Taq* Hot Start 2X Master Mix with Standard Buffer	New England Biolabs	M0484
Opti-MEM Reduced Serum Medium	Thermo Fisher	31985070
PBS Tablets	Life Technologies	18912014
Penicillin/Streptomycin 10,000 U/mL	Life Technologies	15140122
Potassium acetate	Sigma Aldrich	236497
Potassium chloride	Sigma Aldrich	P9541

Item	Company	Catalogue Number
Potassium phosphate monobasic	Sigma Aldrich	P5379-500G
Precision Plus Protein Dual Color Standards	Bio-Rad	1610394
Propan-2ol	Chem-Supply	RP1162
Propidium iodide	Sigma Aldrich	P4170-100mg
Protease inhibitor cocktail	Sigma-Aldrich	05056489001
Protein Assay Dye Reagent Concentrate	Bio-Rad	5000006
PureBlue DAPI Nuclear Staining Dye	Bio-Rad	13151303
QuantiNova Reverse Transcription Kit	Qiagen	205413
QuickExtract DNA Extraction Solution	Gene Target Solutions	QE09050
RealTime-Glo™ MT Viability Assay	Promega	G7911
RNase A	Thermo Fisher	EN0531
RPMI	Life Technologies	21870076
Rubidium chloride	Sigma Aldrich	R2252
S-adenosylmethionine (SAM)	New England Biolabs	B9003
SDS Solution	Bio-Rad	1610418
Seahorse XF 1.0M Glucose Solution	InVitro Technologies	SEA103577100
Seahorse XF 100mM Pyruvate Solution	InVitro Technologies	SEA103578100

Item	Company	Catalogue Number
Seahorse XF 200mM Glutamine Solution	InVitro Technologies	SEA103579100
Seahorse XF Base Medium	InVitro Technologies	SEA103334100
Seahorse XF Calibrant	InVitro Technologies	SEA100840000
Seahorse XF Cell Mito Stress Test Kit	InVitro Technologies	SEA103015100
Seahorse XF DMEM medium	InVitro Technologies	SEA103575100
Seahorse XF Glycolysis Stress Test Kit	InVitro Technologies	SEA103020100
Seahorse XF RPMI medium	InVitro Technologies	SEA103576100
Seahorse XFp Cell Energy Phenotype Test Kit	InVitro Technologies	SEA103275100
Seahorse XFp Cell Mito Stress Test Kit	InVitro Technologies	SEA103010100
Seahorse XFp Glycolysis Stress Test Kit	InVitro Technologies	SEA103017100
Sodium chloride	Thermo Fisher	FSBBP358-212
Sodium deoxycholate	Sigma Aldrich	S1827
Sodium fluoride	Sigma Aldrich	201154
Sodium hydroxide	Sigma Aldrich	221465
Sodium orthovanadate	Sigma Aldrich	450243
Sodium phosphate Dibasic	Sigma Aldrich	S9763
Sodium pyruvate Solution	Life Technologies	11360070
T4 DNA Ligase	New England Biolabs	M0202S
T4 Polynucleotide Kinase	New England Biolabs	M0201

Item	Company	Catalogue Number
TEMED	Sigma Aldrich	T9281-25ML
Triethylammonium bicarbonate buffer	Sigma Aldrich	18597
TRI Reagent	Sigma Aldrich	T9424-200ML
Trizma® base	Sigma Aldrich	T1503
Trypan Blue Solution 0.4%	Sigma Aldrich	T8154-100ML
TrypLE™ Express Enzyme	Life Technologies	12605028
Tween-20	Thermo Fisher	ACR233360010
Type I Bovine Collagen	Stemcell Technologies	07001
Whatman™ paper 3mm	Bio-strategy	WHAT3030-917

2.2 Cell culture and treatments

2.2.1 Cell lines and maintenance

Cell line authenticity was confirmed by the Garvan Molecular Genetics (Sydney, New South Wales, Australia) for MDA-MB-231 and A549 cells. PC3 cells were authenticated by CellBank Australia (Westmead, New South Wales, Australia). The A549 cells expressing an inducible short hairpin RNA (shRNA) were previously provided by Janssen Pharmaceutica (Beerse, Belgium)[59]. MDA-MB-231 (human breast carcinoma) and A549 (human lung carcinoma) cells were grown in high glucose Dulbecco's Modified Eagle Medium (DMEM) – 25 mM D-glucose, 4 mM L-glutamine, 1 mM sodium pyruvate, 10% (v/v) foetal bovine serum (FBS) and 100 U/mL penicillin with 0.1 mg/mL streptomycin (1%

P/S). PC3 (human prostate carcinoma) cells were grown in Roswell Park Memorial Institute (RPMI) 1640 medium – 11.1 mM D-glucose, 2 mM L-glutamine, 1 mM sodium pyruvate, 10% (v/v) FBS, and 1% P/S. The cells were maintained in a 37°C humidified incubator with 5% (v/v) CO_2 and split when grown to approximately 80-90% confluence. To do this, the medium was removed, and the cells were washed twice with 1X phosphate buffered saline (PBS). TrypLE was then added to plates, which were then put in the incubator to detach the cells. Cells were then resuspended in medium and divided into new plates for experimentation or maintenance. To induce eEF2K knock-down in A549 cells, 1 μM IPTG was added to the medium 5 days prior to the start of an experiment.

2.2.2 Cryopreservation of cells

Once the cells were 80-90% confluent, they were washed twice with 1X PBS, trypsinized resuspended in medium and spun down in a centrifuge at 200 x *g* for 5 min. The supernatant was removed, and the cell pellets were resuspended in freezing medium consisting of 95% of either DMEM or RPMI, depending on the cell line, with 5% (v/v) dimethyl sulfoxide (DMSO). The resuspended solution was moved to 1.5 mL cryotubes and stored in a Mr. Frosty container at -80°C overnight. The cryotubes were then moved to liquid nitrogen storage.

To thaw cells for maintenance and experimentation, the cryotubes were thawed in a 37°C water bath prior to the drop-wise addition of medium into the tubes to resuspend the cell pellet. Once resuspended, the medium was moved to a new tube and centrifuged at 200 x *g* for 5 min. The supernatant was removed, and the cells were resuspended in the required

amount of pre-warmed medium for the type of dish that they were grown on. The medium was changed the next day to remove any dead cells and debris.

2.2.3 Trypan Blue cell counts

To seed cells for experiments, cells were washed twice with 1X PBS, trypsinized and resuspended in full medium. The cells were then spun down at 200 x *g* for 5 min and the supernatant was removed. The cells were then resuspended in a small volume of full medium and added to a 0.4% solution of Trypan Blue at a certain dilution (1/5 to 1/20). The mixture was mixed well and 20 µL in total was used fill both chambers of a haemocytometer. The top left, top right, bottom left and bottom right squares of each chamber were counted and the following formula was used to determine the number of cells: number of cells per mL = average number of cells in both chambers x 10,000 x dilution factor. The cells were then seeded at the required density for the experiment.

2.2.4 Cell treatments and harvesting

Cells were treated at 90% confluency. When treating with inhibitors, the corresponding vehicle was used as a control, such as DMSO. For nutrient deprivation experiments, two types of DMEM media were used, both supplemented with 5% (v/v) dialysed FBS and 1% P/S. One type of medium contained no glucose and pyruvate. The other contained no glucose, glutamine, and pyruvate. Prior to changing the medium, the cells were washed once with 1X PBS. Once the treatment was complete, the cells were taken out of the incubator and the medium was aspirated. For experiments involving cell death, the medium was

transferred to a separate tube to collect the dead cells. The plates were kept on ice throughout the process. The plates were washed once with 1X PBS which was then either aspirated or added to separate tubes to collect dead cells. The tubes were then spun for 2 min at 3,000 rpm and the supernatant is removed. Lysis buffer was added to the cells on the plates and the tubes which were also put on ice. In the case of Triton Lysis Buffer, the cells were left with the buffer for at least 5 min prior to scraping them off with the cell scraper. Cells lysed with High Salt Lysis Buffer were left to lyse for at least 20 min. The tubes with the dead cell pellets were combined with the same samples scraped off the plate. The lysates were spun at 4°C at 16,000 x *g* for 15 min. The samples were then used for the Bradford Assay to determine their protein concentration.

2.3 Buffers and bacterial culture media

- Competent Bacteria Transformation Buffer 1: 0.1 M $RbCl_2$, 0.05 M $MnCl_2.4H_2O$, 0.01 M $CaCl_2.2H_2O$, 30 mM potassium acetate pH 7.5, 2 M Glycerol. 0.2 M Acetic acid was used to bring the pH to 5.8 and made up to final volume with Milli-Q. The buffer was sterilised through a 0.22 µm filter.
- Competent Bacteria Transformation Buffer 2: 10 mM MOPS pH 6.8, 10 mM $RbCl_2$, 75 mM $CaCl_2.2H_2O$, 2 M Glycerol. The final volume was made up with water. The buffer was sterilised through a 0.22 µm filter.
- 10X Phosphate Buffer Saline (PBS): 40 mM KCl, 1.7 M NaCl, 100 mM Na_2HPO_4, 22 mM KH_2PO_4. The solids were dissolved in reverse osmosis (RO) water and the pH was brought to 7.4 with sodium hydroxide.
- 1X PBST: 10% (v/v) 10X PBS and 0.1% (v/v) Tween-20.

- Triton Lysis Buffer: 25 mM Tris-HCl pH 7.5, 50 mM KCl, 50 mM β-glycerophosphate, 1 mM EDTA, 1% (v/v) Triton X-100, 2 mM Na_3VO_4, 14.3 mM β-mercaptoethanol, 1X Protease Inhibitor cocktail.
- High Salt Lysis Buffer: 350 mM NaCl, 2.5 mM sodium pyrophosphate ($Na_2H_2P_2O_7$), 50 mM Tris-HCl pH 7.5, 50 mM β-glycerophosphate, 1 mM EDTA, 1 mM EGTA, 10 mM sodium fluoride (NaF), 1% (v/v) Triton X-100, 2 mM Na_3VO_4, 14.3 mM β-mercaptoethanol, 1X Protease Inhibitor cocktail.
- Proteomics Lysis Buffer: 4% (w/v) sodium deoxycholate in 0.1 M triethylammonium bicarbonate (TEAB).
- 5X Sample Buffer: 0.5 M Tris-HCl pH 6.8, 10% (w/v) Sodium Dodecyl Sulfate (SDS), 20% (v/v) Glycerol, 0.12% (w/v) Bromophenol Blue.
- 1X Sample Buffer: 20% (v/v) 5X Sample Buffer, 5% (v/v) β-mercaptoethanol.
- Label-Free Proteomics Lysis Buffer: 150 mM NaCl, 20 mM Tris-HCl pH 7.4, 1 mM EDTA, 1 mM EGTA, 10 mM NaF, 1% (v/v) Triton-X100, 1X PI.
- Luria Broth (LB) medium: Per 1L – 10 g Peptone 140, 5 g Yeast extract, 5 g Sodium Chloride.
- 10X Running Buffer (purchased from Bio-Rad): 25mM Tris, 192 mM glycine, 0.1% SDS, pH 8.3.
- 1X Running Buffer: 10% (v/v) 10X Running Buffer, 90% Milli-Q water.
- 10X Transfer Buffer (purchased from Bio-Rad): 25 mM Tris, 192 mM glycine, pH 8.3.
- 1X Transfer Buffer: 10% (v/v) 10X Transfer Buffer, 10 or 20% (v/v) Methanol (depending on protein of interest molecular weight), 0.01% (v/v) SDS.

- 50X TAE (Tris-acetate EDTA) Buffer: 40 mM Tris, 20 mM acetic acid, 1 mM EDTA.
- Flow Cytometry Staining Buffer: 0.1% (w/v) BSA, 99.9% PBS.
- Dynabeads CD4 Isolation Buffer I: 0.1% (w/v) BSA, 2 mM EDTA in PBS, 0.2 µm sterile filtered.
- Dynabeads CD4 Isolation Buffer II: DMEM (for MDA-MB-231 cells) or RPMI (for PC3 cells) containing 2% (v/v) FBS, 0.2 µm sterile filtered.

2.4 Molecular Biology Techniques

2.4.1 Making of Agar Plates for Bacterial Growth

For a 200 mL mixture of agar, 3 g agar, 5 g LB was added into a bottle and dissolved in Milli-Q water. The mixture was autoclaved and microwaved for 3 min or until the solid is dissolved. The solution was left to cool until warm. Antibiotics were then added to the mixture at a final concentration of 100 µg/mL for carbenicillin or 50 µg/mL for kanamycin. The agar was then poured onto plates (12-15 mL for each plate) and left to solidify. The plates were then stored upside down at 4 °C.

2.4.2 Creation of chemically competent cells

A culture of DH5α cells in 20 mL of Luria Broth (LB) was set up using a 50 mL falcon tube without any antibiotic. A separate culture without any bacteria is used as a control. The cultures are left to shake overnight (>250 rpm) at 37°C. If any growth occurred in the control cultures, the process was started over.

5 mL of the overnight culture was added to 200 mL of LB in a sterile 1 L flask without any antibiotics. The flask was incubated with shaking (>250 rpm) at 37°C until the OD600 was 0.3-0.4. When the culture reached the desired density, it was divided into four 50 mL falcon tubes and placed on ice for 15 min. The tubes were spun at 4,000 rpm for 15 min at 4°C and the supernatant was discarded. Each pellet was resuspended in 16 mL of Competent Bacteria Transformation Buffer 1 and left on ice for 15 min. The tubes were centrifuged at 4,000 rpm for 15 min at 4°C and the supernatant was discarded. Each pellet was resuspended in 16 mL of Competent Bacteria Transformation Buffer 2 and combined into a single tube. The solution was then aliquoted into 50 or 100 µL volumes in 1.5 mL Eppendorf tubes which were then immediately placed on dry ice to snap freeze. The bacteria were then moved into a -80°C freezer for storage.

2.4.3 Transformation

A heat-shock transformation was used on chemically competent DH5α cells. Fifty µL of cells were used per transformation. Cells were defrosted on ice for 5-10 min. The required DNA was spun at 2,000 rpm for 1 min and vortexed. One µL of the DNA was added to the bacterial culture which was then vortexed and left on ice for 30 min. The samples were then heat-shocked at 42°C for 90 s and put on ice for 2 min. One mL of LB was then added to the samples near a Bunsen burner. The samples were put on a shaker (185 rpm) at 37°C for 1 h while agar plates were taken out to bring them to room temperature. The cells were then spun down at 3,000 rpm for 5 min and all but approximately 100 µL of supernatant was removed. Near a flame, the cells were resuspended and spread onto either a carbenicillin or

kanamycin plate depending on the vector used. The plates were then incubated upside down in a 37°C incubator overnight.

2.4.4 Plasmid DNA Purification

Plasmid DNA that was obtained during the transformation stage was then 'midi-prepped'. A single bacterial colony was picked from the desired plate and put into 5 mL of LB with the required antibiotic (100 µg/mL for carbenicillin or 50 µg/mL for kanamycin). The culture was shaken (185 rpm) at 37°C until cloudy. 500 µL of this culture was then added to 100 mL LB (with antibiotic) in an autoclaved flask near a flame and left to shake overnight (185 rpm) at 37°C. The flasks were used in the midi-prep protocol from Macherey-Nagel[120]. The process involves a series of steps – resuspension, cell lysis, neutralisation, extraction of plasmid DNA, washes of the columns and elution of the final product. The DNA was dissolved in a Tris-EDTA (TE) buffer provided with the kit and the concentration was determined via the NanoDrop™ 8000 Spectrophotometer. The DNA was run on a 1% agarose gel alongside the original stock to confirm purity.

The **mini-prep** protocol was used when smaller amounts of plasmid were needed. The protocol is similar to the midi-prep, except smaller columns were used[121].

2.4.5 Agarose Gel Electrophoresis

Agarose was added to 1X TAE Buffer and microwaved for 90 s. Gel Red was diluted in the solution at 1/10 and the agarose mixture was poured into a contained and allowed to set. The gel was moved to a tank filled with 1X TAE. 6X gel loading dye was diluted to 1X in DNA

samples, which were then loaded onto the gel. The gel was run at 100 V for 40 min. The gel was scanned using the ChemiDoc Imaging System from Bio-Rad.

2.5 Transfection

Cells were transfected at approximately 80% confluency in 6-well plates using Lipofectamine 3000 according to manufacturer's instructions[122]. 7.5 µL Lipofectamine 3000 was added to 250 µL Opti-MEM medium in one tube, while 5 µg of DNA or 10 nM siRNA were added to 250 µL of Opti-MEM in another tube. 10 µL of the P3000 reagent was added to the tube with the DNA. P3000 reagent was not used for samples that contained siRNA. The mixture contained DNA or siRNA was then mixed with the tube containing Lipofectamine 3000 and incubated at room temperature for 5 min. The mixture was then added dropwise to the plates and the cells were left in the 37°C, 5% (v/v) CO_2 incubator for 48 h.

2.6 Wound-healing Assay

Once the cells had reached 90% confluency, the medium was changed to either DMEM or RPMI without FBS to synchronise the cells overnight. In the morning, a 1 mL pipette tip was used to make three vertical lines and a horizontal line down the middle of each well. The medium was aspirated, and the cells were washed once with 1X PBS to remove any floating cells. Fully supplemented DMEM or RPMI was then added into each well, alongside 0.5 µg/µL mitomycin C to inhibit cell proliferation. Images were taken using a Zeiss Axio Vert.A1 200 microscope (4X objective lens) at the indicated time points. Images were quantified by ImageJ software (ver 1.52a).

Scrambled siRNA: 5'-UUCUCCGAACGUGUCACGUdTdT-3'; eEF2 siRNA: EHU047821 from Sigma Aldrich.

2.7 Transwell® migration and invasion assays

Transwell® inserts from Corning® were used for these assays (CLS3422). For data related to the eEF2K migration study[123], the protocol was followed as written in the paper. Cells were grown until 90% confluent and serum-starved overnight. **Migration assay:** The bottom wells were coated with 10 µg/mL Type I bovine collagen in 300 µL PBS at 37°C for 1 h. After coating, the PBS was gently removed and replaced with serum-free DMEM. **Invasion assay:** 600 µL of DMEM with 20% FBS was added to the bottom well. Matrigel was diluted in serum free medium to a concentration of 0.5 mg/mL and layered over the Transwell insert in a volume of 100 µL. The gel was left to set at 37°C for 1 h. The unset liquid was then carefully removed prior to seeding the cells.

For both assays, $6x10^4$ MDA-MB-231 cells were seeded into the top well in a volume of 100 µL serum-free medium and allowed to settle at room temperature for 1 h. The cells were left to migrate or invade for 24 h. The medium was then aspirated from the bottom and top wells. 3.7% formaldehyde (500 µL were added to the bottom well and left for 15 min. The insert was then washed twice in PBS and the formaldehyde was replaced with 500 µL of 100% methanol. After 20 min, the inserts were washed twice in PBS and the methanol was replaced with 500 µL of DAPI diluted in PBS to a concentration of 5 µg/mL. The cells were left to stain for 15 min before the DAPI was removed. The top of insert was swabbed with a cotton swab to remove any non-migrated or invaded cells. The Transwell was then cut out with a scalpel and put onto a slide. A 30 µL drop of 80% glycerol was added and the slide was

covered with a coverslip. Six representative images were taken of each insert using the 10X magnification lens on the Nikon Eclipse Ni Fluorescent Microscope with the DAPI filter (340-380 nm excitation, 435-485 nm emission). The number of cells in each image was counted using the NIS Elements BR 4.40.00 software.

2.8 Adhesion Assay

Cells were serum-starved overnight once they had reached 90% confluency. 22.1 mm 12-well plates were coated with Type I bovine collagen at a concentration of 10 µg/mL for 1 h at 37°C in 500 µL PBS. Some wells were left without collagen coating. The collagen solution was carefully removed and allowed to air-dry prior to cell seeding. $3x10^5$ MDA-MB-231 cells were seeded per well and allowed to adhere for the indicated time points, trypsinized and resuspended in serum-free medium containing Calcein-AM at a concentration of 1 µg/mL. Each sample was split into three wells of a black-walled 96-well plate (Corning, CLS3603) and the plate was left for 30 min at 37°C with 5% (v/v) CO_2. Representative images were taken using the Zeiss Axio Vert.A1 200 inverted microscope with the 4X objective lens and GFP filter with 470/40 emission and 525/50 excitation. To measure the fluorescence, the GloMax Discover instrument was used with filters set to 475 nm excitation and 500-550 nm emission wavelengths.

2.9 Sodium dodecyl sulfate-polyacrylamide gel electrophoresis (SDS-PAGE)

2.9.1 Bradford Assay

5X Protein Dye Reagent Concentrate was diluted to 1X using Milli-Q water. Protein standards were made using Bovine Serum Albumin diluted in the lysis buffer that the lysates to be tested are in. The standards used were 4, 2, 1, 0.5, 0.25, 0.125, 0.0625 mg/mL. 9 µL of Milli-Q water was added to wells of a 96-well plate, followed by 1 µL of either standard or lysate. A blank using lysis buffer was used. 250 µL of the 1X dye reagent was added to each well and allowed to incubate for 5 min. The absorbance was then measured on the GloMax Discover instrument using 600 nm filter with a 1 min shake function at 300 rpm. Each sample was measured in duplicate and the concentrations of the lysates were then extrapolated from the absorbance values of the standards using Microsoft Excel.

2.9.2 SDS-PAGE gel preparation

Gels were prepared using the Bio-Rad mini-PAGE system using the solutions listed in **Table 2-1**.

	12.5%		**16%**	
Solution (mL)	**Running gel**	**Stacking gel**	**Running gel**	**Stacking gel**
40% acrylamide	5.3	0.75	6	0.93
2% bis-acrylamide	1.7	0.4	3.2	0.49
1.5M Tris-HCl pH 8.8	4.25	-	3.75	-
1.5M Tris-HCl pH 6.8	-	0.75	-	0.94
Milli-Q Water	5.6	4	1.825	5.03
20% SDS	0.085	0.03	0.1125	0.037
10% APS	0.085	0.03	0.1275	0.0563
TEMED	0.017	0.006	0.017	0.0075

Table 2.1: Solutions used to prepare SDS-PAGE gels. TEMED: N,N,N′,N′-Tetramethyl ethylenediamine; APS: ammonium persulfate.

2.9.3 SDS-PAGE gel running

One portion of 5X sample buffer was added to 4 portions of cell lysates. The lysates were then boiled for 5 min at 100 °C. The samples were then spun at 15,000 x *g* for 30 s. SDS-PAGE gels were secured in a Bio-Rad running tank filled with Running Buffer. 30-40 µg of

samples were loaded onto the SDS-PAGE gels alongside the Precision Plus Protein Dual Color Standard ladder. The gels were run at 100 V until the samples passed through the stacking gel and into the running gel. The voltage was then changed to 180 V for another 40-60 min. The gels were stopped just after the migration front ran off the gel or in the case of high bisacrylamide gels for LC 3 II, just prior to the migration front running off the gel.

2.9.4 Western blotting

Western blot "sandwiches" were made in a tray filled with Transfer Buffer using 4 pieces of 3mm Whatman paper with 2 on each side of the gel. Nitrocellulose membranes were put next to the gel and the sandwich was closed with sponges and a clasp. Air bubbles were removed using a roller as each part of the sandwich was put into place. They were then put into a Bio-Rad wet tank transfer system and run for 100 V for 1 h on ice. Following transfer, the membranes were rinsed in RO water and blocked for 30 min in 5% (w/v) skim milk in 1X PBS. The membranes were then again rinsed in RO water and washed three times for 5 min in 1X PBST. After the final wash, the membranes were put into falcon tubes containing primary antibodies that were diluted in 5% (w/v) BSA in PBST. The tubes were rolled overnight at 4 °C. After primary antibody incubation, the membranes were rinsed in RO water and washed three times for 5 min in PBST. Following this, the membranes were put into LI-COR black boxes containing secondary antibody diluted 1/20,000 in PBST. The membranes were left to incubate for 1 h at room temperature on a shaker, following which they were rinsed in RO water and washed three times for 5 min with PBST. The membranes were then scanned on the LI-COR Biosciences Odyssey imaging system using the 700 and 800 nm wavelength channels. Table **2-2** lists the primary and secondary antibodies used.

Antibody	Company	Catalogue No.	Dilution
β-Actin	CST	A2228	1/5000
ACC	CST	3662	1/1000
eEF2	CST	2332	1/1000
eEF2K	CST	3692	1/1000
eIF2α		9722	1/1000
FLIP	CST	8510	1/1000
IRS1	Millipore	06-148	1/1000
LC3 A/B	CST	12741	1/1000
MCL1	CST	5453	1/1000
Nrf2	CST	12721	1/1000
P62	CST	5114	1/1000
P-ACC Ser79	CST	3661	1/1000
PD-L1	CST	13684T	1/1000
PD-L1 (extracellular domain specific) – Flow Cytometry	CST	86744S	1/1000
P-eEF2 Thr56	Eurogentec	Customised	1/1000 with 1/1000 de-phosphopeptide
P-eIF2α Ser51	CST	3398	1/1000
PKB	CST	4685	1/1000
P-PKB-S473	CST	9271	1/1000
P-rpS6 (Ser 240/244)	CST	4858	1/1000
rpS6	Santa Cruz	Sc-74459	1/1000
Goat anti-rabbit IgG (H +L) Secondary Antibody, DyLight 680	Invitrogen	35568	1/20,000
Goat anti-rabbit IgG (H+L) Secondary Antibody, DyLight 800 4X PEG	Invitrogen	SA5-35571	1/20,000
Rabbit anti-sheep IgG (H+L) Secondary Antibody, DyLight 680	Thermo Fischer	SA5-10058	1/20,000
Goat anti-mouse IgG (H+L) Secondary Antibody, DyLight 680	Invitrogen	35518	1/20,000
Goat anti-mouse IgG (H+L) Secondary Antibody, DyLight 800 4X PEG	Invitrogen	SA5-35521	1/20,000

Table 2.2: List of antibodies and their dilutions that were used in this study. CST – Cell Signaling Technologies. P-: phosphorylated

2.10 Flow Cytometry

2.10.1 Cell Cycle (Propidium Iodide Staining)

Once cells had reached 90% confluency, they were serum-starved overnight to synchronise them. The medium was changed to fully supplemented medium, and the cells were left to proliferate for 8 h. At this time, the cells were washed once with PBS and trypsinized. After detachment, the cells were gathered into 15 mL tubes and spun at 300 x *g* at 4°C for 5 min. The supernatant was removed, and the cells were gently resuspended in 100 µL PBS. 0.9 mL ice-cold methanol was then added dropwise to each sample. The samples were incubated for 30 min at -20°C. The samples were then moved to FACS tubes and spun down at 300 x G for 5 min. The methanol was removed, and the cells were then resuspended in 0.5 mL of PBS/Propidium Iodide (PI)/RNAse mix (4 µg/mL PI, 20 µg/mL RNAse). The signal intensity was then measured using the BD FACS CantoTM II system, gating for single, stained cells and analysed for cell cycle.

2.10.2 Extracellular PD-L1 staining

Following treatment, cells were washed with PBS, trypsinized, transferred to 15 mL tubes and spun at 300 x *g* at 4°C. The supernatant was removed, and the samples were incubated with the extracellular PD-L1 antibody diluted 1/100 in 100 µL of Flow Cytometry staining buffer for 30 min on ice. Cells were washed three times with PBS and incubated in 100 µL of the staining buffer containing Alexa Fluor-conjugated rabbit secondary antibody diluted 1/200 for 30 min on ice. The cells were washed three times with PBS and the intensity of

the signal was measured using the BD FACS CantoTM II system, gating for single, stained cells.

2.11 RNA isolation using Trizol

After treatment in a 6-well plate, the medium was aspirated, and the cells were washed once with PBS. After the PBS was removed, 1 mL of Trizol reagent was added to each well and the cells were left to lyse at room temperature for 5 min. The mixture was then transferred to 1.5 mL Eppendorf tubes and 0.2 mL chloroform was added. The tubes were shaken vigorously by hand for 15 s and incubated at room temperature for 2-3 min. The samples were then centrifuged at 12,000 x *g* for 15 min at 4°C. The colourless aqueous upper phase was transferred to a new tube and 0.5 mL isopropanol was added. The tubes were inverted to mix evenly and incubated at room temperature for 10 min prior to centrifugation at 12,000 x *g* for 10 min at 4°C. The supernatant was discarded, and the samples were washed with 1 mL 75% ethanol. The sample was vortexed and centrifuged at 12,000 x *g* for 5 min at 4°C. The ethanol was carefully removed from the tubes and the RNA pellet was left to air-dry for 15-30 min. The pellet was then resuspended in 20 µL RNAse-free water and the concentration was determined via the NanoDrop^{TM} 8000 Spectrophotometer.

2.12 RT-qPCR

The reverse transcription reaction to create cDNA was done using the QuantiNova Reverse Transcription kit according to manufacturer's instructions[124]. One µg RNA and water reactions were assembled on ice to a final volume of 13 µL. Two µL of gDNA removal mix

was then added per reaction, the tubes were briefly centrifuged and placed in a thermocycler for 2 min at 45°C and brought down to 4°C. 5 µL of the Reverse Transcription 'mastermix' was then added to each tube (4 µL RT mix, 1 µL RT). The tubes were briefly centrifuged and put into a thermocycle with the following program – 3 min at 25°C, 5 min at 85°C, hold at 4°C. The reverse transcription reactions were then diluted with 180 µL Milli-Q water.

For the qPCR reaction, the Fast SYBR Green Master Mix protocol was followed[125]. Each qPCR reaction contained 2 µL of the diluted cDNA, 8 µL nuclease-free water, 0.8 µL of 5 µM forward, 0.8 µL of 5 µM reverse primers and 8.4 µL Fast SYBR Green Master Mix. The reactions were put into MicroAmp Fast Optical 96-well Reaction Plates (Thermo Fisher) and run using the StepOne Plus Real-Time PCR system from Applied Biosciences using the settings stated in **Table 2-3** using Fast Mode. ROX was used as the Passive Reference.

Step	**Temperature (°C)**	**Duration (s)**	**Cycles**
AmpliTaq Fast DNA Polymerase, UP activation	95	20	HOLD
Denature	95	3	40
Anneal/Extend	60	30	

Table 2.3: Settings used on the StepOne Plus Real-Time PCR system to run the RT-qPCR reaction.

The relative expression of the gene of interest was then calculate in Microsoft Excel using the ΔΔ Ct method.

qPCR was performed for PD-L1 with the following human primers, normalised to β-actin:

PD-L1 forward: 5'-TGGCATTTGCTGAACGCATTT-3'

PD-L1 reverse: 5'-TGCAGCCAGGTCTAATTGTTTT-3'

ACTB Forward: 5'-CATGTACGTTGCTATCCAGGC-3'

ACTB Reverse: 5'-CTCCTTAATGTCACGCACGAT-3'.

2.13 96-well Plate Assays

2.13.1 Glucose Uptake-Glo™ Assay

The assay was done according to the manufacturer's protocol[126]. MDA-MB-231, A549 and PC3 cells were seeded at densities of $2.5x10^4$, $2x10^4$ and $3x10^4$ cells per well respectively in an opaque white-walled 96-well plate (Corning, CLS3610). After overnight growth, the medium was changed to 100 µL per well of serum-free medium. After 24 h, the medium was changed to 100 µL of medium supplemented with FBS and containing 100 nM insulin. The cells were incubated for 1 h at 37°C in 5% (v/v) CO_2. The medium was removed and replaced with 50 µL of 1X PBS containing 1 mM 2-DG. The plate was left to incubate at room temperature for 10 min. 25 µL of Stop Buffer was then added to each well and the plate was briefly shaken. This was followed by the addition of 25 µL of neutralization buffer. The plate was briefly shaken and 100 µL of 2DG6P reagent provided by the kit was added into each well. The plate was shaken briefly and then left to incubate at room temperature for 1 h. The luminescence was recorded on the GloMax Discover instrument with a 0.3 s integration time.

2.13.2 Dual-Glo® Luciferase Assay

The assay was conducted according to manufacturer's instructions, as stated in the study the data was used in[127, 128]. Transfected MDA-MB-231 cells were seeded into 96-well white-walled opaque plates at $2.5x10^4$ cells per well in 75 µL medium. After growth overnight, 75 µL of Dual-Glo Luciferase Reagent is added to each well, mixed and left to incubate for 10 min at room temperature. Firefly luminescence was then measured using the GloMax Discover instrument with 0.3 s integration time. Dual-Glo Stop & Glo Reagent (75 µL) was added to each well, mixed and left to incubate for 10 min at room temperature. Renilla luminescence was then measured using the GloMax Discover instrument with 0.3 s integration time. The luminescence was then normalised by dividing the Firefly fluorescence values by the Renilla fluorescence values.

2.13.3 BrdU Cell Proliferation Assay

The assay was performed according to manufacturer's instructions[129]. Once cells reached 90% confluency, they were serum starved overnight and seeded into clear 96-well plates at seeding densities of $2.5x10^4$ and $2x10^4$ cells per well in 100 µL of medium for MDA-MB-231 and A549 cells respectively. 10 µL of 10X BrdU solution was added to each well and the plates were incubated at 37°C in 5% (v/v) CO_2 for 24 h. After incubation, the medium was removed and 100 µL of fixing/denaturing solution was added to each well. The plate was incubated at room temperature for 30 min and the solution was replaced with 100 µL of 1X detection antibody solution. The plate was incubated at room temperature for 1 h and the solution was removed. Each well was washed three times with 1X Wash Buffer. 1X HRP-

conjugated secondary antibody solution (100 µL) was added to each well and incubated for 30 min at room temperature. The solution was removed and each well was washed three times with 1X Wash Buffer. 100 µL of TMB substrate was added to each well and incubated until a color change was seen. At this point, 100 µL of STOP solution was added to each well and the absorbance was read at 450 nm using the GloMax Discover instrument.

2.13.4 CellTox® Green Cytotoxicity Assay

The assay was carried out according to manufacturer's instructions[130] following the Express, No-step addition at dosing method. MDA-MB-231, A549 and PC3 cells were seeded at a density of $3x10^4$, $2x10^4$ and $3.5x10^4$ cells per well respectively in 200 µL of medium inside 96-well black opaque walled plates and left to grow overnight at 37°C in 5% CO_2. Once the cells had reached 90% confluence, the medium was changed to 100 µL of the treatment medium with CellTox Green reagent at a ratio of 10 µL reagent per each 5 mL of medium. The plates were then placed back into the incubator until the indicated time points when the signal intensity was measured by the GloMax Discover instrument at 475 nm excitation and 500-550 nm emission wavelengths. For the Lysis Solution control, 1 µL of Lysis Solution provided in the kit was added to each control well and the plate was put into a 37°C, 5% CO_2 incubator for 30 min prior to fluorescence measurement. Images were taken using the Zeiss Axio Vert.A1 200 inverted microscope with the 4X objective lens and GFP filter with 470/40 nm emission and 525/50 nm excitation.

2.13.5 Propidium Iodide/Calcein-AM assay

The cells were treated in the same way as for the CellTox Green assay. Propidium iodide and Calcein-AM were added to each well 1 h prior to measuring at final concentrations of 10 µM and 1 µM, respectively. The propidium iodide signal was measured at 520 nm excitation and 580-640 nm emission wavelengths using the GloMax Discover instrument. The Calcein-AM signal was measured at 475 nm excitation and 500-500 nm emission wavelengths. Images were taken using the Zeiss Axio Vert.A1 200 inverted microscope with the 4X objective lens and GFP filter with 470/40 nm emission and 525/50 nm excitation.

2.13.6 RealTime-Glo™ MT Cell Viability Assay

The cells were treated in the same way as the CellTox Green assay and the assay was done according to manufacturer's instructions[131] using the continuous-read method at dosing. White opaque-walled plates were used. The MT Cell Viability Substrate and NanoLuc® Enzyme were mixed and added to each well to a final concentration of 1X. Luminescence was read on the GloMax Discover instrument with 0.3 s integration time.

2.13.7 Caspase-Glo® 3/7, Caspase-Glo® 8 and CellTiter-Glo® 2.0 Assays

The cells were treated in the same way as the CellTox Green assay but in white opaque walled plates. The assay was done according to manufacturer's instructions[132-134]. Once the treatments were complete, the plate was allowed to equilibrate to room temperature and 100 µL of either Caspase-Glo 3/7 Reagent, Caspase-Glo 8 Reagent or Cell-Titre Glo 2.0 Reagent was added to each well. The plate was shaken at 300 rpm for 30 s and incubated at room

temperature for 30 min for the caspase assays. The plate was incubated for 10 min at room temperature for the Cell-Titre Glo assay. The luminescence was measured using the GloMax Discover instrument with 0.3 s integration.

2.13.8 Magic Red™ Cathepsin L Assay

The cells were seeded in the same way as the CellTox Green assay and treated with inhibitor in 280 µL of fully supplemented medium in black opaque walled 96-well plates. The manufacturer's instructions were followed to complete the assay[135]. Once the treatment was complete, the 15X diluted Magic Red staining solution was added to each well at 20 µL per well. Hoechst 33342 provided with the kit was also added to a final concentration of 200 µM. The cells were incubated for 1 h at 37°C in 5% (v/v) CO_2 protected from light. The plate was read using the GloMax Discover instrument at 627 nm excitation and 580-640 nm emission for Magic-Red and 365 nm excitation and 415-445 nm emission for Hoechst. The magic red values were normalised to the Hoechst values.

2.13.9 LysoTracker™ Red Assay

The MDA-MB-231 resistant and non-resistant cells were seeded into 96-well black opaque walled plates at a density of $3x10^4$ cells per well. Once the cells had reached 90% confluency, the medium was changed to 100 µL of DMEM lacking glucose and pyruvate with 125 nM Bafilomycin A (BafA) for 1 h. At this point, LysoTracker Red[136] reagent was added to a final concentration of 156 nM alongside Hoechst 33342 to a final concentration of 200 µM. After 1 h incubation period, the LysoTracker Red signal was measured using the GloMax

Discover at 520 nm excitation and 580-640 nm emission. The Hoechst signal was measured at 365 nm excitation and 415-445 nm emission. The LysoTracker signal was normalised to the Hoechst signal.

2.14 Generation of KO cells using CRISPR

2.14.1 CRISPR-Cas9 vector cloning

Annealing and phosphorylating oligonucleotides: The following sgRNA was used to create eEF2K-KO cells: 5'-AGTGAGCGGTATAGCTCCAG-3'. The top strand oligo contained a **GTTTT** 3' overhang, while the bottom strand contained **CGGTG** 3' overhang.

The sgRNA forward and reverse oligonucleotides were resuspended from a pellet to 200 µM and were assembled in a round-topped PCR tubes as follows: 1 µL top strand oligo, 1 µL bottom strand oligo, 1 µL 10X T4 DNA Ligation Buffer, 1 µL T4 PNK, 6 µL Milli-Q water. The tubes were then put into a thermocycler with the following program: 37°C for 30 min; 95°C for 5 min; ramp down to 25°C at 5°C per min. The annealed oligos were diluted 1/200 to acquire a concentration of 0.1 pmol/µL.

Linearisation of vector: The CRISPR/Cas9 vector[137] was linearised with *Bae*I restriction enzyme. A digestion reaction was set-up in a PCR tube as follows: 6 µg of CRISPR/Cas9 vector, 10 µL 10X CutSmart Buffer, 5 µL *Bae*I, to 40 µM final concentration of SAM and topped-up to 100 µL with Milli-Q water. The solution was mixed and briefly centrifuged. The linearisation reaction was left overnight at 25°C in a thermocycler.

6X Purple loading dye was then added to the reaction to make it 1X and the entire volume of the reaction was loaded across multiple wells on a 1% agarose gel. The gel was run at 100

V for 30 min. The vector fragments were viewed under UV light and excised using a sterile scalpel.

Gel Extraction: The DNA was extracted from the gel following the manufacturer's protocol (GeneJET Gel Extraction Kit)[138]. The gels fragments were put into 1.5 mL Eppendorf tubes and weighed. A 1:1 ratio of binding buffer to gel weight was added to the tubes, e.g. for every 100 mg gel, 100 µL of binding buffer was added. The mixture was incubated at 60°C until the gel slice was dissolved. The tubes were inverted every few minutes to speed the process. The mixture was vortexed and loaded onto the column. If the colour of the column was not yellow but orange or violet, 10 µL of 3 M sodium acetate, pH 5.2 was added and mixed to make the pH optimal for extraction. The column was centrifuged for 1 min at 12,000 x *g* and the flow-through was discarded. 100 µL of Binding buffer was added to the column, which was centrifuged 1 min at 12,000 x G. The flow-through was discarded and 700 µL of Wash Buffer was added to the column. The column was centrifuged for 1 min at 12,000 x *g*, the flow-through was removed and the column was centrifuged again to remove residual buffer. The column was transferred to a clean tube and 50 µL of elution buffer were added. The column was centrifuged for 1 min at 12,000 x *g* and the eluted DNA was then quantified via the NanoDrop™ 8000 Spectrophotometer.

Ligation: The ligation reaction was setup as follows: 100 ng CRISPR-Cas9 vector, 2 µL diluted primers, 1 µL 10X T4 Ligase Buffer, 1 µL T4 DNA Ligase, made up to 10 µL with Milli-Q water. A negative control reaction was set-up without the oligos. The reaction was incubated at 16°C overnight in a thermocycler. Five µL of the ligation reaction was then used to transform DH5α cells which were incubated overnight at 37°C. After a successful ligation reaction, more growth was observed on the plates containing cells with the oligos

inserted into the vector compared to negative control. Multiple single colonies were picked from the plates and put into a tube containing 5 mL LB with 100 µg/mL carbenicillin and left to incubate on a shaker (200 rpm) at 37°C overnight. The plasmids were then isolated following the **mini-prep protocol**.

Diagnostic Digests: To screen for successful ligation of the oligos to the vector, *Bae*I-*Eco*RI-HF sequential digests were performed. The reactions were set-up in Eppendorf tubes as follows: 500 ng of DNA isolated from colonies made up to 11.12 µL with Milli-Q water. The Cas9 CRISPR vector was also digested as a control. The following master-mix (3.88 µL) was added to each reaction: 0.5 µL *Bae*I, 1.88 µL 320 µM SAM, 1.5 µL 10X Cutsmart Buffer. The reactions were incubated at 25°C for 15 min. 0.5 µL of *Eco*RI-HF was then added to each tube and incubated further at 37°C for 15 min. An *Eco*RI-HF only reaction was set up as a control to cut the Cas9 CRISPR vector. Five µL of 6X Loading Dye was then added to each reaction and they were loaded onto a 1% agarose gel with GelRed. The gel was run at 100 V for 40 min. The gel was imaged using the ChemiDoc Imaging System from Bio-Rad.

Confirmatory Sequencing: The successfully ligated samples were then sequenced using the forward pCP01 gRNA sequencing primer as follows: 700 ng DNA, 1 µL of 10 µM primer and made up to 12 µL with Milli-Q water.

pCP01 gRNA sequencing primer: 5'-GCATATACGATACAAGGCTGTTAG-3'

2.14.2 Nucleofection

The manufacturer's instructions were followed for nucleofection of MDA-MB-231[139] and PC3[140] cells. Cells were cultured in dishes until 80% confluence, washed with 1X PBS and trypsinized. $3x10^5$ and $4x10^5$ PC3 and MDA-MB-231 cells were seeded into cuvettes in 100 µL of Nucleofector solution which contained Supplement that was provided with the kit at a ratio of 4.5:1. SE Nucleofector solution was used for MDA-MB-231 cells while SF Nucleofector solution was used for PC3 cells. 2 µg of CRISPR-Cas9 plasmid was added to each reaction, with CRISRP-Cas9-eGFP plasmid serving as a control for transfection efficiency. The cuvettes were then placed into the Lonza 4D-Nucleofector and the following programs were used: CH-125 for MDA-MB-231 cells and DS-137 for PC3 cells. 500 µL of pre-warmed medium was then added to resuspend the cells and they were added to 1.5 mL of medium in a 6-well plate. 24 h after nucleofection, the eGFP controls were checked for the efficiency of the process using a fluorescence microscope. The cells were then used in the CD4 positive isolation protocol.

2.14.3 Enrichment of CD4 expressing cells using Dynabeads

The CD4 expressing cells were then isolated following the manufacturer's instructions using the Dynabeads CD4 Positive Isolation Kit[141]. The vial of Dynabeads was resuspended and 25 µL of beads per sample was added to an Eppendorf tube. The tube was put on a Dynal magnetic separator for 1 min after which the supernatant was removed. The beads were resuspended in 100 µL of Buffer I and placed back on the magnetic separator for 1 min. The supernatant was decanted, and the beads were resuspended in 100 µL of Buffer I.

Cells were washed with PBS and trypsinized with TrypLE. The cells were centrifuged at 400 x *g* for 5 min and the supernatant was removed. The cells were washed 2X with 2mL of Buffer I and then resuspended in 900 µL of it. The cells were then added to the tubes containing Dynabeads and put on a rotator at 4°C for 30 min. The tubes were then put on a magnetic separator for 1 min and the supernatant was removed using a pipette. The cells and beads were resuspended in 500 µL of Buffer I and incubated on a rotator for 2 min at room temperature. The tubes were then put on a magnetic separator for 1 min and the supernatant was removed with a pipette. The cells were again resuspended in 500 µL of Buffer I and left on the rotator for 2 min. These wash steps were done a total of **six times**. After the final wash, the cells were resuspended in 100 µL of Buffer II. Ten µL of DETACHaBEAD CD4 was added and the tubes were incubated for 45 min on a rotator at room temperature. The tubes were placed on a magnetic separator for 1 min and the supernatant was transferred to a new tube. The beads were resuspended in 500 µL of Buffer II and placed on a magnetic separator for 1 min. The supernatant was transferred to the same new tube. These washes were done another **three** times to obtain the maximum yield of CD4 positive cells. The tube containing the cells was then filled up to a final volume of 4 mL with Buffer II and centrifuged at 400 x G for 6 min. The enriched cells were resuspended in 500 µL of either DMEM for MDA-MB-231 cells or RPMI for PC3 cells and counted on a haemocytometer. The cells were then seeded in clear 96-well plates at 1, 2 and 3 cells/well. The plates were placed in a 37°C humidified 5% CO_2 (v/v) incubator and allowed to grow.

2.14.4 DNA Extraction with QuickExtract™ Solution

Colonies that formed from single cells were then used for the DNA extraction step. Once the cells were confluent, they were trypsinized and transferred to 24-well plates and allowed to reach 80% confluency prior to DNA extraction. The DNA was extracted according to manufacturer's protocol[142]. The cells were washed, trypsinized and put into sterile Eppendorf tubes. 50 µl of the QuickExtract solution was added to each sample and vortexed for 15 sec. The tubes were the transferred to a heat block set at 65 °C for 6 min. The solution was vortexed for 15 sec and incubated at 98 °C for 2 min. The genomic DNA was then used for PCR.

2.14.5 Polymerase Chain Reaction (PCR)

The reactions were set up on ice as follows: 2 µL genomic DNA, 2 µL of 10 µM forward primer, 2 µL of 10 µM reverse primer, 25 µL of One*Taq* HotStart Master Mix and 19 µL of Milli-Q water. The tubes were put into a thermocycler with the following program: initial denaturation at 94°C for 2 min, followed by 35 cycles of 94°C for 30 s, 56°C for 30 s, 68°C for 45 s. The final extension was at 68°C for 5 min, and the samples were then brought down to 4 °C. Five µL of the reactions were then run on a 1% agarose gel to confirm the correct products were amplified.

2.14.6 Solid Phase Reverse Immobilisation Clean-up

The reactions were then purified using AxyPrep beads. The beads were fully resuspended and 81 µL was added to a tube. The 45 µL PCR reaction was added to the tube and mixed.

The solution was left to stand at room temperature for 5 min and placed into Dynal magnetic racks for 2 min. The supernatant was carefully removed from the tubes while they are in the racks and 500 µL of freshly diluted 70% ethanol was added. The beads were left to collect at the back of the tube and the supernatant was remove with a pipette. Another 500 µL of 70% ethanol was added to the tubes and the beads were left to collect at the back of the tube. As much as possible of the liquid was removed and any remaining liquid was left to evaporate while the tubes remained in the rack. The tubes were then taken out of the rack and the beads were resuspended in 20 µL of 5 mM Tris-HCl pH 8. The tubes were left to stand for 2 min and placed back onto the magnetic racks. The elution buffer was then collected into a fresh tube and the NanoDrop^{TM} 8000 Spectrophotometer was used to determine the concentration.

2.14.7 Restriction Endonuclease Digestion to check for positive clones

The purified DNA was then digested with *Bpm*I to confirm clones that have eEF2K knocked out. The following 10 µL reaction was set up: 200 ng purified DNA, 1 µL 10X NEBuffer 3.1, 0.5 µL *Bpm*I, topped up with Milli-Q water. The reaction was incubated at 37°C for 2 h. DNA of WT cells was also digested as a control. 1.7 µL of 6X Loading Buffer was added to the reactions and they were run on a 2% agarose gel at 100V for 40 min. The gels were imaged on the ChemiDoc Imaging System from Bio-Rad. The samples were then sequenced as previously described in **2.12.1** with the following screening primers:

Forward: 5'-TTAAAATGTGCCTGGGTGCTGC-3'

Reverse: 5'- TGTTGAGGCATCACACAGGACC-3'

2.15 Isobaric tag for relative and absolute quantitation (iTRAQ)

2.15.1 Sample preparation

When cells had reached 80% confluency, the medium was changed to low glucose DMEM (5.55 mM D-glucose) for 1 h. The cells were then treated with 1 mM 2-deoxyglucose (2-DG) for 1 h prior to washing the cells with PBS, trypsinizing and spinning at 400 x *g* for 5 min. The pellets were resuspended in cold PBS and washed three more times. The liquid was removed, and the pellets were snap-frozen on dry ice.

2.15.2 Mass-spectrometry analysis

The samples were analysed by Dr. Antigoni Manousopoulou from Professor Spiros D. Garbis' group (then at the University of Southampton, UK; now Caltech, Pasadena, CA, USA). The iTRAQ protocol followed was used in the study by Dr Bashar Zaidan and Dr Antigoni Manousopoulou[143]. Phospho-proteomics analysis and total protein levels were analysed.

2.16 Generation of Bafilomycin-A Resistant MDA-MB-231 cells

When cells had reached 80% confluency, the medium was changed to DMEM without glucose and pyruvate and the cells were treated with 125 nM BafA for 48 h. After treatment, the medium was aspirated, and the cells were washed with 1X PBS three times to remove any dead cells. The medium was changed back to fully supplemented DMEM with 10% FBS and the cells were left to recover. Once the cells had reached 80% confluency, they were

treated in DMEM without glucose and with BafA. This was repeated until a significant resistance to these conditions was observed. The degree of resistance was quantified using the CellTox Green Cytotoxicity Assay under the same conditions, data being normalised to total protein content.

2.17 Dr. Sushma Rao's Proteomics Protocol

2.17.1 Label-free proteomics and phosphoproteomic analysis

The cells were grown to 90% confluency in T175 flasks and treated for 24 h with 125 nM BafA under conditions with no glucose and pyruvate. The cells were then trypsinized, washed three times in 1X cold PBS and snap frozen on dry ice once all liquid was removed from the pellet. **Please note** that the following protocol is taken directly from the unpublished manuscript attached to the **appendix** of this thesis.

Frozen MDA-MB-231 cell pellets (4 replicates of WT, eEF2K-KO #1, eEF2K-KO #2) with and without BafA, were dissolved in chilled SDC buffer (4% sodium deoxycholate in 0.1 M triethylammonium bicarbonate (TEAB) and lysed using the Precellys®tube homogenise. The cell supernatants were heat-treated for 5 min at 95°C and further lysed using a sonicator probe at 4°C (three 30 s cycles of 1 s on/off at 880% output). The protein concentration was determined using the Nanodrop (Thermo). Equal protein amounts from each sample were used for protein digestions and phosphopeptide enrichment that was performed as according to the Easy-Phos protocol [144] with a slight modification. Phosphopeptide enrichment was performed on WT, eEF2K-KO #1 and eEF2K-KO #2 cell pellets. Following protein

digestion, an equal amount of all the samples were set aside for proteomic profiling experiments. All samples (profiling, phosphopeptide fraction and non-phosphopeptide fractions) were then de-salted using POROS R3 resin (Thermo Scientific), dried, re-suspended in 0.1% (v/v) formic acid and analysed by mass-spectrometry.

2.17.2 LC-MS/MS and data acquisition

The peptide samples were separated by nano-liquid chromatography (nLC) using the NanoElute nLC system (Bruker Daltonics, Germany) coupled online to the trapped-ion mobility spectrometry Time-of-Flight (timsTOF) *Pro* mass spectrometer (Bruker Daltonics, Germany) using the Data Dependent Acquisition- Parallel Accumulation Serial Fragmentation (DDA PASEF) mode. Reverse-phase chromatography was done using a 25 cm, 75 µm ID Odyssey C18 nano column (IonOpticks, Australia) with an integrated emitter. The peptides were eluted using a 120 min gradient from 0% to 35% buffer B (acetonitrile in 0.1% formic acid) at a rate of 400 nL/min. Buffer A consisted of 0.1% (v/v) formic acid.

2.17.3 Data processing and analysis

The raw data files from each sample generated on the timsTOF Pro mass spectrometer was processed using the software package MaxQuant version 1.6.14 (Max Planck Institute of Biochemistry, Martinsried, Germany; [145]). The data was searched against the UniProt reference proteome for *Homo sapiens* with the following parameters: variable modifications - deamidation (N/Q), oxidation (M); fixed modification – methylthio (C); enzyme – trypsin; missed cleavages – 2; all other parameters were default settings. Only proteins with a false discovery rate (FDR) of ≤ 1% were reported. For phosphopeptide analysis all settings were

set to default except of the peptide spectrum match (PSM) was set to FDR 0.05. Samples set aside for profiling experiment was used for protein abundance analysis. Phosphopeptide analysis was performed using data obtained from the phosphopeptide fraction following enrichment. Data analysis was done using the software Perseus [146]. Briefly, raw data were cleaned to remove reverse hits and contaminants, transformed to log_2 and multi-sample ANOVA performed to identify statistically significant proteins. The post-hoc Tukey's test was used to identify significant pairs (FDR < 0.01) and the proteins were further classified into relevant GO Biological process groups for data interpretation.

2.18 Seahorse Assays

2.18.1 8-well Seahorse Assays

8-well Seahorse XFp sensor cartridges (SEA103022-100) were prepared following manufacturer's instructions[147]. Seahorse Calibrant was put into a tube and left to incubate in a non-CO_2 37°C incubator overnight. At the same time, each well of the utility plate for the sensor cartridges was filled with 200 µL sterile water. Each moat section was filled with 400 µL of sterile water and the cartridges were gently lowered into the wells, ensuring no bubbles were created. The plates were placed in a non-CO_2 37°C incubator overnight. On the same day, MDA-MB-231 cells were seeded into XFp cell culture miniplates at a density of $2.5x10^4$ cells per well in 80 µL of DMEM, following manufacturer's instructions[148]. The two outer wells were filled with 80 µL of DMEM to be used as background controls. The moat sections were filled with 400 µL of sterile PBS. The plates were left for 1 h inside the cell culture hood to attach prior to being put into a 37°C humidified 5% CO_2 (v/v) incubator.

On the day of the assay, the sensor cartridge was taken out of the incubator and the water was discarded. Each well of the utility plate was filled with 200 µL of XF Calibrant while the moats were filled with 400 µL of calibrant. The sensor cartridge was lowered into the wells and the plate was put into a non-CO_2 37°C incubator for 1 h prior to the loading of the drug ports.

The medium was prepared on the day of the assay according to manufacturer's instructions[149]. The medium was warmed in a 37°C water bath and supplemented with 10 mM D-Glucose, 1 mM sodium pyruvate and 2 mM L-glutamine. In the case of the **Glycolysis Stress Test**, the medium was supplemented only with 2 mM L-glutamine. The pH was brought to 7.4 using 0.1 M NaOH. The medium was then sterilised using 0.1 µm filters and warmed to 37°C again.

Prior to the assay, all but 20 µL of medium was removed from the cells and 180 µL of assay medium was added to each well. This was repeated twice, with the final volume of each well ending up being 180 µL of assay medium.

XFp Cell Energy Phenotype Test: The test was performed according to manufacturer's instructions[150]. Oligomycin and FCCP powders were resuspended with XF medium to a final concentration of 50 µM and following manufacturer's instructions, a mixture of FCCP and oligomycin was added to Port A on the calibrant plate to make up a final concentration of 1 µM FCCP and 1 µM oligomycin in each well. The cartridge was then placed on top of the cell culture plate and moved into the XF HS Mini Analyzer. The XFp Cell Energy Phenotype program was chosen and the ECAR and OCR was measured by the instrument. The values

were normalised to total protein content of each well, measured via Bradford Assay (**2.7.1**) after the cells were lysed in 20 µL of Triton Lysis Buffer.

XFp Glycolysis Stress Test: The test was performed according to manufacturer's instructions[151]. The solids were resuspended with XF medium to a final concentration of 100 mM D-glucose, 50 µM oligomycin, 500 mM 2-DG. The constant compound approach was used to load the compounds into the ports. The final concentrations per well were 10 mM D-glucose in Port A, 1 µM oligomycin in Port B, and 50 mM 2-DG in Port C. The cartridge was then placed on top of the cell culture plate and moved into the XF HS Mini Analyzer. The XFp Glycolysis Stress Test program was chosen and the ECAR (extracellular acidification rate) and OCR (oxygen consumption rate) was measured by the instrument. The values were normalised to total protein content of each well, measured via Bradford Assay (**2.7.**1) after the cells were lysed in 20 µL of Triton Lysis Buffer.

XFp Cell Mito Stress Test: The test was performed according to manufacturer's instructions[152]. The solids were resuspended with XF medium to a final concentration of 45 µM oligomycin, 50 µM FCCP, and 25 µM rotenone/antimycin A mix. The constant compound approach was used to load the compounds into the ports. The final concentrations per well were 1.5 µM oligomycin in Port A, 1 µM FCCP in Port B, and 0.5 µM rotenone/antimycin A mix in Port C. The cartridge was then placed on top of the cell culture plate and moved into the XF HS Mini Analyzer. The XFp Cell Mito Stress Test program was chosen and the ECAR and OCR were measured by the instrument. The values were

normalised to total protein content of each well, measured via Bradford assay (**2.7.**1) after the cells were lysed in 20 µL of Triton Lysis Buffer.

2.18.2 96-well Seahorse Assays

96-well Seahorse XF sensor cartridges (SEA103729100) were prepared following manufacturer's instructions[153]. The protocol for the hydration of cartridges and cell seeding is the same as in the 8-well plate format[154]. $2.5x10^4$ MDA-MB-231 cells were seeded per well of the cell culture plate in 80 µL of DMEM. The cells were washed in the same ways as the 8-well format following manufacturer's protocol 1 h prior to the beginning of the assay[155]. The medium used in these experiments contained HEPES and did not requiring pH adjustment. The medium for the **Cell Mito Stress Test** was supplemented with 10 mM D-glucose, 2 mM L-glutamine and 1 mM sodium pyruvate. The medium for the **Glycolysis Stress Test** was supplemented only with 2 mM L-glutamine.

XF Glycolysis Stress Test: The test was performed according to manufacturer's instructions[156]. The solids were resuspended with XF medium to a final concentration of 100 mM D-glucose, 100 µM oligomycin and 500 mM 2-DG. The constant compound approach was used to load the compounds into the ports. The final concentrations per well were 10 mM D-glucose in Port A, 1 µM oligomycin in Port B, and 50 mM 2-DG in Port C. The cartridge was then placed on top of the cell culture plate and moved into the XFe 96 Analyzer. The XF Glycolysis Stress Test program was chosen and the ECAR and OCR were measured by the instrument. Hoechst33342 was then added to each well to a concentration of 200 µM and allowed to incubate for 1 h in a 37°C humidified 5% (v/v) CO_2 incubator.

The fluorescence was measured at 365nm excitation and 415-445nm emission for Hoechst using the GloMax Discover and the OCR (oxygen consumption rate) and ECAR (extracellular acidification rate) values were normalised to the Hoechst fluorescent signal.

XF Cell Mito Stress Test: The test was performed according to manufacturer's instructions[157]. The solids were resuspended with XF medium to a final concentration of 100 µM oligomycin, 100 µM FCCP, and 50 µM rotenone/antimycin A mix. The constant compound approach was used to load the compounds into the ports. The final concentrations per well were 1.5 µM oligomycin in Port A, 1 µM FCCP in Port B, and 0.5 µM rotenone/antimycin A mix in Port C. The cartridge was then placed on top of the cell culture plate and moved into the XFe 96 Analyzer. The XF Cell Mito Stress Test program was chosen and the ECAR and OCR were measured by the instrument. The values were then normalised by the Hoechst33342 signal as described in the **XF Glycolysis Stress Test** section above.

3.1 Introduction

3.1.1 eEF2K and autophagy

The relationship between autophagy and eEF2K has been examined in multiple studies but there is currently no clear picture as to whether eEF2K positively or negatively regulates autophagy, or indeed if it regulates it at all. Separate studies by Py *et al*., Wu *et al*., Cheng *et al*. and Wang *et al*. suggested that eEF2K positively regulates autophagy to protect cells under metabolic stress conditions[113-118, 158]. These studies looked at MCF-7, MDA-MB-468 and MDA-MB-231 human breast cancer cell lines, T98G, U138MG and LN-229 human glioblastoma cell lines and mouse embryonic fibroblasts (MEFs). It was reported that inhibiting or silencing eEF2K in human breast cancer and glioblastoma cell lines decreased autophagic flux as indicated by the lowering of LC3-II protein levels and that this was associated with increased death of cells under nutrient-deprived conditions.

However, contrasting to those reports, a study by Xie *et al*.[119] found that eEF2K negatively regulates autophagy in human colon cancer cells. Silencing of eEF2K in HT-29 and HCT-116 cell lines led to a decrease in LC3-II levels, suggesting autophagic flux is increased. In this case, silencing eEF2K promoted colon cancer cell survival in response to the chemotherapy drug oxaliplatin.

On the other hand, a study by Moore *et al*.[58] from our group investigated the link between autophagy and eEF2K in A549 lung carcinoma and MEF cells. The silencing of eEF2K via inducible shRNA in A549 cells or its knock-out in MEF cells did not lead to any changes in LC3-II protein levels. This was the case even with treatment of cells with 2-deoxyglucose (2-DG) or in medium lacking glucose. Once 2-DG is transported into the cells, it is

phosphorylated into 2-deoxy-D-glucose-6-phosphate (2-DG-6-P) which is a charged compound that becomes trapped inside the cell. However, as this compound lacks the 2-OH group, it cannot be metabolised to fructose-6-P and therefore the cells cannot use it as an energy source[159]. Thus, 2-DG mimics glucose starvation conditions. In contrast to previous findings, this study concluded that eEF2K does not affect autophagy in these cell types.

These conflicting findings show that more research is required to understand the relationship between eEF2K and autophagy in a variety of cell lines. A major drawback of most of these studies is that autophagic flux was assessed solely by looking at LC3-II protein levels. As LC3-II is an intermediate in the autophagic process, any change in its levels could mean either an increase or a decrease in autophagic flux. This protein is required for autophagy but is also degraded by it[160]. Other methods to assess autophagic flux are required to further understand the role of eEF2K in this process.

eEF2K and autophagy both play roles in cell survival under nutrient deprivation although eEF2K-KO mice have no obvious phenotype under standard vivarium conditions[70]. Several studies have previously suggested that inhibition of eEF2K itself or in combination with another pathway may be a viable strategy in treating some cancers[56, 57, 61, 161-163]. Autophagy has also been singled out as a potential target for cancer therapy[164-168]. Chloroquine, an autophagy inhibitor has been used in clinical studies to treat glioblastoma with promising results[169, 170]. As many tumours and the tumour microenvironment are under constant nutrient stress, this presents an interesting possibility for cancer therapy of targeting eEF2K and autophagy at the same time, without undue side-effects of eEF2K inhibition.

For these reasons, the effects of inhibiting these two pathways must first be tested in a variety of cancer cells, which is what this Chapter aims to do.

3.1.2 Aims of this Chapter

Due to the conflicting findings regarding the effects that eEF2K has on autophagy and cell survival, this study focused on three different cancer cell lines to test the effect of inhibiting, silencing, or knocking out eEF2K on autophagy. Since currently available eEF2K inhibitors are not very potent or have off-target effects, creating eEF2K-KO cells would allow the gathering of more reliable data.

There are two main aims of this chapter – to create eEF2K knock-out (KO) MDA-MB-231 triple negative breast carcinoma and PC3 Androgen Receptor negative prostate carcinoma cell lines via a CRISPR-Cas9 approach. The other aim is to test the hypothesis that cells can use eEF2K and autophagy as independent cell survival mechanisms under nutrient-deprived conditions. A figure schematic of this is shown in **Figure 3.1**.

Figure 3.1

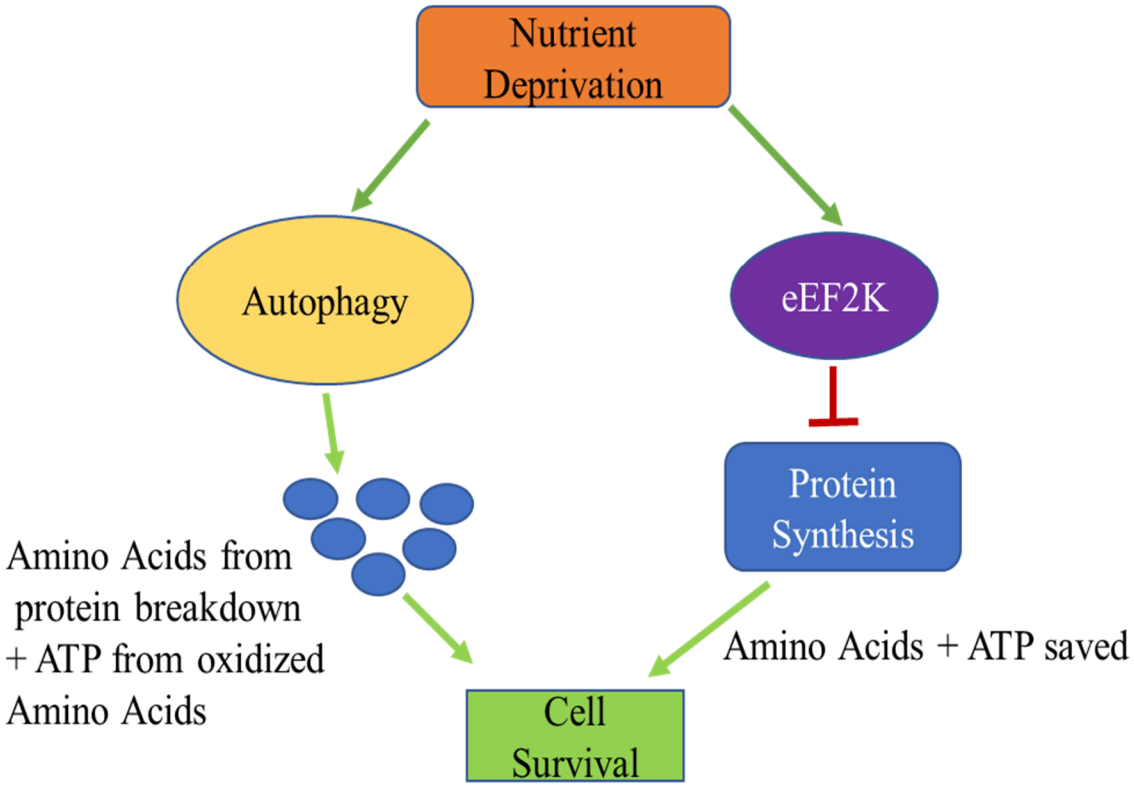


Figure 3.1: **Schematic of the hypothesis.** eEF2K and autophagy may play separate roles in cell survival under nutrient deprived conditions. Autophagy assists cells to save amino acids and ATP that is oxidized from them. eEF2K inhibits protein synthesis, saving amino acids and ATP that would otherwise have been used to make new proteins.

3.2 Results

Some of the results in this chapter were used in a manuscript which is attached in the Appendix folder of this thesis. The link below can be used to access it: https://universityofadelaide.box.com/s/qrodwr56kv6zgkr8mzqyw8ebzsnud9mf

3.2.1 eEF2K inhibition via JAN384 has no cytotoxic effect on breast cancer cells experiencing nutrient deprivation.

Initial experiments were performed in the MDA-MB-231 triple negative breast cancer cell line which lack the oestrogen receptor (ER), progesterone receptor (PR) and human epidermal growth factor receptor 2 (HER2), thus making it difficult to treat corresponding tumours with chemotherapy[171]. Triple negative breast cancers thus have poorer prognosis than luminal tumours that do contain these receptors[172, 173]. Treatments that target the ER, PR and HER2 of cancer cells, e.g., by blocking the hormones from attaching to the cancer cells, will have no effect on triple negative cancers. Because of the lack of these three receptors, triple-negative cancers tend to grow quicker as they are no longer reliant on these hormones, resulting in poorer prognosis for patients. Therefore, it is necessary to find out how to slow down the growth and treat these types of cancers.

The MDA-MB-231 cell line is commonly used to model late stage breast cancer, is invasive and metastatic[174]. Previous, unpublished data also showed a high level of phosphorylated eEF2 in breast tumour tissue (Dr. Marina Kochetkova, University of South Australia). So far, two main inhibitors of eEF2K have been reported in the literature – NH125 and A484954. After NH125 was initially reported to be an eEF2K inhibitor[175], it was found that

it actually increased the phosphorylation of eEF2 in some types of cells[176, 177], showing that it has off-target effects elsewhere. A484954 does not appear to have the issue that NH125 does, however it is only weakly effective against eEF2K and therefore needs to be used at high concentrations[176, 178]. Rottlerin has also been reported as inhibiting eEF2K but also affects a number of other protein kinases as well as the function of mitochondria[179, 180]. Our group was kindly given a set of eEF2K inhibitors by Janssen Pharmaceutica (Beerse, Belgium). The most promising candidates were JAN384 and JAN978.

To test the effectiveness of JAN384, MDA-MB-231 cells at 80% confluency were treated under conditions of high glucose (+Glc: 25 mM D-glucose, 4 mM L-glutamine, 1 mM sodium pyruvate) and no glucose or pyruvate (-Glc) for up to 16 h with or without 3 µM of JAN384 After treatment, the cells were lysed, and samples were run on SDS-PAGE/immunoblot. When cells are deprived of nutrients, it was expected that eEF2K would be activated and phosphorylate eEF2 at threonine 56 (Thr56), thus inhibiting translation elongation and hence slowing down protein synthesis. This occurs because mTORC1 is inactivated under nutrient deprived conditions, removing its inhibitory phosphorylation of eEF2K. In turn, AMPK is activated due to the lowering of cellular ATP, phosphorylating eEF2K on separate sites that activate it or inhibiting mTORC1 signalling[45, 48]. Since eEF2K is the only kinase that acts at Thr56 in eEF2, eEF2 phosphorylated at this site is used as a reliable readout of eEF2K activity in all experiments. As is evident in **Figure 3.2**, MDA-MB-231 cells have a high basal level of eEF2 phosphorylation (p-eEF2) after 16 h of growth in +Glc medium. This is likely because eEF2K becomes activated as cells become more confluent and compete for nutrients in the medium. As expected, -Glc conditions further increased p-eEF2 levels, even after 2 h, showing that eEF2K is activated. At the 16 h time point, it is evident that the phosphorylation levels of eEF2 are similar in both +Glc and -Glc

conditions. This could mean that all eEF2 has been phosphorylated in the cell. Further evidence that eEF2K becomes more active in -Glc conditions over time is that JAN384 is not as effective at blocking eEF2 phosphorylation at 16h in -Glc conditions, while it effectively reduced p-eEF2 levels to very low levels in +Glc at the same time point. Furthermore, it is important to remember that as eEF2K becomes active, it is degraded by the ubiquitin proteasome system, perhaps to allow the resumption of translation elongation, but this does not mean that eEF2 levels will immediately fall[181]. This is supported by the reduced levels of eEF2K at 16 h in -Glc conditions compared to +Glc, yet the phosphorylation of eEF2 still being high. However, over longer periods of time in stressed conditions, eEF2K may be degraded to very low levels, meaning that one might not see the expected increase in p-eEF2 compared to optimal conditions.

Figure 3.2B shows the treatment of MDA-MB-231 cells with a higher concentration of JAN384 (5 μM). In this case, it is evident that even after 24 h, p-eEF2 is almost completely gone. Again, it is of note that p-eEF2 is increased under -Glc conditions compared to +Glc, showing eEF2K's activation under nutrient deprived conditions. Interestingly, it is also evident that p-eEF2 is decreased at 24 h in +Glc medium, compared to 16 h in +Glc. This activation of eEF2K at 16 h could be a transient event, perhaps due to the 'stress' of the cells due to the confluence of the 16 h time point samples. Once the cells have slowed down protein synthesis and their energy consumption rate, eEF2 phosphorylation was no longer elevated and thus fell by 24 h.

Figure 3.2

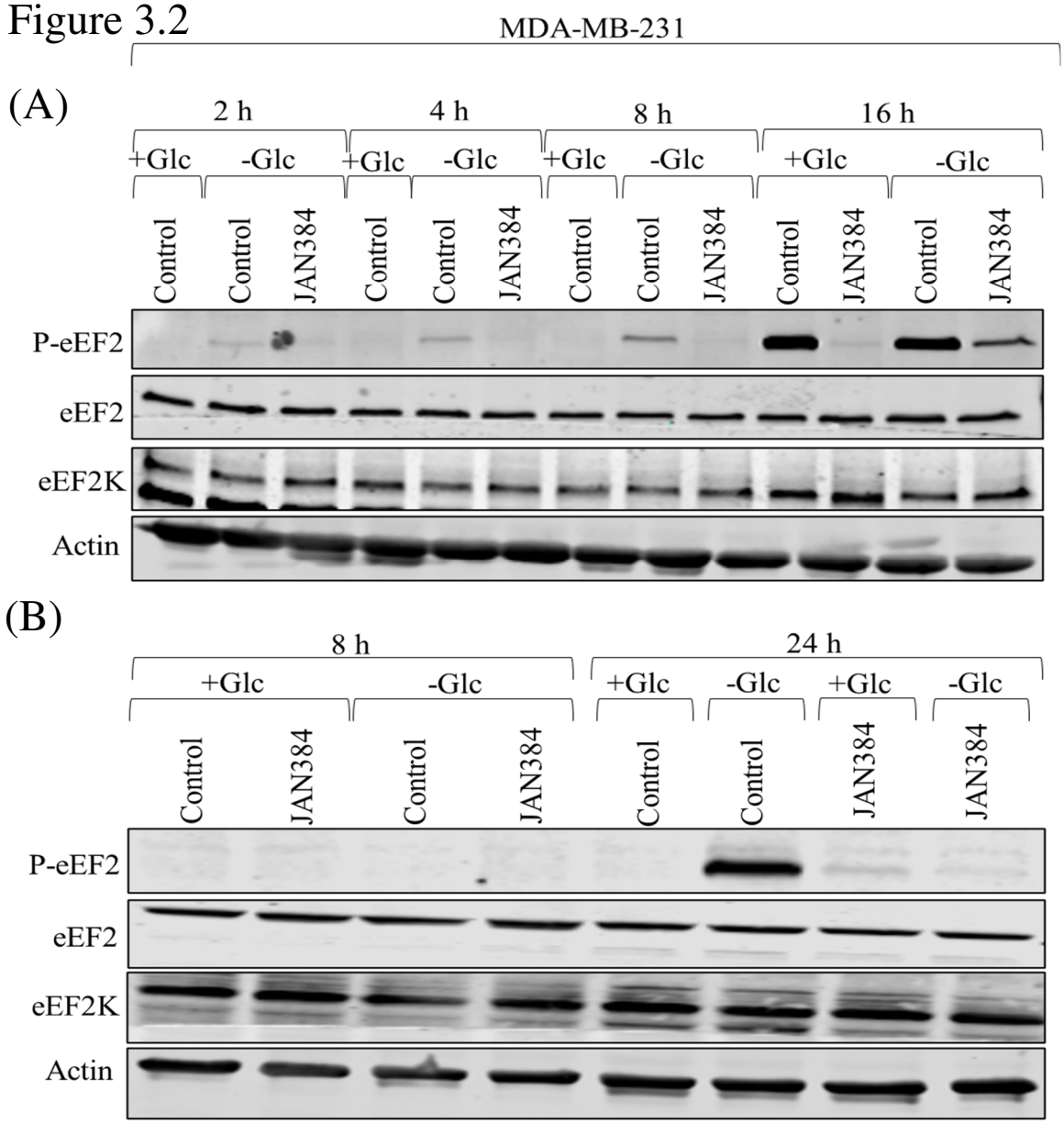


Figure 3.2: **eEF2K is successfully inhibited by JAN384 in MDA-MB-231 cells. A:** MDA-MB-231 cells were treated in medium with or without glucose and with or without 3 µM of JAN384 for the indicated times and lysed. **B:** Cells were treated in medium with or without Glc/Pyr and with or without 5 µM of JAN384 for the indicated times and lysed. The lysates were run on (12.5%) SDS-PAGE and analysed by immunoblot for the indicated proteins and phosphoproteins. The western blot images are indicative of n=3. **+Glc:** DMEM with 25 mM D-Glucose, 4 mM L-Glutamine, 1 mM sodium pyruvate. **–Glc:** DMEM without glucose and sodium pyruvate but containing 4 mM L-Glutamine.

Next, the other eEF2K inhibitors from Janssen were tested. JAN452, a compound that is related to JAN384 and JAN978 (both active compounds) but inactive against eEF2K, was used as a negative control. As shown in **Figure 3.3A and B**, both JAN384 and JAN978 effectively inhibit eEF2K at a concentration of 3 μM at the 6 h time point. As expected, the negative control compound JAN452 did not significantly alter p-eEF2 levels. However, an issue arose with JAN978 as it precipitated out of solution in the medium and was therefore not used in any future experiments. It is also of note that a lower level of eEF2 phosphorylation was evident under -Glc conditions compared to +Glc. This is likely due to degradation of eEF2K, as shown by the reduction of eEF2K levels under -Glc conditions compared to +Glc (**Figure 3.3A**). Thus, p-eEF2 is not always higher under -Glc conditions.

The next step was to test whether eEF2K inhibition reduced cell survival under nutrient-deprived conditions as shown by Leprivier *et al*.[57]. For this, a CellTox Green Cytotoxicity Assay from Promega was performed[130]. This assay uses a cell membrane-impermeable fluorescent DNA-binding dye. This dye cannot enter viable cells, but as cells undergo cell death, the membrane ruptures, allowing the dye entry. The dye then binds DNA, enhancing its fluorescent properties which can then be measured via a plate reader. MDA-MB-231 cells were treated for 48 h in +Glc and -Glc conditions with or without 6 μM JAN384. After 48 h, the CellTox Green signal was measured via plate reader and the relative fluorescence units (RFU) were normalised to the total protein content of each sample. The results are shown in **Figure 3.3C**. As expected, in +Glc control conditions, there was very little CellTox Green fluorescence, signifying very little cell death. The addition of JAN384 in +Glc conditions did not induce more cell death, indicating this compound is not cytotoxic by itself. Under -Glc conditions, the cells are clearly dying as the fluorescence intensity increases more than 40 times that of the +Glc signal intensity. However, the addition of JAN384 and thus

inhibition of protein synthesis did not significantly affect cell death compared to control. This could mean that MDA-MB-231 cells do not use eEF2K to assist them in surviving these conditions or another mechanism is involved, such as autophagy. It is possible that when eEF2K is inhibited, autophagy is able to substitute as another survival mechanism, allowing cells to scavenge their own proteins for amino acids and energy.

Figure 3.3

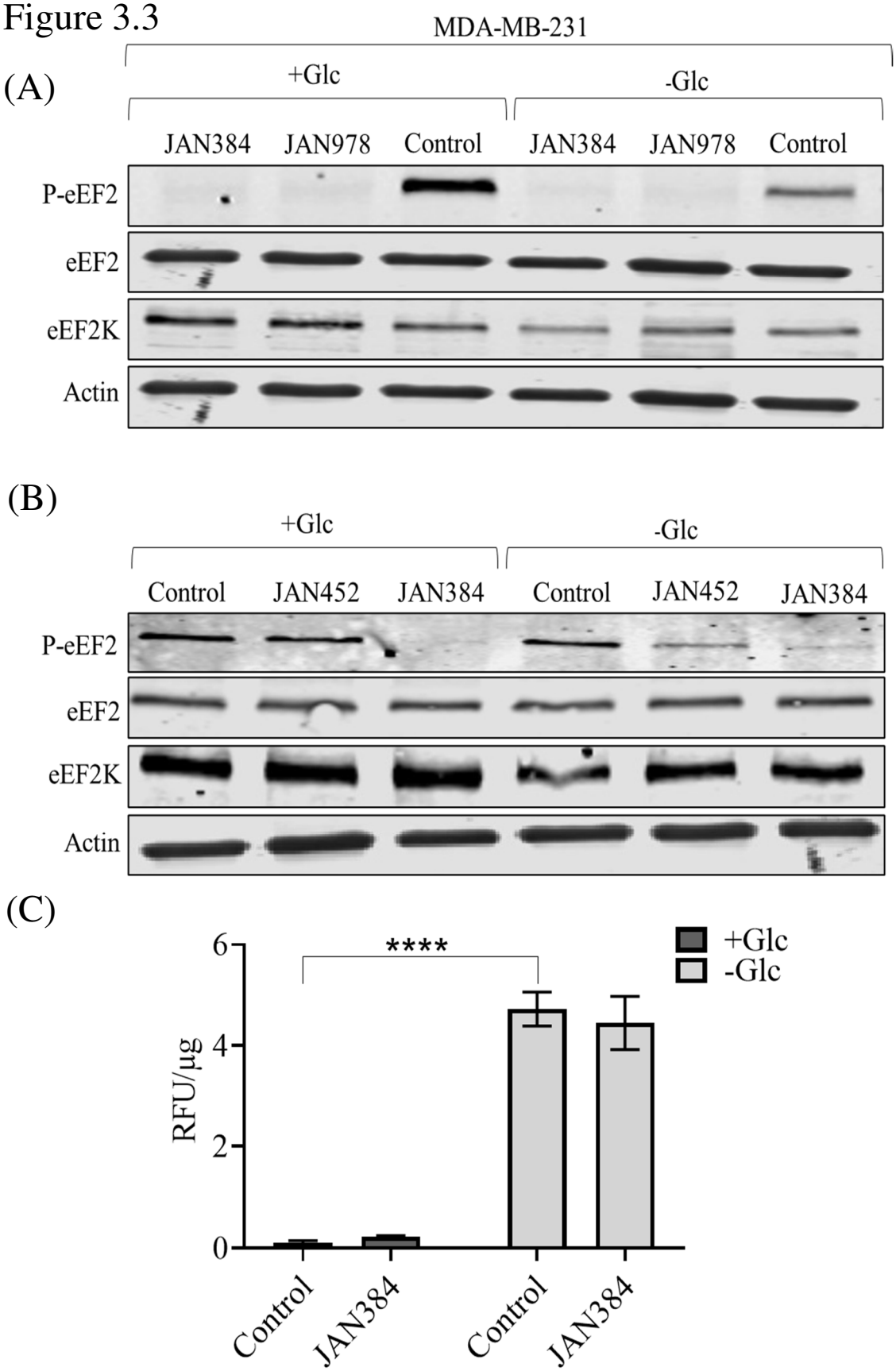

(A)
MDA-MB-231
+Glc
-Glc
JAN384
JAN978
Control
JAN384
JAN978
Control
P-eEF2
eEF2
eEF2K
Actin
(B)
+Glc
-Glc
Control
JAN452
JAN384
Control
JAN452
JAN384
P-eEF2
eEF2
eEF2K
Actin
(C)
****
+Glc
-Glc
RFU/µg
6
4
2
0
Control
JAN384
Control
JAN384

Figure 3.3: eEF2K inhibition via JAN384 has no effect on breast cancer cell cytotoxicity under nutrient deprived conditions. A: MDA-MB-231 cells were treated in medium with or without Glc/Pyr and with 3 μM of either JAN384 or JAN978 for 6 h, lysed. **B:** Cells were treated in medium with or without Glc/Pyr and with 3 μM of either JAN384 or JAN452 for 6 h. The lysates were run on (12.5%) SDS-PAGE and analysed by immunoblot. Western blot images are representative of n=3. **C:** CellTox Green Cytotoxicity Assay of MDA-MB-231 cells treated with 6 μM JAN384 in medium with or without glucose for 48 h. Error bars represent S.D. (n=3). The p-values were calculated using Two-Way ANOVA with the Tukey multiple comparisons test. RFU was normalised by total protein content.

3.2.2 Concurrent inhibition of eEF2K via JAN384 and autophagy via BafA leads to increased MDA-MB-231 and A549 cell cytotoxicity under nutrient deprivation.

To test whether autophagy and eEF2K both assist MDA-MB-231 cells to survive nutrient deprivation, BafA was used alongside JAN384. BafA is a V-ATPase inhibitor which inhibits the fusion between the lysosomes and the autophagosomes as well as decreasing lysosomal acidity, preventing the autophagic process from degrading proteins[182]. To ensure that BafA can efficiently inhibit autophagy, the Magic Red Cathepsin L assay from Bio-Rad was used. Cathepsin L is an important lysosomal protease which is involved in protein degradation[183]. As BafA inhibits the fusion between the lysosomes and autophagosomes, cathepsin L cannot act on the proteins it is supposed to degrade and therefore its activity should be much lower in cells treated with BafA. The Magic Red Cathepsin L assay utilises a cresyl violet fluorophore that can enter cells. If cathepsin L is active in the cells, it will cleave off the cathepsin targeting sequences on the fluorophore, allowing it to become fluorescent upon excitation.

MDA-MB-231 cells were treated in -Glc conditions with or without BafA for 24 h prior to the addition of the magic red fluorophore. As expected, the fluorescence was high under control conditions as autophagy is activated under nutrient deprived conditions (**Figure 3.4 A**). However, treatment with BafA almost completely suppressed cathepsin L activity, confirming that it is an effective inhibitor of autophagic flux under these conditions.

The next step was to test the effects of eEF2K and autophagy inhibition on cell survival under nutrient deprivation in MDA-MB-231 and A549 cells. A549 lung carcinoma cells

Figure 3.4

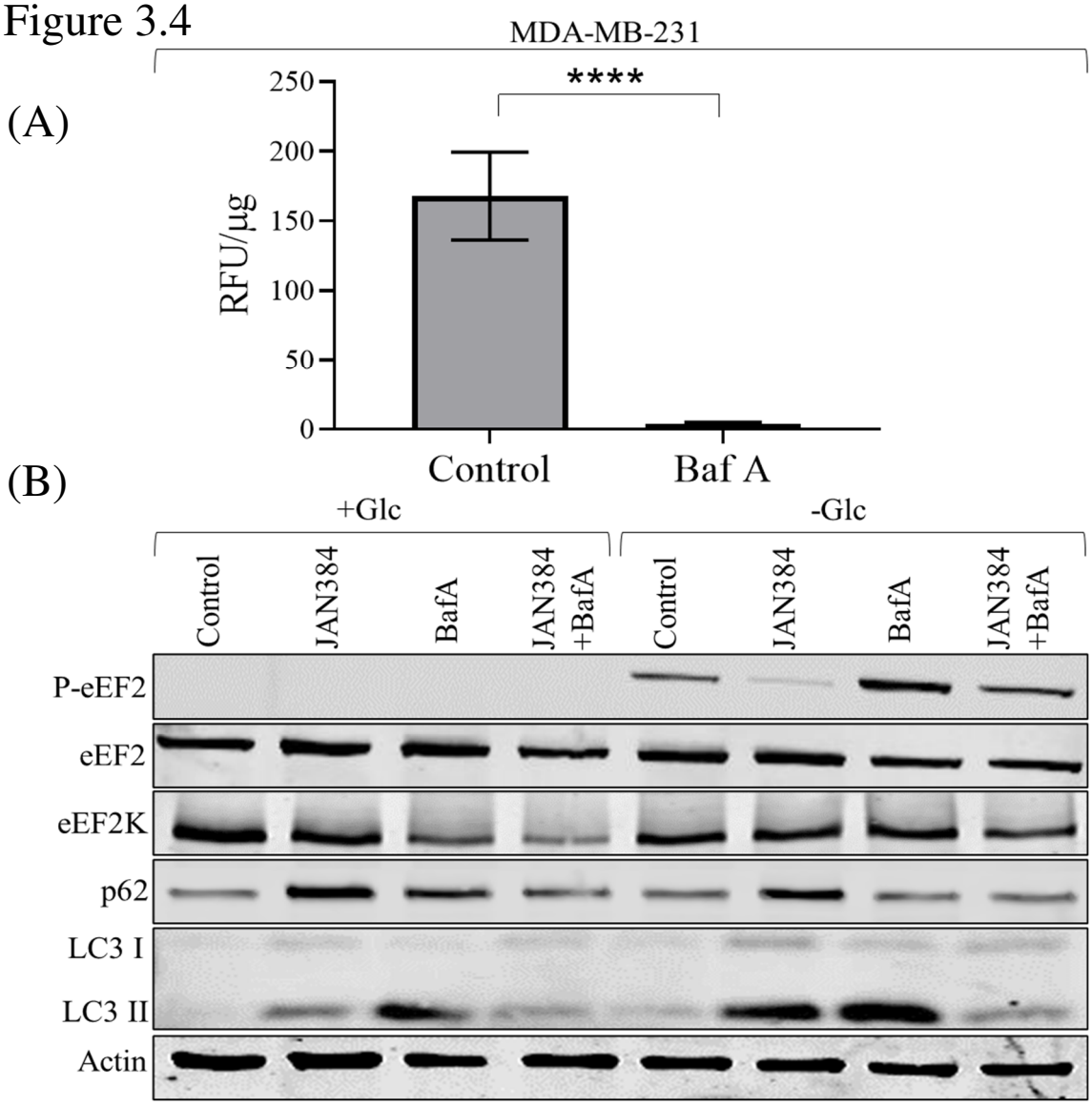


Figure 3.4: **Bafilomycin A successfully inhibits autophagic flux in MDA-MB-231 cells.** **A:** Magic Red Assay – MDA-MB-231 cells were treated in medium lacking Glc/Pyr conditions for 24 h with 125 nM BafA. Error bars represent S.D. (n=3). The p-values were calculated using an unpaired, parametric, two-tailed T-test with Welch's correction. P-value: ****≤0.0001. RFU was normalised to total protein content. **B: C**ells were treated in medium with or without Glc/Pyr and with either 6 µM JAN384, 125 nM BafA or both for 48 h. The cells were lysed, the samples were run on either (16%) SDS-PAGE for low molecular weight proteins or (12.5%) SDS-PAGE for others, followed by analysis via immunoblot. The western blot images are representative of n=3.

were previously used by Moore and others in our group's study in 2015 looking at eEF2K's role in hypoxia[78]. These cells contain an inducible shRNA which silences eEF2K upon the addition of 1 mM IPTG for 5 days.

MDA-MB-231 and A549 cells were treated in +Glc and -Glc conditions with JAN384, BafA or the two compounds together. eEF2K was also silenced in A549 cells to compare the effect of JAN384 and shRNA. **Figures 3.4B and 3.5** show the levels of proteins of interest after these treatments in both cell lines. JAN384 effectively inhibited eEF2K activity, as evident by P-eEF2 being almost completely lost in ±Glc conditions. It is important to note that there is no eEF2 phosphorylation in -Glc conditions. Western blots are an end-point assay and p-eEF2 may well have gone up prior to this time point to protect cells, falling later as eEF2K is degraded.

P62, otherwise known as SQSTM1, is an autophagosome cargo protein that targets other proteins for degradation via autophagy[184]. This protein is mainly degraded through selective autophagy and is commonly used to monitor autophagic flux[185, 186]. When autophagy is inhibited, p62 is no longer degraded via this process and its levels are thus expected to increase. After BafA treatment, p62 levels significantly increased under either +Glc or -Glc conditions, further confirming that BafA blocks autophagy.

During autophagy, LC3-I is covalently modified with phosphatidylethanolamine and forms LC3-II. LC3-II enters the phagophore, promoting the biogenesis of the autophagosome, as well as playing a role in substrate selection. During autophagy, LC3-II is degraded[160]. As BafA blocks the fusion of the autophagosome and the lysosome, LC3-II cannot be degraded and is therefore a good marker of autophagic inhibition. Upon treatment with BafA, it is

evident that LC3-II levels were greatly increased in ±Glc conditions. This provides further evidence that BafA does indeed inhibit autophagy under these conditions.

Next, the CellTox Green assay was performed on both cell lines to measure cytotoxicity of the cells under the same conditions. As shown in **Figure 3.6A**, treatment with BafA even in +Glc conditions increased cell death 19-fold compared to control in MDA-MB-231 cells. After 48 h of treatment, cells would have become overconfluent, using up the nutrients in the +Glc medium. Without autophagy, these cells cannot scavenge their own proteins for energy and would thus start dying. This shows that autophagy is necessary for cell survival under these conditions as the cells that can no longer scavenge their own proteins for extra amino acids and energy do not survive. The addition of JAN384 concurrently to BafA did not significantly alter cell death under these conditions. In -Glc conditions, the addition of JAN384 or BafA separately did not significantly increase cell death compared to control conditions. However, when both inhibitors are used at the same time, cell death is increased by more than 2-fold. This suggests that when either eEF2K or autophagy is inhibited separately, the other pathway substitutes for the inactive pathway, allowing cells to save nutrients and survive for longer. However, when both pathways are blocked, the cells can no longer control their translation elongation or break down their own proteins for amino acids and ATP, leading to quicker cell death.

Figure 3.5

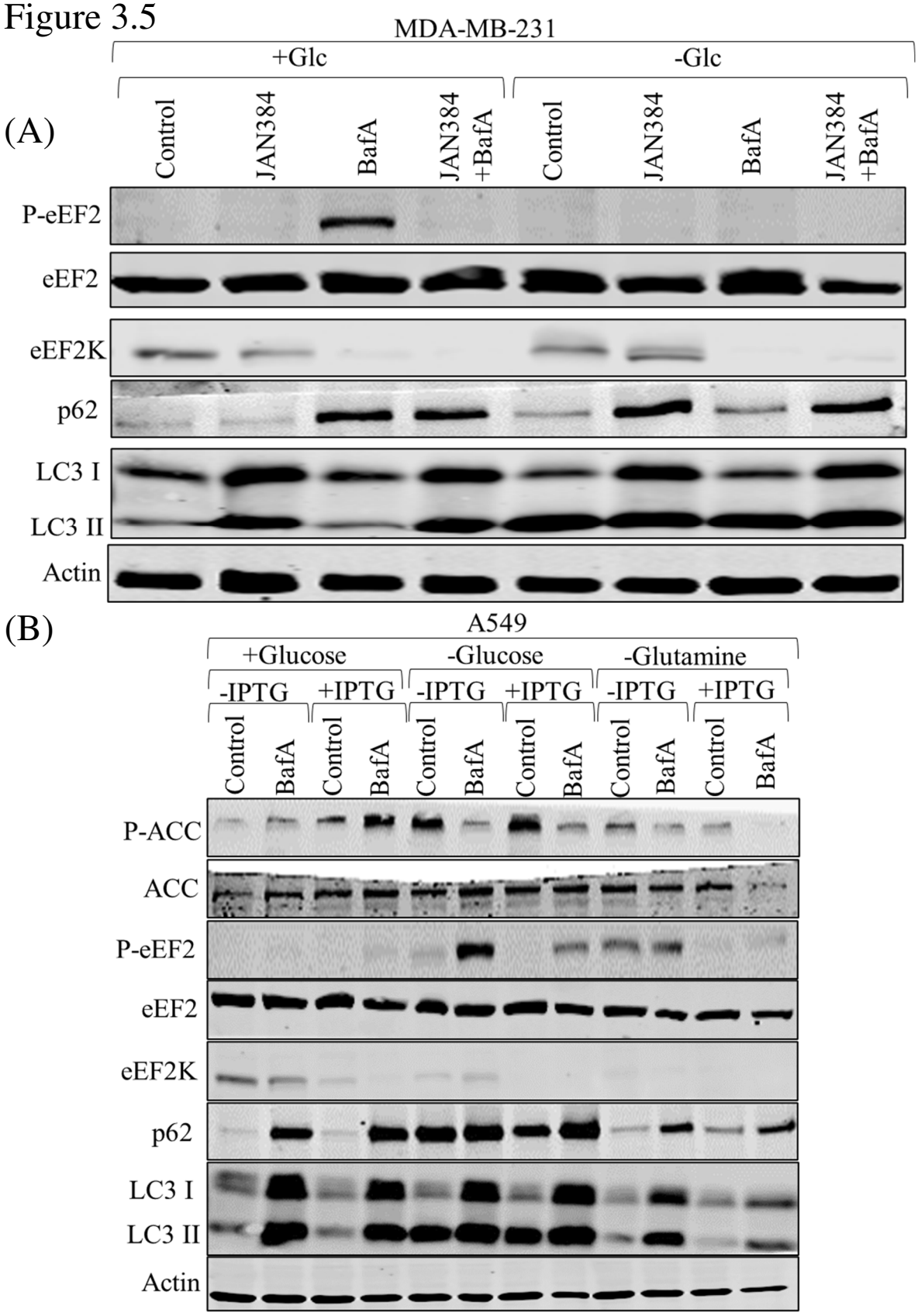

(A)
MDA-MB-231
+Glc
-Glc
Control
JAN384
BafA
JAN384 +BafA
Control
JAN384
BafA
JAN384 +BafA
P-eEF2
eEF2
eEF2K
p62
LC3 I
LC3 II
Actin
(B)
A549
+Glucose
-Glucose
-Glutamine
-IPTG
+IPTG
-IPTG
+IPTG
-IPTG
+IPTG
Control
BafA
Control
BafA
Control
BafA
Control
BafA
Control
BafA
Control
BafA
P-ACC
ACC
P-eEF2
eEF2
eEF2K
p62
LC3 I
LC3 II
Actin

Figure 3.5: **Bafilomycin A successfully inhibits autophagic flux in A549 cells. A:** A549 cells were treated in medium with or without Glc/Pyr and with either 6 μM JAN384, 125 nM BafA or both for 48 h. **B:** Cells were treated in medium lacking Glc/Pyr or Glc/Pyr/Gln and with or without 125 nM BafA for 48 h. eEF2K silencing was done by adding 1 mM IPTG to cells 5 days prior to the experiment. The cells were lysed, the samples were run on either (16%) SDS-PAGE for low molecular weight proteins or (12.5%) SDS-PAGE for others, followed by analysis via immunoblot. The western blot images are representative of n=3. –Glutamine: DMEM that lacks glucose, pyruvate and glutamine.

Figure 3.6

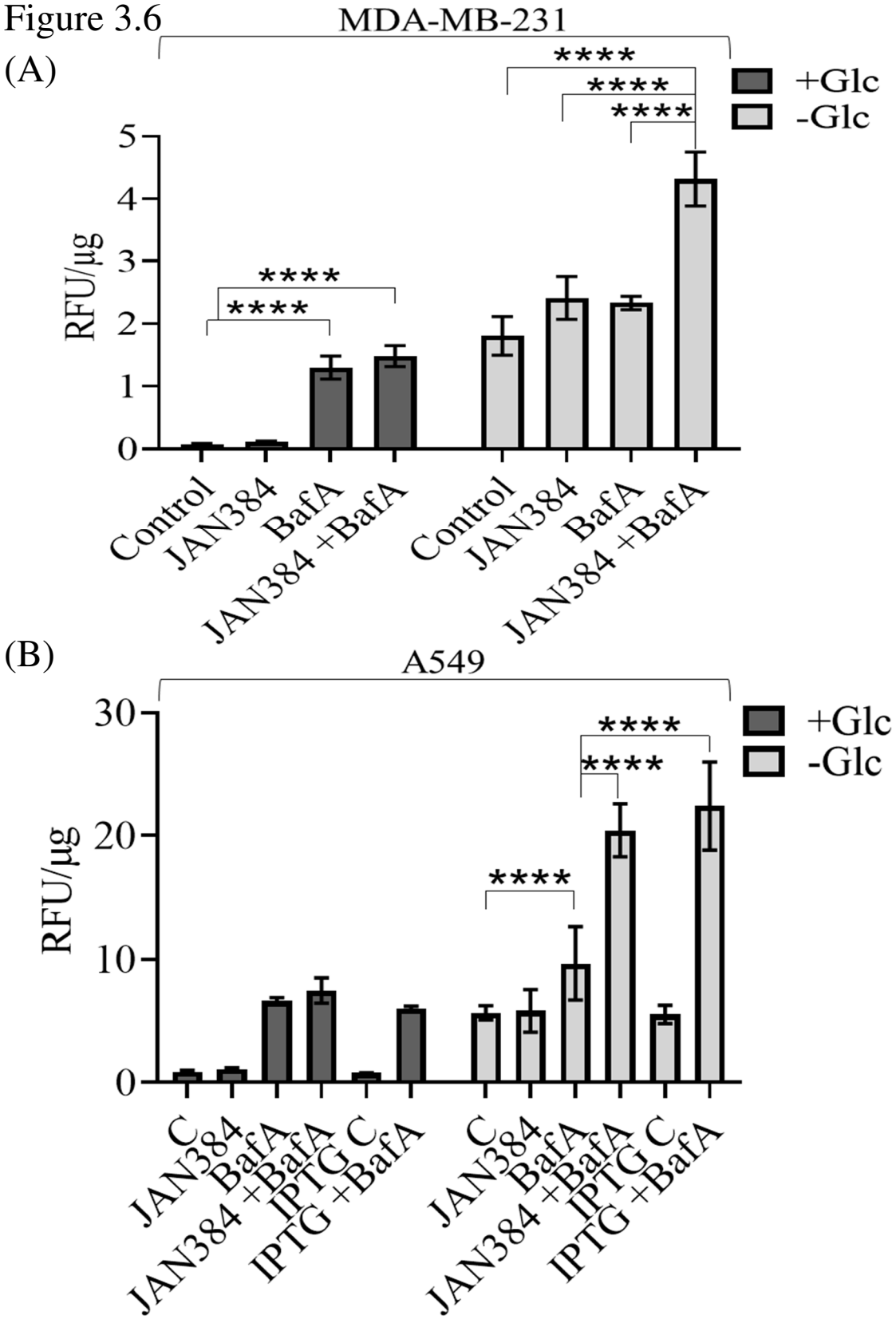

(A)
MDA-MB-231
+Glc
-Glc
RFU/µg
0
1
2
3
4
5
****
****
****
****
****
Control
JAN384
BafA
JAN384 +BafA
Control
JAN384
BafA
JAN384 +BafA
(B)
A549
+Glc
-Glc
RFU/µg
0
10
20
30
****
****
****
C
JAN384
BafA
JAN384 +BafA
IPTG C
IPTG +BafA
C
JAN384
BafA
JAN384 +BafA
IPTG C
IPTG +BafA

Figure 3.6: **A combination of eEF2K and autophagy inhibition or silencing leads to increased cell death under nutrient deprived conditions than when either pathway is inhibited individually in MDA-MB-231 and A549 cells.** Cell death was measured via the CellTox Green Assay. **A:** MDA-MB-231 cells were treated in medium with or without Glc/Pyr and with either 6 μM JAN384, 125 nM BafA or both for 48 h. **B:** A549 cells were treated in medium with or without Glc/Pyr and with either 6 μM JAN384, 125 nM BafA or both for 48 h. eEF2K shRNA was induced with 1mM IPTG treatment for 5 days prior to the experiment. Error bars represent S.D. (n=3). The p-values were calculated using Two-Way ANOVA with the Tukey multiple comparisons test. P-values: ****≤0.0001. RFU was normalised by total protein content.

This data is further supported by data for A549 cells shown in **Figure 3.6B.** Treatment with BafA leads to increased cell death under +Glc conditions, while the addition of JAN384 or silencing of eEF2K with IPTG-induced shRNA does not. In -Glc conditions, inhibition or silencing of eEF2K did not increase cell death by itself, although unlike in MDA-MB-231 cells, BafA did increase cell death under these conditions by approximately 1.7-fold. However, when both pathways were inhibited, cell death quadrupled. This also shows that this increase in cell death is not due to an off-target effect of JAN384, as eEF2K silencing via IPTG and BafA treatment show the same increase in cell death as using JAN384 and BafA together. CellTox Green images that complement these data are shown in **Figures 3.7 and 3.8**. Cells that are stained green are dead or dying.

To augment these findings, RealTime-Glo™ MT Cell Viability Assay from Promega was used[131]. This assay measures cell metabolism by quantifying the reduction potential of the cells. Cells need to reduce various molecules to survive. For example, the aerobic catabolism of glucose leads to the production of ATP. In this reaction, glucose is oxidised to carbon dioxide, while oxygen accepts electrons and is reduced to water. This reduction potential of cells gives an idea of their viability. Viable cells can reduce the prosubstrate added to them, creating a substrate for NanoLuc® Luciferase which then uses it to release a luminescent signal that can be measured on a plate reader. Dead or dying cells cannot reduce the substrate, leading to a low signal measurement. Thus, it was expected that this assay would produce results that are the opposite of the CellTox Green results, i.e., when eEF2K and autophagy are inhibited at the same time, cell viability was further reduced. MDA-MB-231 and A549 cells were treated under the same conditions as in the CellTox Green assay and the luminescence was measured. As shown in **Figure 3.9A and B**, the cell viability trend was indeed the direct opposite of the cell death trend. In both MDA-MB-231 and A549 cells,

treatment with BafA significantly reduced cell viability even under +Glc conditions. eEF2K inhibition under +Glc conditions alongside BafA treatment did not further decrease cell viability. In -Glc conditions, inhibiting eEF2K or autophagy separately did not significantly alter cell viability compared to control. However, when both pathways were inhibited, the viability is decreased 5-fold for MDA-MB-231 cells and 2-fold for A549 cells. This further confirms the CellTox Green data.

Taken together, these data lend support to the hypothesis that eEF2K and autophagy are both used, 'in parallel', by these cancer cell lines under nutrient deprived conditions to help them to survive. When one process is turned off, the other pathway acts as a substitute; however, when both pathways are turned off, the cells cannot cope and succumb to nutrient deprivation much quicker. Unfortunately, inhibitors tend to have side effects. This is evident when looking at **Figure 3.4B and 3.5A**, where JAN384 seems to increase both p62 and LC3-II levels compared to control without the addition of BafA. On the other hand, silencing of eEF2K in A549 cells did not lead to any changes in p62 or LC3-II levels (**Figure 3.5B**). Due to the potentiawl of JAN384 having an off-target effect, the data in MDA-MB-231 cells needed to be confirmed using knock-out (KO) cells.

Figure 3.7

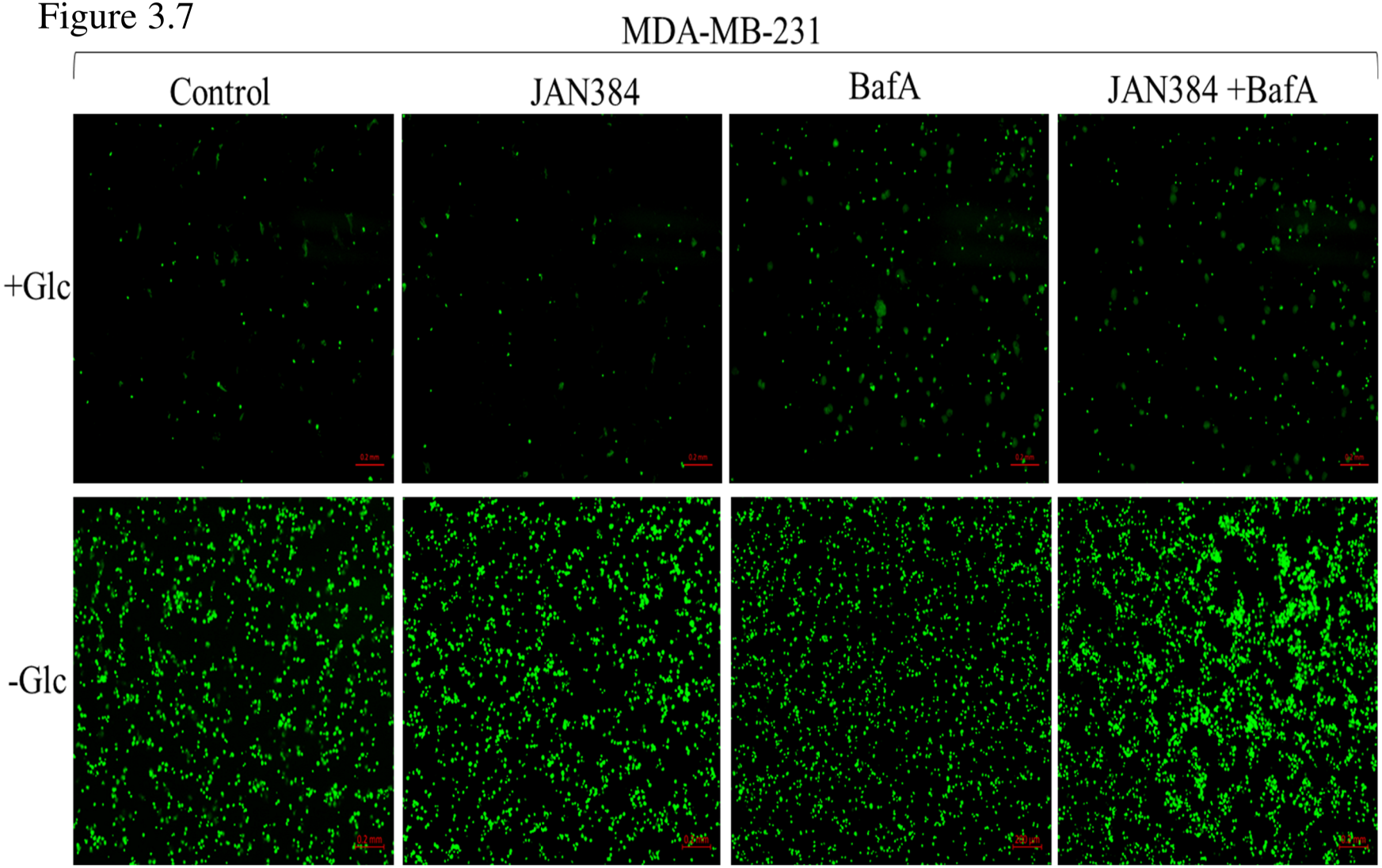


Figure 3.7: **A combination of eEF2K and autophagy inhibition or silencing leads to increased cell death under nutrient deprived conditions than when either pathway is inhibited individually in MDA-MB-231 cells (CellTox Green images).** CellTox Green Assay images **–** MDA-MB-231 cells were treated in medium with or without Glc/Pyr with either 6 μM JAN384, 125 nM BafA or both for 48 h. Images of Cell-Tox Green fluorescence were taken using the GFP filter on a Zeiss Axio Vert.A1 200 microscope with the 4X magnifying lens Each image is representative of 15 images total from 3 biological replicates.

Figure 3.8

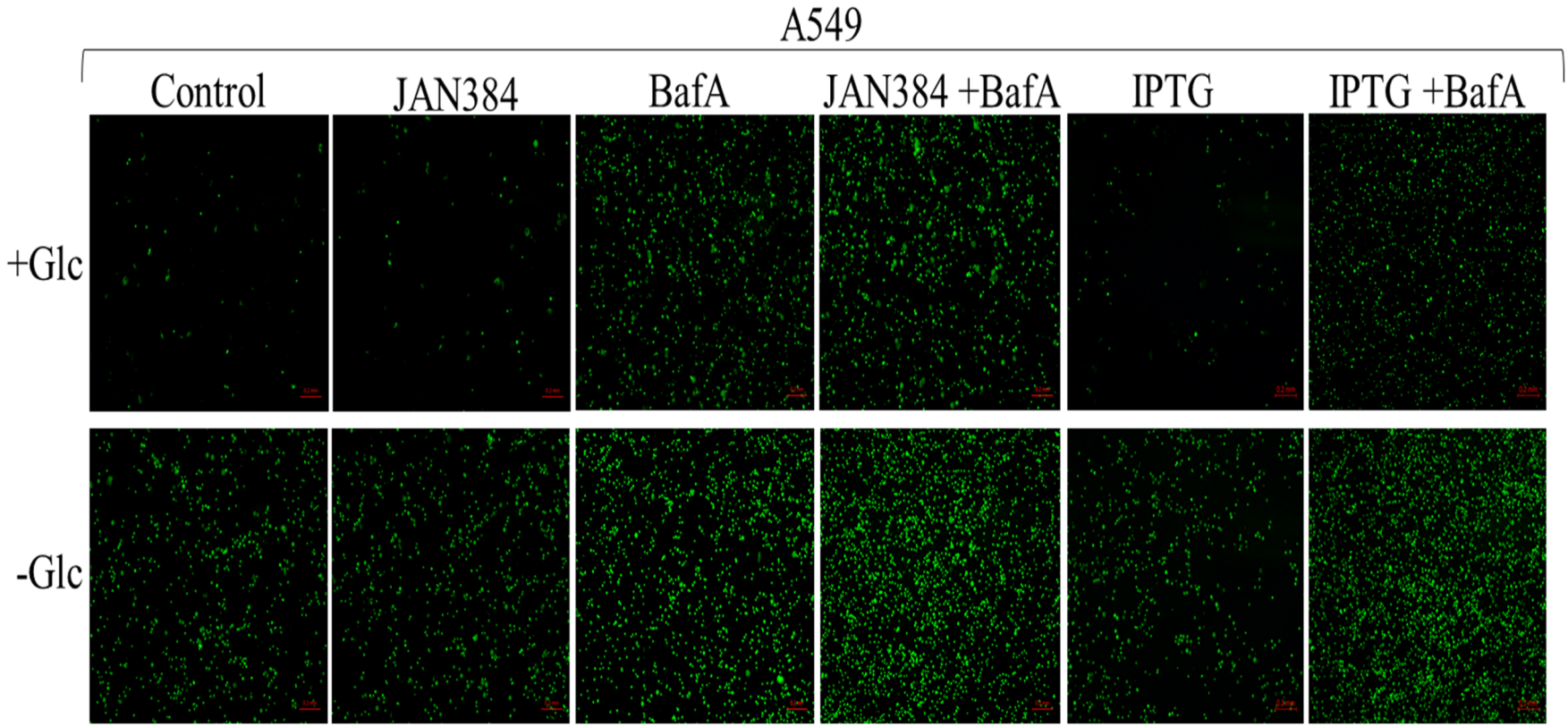


Figure 3.8: **A combination of eEF2K and autophagy inhibition or silencing leads to increased cell death under nutrient deprived conditions than when either pathway is inhibited individually in A549 cells (CellTox Green images).** CellTox Green Assay images – A549 cells were treated in medium with or without Glc/Pyr with either 6 μM JAN384, 125 nM BafA or both for 48 h. eEF2K shRNA was induced with 1 mM IPTG treatment for 5 days prior to the experiment. Images of Cell-Tox Green fluorescence were taken using the GFP filter on a Zeiss Axio Vert.A1 200 microscope with the 4X magnifying lens Each image is representative of 15 images total from 3 biological replicates.

Figure 3.9

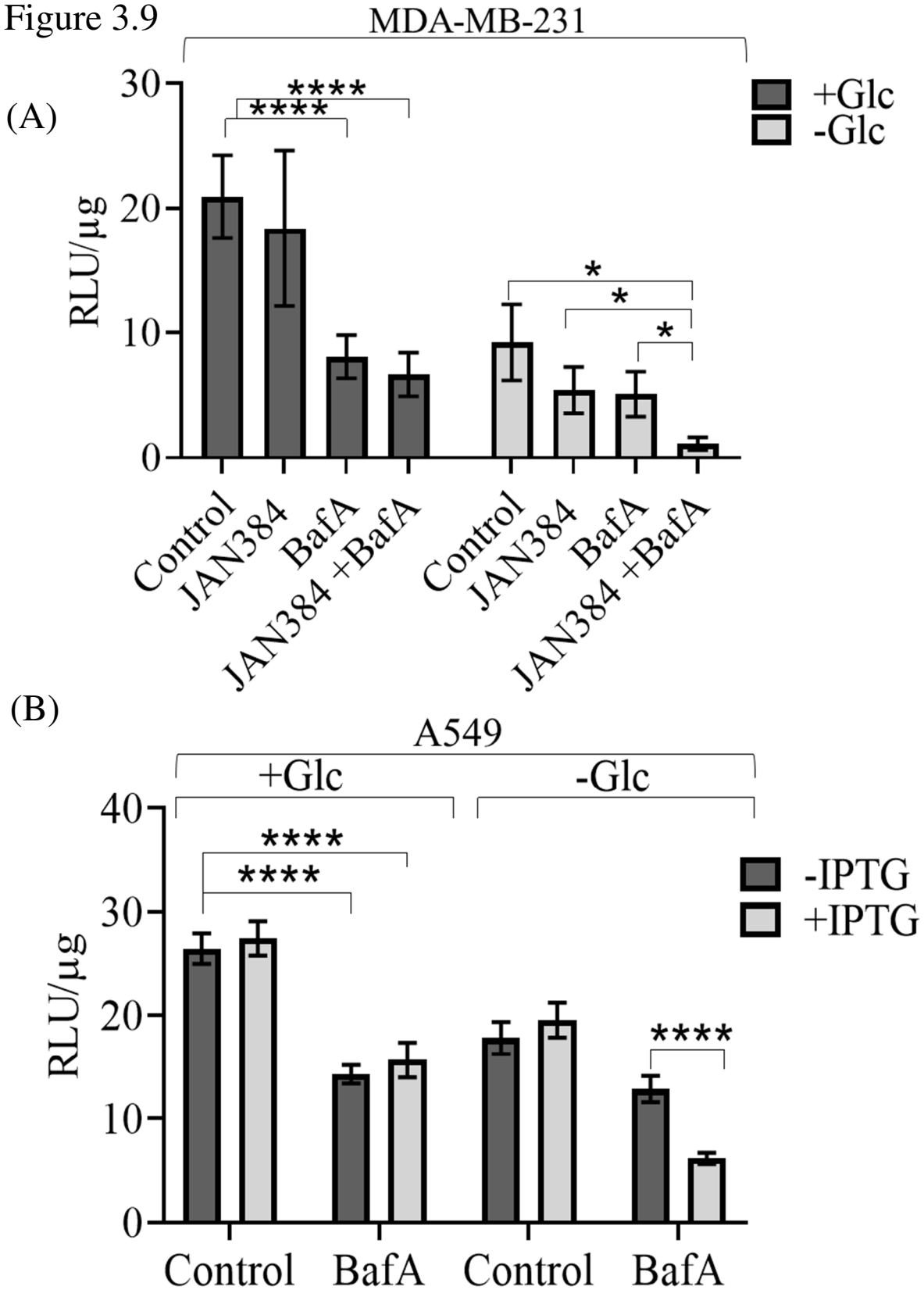

(A)
MDA-MB-231
+Glc
-Glc
RLU/µg
30
20
10
0
****
****
*
*
*
Control
JAN384
BafA
JAN384 +BafA
Control
JAN384
BafA
JAN384 +BafA
(B)
A549
+Glc
-Glc
-IPTG
+IPTG
RLU/µg
40
30
20
10
0
****
****
****
Control
BafA
Control
BafA

Figure 3.9: **A combination of eEF2K and autophagy inhibition or silencing leads to decreased cell viability under nutrient deprived conditions than when either pathway is inhibited individually in MDA-MB-231 and A549 cells.** Cell viability was measured via the RealTime-Glo Cell Viability Assay. **A:** MDA-MB-231 cells were treated in medium with or without Gl/Pyr and with either 6 μM JAN384, 125 nM BafA or both for 48 h. **B:** A549 cells were treated in medium with or without Glc/Pyr and with either 6 μM JAN384, 125 nM BafA or both for 48 h. eEF2K shRNA was induced with 1mM IPTG for 5 days prior to the experiment. Error bars represent S.D. (n=3). The p-values were calculated using Two-Way ANOVA with the Tukey multiple comparisons test. P-values: *≤0.05; ****≤0.0001. RLU was normalised by total protein content.

3.2.3 Creation of eEF2K knock-out MDA-MB-231 and PC3 cells using CRISPR-Cas9 Genome Editing

The eEF2K-KO MDA-MB-231 cells created in this section were used in the study by Dr. Jianling Xie from our group who looked into eEF2K's effect on translation fidelity[128]. This effect on translation fidelity will be further discussed in Chapter 5. PC3 is an aggressive prostate cancer cell line which is androgen independent and does not respond to glucocorticoid or fibroblast growth factors, making it a useful cell line to investigate prostate cancer[187]. The PC3 eEF2K-KO cells were created by Danielle Fang following my method. These cells were used in a study done by our group[188] and others investigating the effects of eEF2K on PD-L1 (programmed cell death 1 ligand 1), which will also be discussed in Chapter 5.

The first step to creating eEF2K-KO cells was to design the sgRNA. This sgRNA was designed to cut the end of exon 2 of eEF2K which is the beginning of its open reading frame. This cut would prevent the rest of the protein from being synthesised. A successful cut would also remove the nearby *Bpm*I recognition sequence which is then later used to screen possible knock-out clones. A schematic of where the sgRNA targets the gene is shown in the Benchling[189] diagram in **Figure 3.10**.

Figure 3.10

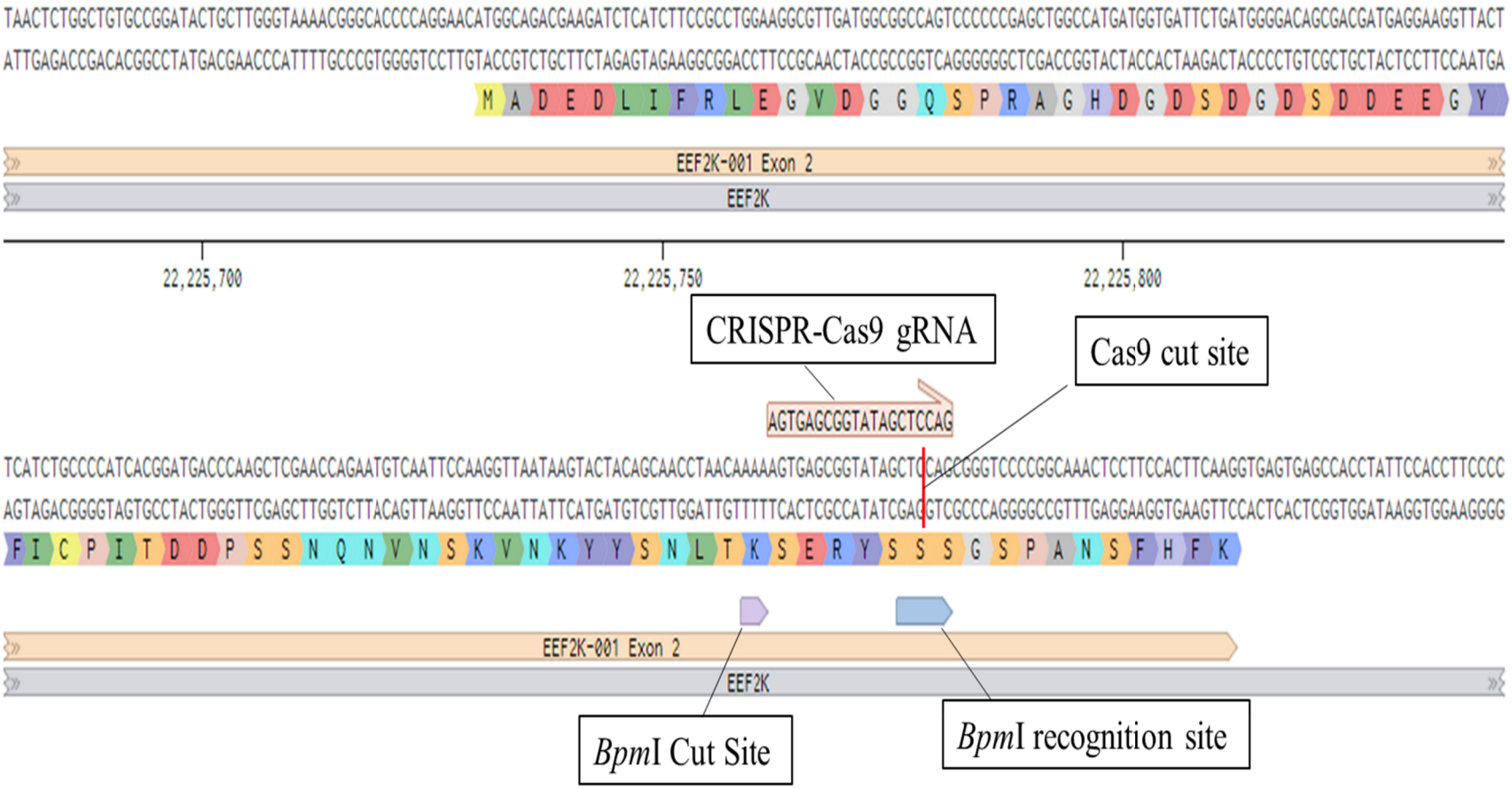


Figure 3.10: Creation of eEF2K KO MDA-MB-231 and PC3 cells using CRISPR-Cas9. A Benchling[177] diagram showing the location of the Cas9 gRNA within exon 2. The Cas9 cut site, *Bpm*I cut and recognition sites are also shown. If the Cas9 successfully introduces an indel, the *Bpm*I recognition site will be lost.

The next step was to ligate the sgRNA that will cut the eEF2K sequence into the CRISPR-Cas9 vector. The sgRNA top and bottom strands were phosphorylated and annealed. They were then ligated into a linearised CRISPR-Cas9 CD4 vector using T4 DNA ligase. The ligated product was transformed into DH5α cells alongside a negative control vector. Single colonies were picked from the plates that showed more growth than the negative control, and colonies were grown and DNA mini-prepped. Sequential digests using *Bae*I first and then *Eco*RI-HF restriction enzymes were performed. An example of this is shown in **Figure 3.11A**. Successfully ligated vectors showed up as one band, at the same size as the vector control digested only with *Eco*RI-HF. This *Bae*I recognition sequence is removed when the sgRNA is ligated into the vector. After confirmatory sequencing, the ligated sgRNA-CRISRP-Cas9 CD4 vector was nucleofected into MDA-MB-231 and PC3 cells. Cells that have taken up the vector were able to express CD4 and were isolated using Dynabeads that were coupled together with an anti-human CD4 antibody. After counting the cells, a range of cell dilutions was used to seed cells into 96-well plates to grow single-celled colonies. From these colonies, two screening strategies were performed to isolate eEF2K-KO clones – *Bpm*I restriction enzyme digests and western blotting after hydrogen peroxide (H_2O_2) treatment. A schematic of this process is shown in **Figure 3.12**. To perform the *Bpm*I restriction enzyme screening, whole cell genomic DNA was extracted, and PCR was performed with a pair of primers surrounding the CRISRP-Cas9 cut site. **Figures 3.11B and C** show the successful PCR amplification from MDA-MB-231 and PC3 cells respectively, with a single band product at the expected size being visible on an agarose gel.

The *Bpm*I restriction enzyme digestion was then used to screen for potential eFE2K-KO clones. If the Cas9 had cut in the correct location, it would have removed the *Bpm*I recognition site, meaning the enzyme could no longer cut the sequence. Therefore, for

potential eEF2K-KO clones, the DNA would appear as single uncut bands. For clones that showed two bands, the CRISPR-Cas9 either had not cut or had cut elsewhere and they were not used for the next step in the screening process. An example of this is shown in **Figures 3.13A and B** for MDA-MB-231 and PC3 cells respectively.

The final stage of the screening process involved treating potential eEF2K-KO clones with hydrogen peroxide (H_2O_2) for 4 h. H_2O_2 rapidly stimulates eEF2K [190], allowing for a quick experiment to be performed to screen many potential candidates for presence or absence of eEF2K activity. As shown in **Figures 3.14A and B**, wild-type (WT) MDA-MB-231 and PC3 cells' p-eEF2 is increased, meaning eEF2K is stimulated by the addition of H_2O_2. According to the western blot, some of the potential eEF2K-KO clones did not show any p-eEF2 (indicating a complete lack of eEF2K activity) and did not contain any eEF2K protein, indicating successful knockout of eEF2K and that this is the only kinase acting on Thr56 in eEF2. Two clones from both MDA-MB-231 and PC3 cells were chosen for all future experiments with KO cells. Comparing two different eEF2K-KO clones allowed for confirmation that any data gathered regarding the KO is not due to an off-target effect of the CRISRP-Cas9.

Figure 3.11

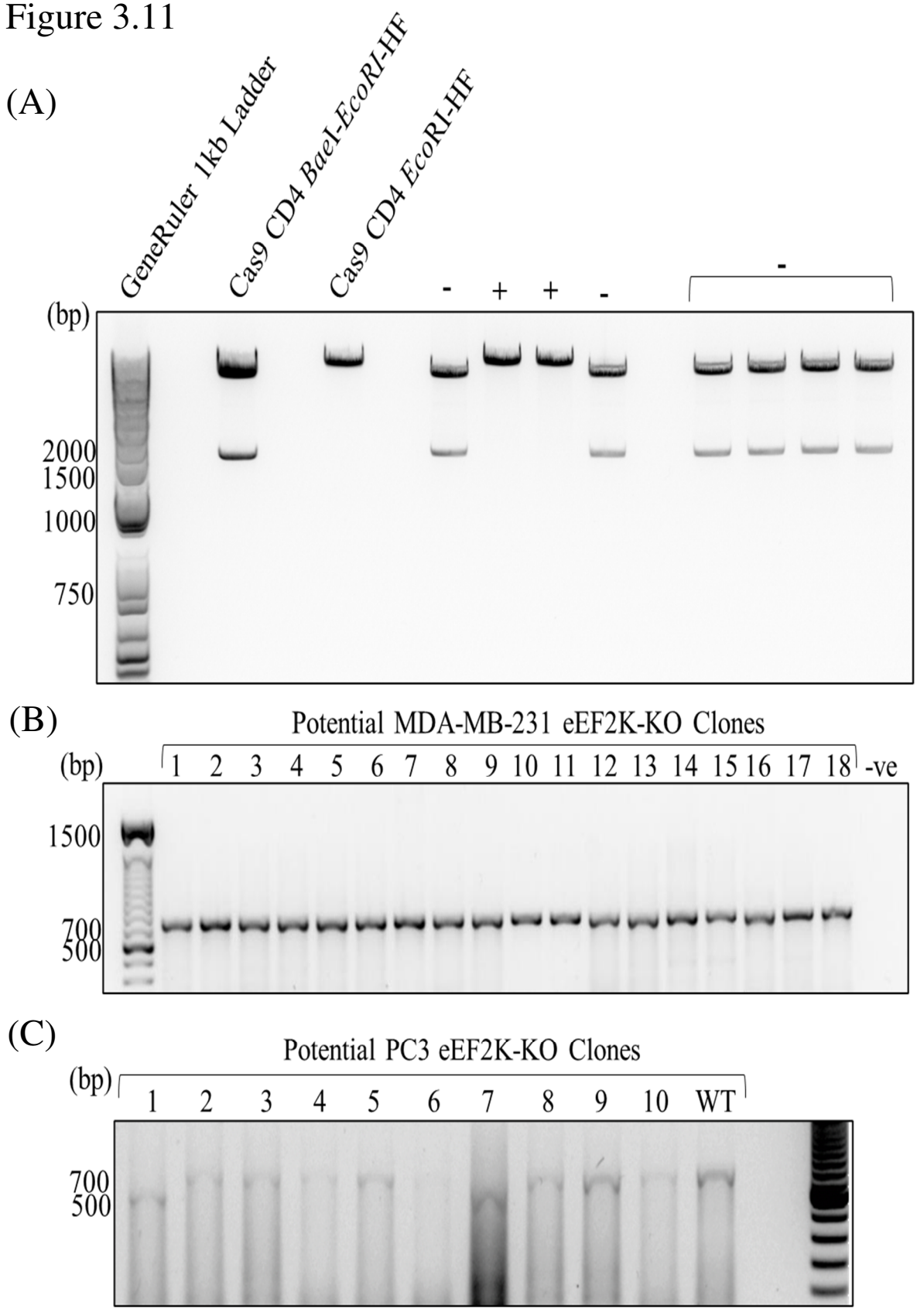

(A)
GeneRuler 1kb Ladder
Cas9 CD4 BaeI-EcoRI-HF
Cas9 CD4 EcoRI-HF
-
+
+
-
-
(bp)
2000
1500
1000
750
(B)
Potential MDA-MB-231 eEF2K-KO Clones
(bp)
1 2 3 4 5 6 7 8 9 10 11 12 13 14 15 16 17 18
-ve
1500
700
500
(C)
Potential PC3 eEF2K-KO Clones
(bp)
1 2 3 4 5 6 7 8 9 10 WT
700
500

Figure 3.11: Ligation of CRISPR-Cas9 CD vector with gRNA and possible eEF2K-KO clone digests. A: *Bae*I and *Eco*RI-HF sequential restriction enzyme digests of ligation products were run on a 1% agarose gel. Unsuccessful ligations are marked with '-'. Successful ligations are marked with '+'. **B, C:** PCR amplification was performed on the genomic DNA of potential eEF2K-KO's clones from MDA-MB-231 and PC3 cells respectively. The DNA was run on a 1% agarose gel. Milli-Q water was used as a negative (-ve) control. The expected product size was 722 bp. The data for part **C** was obtained by Ms. Danielle Fang.

Figure 3.12

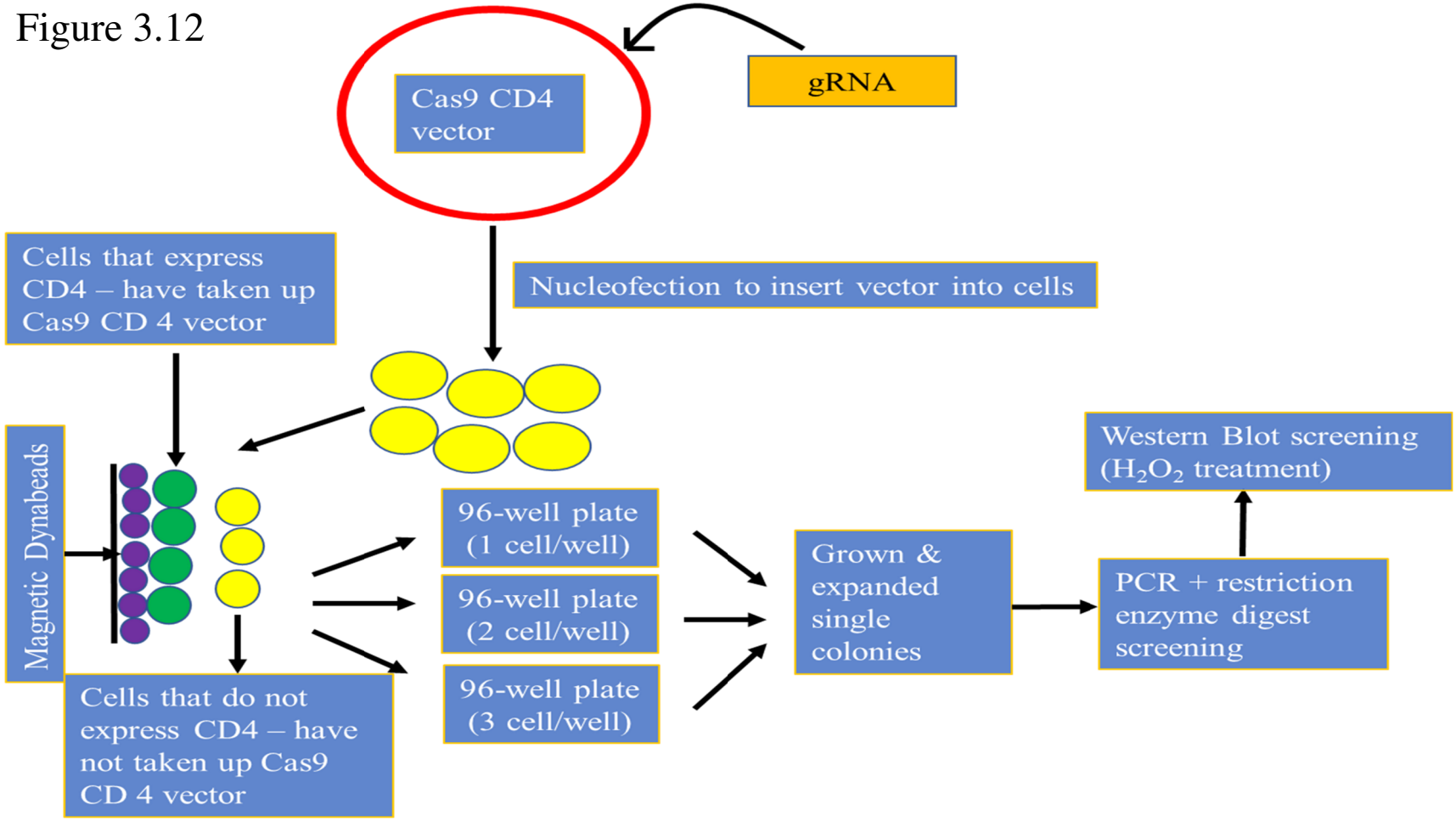


Figure 3.12: Schematic of the isolation of possible eEF2K-KO clones. Cells that have successfully taken up the Cas9 vector expressed CD4 and were isolated via magnetic CD4 Dynabeads. They were then seeded into 96-well plates and single cell colonies were grown and expanded. Each colony was tested via PCR followed BpmI restriction enzyme digests and western blotting after treatment with H_2O_2.

Figure 3.13

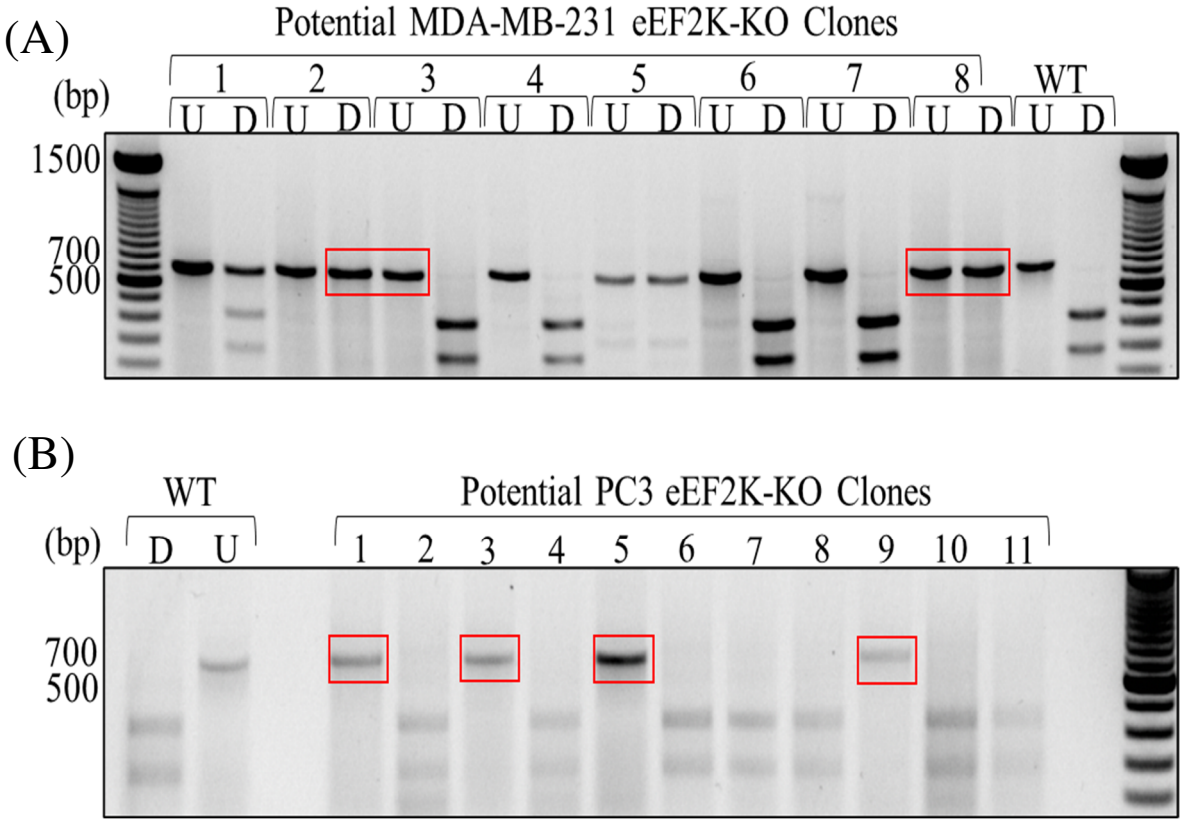


Figure 3.13: **Screening of potential eEF2K-KO clones. A, B:** *Bpm*I restriction enzyme digests of PCR amplification products of MDA-MB-231 and PC3 cells respectively were run on a 2% agarose gel. Potentially successfully eEF2K-KO Clones are outlined in red. U: undigested; D: digested. The data for part **B** was obtained by Ms. Danielle Fang.

Figure 3.14

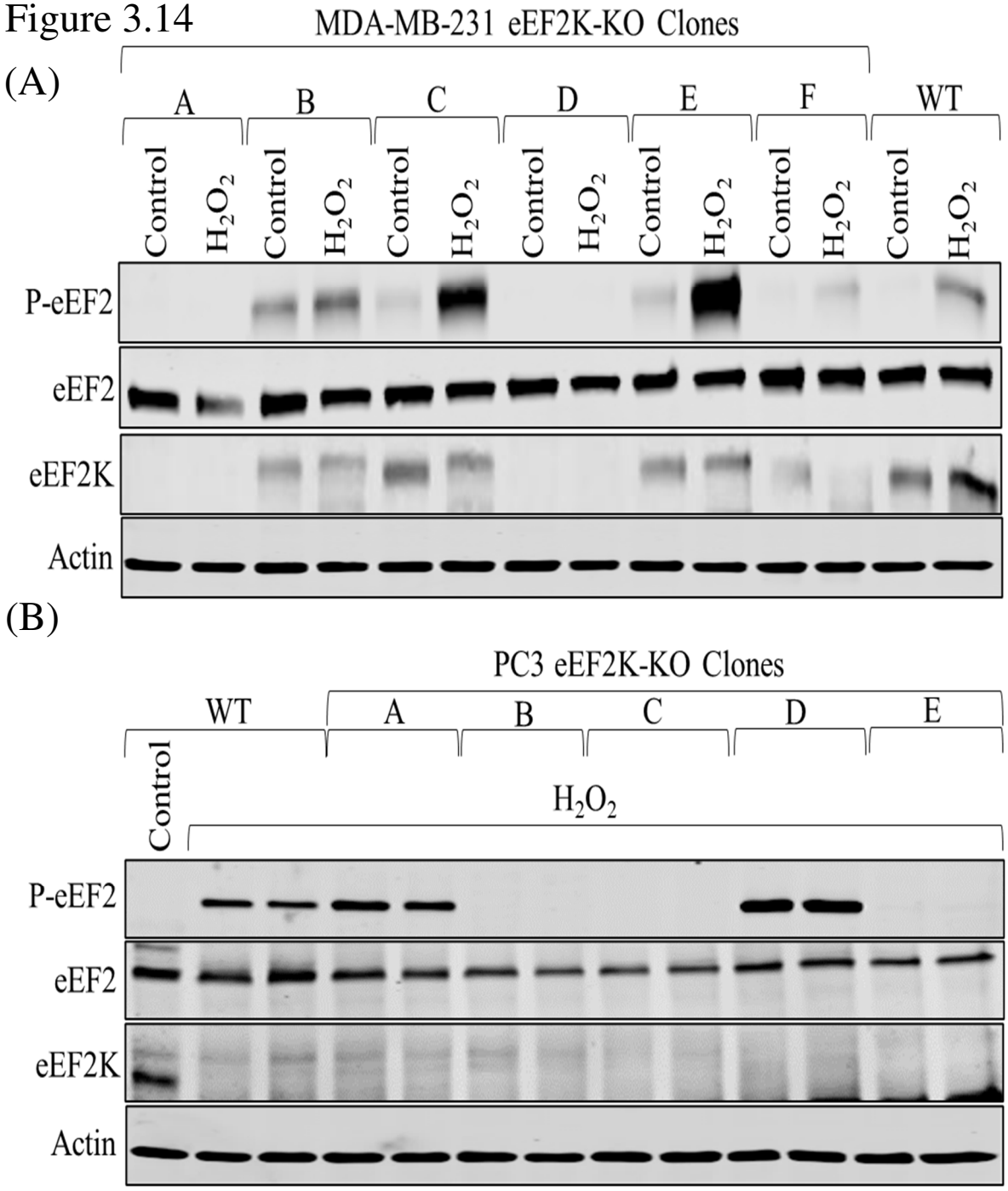


Figure 3.14: **Screening of potential eEF2K-KO clones. A, B:** MDA-MB-231 and PC3 cells respectively were treated with 3 mM H_2O_2 for 4 h in fully supplemented DMEM. The cells were lysed, the samples were run on (12.5%) SDS-PAGE and analysed by immunoblot for the indicated proteins or phosphoproteins. The PC3 western blot shows biological replicates treated with H_2O_2. The data for part **B** was obtained by Ms. Danielle Fang.

The most promising eEF2K-KO clones were then sequenced and analysed using the Tracking of Indels by Decomposition (TIDE)[191] program. This program can compare the sequence between the WT and KO cells, considering the sgRNA sequence, and show what type of indels have occurred due to the Cas9 cut. The program can also show the percentage of aberrant signal in the sequence and the probability of which base pair is inserted if the Cas9 caused an insertion to occur. Looking at **Figure 3.15A** which compares the WT sequence to the KO #1 sequence of MDA-MB-231 cells, it can be seen that 32 % of the sequences contained a -1 (one base pair) deletion, while 40.4% contained a -2 (two base pairs) deletion. **Figure 3.15B** shows that after the expected cut site, the percentage of aberrant sequences increases drastically as expected if the Cas9 had cut where it should have done. **Figure 3.16A** shows MDA-MB-231 eEF2K-KO #2 has 48.9% of the sequence containing a -1 deletion, and 37.6% containing a +2 (two base pair) insertion. **Figure 3.16B** shows a very similar result to clone #1, with the aberrant sequences increasing after the expected cut site. **Figure 3.16C** shows that the probability of the insertions being two adenines is very high. **Figure 3.17A** shows an alignment of the sequences using the Benchling program. Vertical bars in the figure show the quality of the sequence. As expected, the sequence of the KO clones drastically decreases in quality around the cut site, further supporting the evidence that these are indeed eEF2K-KO cells. The sequencing also confirms the -1 deletion in KO #2. **Figure 3.17B** shows what happens to the eEF2K sequence after the indels shown in TIDE are input into Benchling. The STOP codon in exon 3 appeared due to the -1 deletion in KO #1 and #2. The STOP codons in exon 4 appeared due to the -2 deletion in KO #1 and the +2 insertion in KO #2.

Figure 3.15

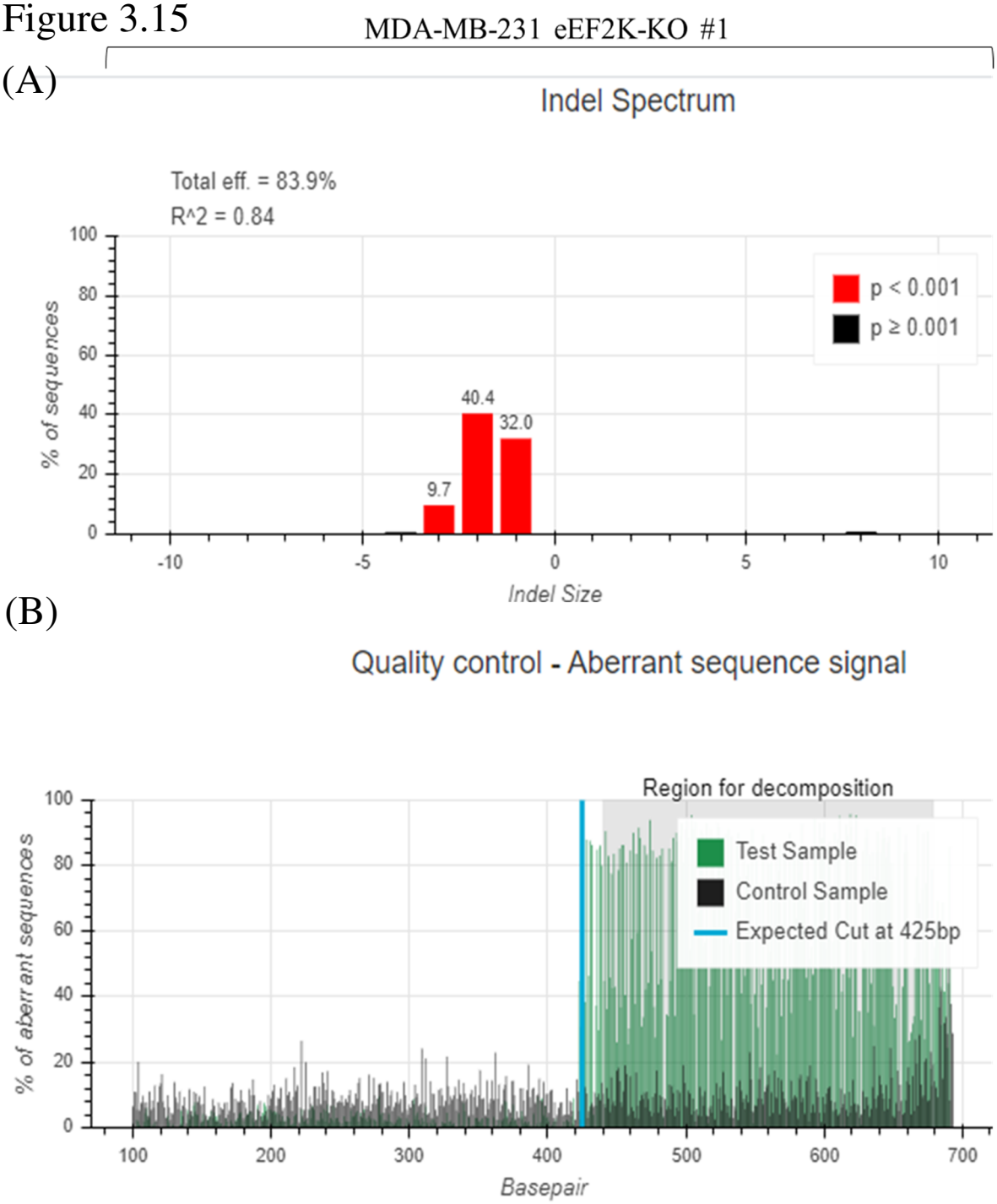
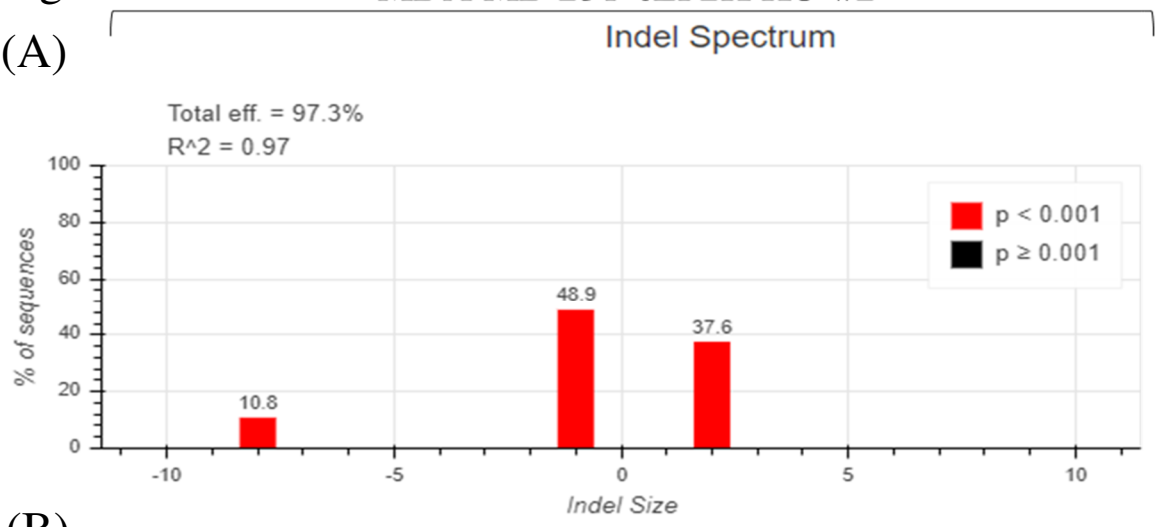


Figure 3.15: Confirmation of MDA-MB-231 eEF2K-KO Clone #1. WT and KO Clone #1 sequences of MDA-MB-231 cells were compared using the TIDE software[179]. **A:** The indel spectrum showing the percentage of sequence with indels. **B:** The percentage of aberrant sequence in WT vs KO #1 cells. The increase in aberrant sequence signal past the cut site indicates that the Cas9 cleavage was successful.

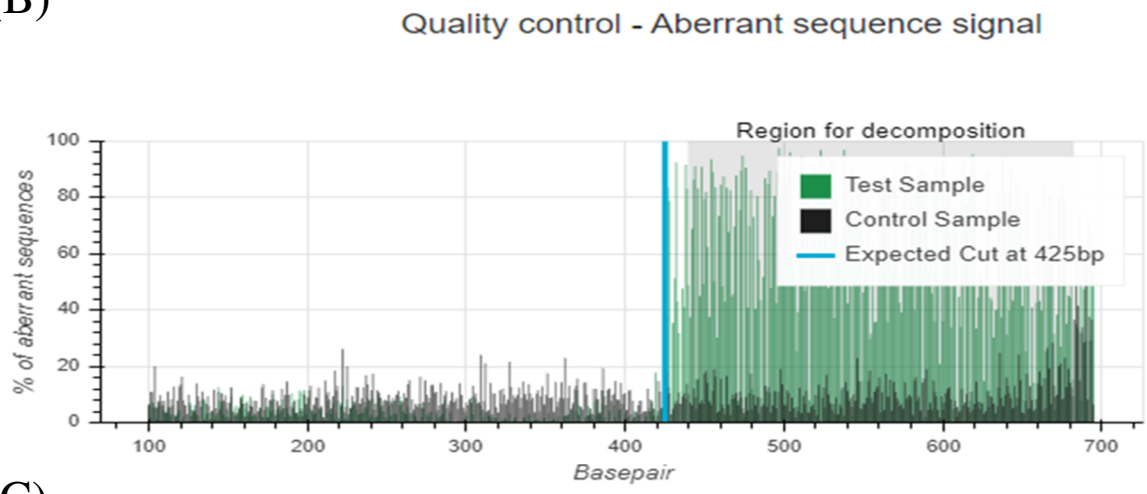
Figure 3.16

MDA-MB-231 eEF2K-KO #2

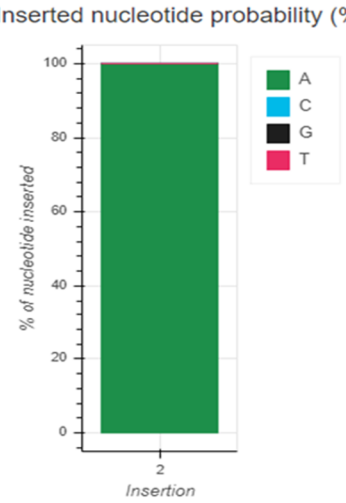
(A)



(B)



(C)



The original base at base position 0 (derived from the control sequence) is "C". Please note that point mutations are not taken into account when calculating the genome editing efficiency.

	A	C	G	T
2	100.0	0.0	0.0	0.0

Figure 3.16: Confirmation of MDA-MB-231 eEF2K-KO Clone #2. WT and KO Clone #1 sequences of MDA-MB-231 cells were compared using the TIDE software[179]. **A:** The indel spectrum showing the percentage of sequence with indels. **B:** The percentage of aberrant sequence in WT vs KO #2 cells. The increase in aberrant sequence signal past the cut site indicates that the Cas9 cleavage was successful. **C:** Probability of inserted nucleotides.

Figure 3.17

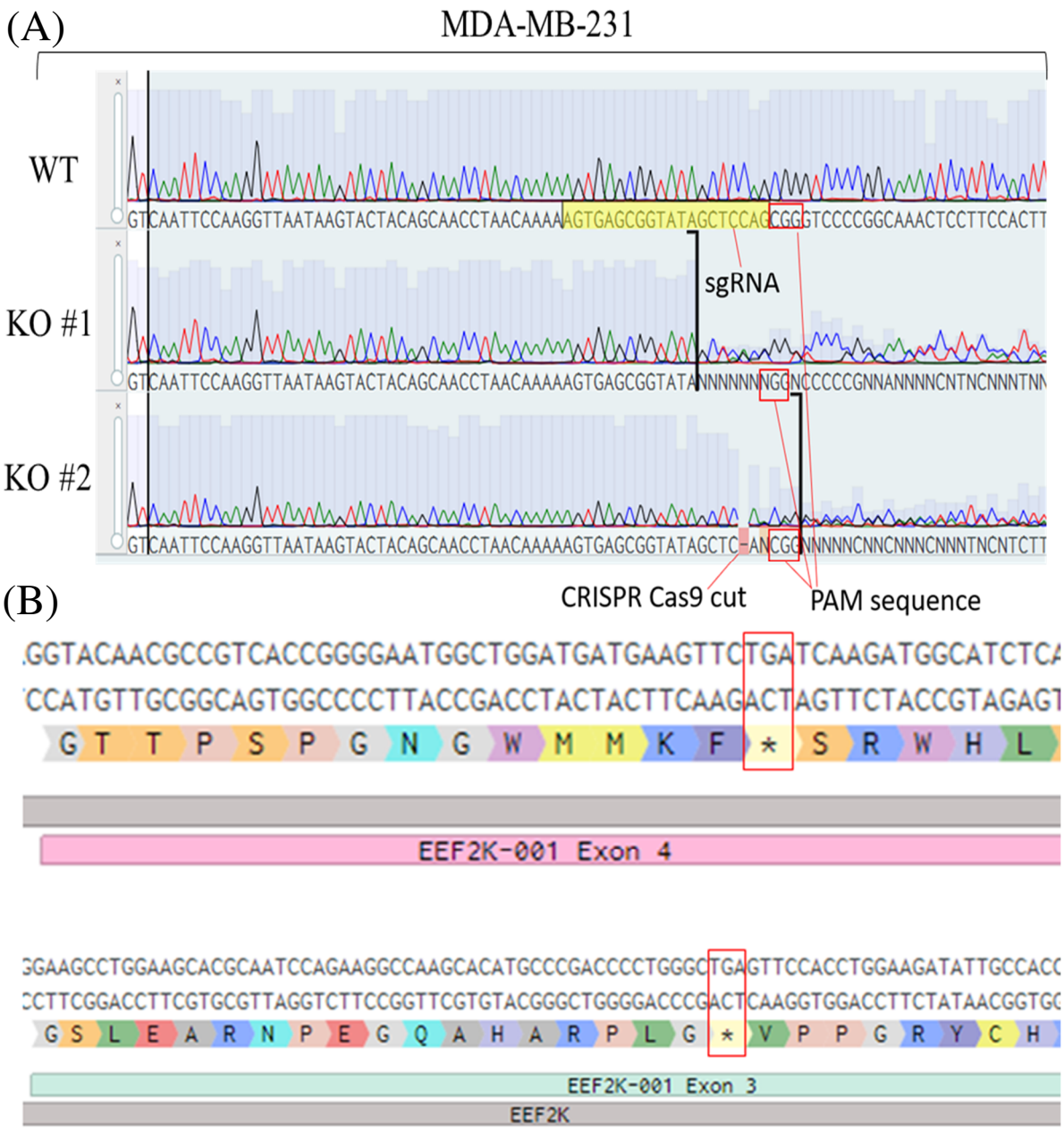


Figure 3.17: Confirmation of the MDA-MB-231 eEF2K-KO Clones via Benchling.

A: eEF2K exon 2 sequences of both eEF2K-KO clones of MDA-MB-231 cells were aligned against the wildtype eEF2K gene and analysed via Benchling[177]. Vertical bars show the quality of the sequence signal. **B**: Benchling diagrams showing the location of the STOP codons caused by CRISPR-Cas9 cuts, denoted with a star. Exon 4 STOP codons were caused by the -1 deletion and +2 insertion. Exon 3 STOP codon was caused by the -2 deletion.

Figure 3.18A shows that PC3 eEF2-KO #2 has a -1 deletion. **Figure 3.18B** confirms that the percentage of aberrant sequences increases after the expected cut site. PC3 eEF2K-KO #1 could not be analysed by TIDE due to problems with the sequencing quality but looking at **Figure 3.19A**, it has a large deletion, further confirming it is indeed an eEF2K knock-out. The Benchling alignment also confirms that KO #2 has a -1 deletion. **Figure 3.19B** shows the STOP codons created in exon 4 due to the -1 deletion in KO #2 and the large deletion in KO #1. Taken together, these data confirm that two clones of eEF2K-KO cells were successfully generated for both MDA-MB-231 and PC3 cells. These clones of cells were used for further experiments.

Figure 3.18

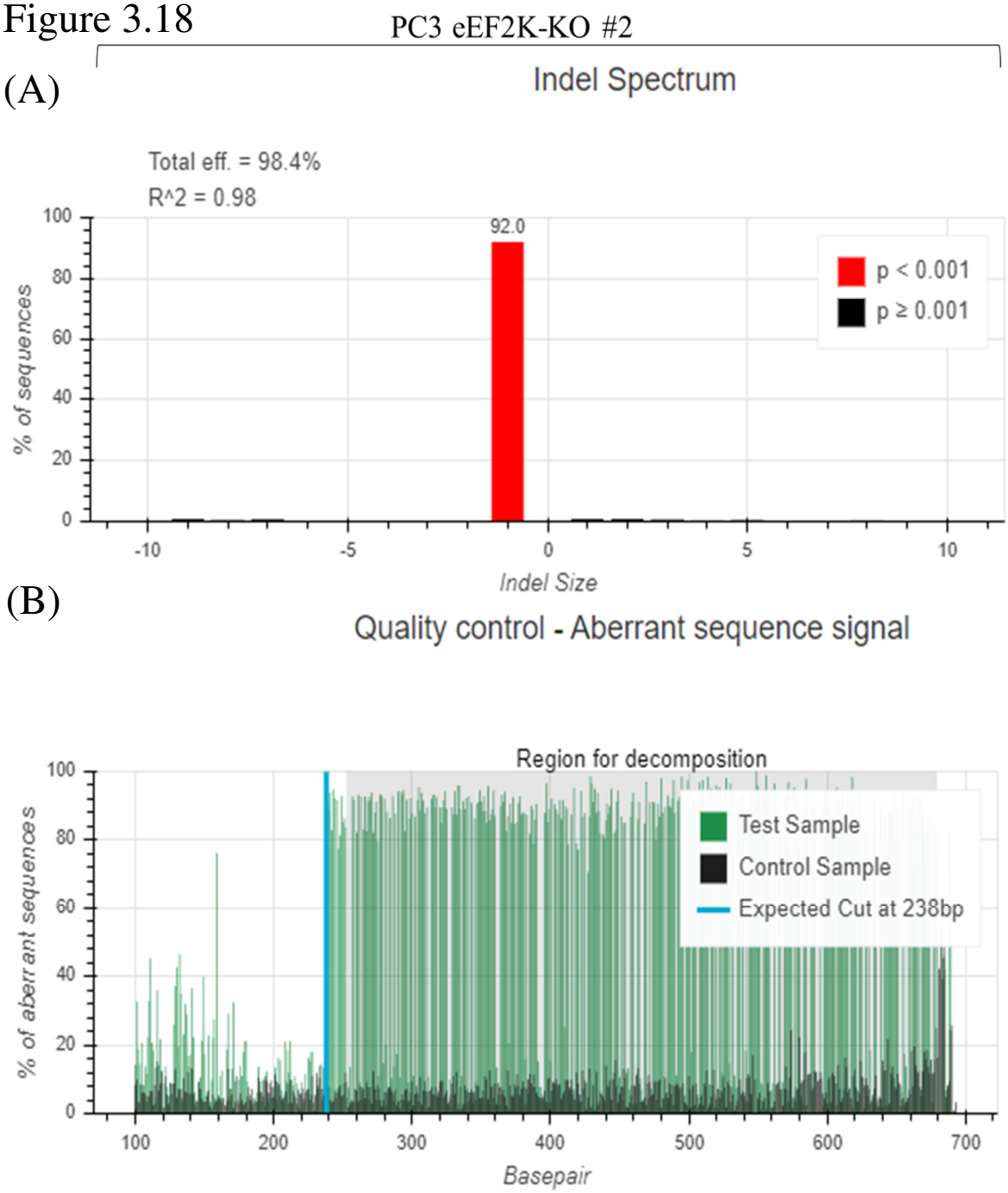


Figure 3.18: Confirmation of PC3 eEF2K-KO Clone #2. WT and KO Clone #2 sequences of PC3 cells were compared using the TIDE software[179]. **A:** The indel spectrum showing the percentage of sequence with indels. **B:** The percentage of aberrant sequence in WT vs KO #1 cells. The increase in aberrant sequence signal past the cut site indicates that the Cas9 cleavage was successful. The sequencing data was obtained by Ms. Danielle Fang.

Figure 3.19

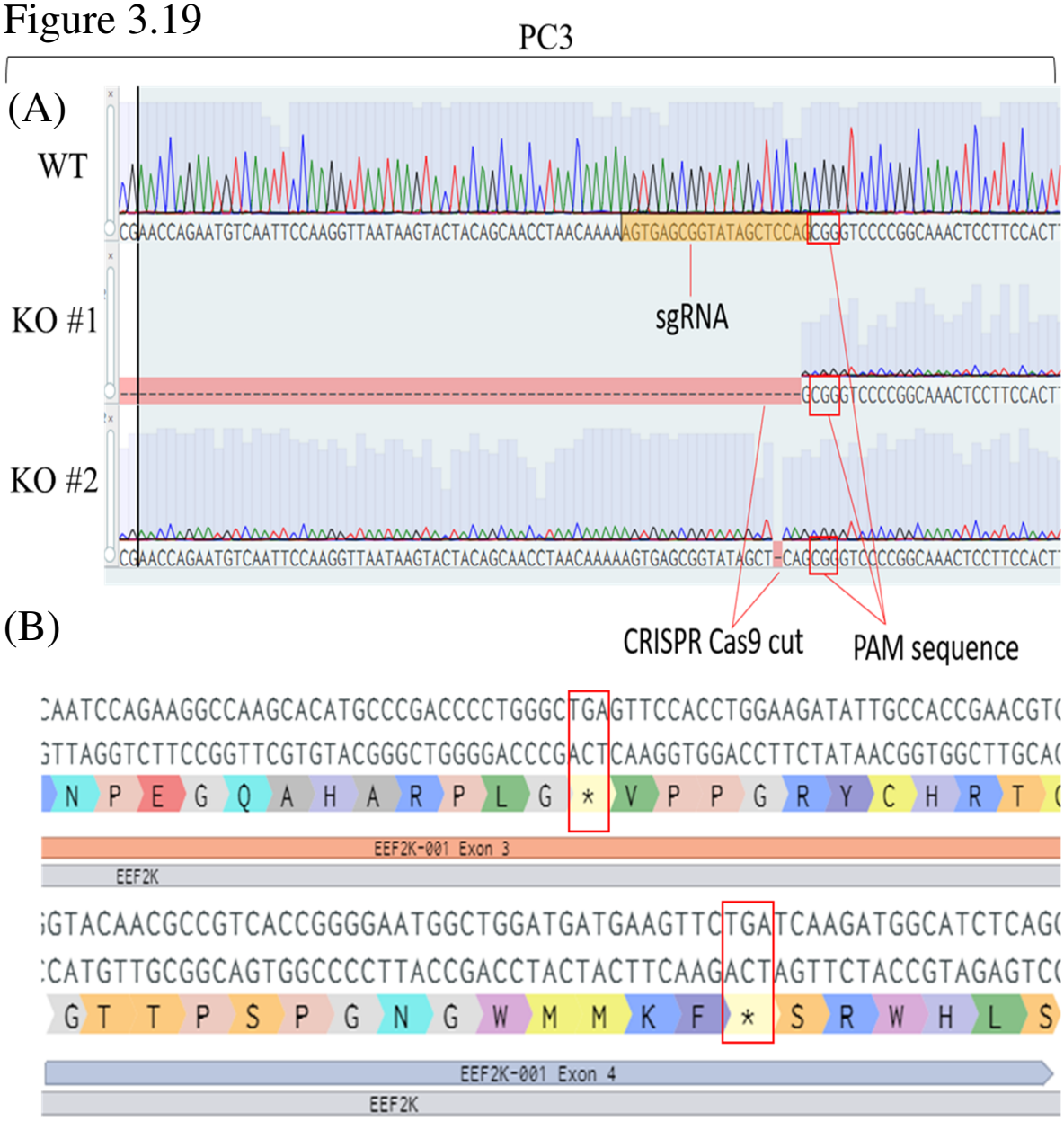


Figure 3.19: Confirmation of the eEF2K KO Clones via Benchling. A: eEF2K exon 2 sequences from both eEF2K-KO clones of PC3 cells were aligned against the wildtype eEF2K gene and analysed via Benchling[177]. Vertical bars show the quality of the sequence signal. **B**: Benchling diagrams showing the location of the STOP codons caused by CRISPR-Cas9 cuts, denoted with a star. Exon 3 STOP codons were caused by the large deletion in KO #1 and exon 4 STOP codons by the -1 deletions in KO #2. The sequencing data was obtained by Ms. Danielle Fang.

3.2.4 A lack or inhibition of eEF2K and autophagy leads to increased cell death of MDA-MB-231 and A549 cells under nutrient deprivation.

After the creation of eEF2K-KO cells using CRISRP-Cas9, the next step was to confirm the cell survival result obtained using JAN384. However, as JAN384 had potential side effects (increasing p62 and LC3-II as shown in **Figures 3.4B and 3.5A**), it was decided to continue experiments using the eEF2K inhibitor A484954 (A484 for short). Its' effectiveness to block eEF2K activity can be observed in **Figure 3.20A**. A much higher concentration (30 μM) than JAN384 (6 μM) had to be used but it was necessary to avoid JAN384's side effects. First, the Magic Red assay was used to compared eEF2K-WT and KO cell's cathepsin L activity (a measure of autophagy). It was shown that there was no significant difference in cathepsin L activity between WT and both eEF2K-KO clones, with BafA effectively reducing the Magic Red signal to negligible amounts in all three cell lines (**Figure 3.20B**).

A484 effectively blocked the phosphorylation of eEF2 in WT cells and did not lead to an increase in p62 or LC3-II levels, unlike JAN384 (**Figure 3.20C**). This shows it does not have the same off-target effect. The KO clones showed no phosphorylation of eEF2 and no eEF2K protein, as expected. Treatment with BafA caused an upregulation of p62 and LC3-II, again showing its' inhibition of autophagic flux. It is also of note that the phosphorylation of acetyl-CoA carboxylase (ACC) on Ser79 is increased under -Glc conditions. AMPK phosphorylates ACC under conditions of nutrient stress, when AMPK is active, which in turn leads to the phosphorylation and activation of eEF2K[47, 48, 192]. Interestingly, BafA increased the phosphorylation of eEF2 in -Glc conditions, although the p-ACC levels remained unchanged compared to control, suggesting this is not due to AMPK trying to compensate for the lack of autophagy. A separate experiment was also done to test for

JAN384's off-target effects in eEF2K-KO as well as JAN384's and A484's effects on KO cell survival. CellTox Green assays were performed on WT and eEF2K-KO cells in medium lacking glucose and pyruvate, treated with BafA and either JAN384 or A484. **Figures 3.21A and B** show that neither inhibitor significantly affected eEF2K-KO cell survival. However, **Figure 3.21C** shows that JAN384 does indeed raise p62 and LC3-II levels in both WT and eEF2K-KO cells compared to the controls of each cell line. This further puts into question what side effects JAN384 has to affect autophagy in such a way. Importantly, FLIP (cellular FLICE-like inhibitory protein) and MCL1 (induced myeloid leukemia cell differentiation factor Mcl-1) levels were not significantly altered in either of the KO clones compared to WT cells. These proteins are involved in the regulation of apoptosis. No changes in these proteins suggests that eEF2K affects cell survival by down-regulating protein synthesis, rather than affecting the abundance of proteins related to cell survival. It is also of note that BafA again increased p-eEF2. It can be seen that BafA decreased the phosphorylation on Ser 240/244 (p-S6) of ribosomal protein S6, a component of the 40S ribosomal subunit, important in regulating cell size, proliferation and glucose homeostasis[193]. This phosphorylation event is frequently used as a readout of mTORC1 activation, as it is a target of p-S6K1 which mTORC1 activates. As BafA decreased this phosphorylation, it can be inferred that it somehow interferes with mTORC1 signalling and therefore eEF2K activation, presumably thus increasing p-eEF2[45,194]. JAN384 also caused a decrease in p-S6, which could be a result of its possible off-target effect on autophagy, similar to the effects of the autophagy inhibitors BafA and CQ which also impair mTORC1 signalling, as shown by Fedele & Proud[194].

Figure 3.20

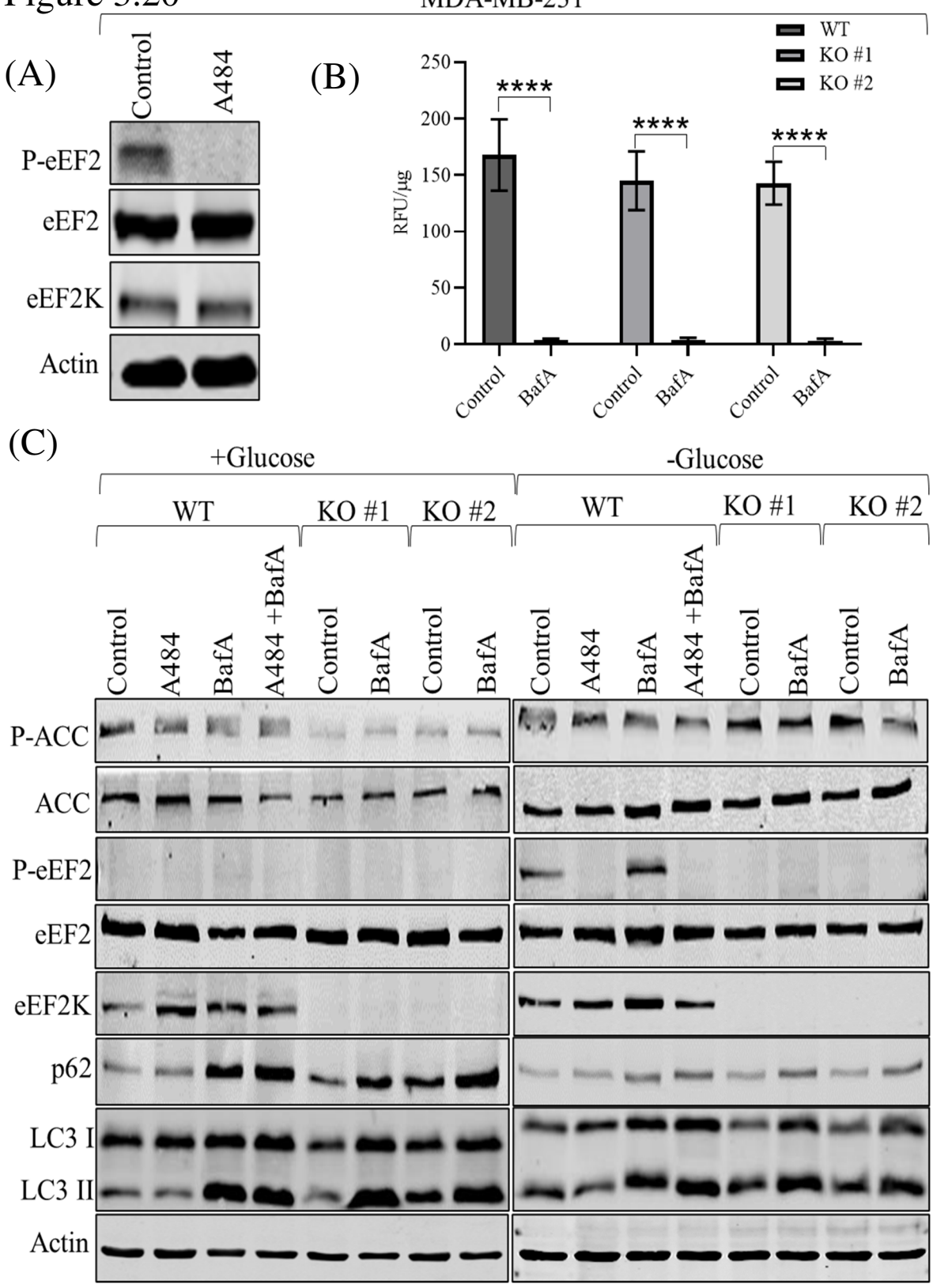

MDA-MB-231
(A)
Control
A484
P-eEF2
eEF2
eEF2K
Actin
(B)
WT
KO #1
KO #2
RFU/µg
250
200
150
100
50
0
****
****
****
Control
BafA
Control
BafA
Control
BafA
(C)
+Glucose
-Glucose
WT
KO #1
KO #2
WT
KO #1
KO #2
Control
A484
BafA
A484 +BafA
Control
BafA
Control
BafA
Control
A484
BafA
A484 +BafA
Control
BafA
Control
BafA
P-ACC
ACC
P-eEF2
eEF2
eEF2K
p62
LC3 I
LC3 II
Actin

Figure 3.20: **Bafilomycin A successfully inhibits autophagic flux in MDA-MB-231 WT and eEF2K-KO cells. A:** MDA-MB-231 WT cells were treated with 30 μM A484954 in +Glc conditions for 48 h, lysed, the lysates were run on 12.5% SDS-PAGE and analysed by immunoblot. **B:** Magic Red Assay – cells were treated in medium lacking Glc/Pyr for 24 h with or without 125 nM BafA. Error bars represent S.D. (n=3). The p-values were calculated using an unpaired, two-tailed, parametric T-test with Welch's correction. P-values: ****≤0.0001. RFU was normalised to total protein content. **C:** WT and eEF2K-KO cells were treated in medium lacking Glc/Pyr and with either 30 μM A484954, 125 nM BafA or both for 48 h. The cells were lysed, the samples were run on either (16%) SDS-PAGE for low molecular weight proteins or (12.5%) SDS-PAGE for others, followed by analysis via immunoblot. The western blot images are representative of n=3.

Figure 3.21

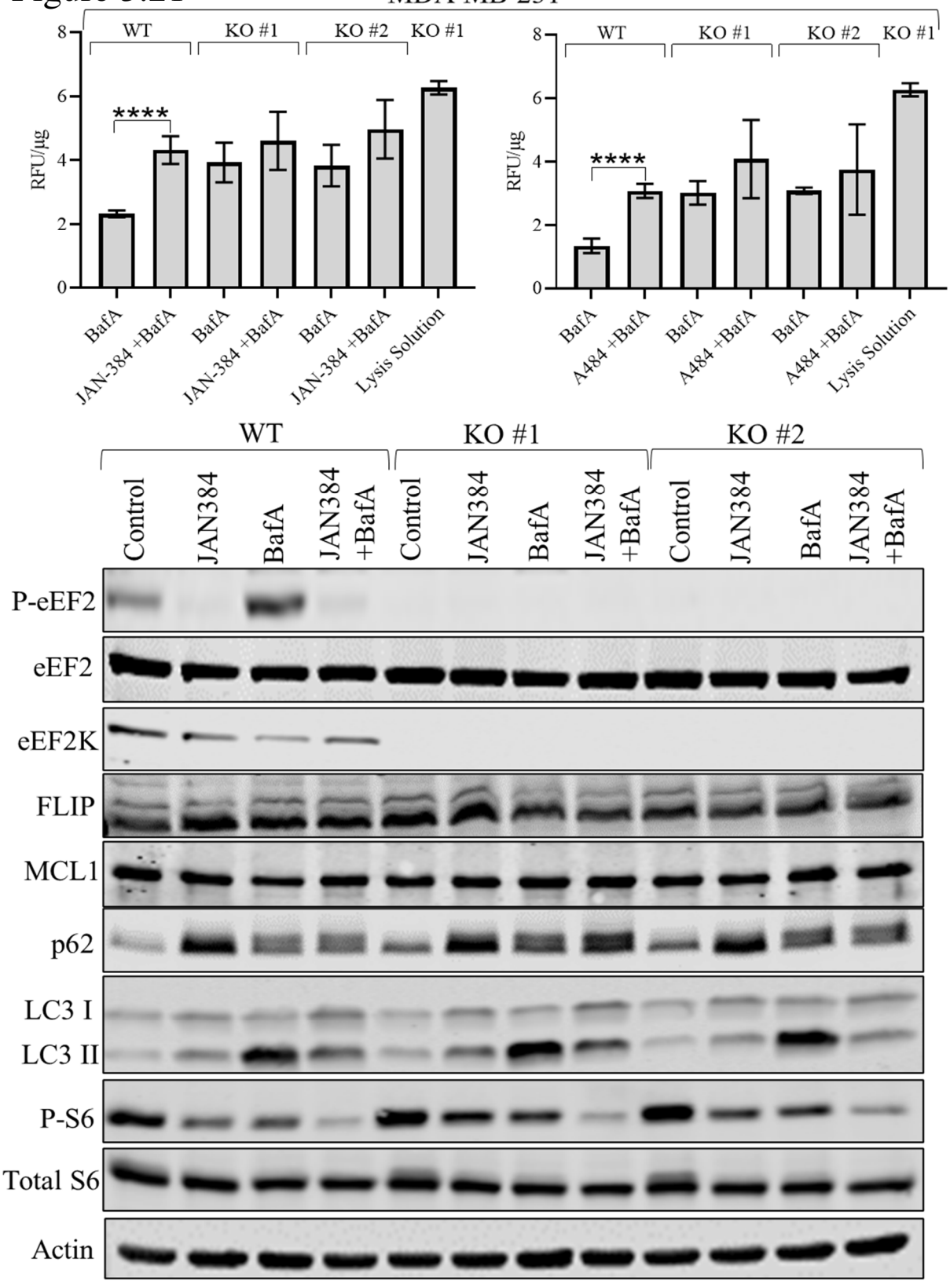

MDA-MB-231
WT
KO #1
KO #2
KO #1
RFU/µg
****
BafA
JAN-384 +BafA
Lysis Solution
A484 +BafA
Control
JAN384
JAN384 +BafA
P-eEF2
eEF2
eEF2K
FLIP
MCL1
p62
LC3 I
LC3 II
P-S6
Total S6
Actin

Figure 3.21: **JAN384 and A484954 do not significantly alter cell survival of eEF2K-KO MDA-MB-231 cells; JAN384 increases p62 and LC3 II levels. A, B:** MDA-MB-231 WT and eEF2K-KO cells were treated in medium without Glc/Pyr. With 125 nM BafA and either 6 µM JAN384 (**A**) or 30 µM A484954 (**B**) for 48 h. For the Lysis Solution control, 1 µl of Lysis Solution was added to wells of KO #1 cells grown in high glucose medium for 48 h and incubated for 30 min prior to fluorescence measurement. The p-values were calculated using Two-Way ANOVA with the Tukey multiple comparisons test. P-values: ****≤0.0001. RFU was normalised to total protein content. **C:** WT and eEF2K-KO cells were treated with either 6 µM JAN384, 125 nM BafA or both in +Glc conditions for 48 h, lysed, the lysates were run on (16%) SDS-PAGE for low molecular weight proteins or (12.5%) SDS-PAGE for others, followed by analysis via immunoblot. The western blot image is representative of n=3.

Looking at the +Glc conditions in the CellTox Green Assay seen **Figure 3.22A**, it can be observed that A484 does not increase cell cytotoxicity, just like JAN384 and the eEF2K-KO clones. BafA significantly increased cell death under +Glc conditions, however A484 did not further increase this, as expected. This is very similar to JAN384's effect under +Glc conditions. The two eEF2K-KO clones showed a 2.6-fold increase in cell death when treated with BafA in +Glc conditions. This could be attributed to the fact that these cells do not possess any eEF2K protein, whereas WT cells have had eEF2K inhibited for only 48 h. Looking at the -Glc conditions, it can be seen that A484 or BafA individually did not further increase cell death in WT cells compared to control. However, when cells are treated with both compounds together, cell death was increased 2-fold. This was also seen in both KO clones. Both KO clone showed no significant difference in cell death compared to WT cells, however, treatment with BafA greatly increased their cytotoxicity, further supporting the original data found in WT cells. CellTox Green images to accompany this data are shown in **Figure 3.23**. This data further supports the data already gathered using JAN384 and BafA on WT MDA-MB-231 cells.

To further augment the cell death data, a combined cell death and viability assay was used. This assay involved treating the cells in the same way as in the CellTox Green Assay, but with the addition of propidium iodide and Calcein-AM. Propidium iodide acts in a similar way to CellTox Green dye. It cannot enter intact cell membranes but once the membrane is ruptured when the cells start dying, it can bind the DNA and fluoresce[195]. Calcein-AM, on the other hand, can enter viable cells whereupon intracellular esterases cleave the acetoxymethyl (AM) ester group from it, leaving the cell impermeable and fluorescent Calcein dye[196].

The propidium iodide data (**Figure 3.22B**) are very similar to the CellTox Green data. Namely, treatment with BafA in +Glc conditions increased cell death for both eEF2K-KO clones even further than WT cells. In -Glc conditions, treatment with A484 or BafA alone did not further increase cell death compared to control. Only when both inhibitors were used concurrently, was cell death further increased (more than 2-fold). Treating KO cells with BafA under these conditions also led to significantly increased cell-death.

The Calcein-AM data mirrors the CellTox Green and propidium iodide assays (**Figure 3.24**; Calcein-AM images in **Figure 3.25.** Viable cells are stained green). In +Glc conditions, BafA lowered cell viability, while A484 did not significantly alter it. The addition of BafA to KO cells lowered the viability even further than in WT cells. Under -Glc conditions, A484 or BafA did not alter cell viability significantly from control but when used together, cell viability was decreased 3.5-fold. For the KO clones, cell viability was not decreased under -Glc control conditions compared to WT, again showing the cells possess a survival pathway distinct from eEF2K, but the addition of BafA decreased it to similar levels as WT cells treated with A484 and BafA at the same time. Taken together, these data further support the theory that autophagy and eEF2K are vital but separate processes that MDA-MB-231 cells used to survive nutrient deprivation.

Figure 3.22

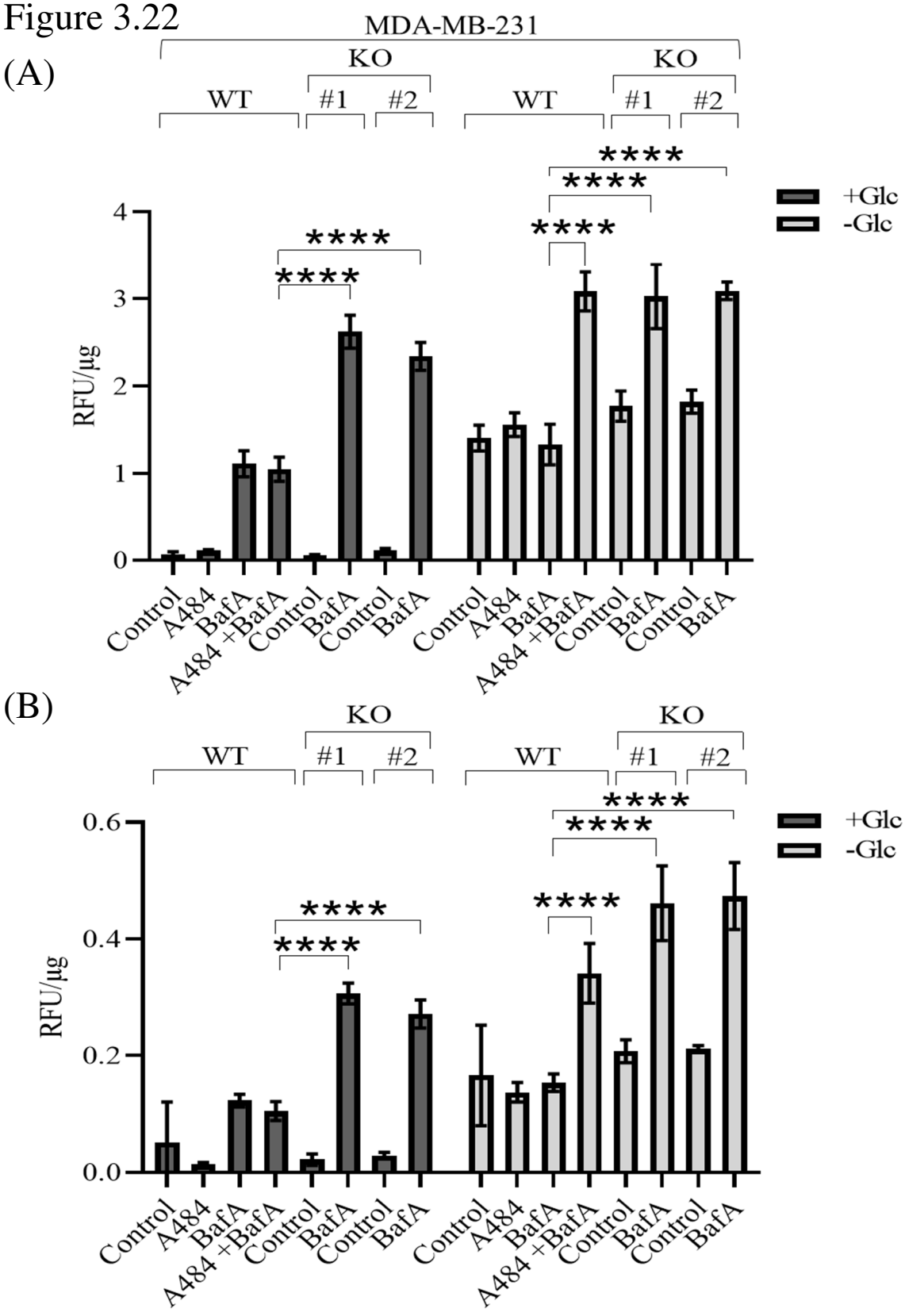

(A)
MDA-MB-231
WT
KO
#1
#2
WT
KO
#1
#2
****
****
****
****
****
+Glc
-Glc
RFU/µg
0
1
2
3
4
Control
A484
BafA
A484 +BafA
Control
BafA
Control
BafA
Control
A484
BafA
A484 +BafA
Control
BafA
Control
BafA
(B)
WT
KO
#1
#2
WT
KO
#1
#2
****
****
****
****
****
+Glc
-Glc
RFU/µg
0.0
0.2
0.4
0.6
Control
A484
BafA
A484 +BafA
Control
BafA
Control
BafA
Control
A484
BafA
A484 +BafA
Control
BafA
Control
BafA

Figure 3.22: A combination of eEF2K inhibition or knock-out and autophagy inhibition leads to increased cell death under nutrient deprived conditions than when either pathway is inhibited individually in MDA-MB-231 cells. MDA-MB-231 cells were treated for 48 h with 30 μM A484954, 125 nM BafA or a combination in medium with or without Glc/Pyr prior to measuring cell cytotoxicity via CellTox Green **(A)** and propidium iodide **(B).** 10 μM propidium iodide was added 1 h prior to measurement. Error bars represent S.D. (n=3). The p-values were calculated using Two-Way ANOVA with the Tukey multiple comparisons test. P-values: ****≤0.0001. RFU was normalised by total protein content.

Figure 3.23

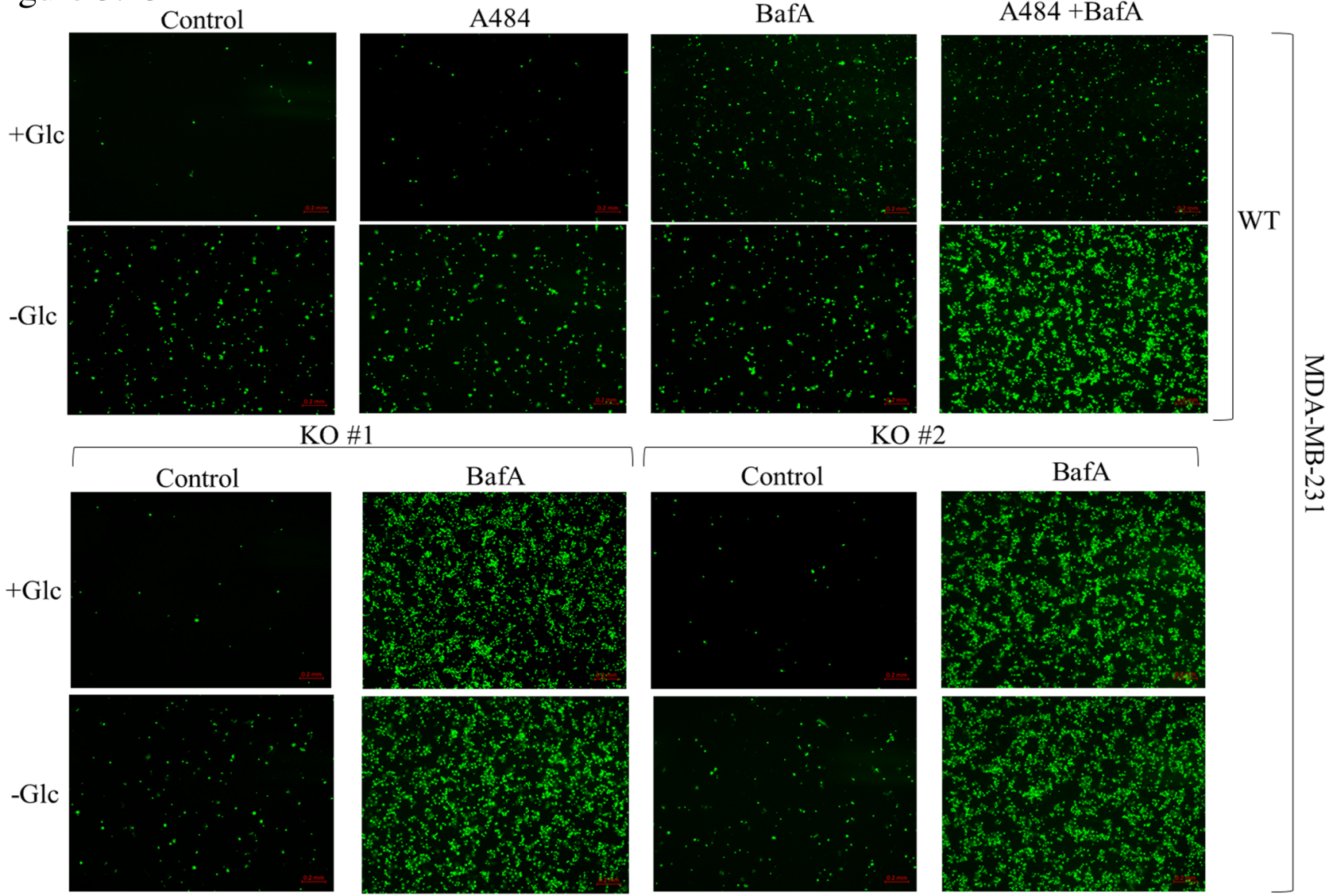

Control
A484
BafA
A484 +BafA
+Glc
-Glc
WT
KO #1
KO #2
Control
BafA
Control
BafA
+Glc
-Glc
MDA-MB-231

Figure 3.23: A combination of eEF2K inhibition or knock-out and autophagy inhibition leads to increased cell death under nutrient deprived conditions than when either pathway is inhibited individually in MDA-MB-231 cells (CellTox Green images). MDA-MB-231 WT and eEF2K-KO cells were treated for 48 h with 30 μM A484954, 125 nM BafA or a combination in medium with or without Glc/Pyr with CellTox Green Dye prior to taking images with a GFP filter. Images of Cell-Tox Green fluorescence were taken using the GFP filter on a Zeiss Axio Vert.A1 200 microscope with the 4X magnifying lens. Each image is representative of 15 images total from 3 biological replicates.

Figure 3.24

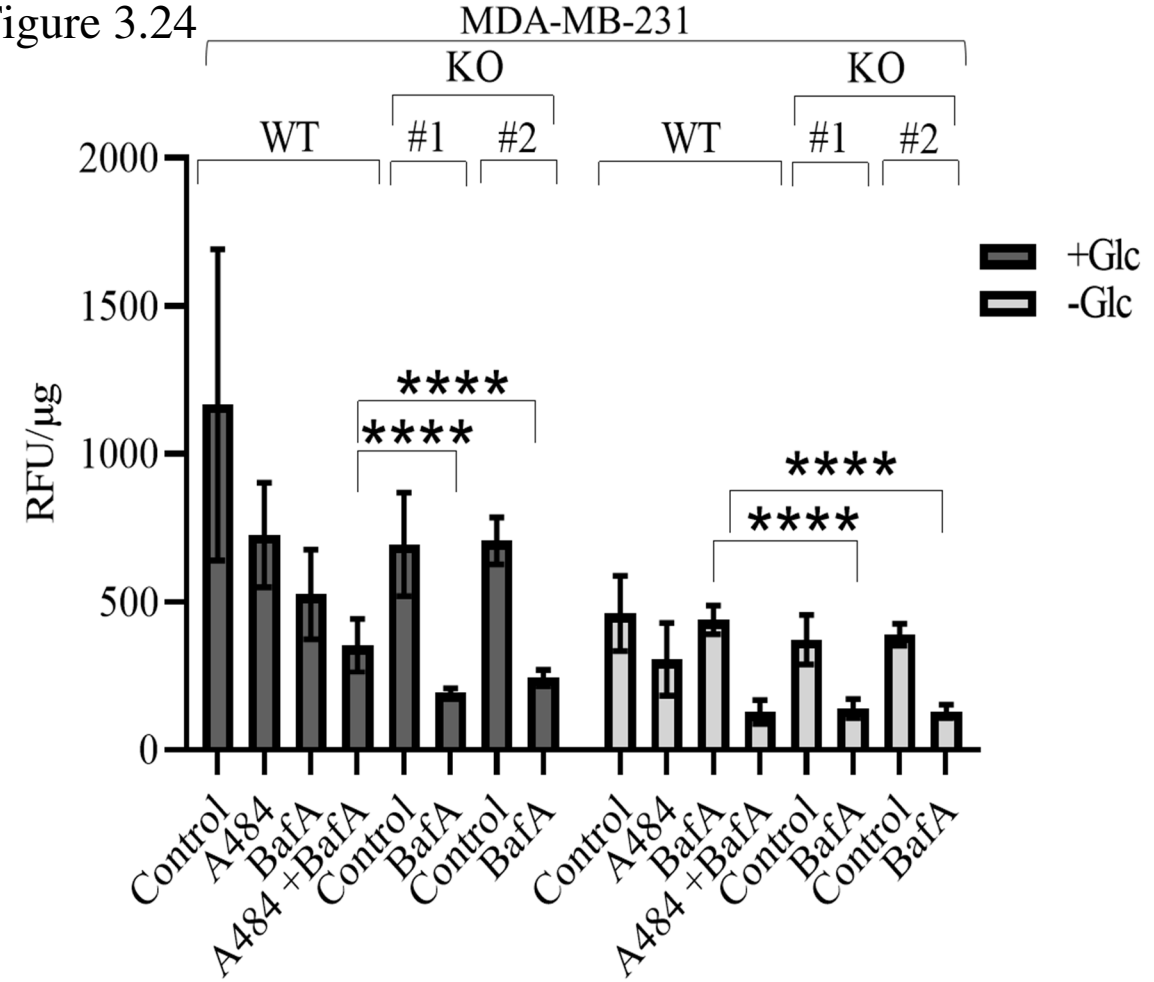


Figure 3.24: A combination of eEF2K inhibition or knock-out and autophagy inhibition leads to decreased cell viability under nutrient deprived conditions than when either pathway is inhibited individually in MDA-MB-231 cells. Calcein-AM Assay – MDA-MB-231 cells were treated for 48 h with 30 µM A484954, 125 nM BafA or a combination in medium with or without Glc/Pyr. Calcein-AM was added 1 h prior to measurement to a final concentration of 1µM. Error bars represent S.D. (n=3). The p-values were calculated using Two-Way ANOVA with the Tukey multiple comparisons test. P-values: ****≤0.0001. RFU was normalised by total protein content.

A549 cells were also tested under the same conditions, using IPTG to silence eEF2K. Additionally, A549 cells were also tested using medium without any glutamine, glucose and pyruvate (-Gln), removing all three major carbon sources that are required for glycolysis or the citric acid cycle. MDA-MB-231 cells that were tested in -Gln conditions died too quickly for any useful data to be obtained. To test the effectiveness of eEF2K silencing and autophagy inhibition in -Gln conditions, a western blot was run after 48 h of treatment (**Figure 3.5 B**). IPTG-induced silencing of eEF2K effectively removed eEF2K protein itself and prevented the phosphorylation of eEF2 in almost all the conditions. The one condition where the eEF2K silencing was not fully effective was in -Glc, when cells were treated with BafA. Here p-eEF2 is still present (although lower than in non-silenced cells), although eEF2K is absent. Under the same conditions, p-ACC was lower, showing that this increase in p-eEF2 is not due to the activation of AMPK. BafA significantly increased p62 and LC3-II levels, confirming autophagic flux is inhibited in these cells.

Figure 3.25

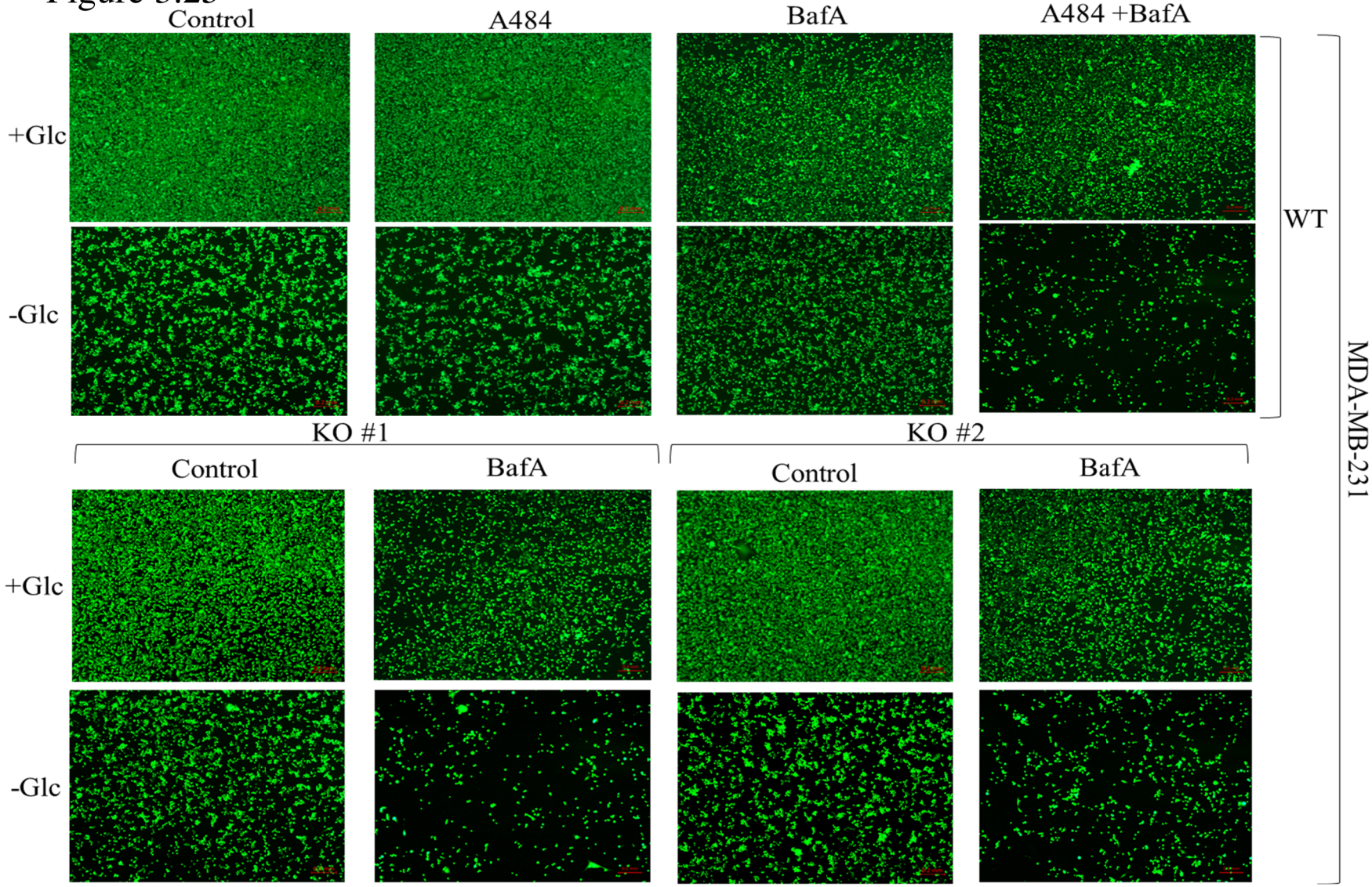

Control
A484
BafA
A484 +BafA
+Glc
-Glc
WT
KO #1
KO #2
Control
BafA
Control
BafA
+Glc
-Glc
MDA-MB-231

Figure 3.25: A combination of eEF2K inhibition or knock-out and autophagy inhibition leads to decreased cell viability under nutrient deprived conditions than when either pathway is inhibited individually in MDA-MB-231 cells (Calcein-AM images). MDA-MB-231 WT and eEF2K-KO cells were treated for 48 h with 30 µM A484954, 125 nM BafA or a combination in medium with or without Glc/Pyr. Calcein-AM dye (1µM final) was added 1 h prior to taking images with a GFP filter. Images of Calcein-AM fluorescence were taken using the GFP filter on a Zeiss Axio Vert.A1 200 microscope with the 4X magnifying lens. Each image is representative of 15 images total from 3 biological replicates.

Next, A549 cells were tested using CellTox Green and the propidium iodide/calcein-AM assay (**Figure 3.26A and B**; CellTox Green images are in **Figure 3.27**). The results are similar between the CellTox Green and the propidium iodide assay and follow the trend shown for MDA-MB-231 cells. Treatment of cells with BafA in +Glc conditions raised cytotoxicity but silencing eEF2K had no effect on it. In -Glc conditions, eEF2K silencing alone did not increase cell death compared to control. Unlike in MDA-MB-231 cells, BafA treatment of A549 cells in -Glc conditions did increase cell death further. However, the cell death caused by silencing of eEF2K and treatment with BafA was double that of treatment with BafA alone. Interestingly, under -Gln conditions, silencing of eEF2K alone led to a 1.5-fold increase in cell death compared to the -IPTG control. This suggests that under conditions of extreme stress, autophagy alone cannot cope to ensure cell survival and eEF2K is even more necessary for this. Silencing eEF2K and blocking autophagy together under these conditions further increased cell death, but not to the same extent as under -Glc conditions. This is likely because too many cells have died under these conditions to show a larger difference.

The results from the Calcein-AM assay mirrored the results of the cell death assays (**Figure 3.28**; images are in **Figure 3.29**). Silencing of eEF2K alone did not decrease cell viability but treatment with BafA of silenced cells further decreased cell viability. eEF2K silencing had a larger effect in -Gln conditions, where it alone further decreased cell viability. The addition of BafA to eEF2K silenced cells under -Gln conditions further decreased cell viability.

Overall, the data from MDA-MB-231 and A549 cells show that autophagy and eEF2K act as separate and complementary pathways to assist these cells in surviving nutrient deprivation.

Figure 3.26

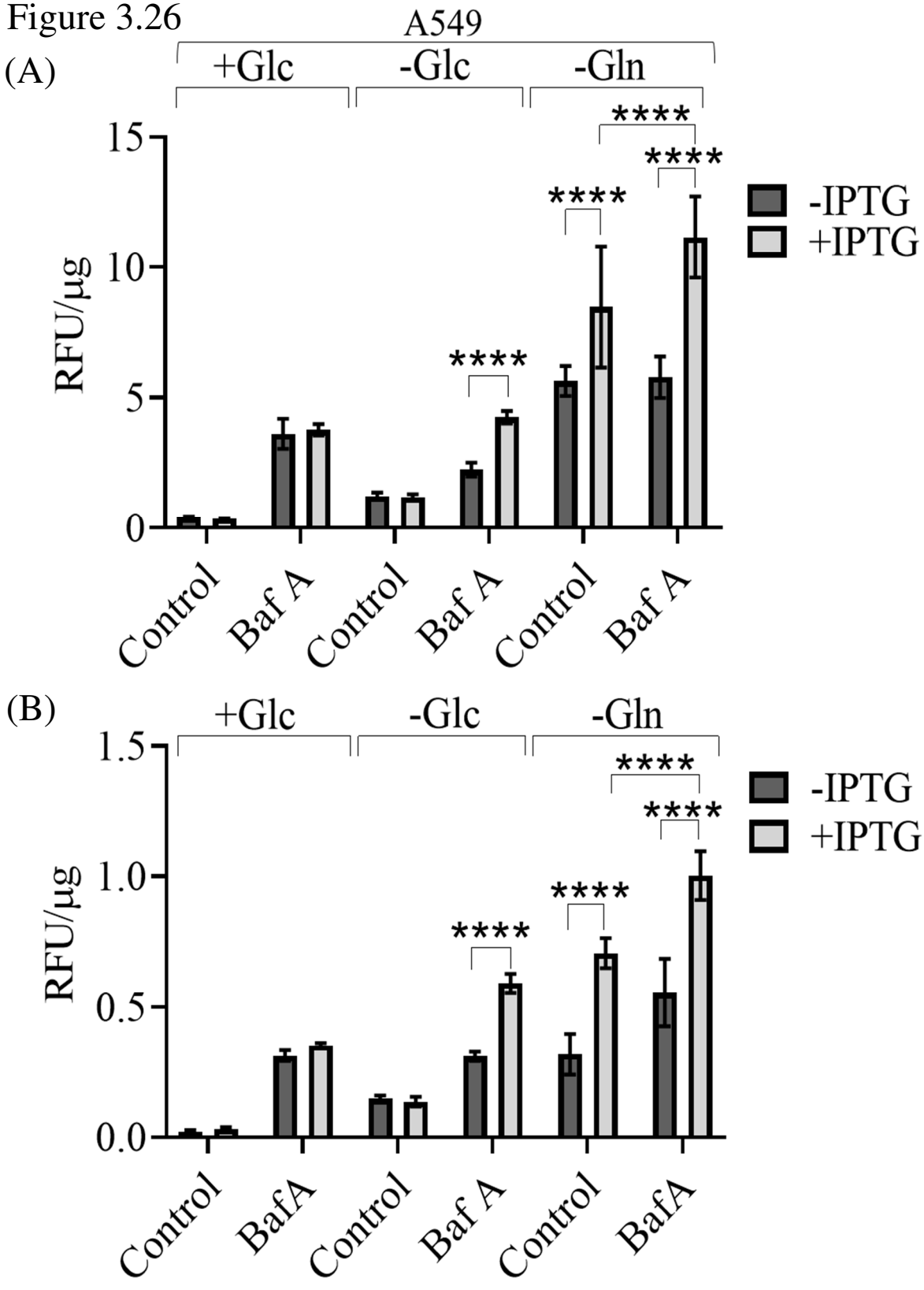

A549
(A)
+Glc
-Glc
-Gln
RFU/µg
15
10
5
0
****
****
****
****
-IPTG
+IPTG
Control
Baf A
Control
Baf A
Control
Baf A
(B)
+Glc
-Glc
-Gln
RFU/µg
1.5
1.0
0.5
0.0
****
****
****
****
-IPTG
+IPTG
Control
BafA
Control
Baf A
Control
BafA

Figure 3.26: A combination of eEF2K inhibition or knock-down and autophagy inhibition leads to increased cell death under nutrient deprived conditions than when either pathway is inhibited individually in A549 cells. A549 cells were treated for 48 h with or without 125 nM BafA in medium with or without Glc/Pyr or Glc/Pyr/Gln. eEF2K was silenced via addition of IPTG (1 mM final) for 5 days prior to the experiment. Cell death was measured via CellTox Green **(A)** and propidium iodide **(B).** 10 µM propidium iodide was added 1 h prior to measurement. Error bars represent S.D. (n=3). The p-values were calculated using Two-Way ANOVA with the Tukey multiple comparisons test. P-values: ****≤0.0001. RFU was normalised by total protein content.

Figure 3.27

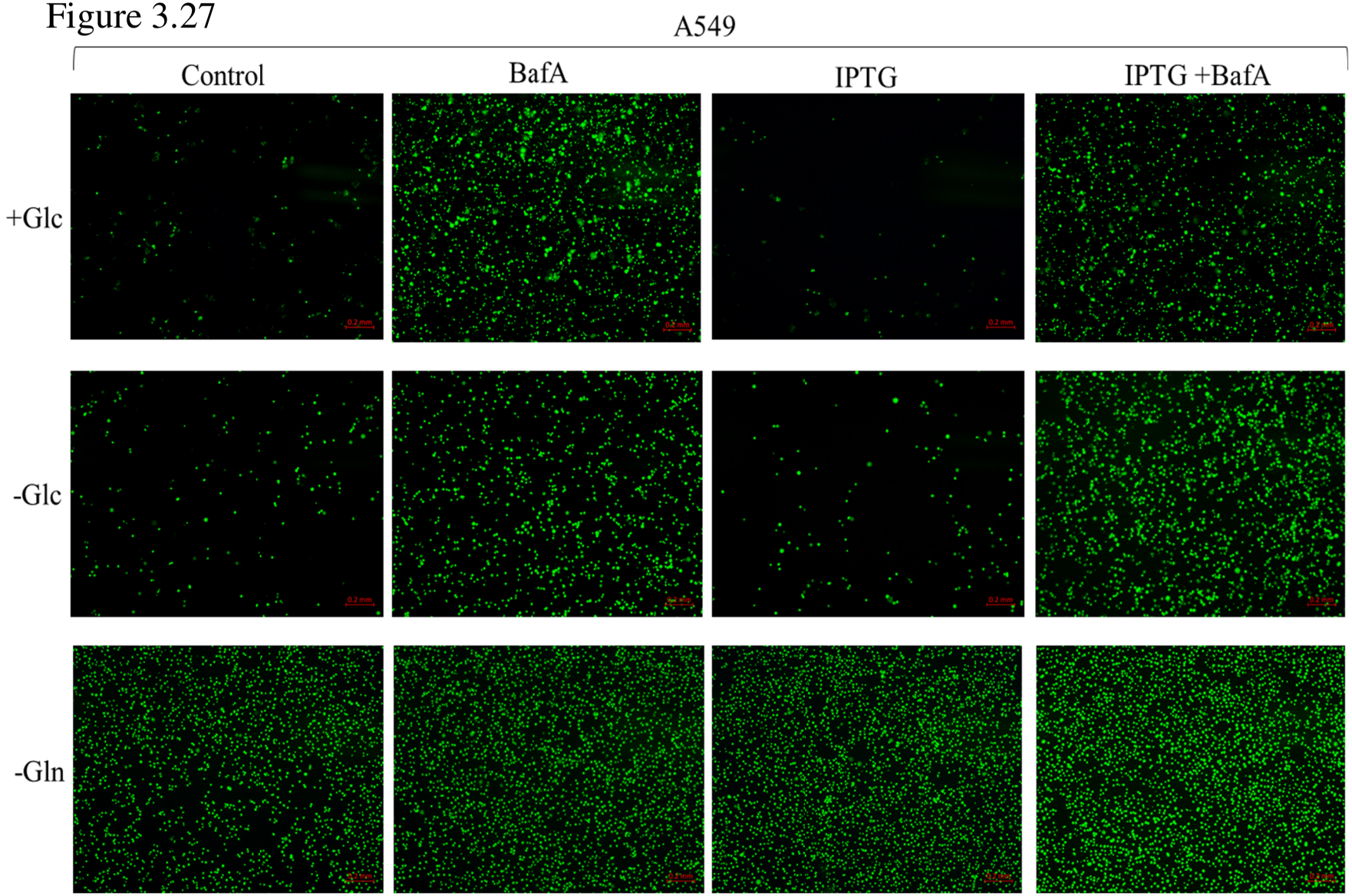


Figure 3.27: A combination of eEF2K inhibition or knock-down and autophagy inhibition leads to increased cell death under nutrient deprived conditions than when either pathway is inhibited individually in A549 cells (CellTox Green images). A549 cells were treated for 48 h with or without 125 nM BafA in medium with or without Glc/Pyr or Glc/Pyr/Gln. eEF2K was silenced via addition of IPTG (1 mM final) for 5 days prior to the experiment. Images of CellTox Green fluorescence were taken using the GFP filter on a Zeiss Axio Vert.A1 200 microscope with the 4X magnifying lens. Each image is representative of 15 images total from 3 biological replicates.

Figure 3.28

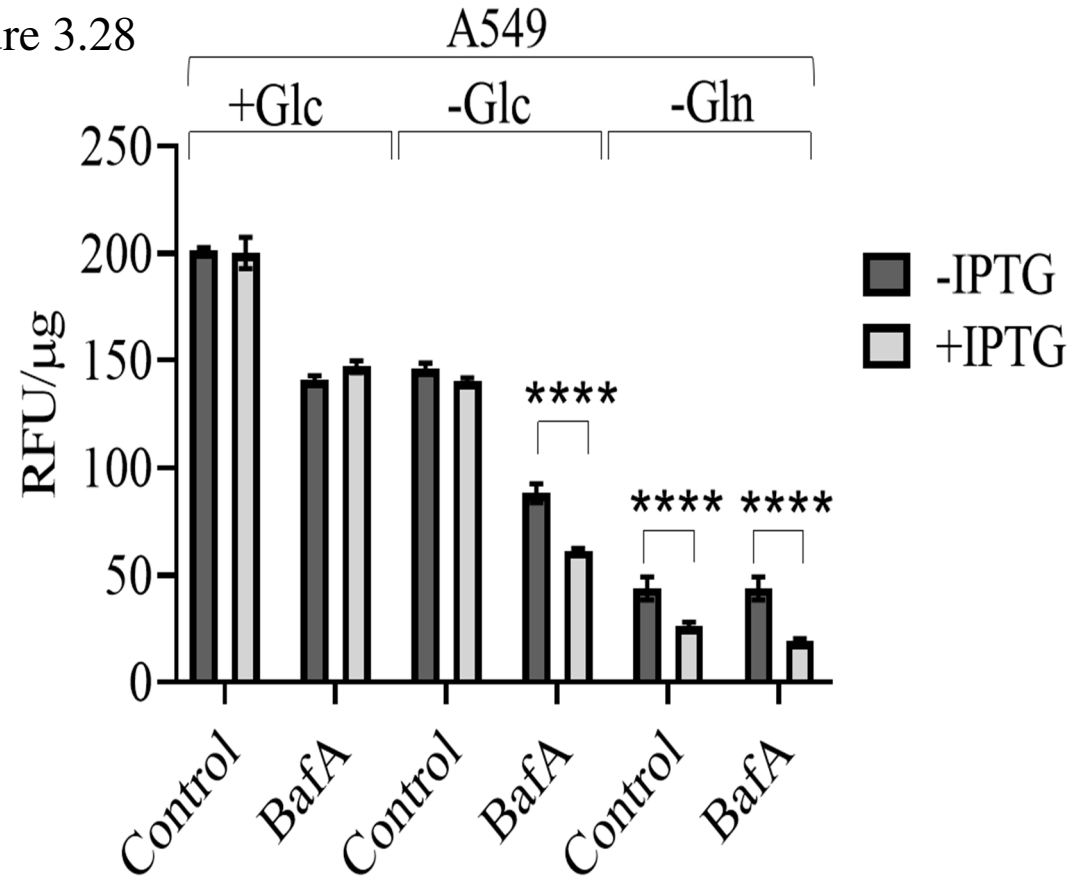


Figure 3.28: A combination of eEF2K inhibition or knock-down and autophagy inhibition leads to decreased cell viability under nutrient deprived conditions than when either pathway is inhibited individually in A549 cells. Calcein-AM Assay - A549 cells were treated for 48 h with or without 125 nM BafA in medium with or without Glc/Pyr or Glc/Pyr/Gln. eEF2K was silenced via addition of IPTG (1 mM final) for 5 days prior to the experiment. Cell viability was measured by adding 1 µM Calcein-AM 1 h prior to measurement on a plate reader. Error bars represent S.D. (n=3). The p-values were calculated using Two-Way ANOVA with the Tukey multiple comparisons test. P-values: ****≤0.0001. RFU was normalised by total protein content.

Figure 3.29

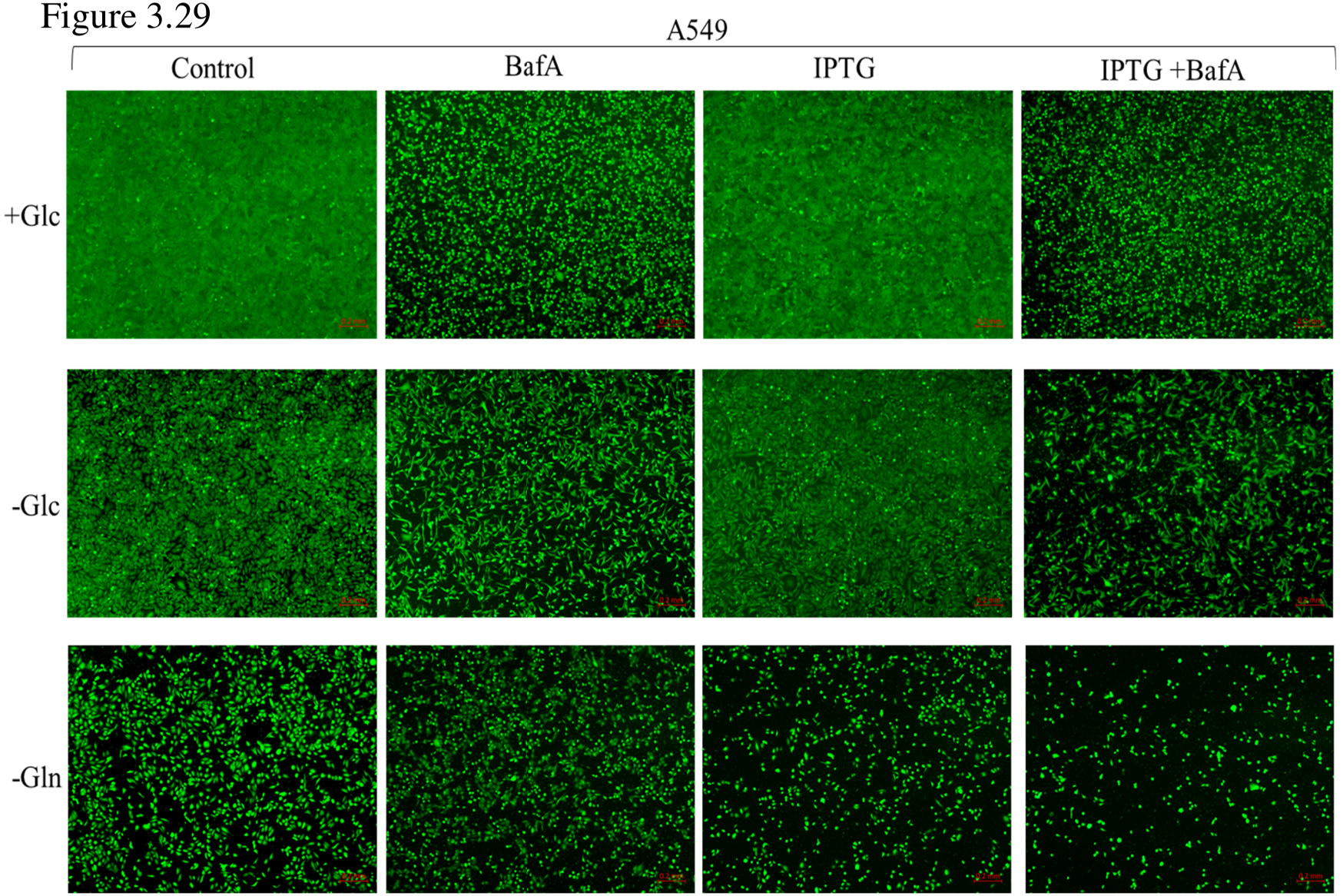


Figure 3.29: A combination of eEF2K inhibition or knock-down and autophagy inhibition leads to decreased cell viability under nutrient deprived conditions than when either pathway is inhibited individually in A549 cells (Calcein-AM images). A549 cells were treated for 48 h with or without 125 nM BafA in medium with or without Glc/Pyr or Glc/Pyr/Gln. eEF2K was silenced via addition of IPTG (1 mM final) for 5 days prior to the experiment. Calcein-AM dye (1µM final) was added 1 h prior to taking images with a GFP filter. Images of Calcein-AM fluorescence were taken using the GFP filter on a Zeiss Axio Vert.A1 200 microscope with the 4X magnifying lens. Each image is representative of 15 images total from 3 biological replicates.

3.2.5 A lack of eEF2K assists cell survival of PC3 cells under nutrient deprived conditions.

The same experiments were performed using PC3 WT and eEF2K-KO cells. PC3 WT and eEF2K-KO cells were treated for 24 h under ±Glc or -Gln conditions with or without BafA. Looking at the western blot in **Figure 3.30,** eEF2K-KO clones showed no p-eEF2 or eEF2K, as expected. BafA increased p62 and LC3-II levels, showing it effectively inhibited autophagic flux in these cells. Interestingly, BafA increased p-eEF2 under +Glc conditions but not under -Glc conditions in these cells.

To test cell death and viability, CellTox Green and propidium iodide/calcein-AM assays were used. As seen in **Figures 3.31A and B**, the CellTox Green and propidium iodide assays showed similar results, which are quite different from the results for MDA-MB-231 and A549 cells. CellTox Green images are shown in **Figure 3.32**. Neither BafA, nor knocking-out eEF2K significantly affected cell cytotoxicity under +Glc conditions. In these cells BafA did not further increase cytotoxicity compared to control. The most surprising observation is that both eEF2K-KO clones showed decreased death whether they are treated with BafA or not in both -Glc and -Gln conditions. This is confirmed using the Calcein-AM viability assay, shown in **Figure 3.33 with images in Figure 3.34**. Treatment with BafA alone did not further decrease cell viability in any of the three media. However, eEF2K-KO cells showed an almost doubling in cell viability compared to WT cells in -Glc and -Gln conditions. This is the opposite of the results observed in MDA-MB-231 and A549 cells. However, this does not seem to be dependent on autophagy, as found by Xie *et al*.[119] in colon cancer cells. In that study, silencing eEF2K led to an increase in p62 and LC3-II levels. In the case of PC3 cells, eEF2K-KO did not lead to any changes in p62 or LC3-II levels

compared to WT (**Figure 3.30**), further supporting the hypothesis that these are two separate pathways in these cells. Clearly, silencing eEF2K has distinct effects on different cell lines and must be tested on each cell line individually.

Figure 3.30

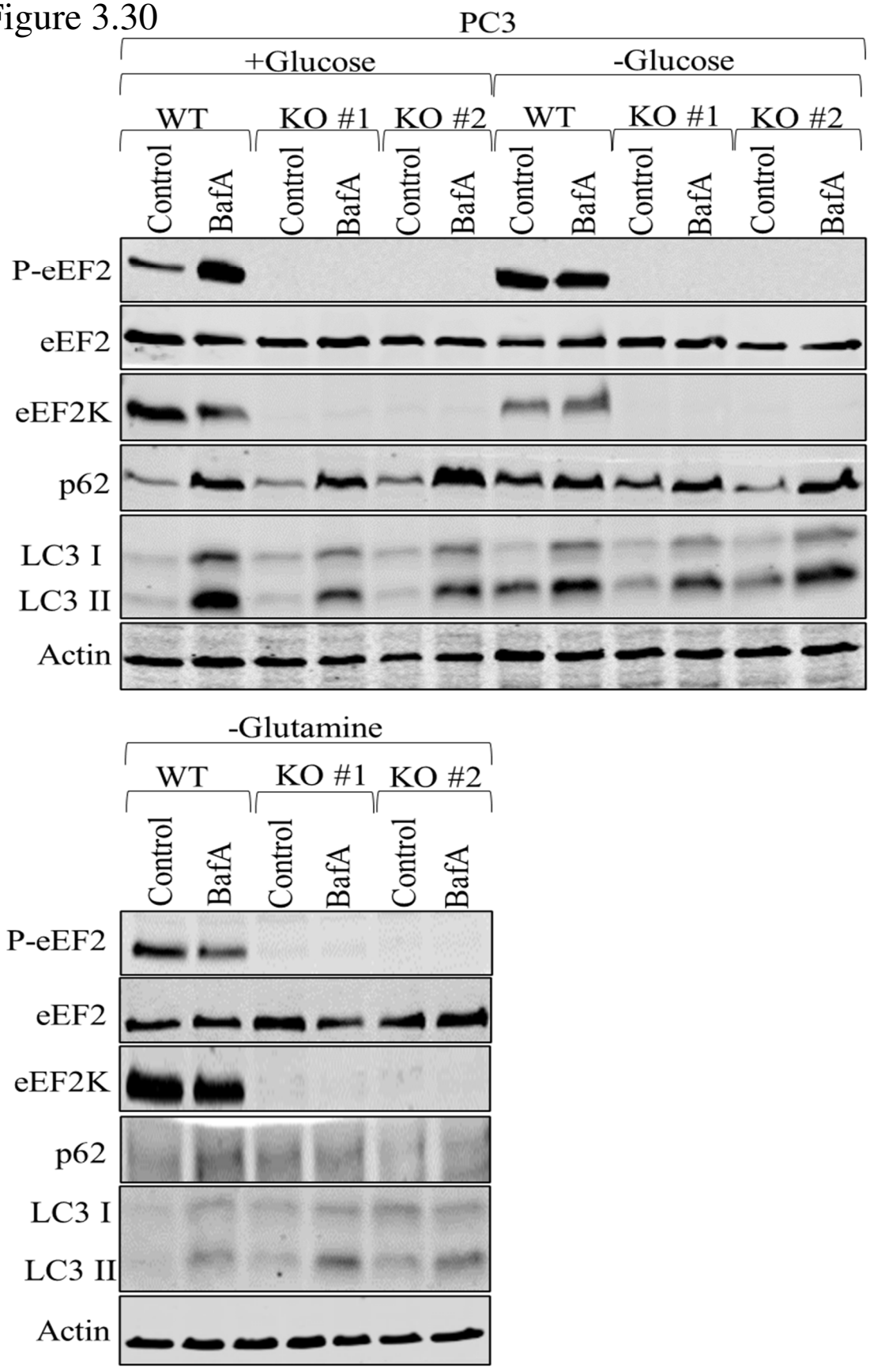

PC3
+Glucose
-Glucose
WT
KO #1
KO #2
WT
KO #1
KO #2
Control
BafA
P-eEF2
eEF2
eEF2K
p62
LC3 I
LC3 II
Actin
-Glutamine
WT
KO #1
KO #2
Control
BafA
P-eEF2
eEF2
eEF2K
p62
LC3 I
LC3 II
Actin

Figure 3.30: **Bafilomycin A successfully inhibits autophagic flux in PC3 WT and eEF2K-KO cells.** PC3 WT and eEF2K KO cells were treated in medium with or without Glc/Pyr or Glc/Pyr/Gln and with or without 125 nM BafA for 48 h. The cells were lysed, the samples were run on either (16%) SDS-PAGE for low molecular weight proteins or (12.5%) SDS-PAGE for others, followed by analysis via immunoblot. The western blot images are representative of n=3.

Figure 3.31

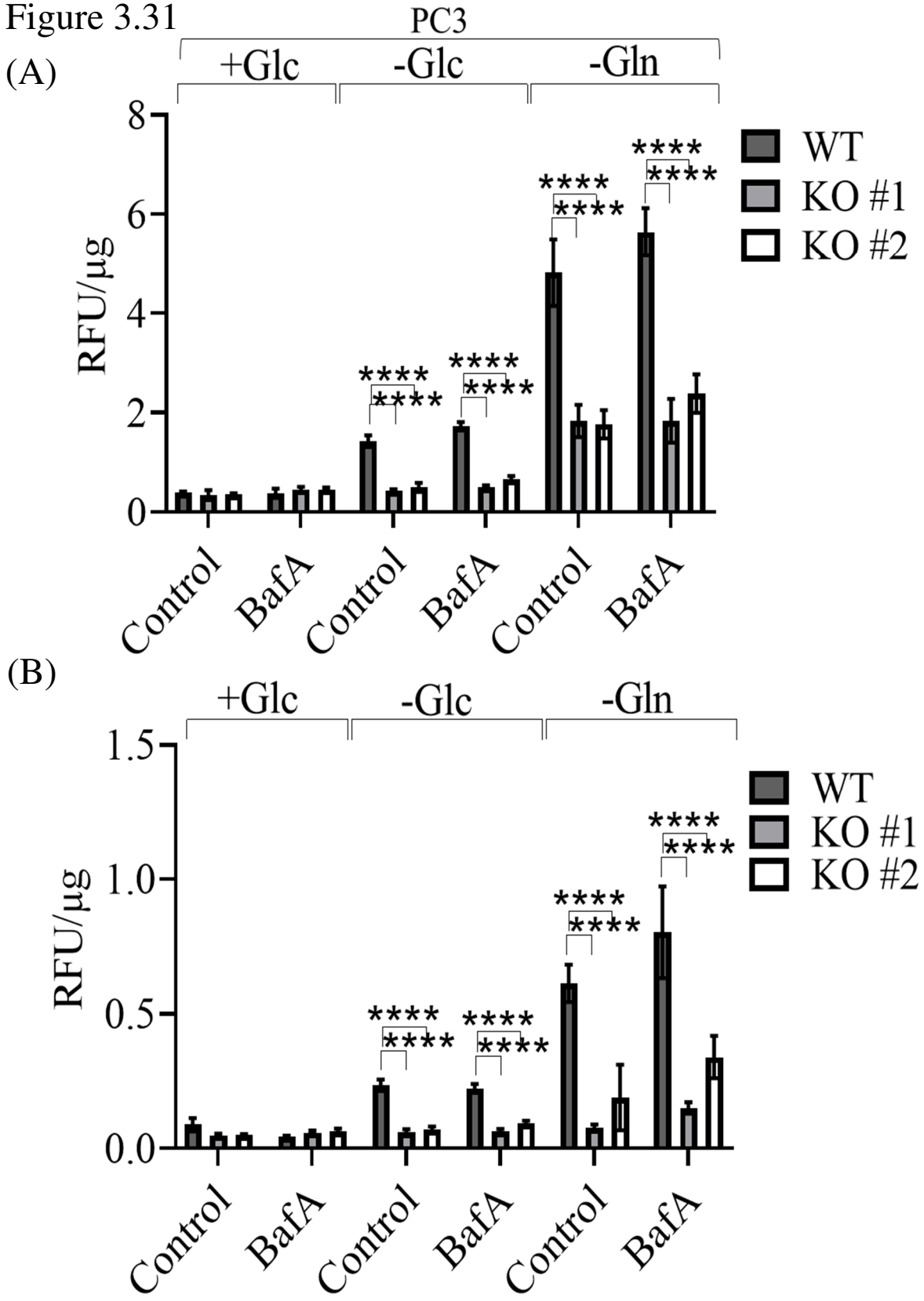

(A)
PC3
+Glc
-Glc
-Gln
RFU/µg
0
2
4
6
8
WT
KO #1
KO #2
****
Control
BafA
(B)
+Glc
-Glc
-Gln
RFU/µg
0.0
0.5
1.0
1.5
WT
KO #1
KO #2
****
Control
BafA

Figure 3.31: A lack of eEF2K reduces cytotoxicity of PC3 cells under nutrient deprived conditions. PC3 WT and eEF2K-KO cells were treated for 24 h with or without 125 nM BafA in medium with or without Glc/Pyr or Glc/Pyr/Gln prior to measuring cell cytotoxicity via CellTox Green **(A)** and propidium iodide **(B).** 10 µM propidium iodide was added 1 h prior to measurement. Error bars represent S.D. (n=3). The p-values were calculated using Two-Way ANOVA with the Tukey multiple comparisons test. P-values: ****≤0.0001. RFU was normalised by total protein content.

Figure 3.32

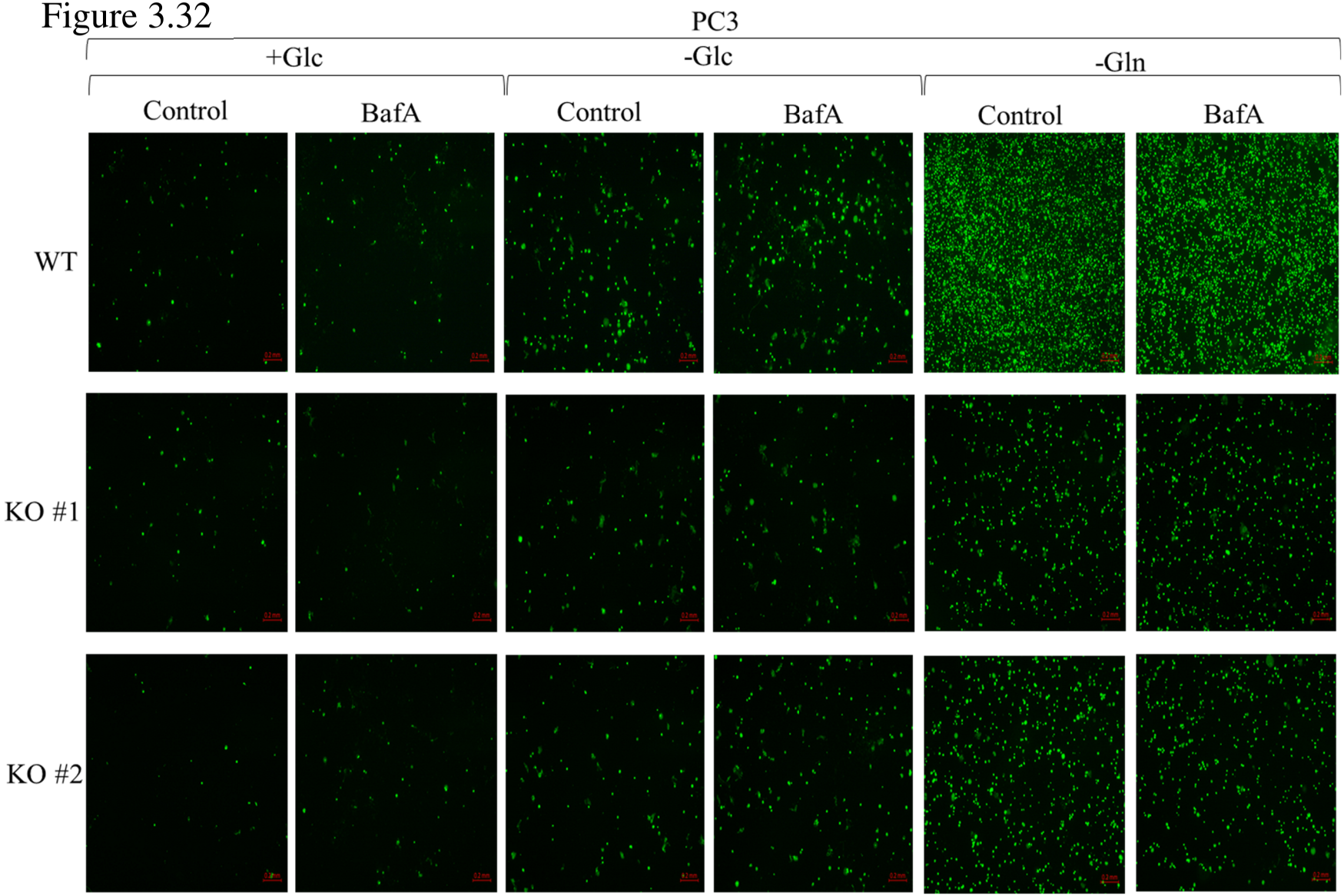

PC3
+Glc
-Glc
-Gln
Control
BafA
Control
BafA
Control
BafA
WT
KO #1
KO #2

Figure 3.32: A lack of eEF2K reduces cytotoxicity of PC3 cells under nutrient deprived conditions (CellTox Green images). PC3 WT and eEF2K-KO cells were treated for 24 h with or without 125 nM BafA in medium with or without Glc/Pyr or Glc/Pyr/Gln prior to taking images. Images of CellTox Green fluorescence were taken using the GFP filter on a Zeiss Axio Vert.A1 200 microscope with the 4X magnifying lens. Each image is representative of 15 images total from 3 biological replicates.

Figure 3.33

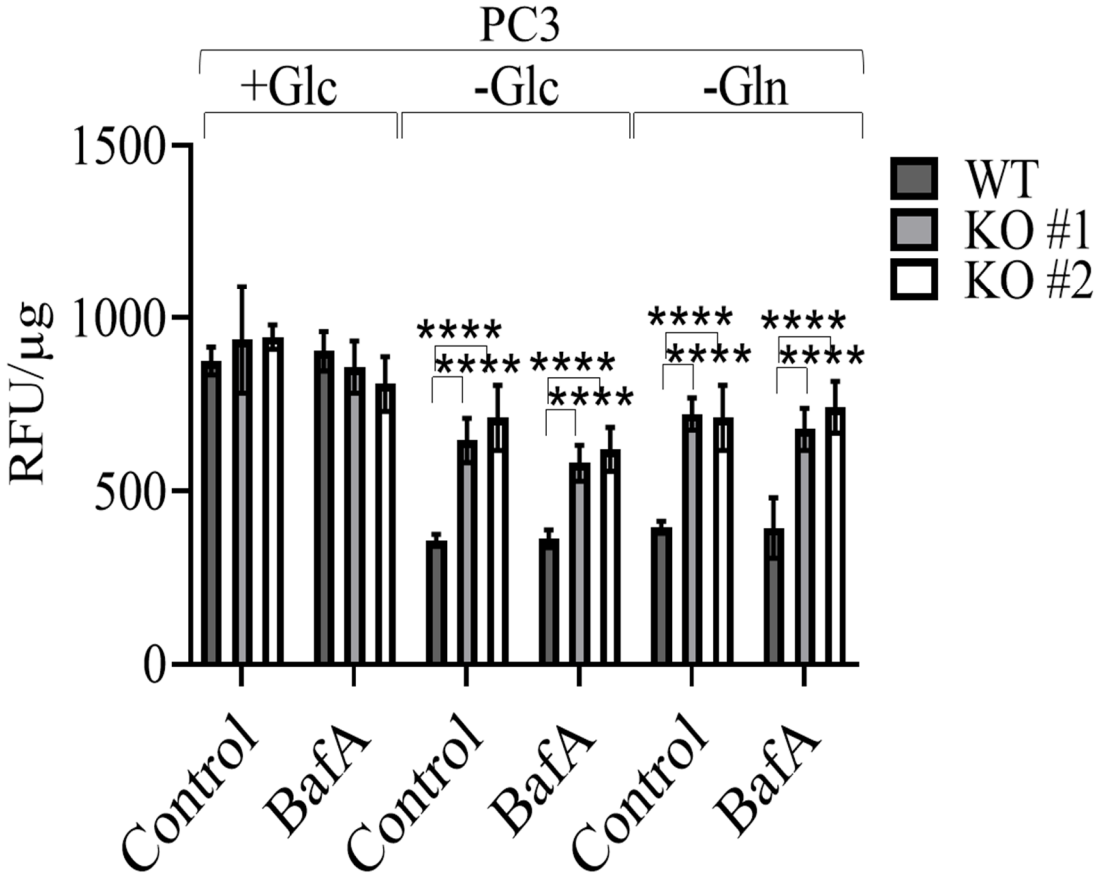


Figure 3.33: A lack of eEF2K increases the viability of PC3 cells under nutrient deprived conditions. Calcein-AM assay - PC3 WT and eEF2K-KO cells were treated for 24 h with or without 125 nM BafA in medium with or without Glc/Pyr or Glc/Pyr/Gln. Calcein-AM was added 1 h prior to measurement to a final concentration of 1µM. Error bars represent S.D. (n=3). The p-values were calculated using Two-Way ANOVA with the Tukey multiple comparisons test. P-values: ****≤0.0001. RFU was normalised by total protein content.

Figure 3.34

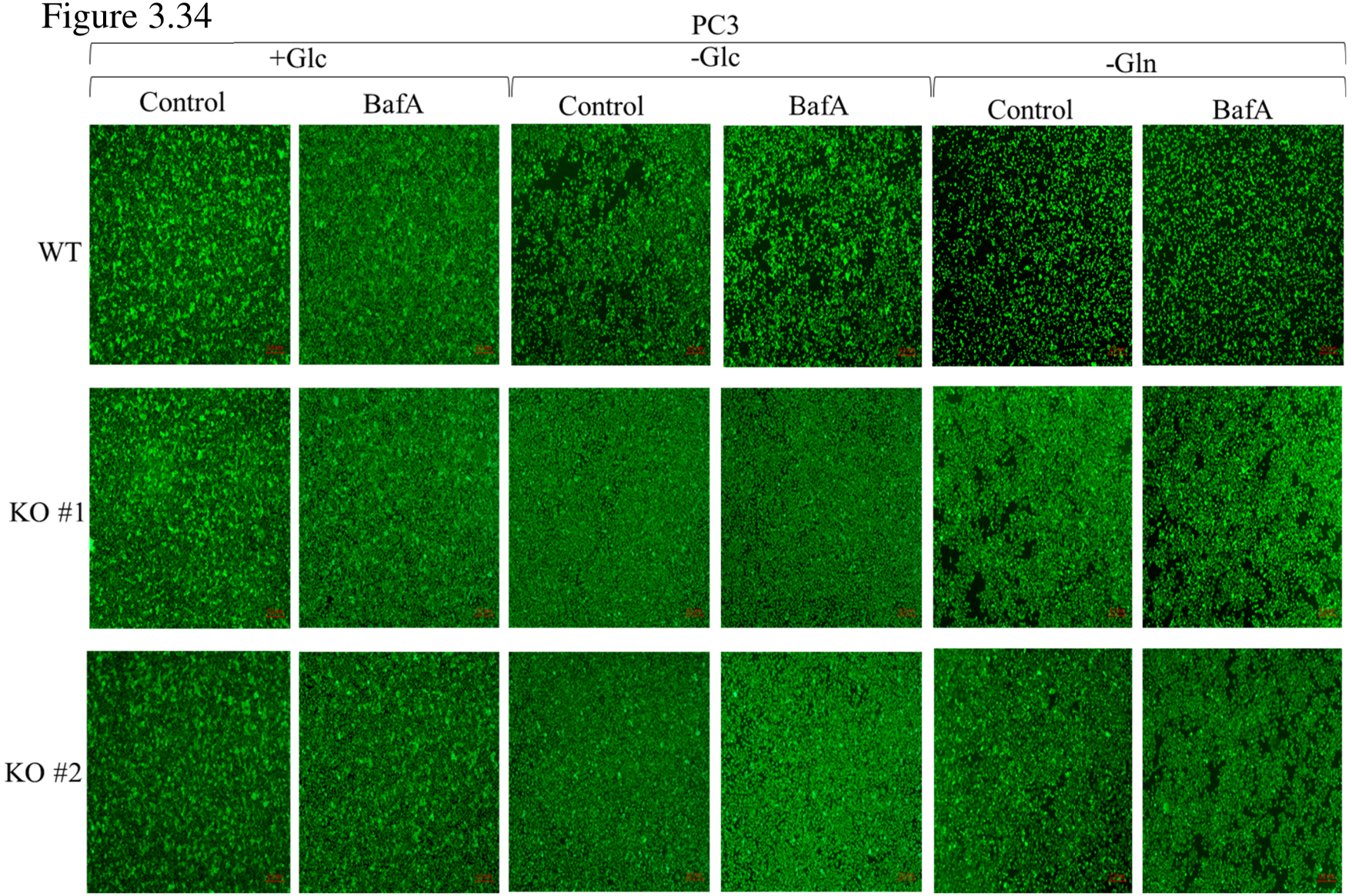

PC3
+Glc
-Glc
-Gln
Control
BafA
Control
BafA
Control
BafA
WT
KO #1
KO #2

Figure 3.34: A lack of eEF2K increases cell viability of PC3 cells under nutrient deprived conditions (Calcein-AM images). PC3 WT and eEF2K-KO cells were treated for 24 h with or without 125 nM BafA in medium with or without Glc/Pyr or Glc/Pyr/Gln. 1 μM Calcein-AM was added 1 h prior to taking images. Images of Calcein-AM fluorescence were taken using the GFP filter on a Zeiss Axio Vert.A1 200 microscope with the 4X magnifying lens. Each image is representative of 15 images total from 3 biological replicates.

3.2.6 Caspase activity is increased in MDA-MB-231 and A549 cells that lack eEF2K.

Another important factor to consider was how the cells undergo die under nutrient deprived conditions with a blockage of eEF2K and autophagy. Apoptosis is a form of programmed cell death which involves initiator caspases (such as caspase 8) cleaving and thus activating executor caspases (such as caspases 3 and 7). These executor caspases in turn form either the apoptosome or the Death Inducing Signalling Complex (DISC) depending on the original stimulus that caused the process to start. These complexes then cleave intracellular proteins which leads to the collapse of the cytoskeleton, fragmentation of DNA and the shrinking of the cell. The cells can then be removed by phagocytes, preventing an immune response which could damage the surrounding cells[197, 198]. If the cells undergo necrosis, however, they lose their membrane integrity, rupture, releasing their contents including pro-inflammatory molecules which can then cause an immune response that could damage the surrounding healthy tissue[199]. If blocking eEF2K and autophagy under nutrient deprived conditions leads to necrosis, such a treatment could cause more damage to the body than good. Therefore, it is important to distinguish what type of cell death occurs. One such way is to look at the activity of initiator and executor caspases. Caspases 3 and 7 are executor caspases that are directly involved in degrading cellular components. The Caspase-Glo 3/7 Assay from Promega allows the measurement of the activity of these caspases[132]. The assay uses a luminogenic caspase 3/7 substrate which when cleaved by the caspases 3 and 7 releases a substrate for luciferin. This then results in a luciferase reaction, creating luminescence which can be measured on a plate reader. The combined activity of both caspases is directly proportionate to the luminescent signal.

MDA-MB-231 and A549 WT and eEF2K-KO or silenced cells were treated in the same conditions as for the assays that measured cell death and viability. Namely, MDA-MB-231 WT cells were treated for 48 h in ±Glc medium with A484954, BafA or a combination. eEF2K-KO cells were only treated with BafA. A549 cells were also treated in -Gln conditions with or without BafA. Caspase 3 and 7 activity was then measured (**Figure 3.35**). The most striking difference seen is that under -Glc or -Gln conditions, the caspase 3/7 activity was lower than in +Glc conditions. This could be due to cells undergoing another form of cell death such as necroptosis or autophagic cell death. However, caspase 3 is itself quickly degraded through the ubiquitin proteasome pathway after its activation[200, 201]. This is likely the reason for such a large drop in the total caspase 3/7 activity since the end-point of the experiment was 48 h. Cells would start to become stressed and begin the apoptotic process before the point of measurement and by 48 h the caspases in apoptotic cells would be degraded. Looking at MDA-MB-231 cells, treatment with A484954 did not significantly alter caspase activity. As expected, treatment with BafA increased caspase activity but a combination treatment with A484 does not significantly alter it in ±Glc conditions. It is interesting to see that even in +Glc conditions, both eEF2K-KO clones had increased caspase 3/7 activity (by approximately 1.5-fold) compared to WT cells. This could be due to the fact that after 48 h in fully supplemented medium, the cells were overconfluent and stressed. Cells without eEF2K cannot cope with this stress and start to apoptose. A large difference can be seen when eEF2K-KO clones were treated with BafA in +Glc conditions. This is similar to what was seen in the CellTox Green and propidium iodide assays. This large increase in caspase activity could be because these cells lack eEF2K completely instead of it being inhibited for only 48 h. In -Glc conditions, it can also be seen that the KO clones had increased caspase activity even without BafA. BafA treatment did not significantly alter this. The results are different in A549 cells. Under control conditions in all three types of

medium, eEF2K silencing did not affect caspase activity. However, in +Glc conditions with BafA treatment, there was a 1.5-fold increase in caspase activity in eEF2K silenced cells. This further shows the differing effects that a lack of eEF2K have in different cell lines.

Another way to measure apoptotic cell death is by measuring the activity of caspase 8. Caspase 8 is an inhibitor of necroptosis which is a form of programmed necrosis. Caspase 8 suppresses the function of receptor-interacting protein kinase 1 (RIPK1) which is necessary to activate mixed lineage kinase domain (MLKL), an executor molecule of necroptosis[202-204]. Caspase 8 directly cleaves and activates caspases 3 and 7, thus initiating apoptosis[205]. To measure its activity, the Caspase-Glo 8 Assay from Promega was used[133]. The assay works in a similar way to the Caspase-Glo 3/7 assay. A luminogenic caspase-8 substrate is cleaved by caspase 8. This then produces luminescence which can be measured on a plate reader. MDA-MB-231 and A549 cells were treated in the same manner as the caspase 3/7 assay (**Figure 3.36**). Looking at +Glc conditions for MDA-MB-231 cells, the results were similar to the caspase 3/7 assay. Caspase 8 activity was not changed in WT cells by A484 or BafA treatment. However, eEF2K-KO cells had significantly higher caspase 8 activity in control and BafA treated conditions. In -Glc conditions, similar to the caspase3/7 data, caspase 8 activity was also much lower than in +Glc conditions. However, in this case the treatment with A484 and BafA together increased caspase 8 activity 1.5-fold. eEF2K-KO by itself also caused an increase in caspase 8 activity in -Glc conditions. Treatment of eEF2K-KO cells with BafA further increased caspase 8 activity by 1.5-fold. A similar trend was seen in A549 cells. Unlike the caspase 3/7 activity, BafA treatment under +Glc conditions did not alter caspase 8 activity in IPTG treated cells. Under -Glc conditions and treatment with BafA, IPTG-treated cells had almost double the caspase-8 activity of WT cells. It is also of note that caspase 8 activity in these cells was decreased in -Glc conditions compared to +Glc but

was increased when cells were treated with BafA and in -Gln conditions. eEF2K-silenced cells also exhibited higher caspase 8 activity in both control conditions and BafA treatment in -Gln medium. The data in **Figure 3.36B** show that the combination of knockdown of eEF2K and BafA promotes apoptotic cell death.

Overall, these data further support the trend shown by the cytotoxicity data and that the cells are dying via apoptosis. If the cells were dying via necrosis, there would be almost no caspase activity as caspases are not required for that process. It appears that a lack of eEF2K tends to lead to an overall increase in caspase 3/7 and 8 activity in MDA-MB-231 cells, while in A549 cells, this increase is only evident when cells are treated with BafA or in -Gln conditions.

Figure 3.35

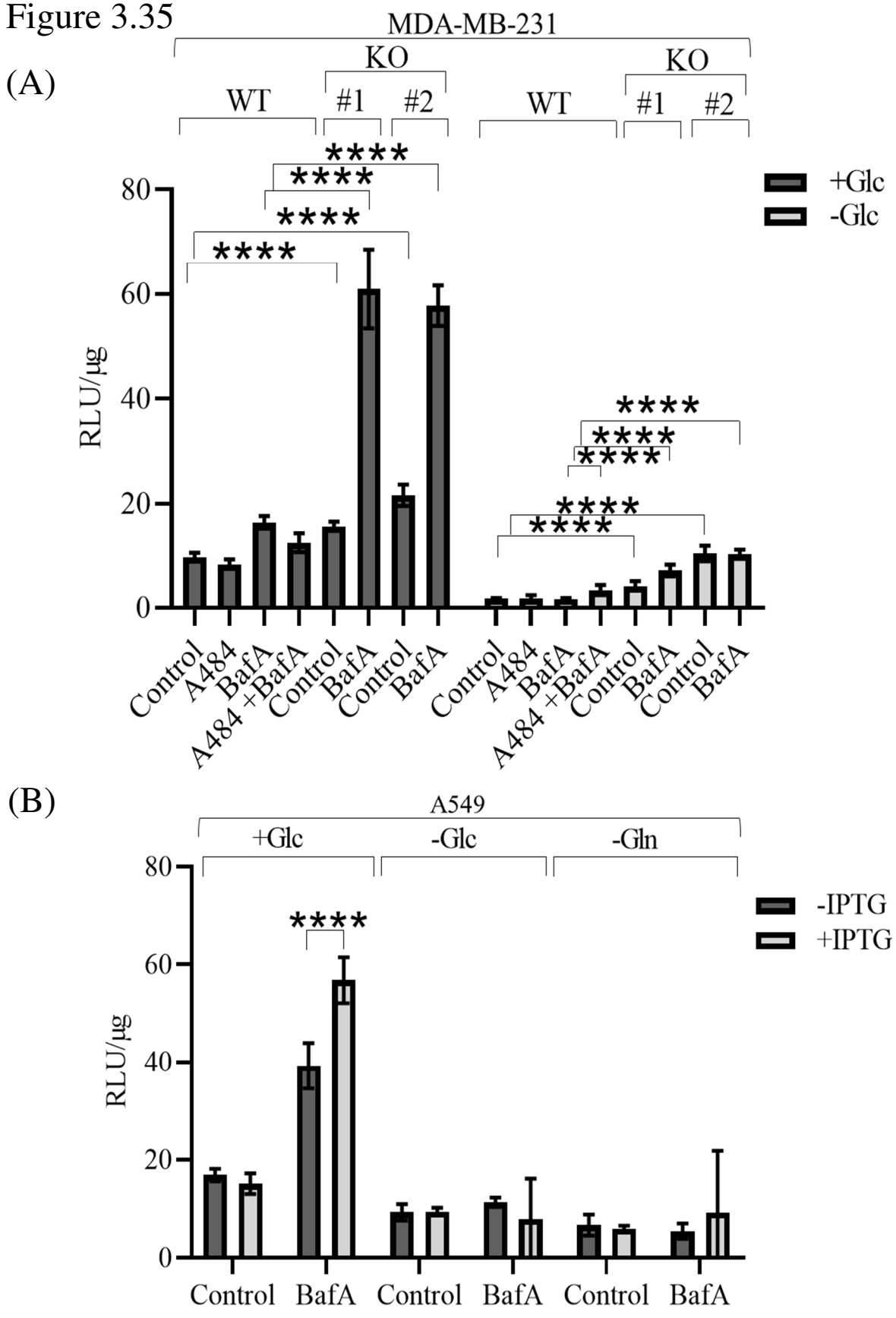

(A)
MDA-MB-231
KO
KO
WT
#1
#2
WT
#1
#2
****
****
****
****
****
****
****
****
****
80
60
40
20
0
RLU/µg
+Glc
-Glc
Control
A484
BafA
A484 +BafA
Control
BafA
Control
BafA
Control
A484
BafA
A484 +BafA
Control
BafA
Control
BafA
(B)
A549
+Glc
-Glc
-Gln
****
80
60
40
20
0
RLU/µg
-IPTG
+IPTG
Control
BafA
Control
BafA
Control
BafA

Figure 3.35: Knocking out or silencing of eEF2K leads to an increase in caspase 3 and 7 activity. Caspase-Glo 3/7 Assay. **A:** MDA-MB-231 WT and eEF2K-KO cells were treated for 48 h with 30 μM A484954, 125 nM BafA, or a combination in medium with or without Glc/Pyr. **B:** A549 cells were treated in medium with or without Glc/Pyr or Glc/Pyr/Gln and with or without 125nM BafA for 48 h. 1 mM IPTG was used to induced eEF2K silencing 5 days prior. Error bars represent S.D. (n=3). The p-values were calculated using Two-Way ANOVA with the Tukey multiple comparisons test. P-values: ****≤0.0001. RLU was normalised by total protein content.

Figure 3.36

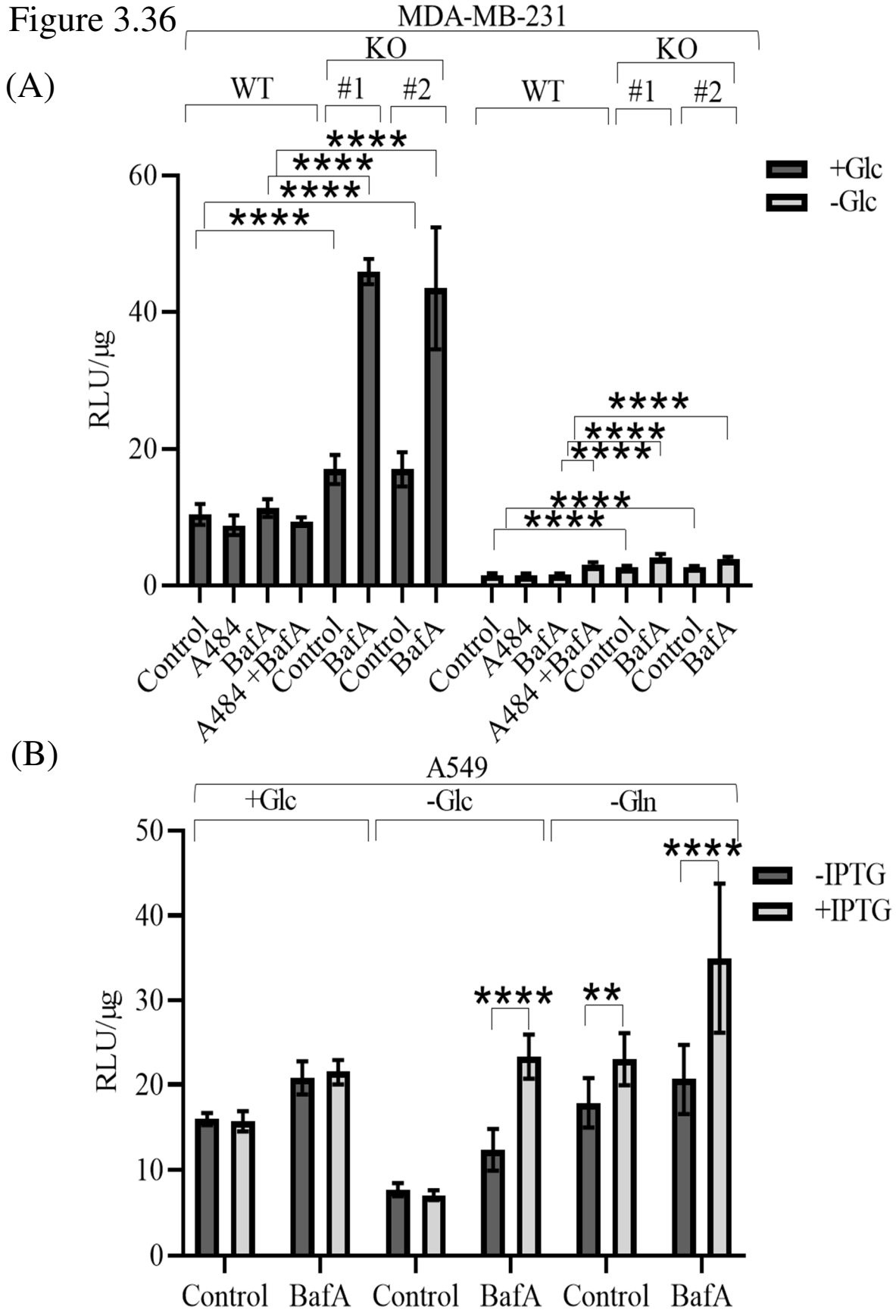

(A)
MDA-MB-231
KO
KO
WT
#1
#2
WT
#1
#2
****
****
****
****
****
****
****
****
****
60
40
20
0
RLU/µg
+Glc
-Glc
Control
A484
BafA
A484 +BafA
Control
BafA
Control
BafA
Control
A484
BafA
A484 +BafA
Control
BafA
Control
BafA
(B)
A549
+Glc
-Glc
-Gln
50
40
30
20
10
0
RLU/µg
****
**
****
-IPTG
+IPTG
Control
BafA
Control
BafA
Control
BafA

Figure 3.36: Knocking out or silencing of eEF2K leads to an increase in caspase 8 activity. Caspase-Glo 8 Assay. **A:** MDA-MB-231 WT and eEF2K-KO cells were treated for 48 h with 30 µM A484954, 125 nM BafA, or a combination in medium with or without Glc/Pur. **B:** A549 cells were treated in medium with or without Glc/Pyr or Glc/Pyr/Gln and with or without 125nM BafA for 48 h. 1 mM IPTG was used to induced eEF2K silencing 5 days prior. Error bars represent S.D. (n=3). The p-values were calculated using Two-Way ANOVA with the Tukey multiple comparisons test. P-values: **≤0.01; ****≤0.0001. RLU was normalised by total protein content.

3.2.7 An inhibition or lack of eEF2K lowers or increases cellular ATP depending on cell type.

The hypothesis behind how eEF2K protects cells from nutrient deprivation is by slowing translation elongation and thus allowing the cells to maintain a larger reserve of metabolic energy (ATP). To test this, the CellTiter-Glo 2.0 Assay from Promega was used to measure ATP levels[134]. The assay uses the reaction of luciferin which is oxygenated in the presence of ATP and luciferase. This then produces luminescence which can be measured. This luminescence is directly proportional to the amount of ATP in cells.

MDA-MB-231, A549 and PC3 cells were treated under the same conditions as for the cytotoxicity assays. After 48 h, cell-titre Glo 2.0 reagent was added, and the luminescence was measured. Looking at **Figure 3.37A,** knocking out eEF2K had no effect on cellular ATP levels in +Glc conditions. A484954 treatment did not affect ATP levels either. Treatment with BafA alone significantly lowered ATP levels but a combination treatment with A484 and BafA did not alter this. As BafA is in an inhibitor of the V-ATPase, is seems counterintuitive that it decreases ATP levels in cells. However, BafA has been reported to reduce the activity of citrate synthase, the enzyme responsible for catalysing the conversion of acetyl-CoA and oxaloacetate to form citrate as part of the Krebs cycle, in primary neurons[206]. It has also been reported to reduce the extracellular acidification rate (ECAR; a measure of the cells' glycolytic activity) and oxygen consumption rate (OCR; a measure of the cells' mitochondrial respiration)[206].

Furthermore, treatment with BafA of eEF2K-KO cells more than halved cellular ATP compared to WT cells. This suggests that a complete lack of eEF2K in cells has a large effect on ATP levels when autophagy is also inhibited. In -Glc conditions, overall ATP levels were lower, as expected. Treatment with A484 or BafA alone did not significantly alter ATP compared to WT control. However, combining A484 and BafA treatment decreased ATP levels by more than half. In -Glc conditions, knocking out eEF2K alone lowered ATP levels by 1.4-fold compared to WT. This could be because the cells do not decrease their protein synthesis rates even under nutrient stress conditions due to the lack of eEF2K, leading to higher energy usage. Treatment of eEF2K-KO cells with BafA lowered ATP levels to the same level as WT cells co-treated with A484 and BafA. It is of note that such large decreases in ATP levels in the KO cells treated with BafA may be what leads to such high levels of cell death, as evidenced by CellTox Green and PI staining (**Figures 3.22, 3.23**).

Looking at the data for A549 cells in **Figure 3.37B,** cellular ATP levels were unaffected by eEF2K silencing in +Glc conditions. Treatment with BafA lowered ATP levels, however, unlike in MDA-MB-231 cells, eEF2K silencing did not further lower them. In -Glc control conditions, IPTG induced cells' ATP level was not changed. However, treatment with BafA of IPTG-treated cells lowered ATP levels by 1.7-fold compared to non-induced cells. No Gln conditions lowered cellular ATP levels to such low levels that no changes were significant. Overall, these data showed that eEF2K plays a significant role in maintaining cellular ATP levels in MDA-MB-231 cells under nutrient deprived conditions and when autophagy is also inhibited. In A549 cells, eEF2K seems to play a large role only when autophagy is inhibited in the absence of Glc.

Figure 3.37

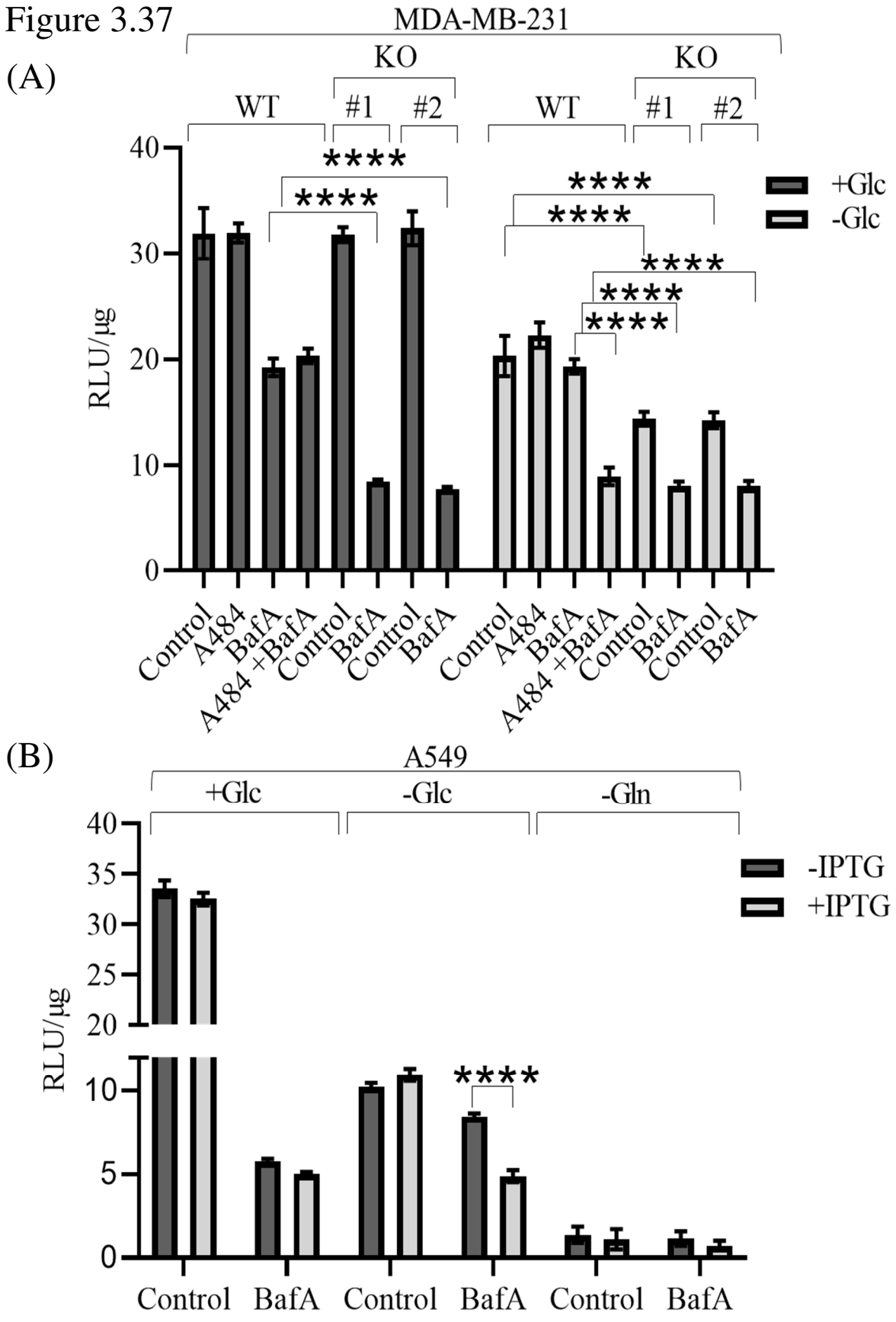

(A)
MDA-MB-231
KO
KO
WT
#1
#2
WT
#1
#2
40
30
20
10
0
RLU/μg
****
****
****
****
****
****
****
+Glc
-Glc
Control
A484
BafA
A484 +BafA
Control
BafA
Control
BafA
Control
A484
BafA
A484 +BafA
Control
BafA
Control
BafA
(B)
A549
+Glc
-Glc
-Gln
40
35
30
25
20
10
5
0
RLU/μg
****
-IPTG
+IPTG
Control
BafA
Control
BafA
Control
BafA

Figure 3.37: A lack of or inhibition of eEF2K leads to a decrease in ATP levels in MDA-MB-231 and A549 cells. CellTiter-Glo 2.0 Assay**. A:** MDA-MB-231 WT and eEF2K-KO cells were treated for 48 h with 30 µM A484954, 125 nM BafA, or a combination in medium with or without Glc/Pyr. **B:** A549 cells were treated in medium with or without Glc/Pyr or Glc/Pyr/Gln and with or without 125nM BafA for 48 h. 1 mM IPTG was used to induced eEF2K silencing 5 days prior. Error bars represent S.D. (n=3). The p-values were calculated using Two-Way ANOVA with the Tukey multiple comparisons test. P-values: ****≤0.0001. RLU was normalised by total protein content.

For PC3 cells, in +Glc conditions with or without BafA, knocking out eEF2K unexpectedly increased ATP levels (**Figure 3.38**). eEF2K-KO did not affect ATP levels in -Glc conditions. However, in -Gln medium, eEF2K-KO showed a large increase in ATP in both control and BafA treatment conditions. This is the opposite of what was shown in MDA-MB-231 and A549 cells but this may explain why PC3 eEF2K-KO cells survived nutrient stress for longer than WT cells (by having more ATP stores to survive for a longer time period).

Figure 3.38

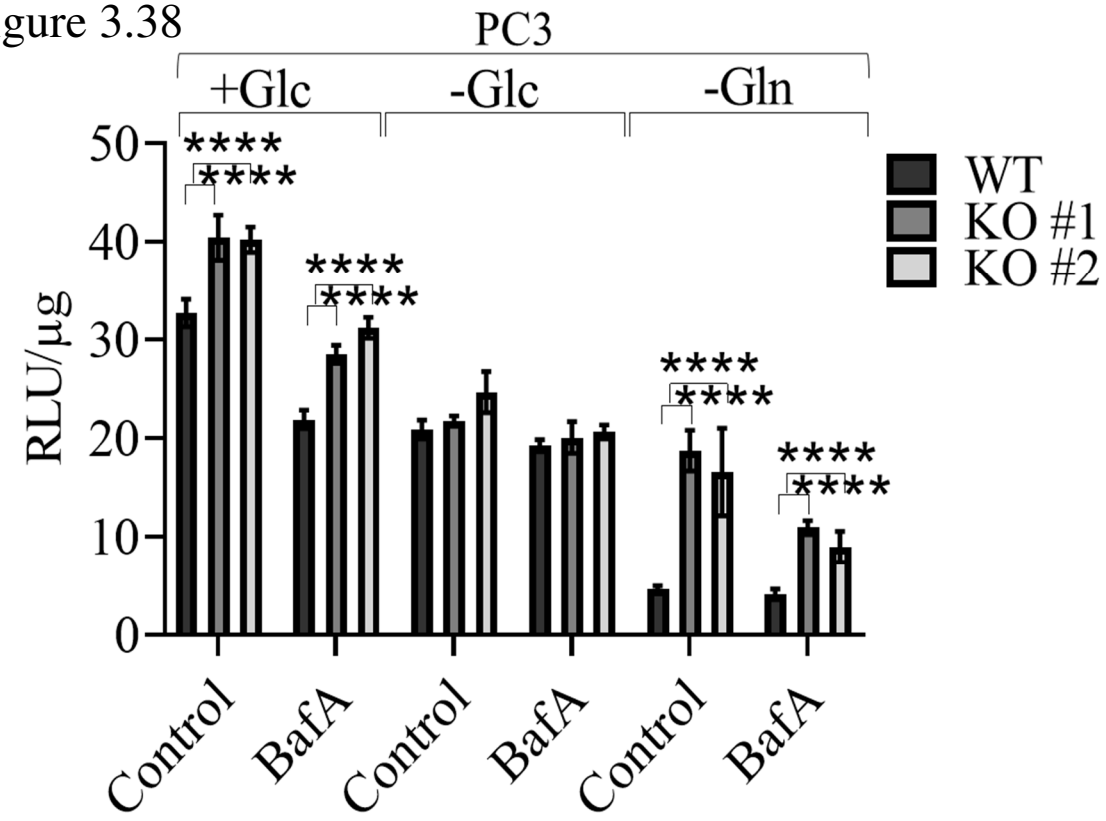


Figure 3.38: Knocking out eEF2K leads to an increase in ATP levels in PC3 cells under –Gln conditions. CellTiter-Glo 2.0 Assay **–** PC3 WT and eEF2K-KO cells were treated for 48 h with or without 125 nM BafA in medium with or without Glc/Pyr or Glc/Pyr/Gln. Error bars represent S.D. (n=3). The p-values were calculated using Two-Way ANOVA with the Tukey multiple comparisons test. P-values: ****≤0.0001. RLU was normalised by total protein content.

3.2.8 Knocking out or silencing eEF2K does not significantly alter cell glycolysis or mitochondrial oxidation.

A study by Cheng *et al*.[207] in 2016 using MCF-7 and MDA-MB-231 cells suggested that silencing of eEF2K led to increased glycolysis. Their data also showed a decrease in the OCR (oxygen consumption rate) of eEF2K silenced cells. Work done by Jan *et al*.[208] in 2018 showed that N2A neuroblastoma cells had increased basal and maximal respiration upon silencing of eEF2K. These experiments were done using the Seahorse cell metabolism analyser. This equipment can also measure changes in ECAR accurately. ECAR measures the levels of lactic acid generated by glycolysis[209]. This allows for the measurement in changes of cell glycolysis and mitochondrial oxidation.

The initial tests were performed in the Seahorse XF HS Analyzer, the only one available to us. This machine can only take 8-well plates. This means that the output can only be three wells per condition, as two wells are used for blanks. The first test done was using the Cell Energy Phenotype Test Kit[150]. This experiment used oligomycin and FCCP at the same time. Oligomycin inhibits ATP production by the mitochondria via the inhibition of ATP synthase by blocking the proton channel which is necessary for oxidative phosphorylation of ADP to ATP. This leads to a compensatory increase in the glycolysis pathway as cells try to recoup the energy lost. FCCP depolarises the mitochondrial membrane by allowing protons to cross it freely. This causes the oxygen consumption rates of cells to peak, as electron flow through the electron transport chain is no longer inhibited. This experiment was initially done to compare MDA-MB-231 WT and KO #1 cells, as shown in **Figure 3.39**. After the injection of the compounds, the OCR was more than doubled while the ECAR increased slightly. However, there was no significant difference between the WT and eEF2K-KO cells. The

WT cells trended towards being more energetic, i.e., their glycolysis and mitochondrial respiration was slightly higher than the KO cells, although not statistically significantly.

To further explore this, the Cell Glyco Stress Test kit was used[151]. This allows for more in-depth analysis of the glycolytic functions of the cells. The experiment started off in -Glc medium to measure the non-glycolytic acidification. Glucose was then added to measure the rate of glycolysis. Oligomycin was added next to measure the total glycolytic capacity of cells. Oligomycin addition increases AMP levels in cells which in turn activates ATP-dependent 6-phosphofructokinase (PFK1), increasing glycolytic flux. AMPK would also be active due to the lowered ATP/AMP ratio, phosphorylate and activate 6-phosphofructo-2-kinase (PFKFB3), an enzyme that has been reported to be overexpressed in a variety of human cancer cells[210] and which increases fructose-2,6-bisphosphate concentrations, contributing to increased glycolysis. Lastly, 2-DG was added last which measured the glycolytic reserve. A diagrammatic representation of this is shown in **Figure 3.40**. Once again, WT and eEF2K-KO #1 cells were compared. **Figure 3.40** shows that, overall, there was no significant difference in overall glycolysis, glycolytic capacity, or the glycolytic reserve between WT and eEF2K-KO #1 cells.

Figure 3.39

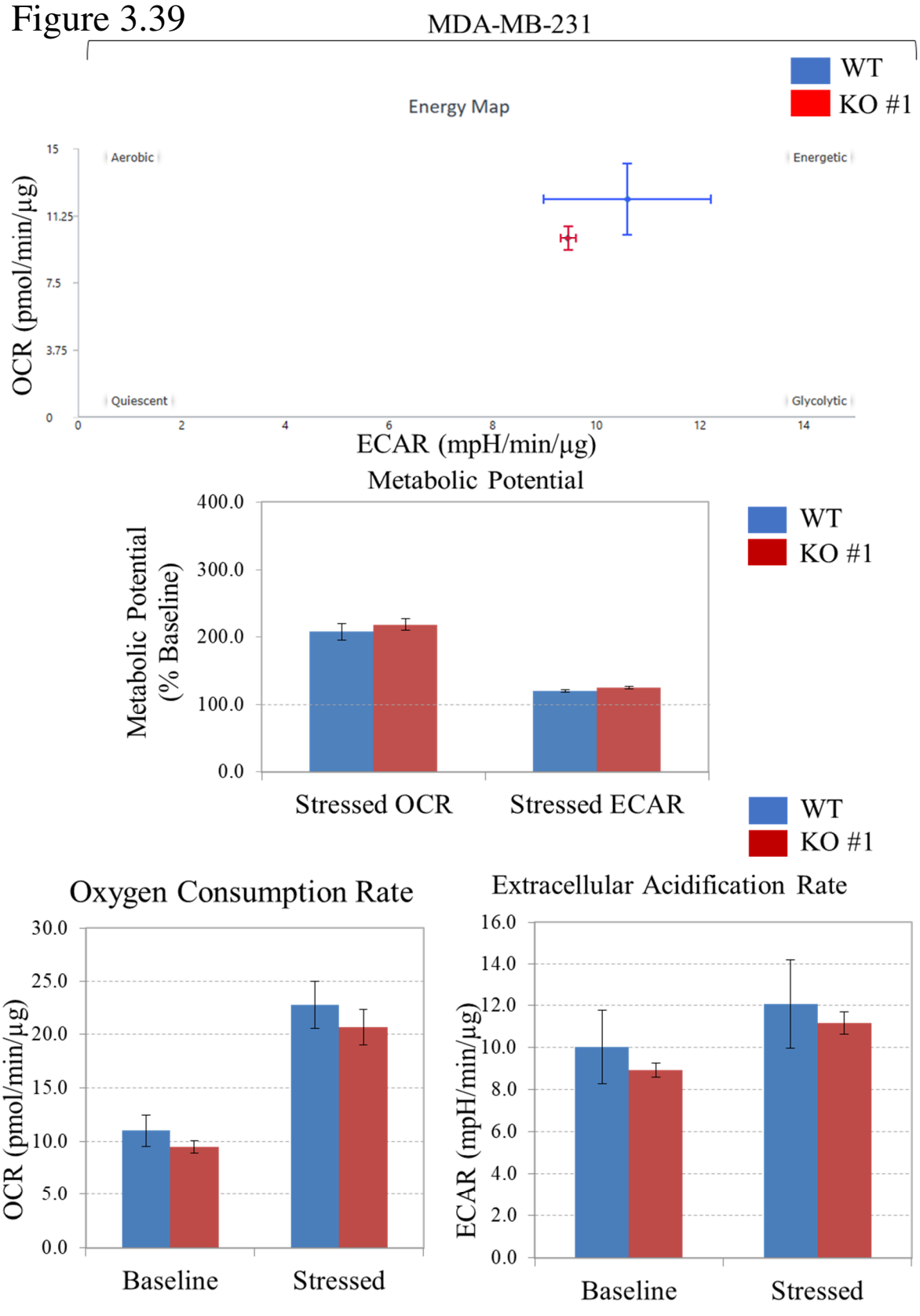
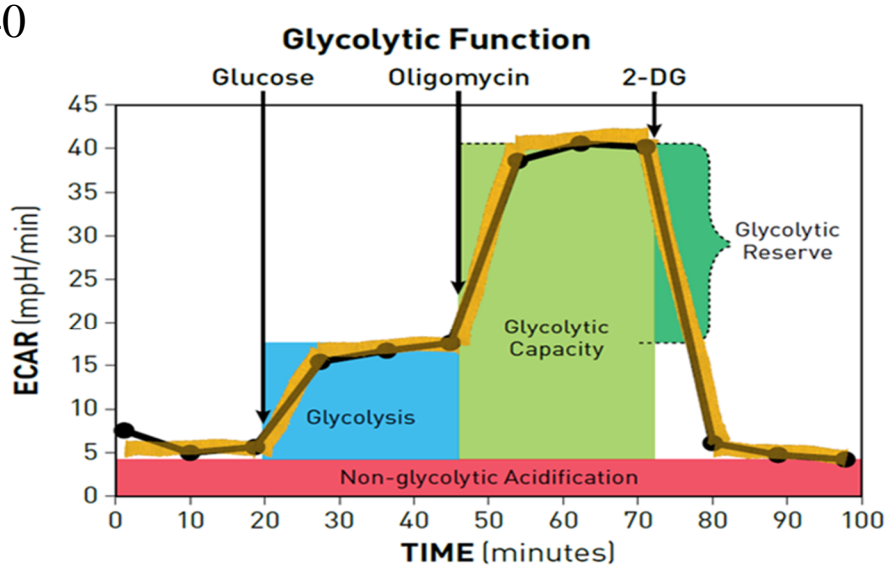

MDA-MB-231
Energy Map
WT
KO #1
Aerobic
Energetic
Quiescent
Glycolytic
OCR (pmol/min/µg)
ECAR (mpH/min/µg)
Metabolic Potential
Metabolic Potential (% Baseline)
Stressed OCR
Stressed ECAR
Oxygen Consumption Rate
Extracellular Acidification Rate
Baseline
Stressed

Figure 3.39: Knocking out eEF2K does not affect the metabolic potential of MDA-MB-231 cells. MDA-MB-231 cells were grown in fully supplemented medium for 24 h prior to performing the XFp Cell Energy Phenotype Assay. Error bars represent S.D. (n=3). The assay was normalised to total protein content.

Figure 3.40

(A)



(B)

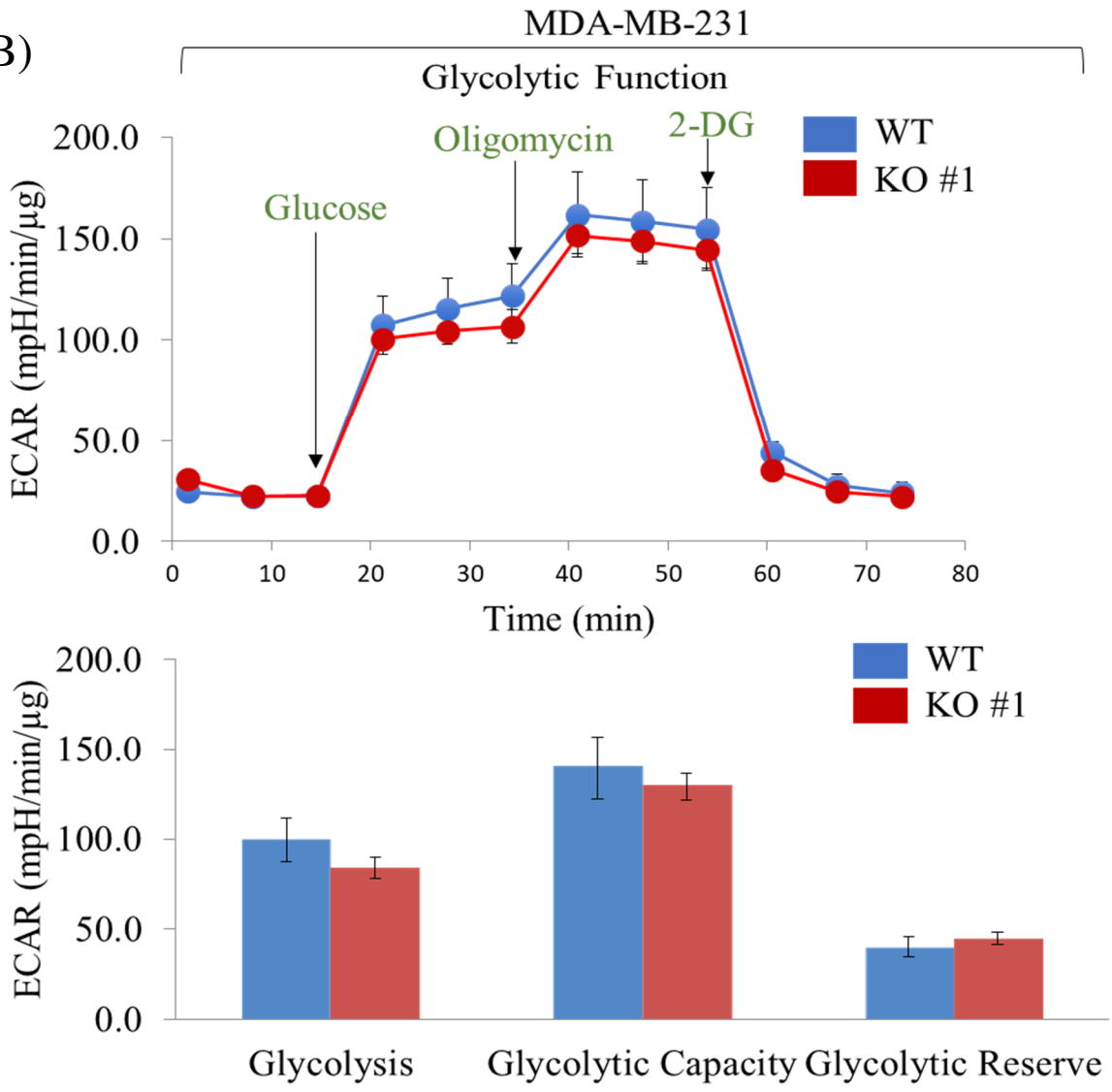


Figure 3.40: Knocking out eEF2K does not affect the glycolysis of MDA-MB-231 cells. **A:** Schematic of the XFp Glyco Stress Test Kit showing the features of glycolysis measured. The diagram was taken from the assay manual[141]. **B:** MDA-MB-231 cells were grown in fully supplemented medium for 24 h prior to performing the XFp Glyco Stress Test. Arrows indicate the time point at which compounds were injected into the wells. Error bars represent S.D. (n=3). The assay was normalised to total protein content.

To explore mitochondrial respiration in greater detail, another assay called the Mito Stress Test was performed[152]. The assay initially measures basal respiration. The first injection contained oligomycin, inhibiting the ATP synthase complex V. This allowed for the measurement of ATP linked respiration and the proton leak. Upon the addition of FCCP, maximal respiration was measured. A mixture of rotenone and antimycin A was then injected. Rotenone blocks the complex I of mitochondria, while antimycin A blocks complex III. This shuts down mitochondrial respiration, allowing for the measurement of non-mitochondrial oxygen consumption. A schematic of this is shown in **Figure 3.41**. Comparing MDA-MB-231 WT and eEF2K-KO #1 cells, there was no significant difference between the basal and spare respiratory capacity. There was also no significant change in the proton leak and ATP production.

The effects of the eEF2K inhibitors JAN384 and A484954 (**Figures 3.42 and 3.43** respectively) were also tested using the Glyco Stress Test. Inhibiting eEF2K using JAN384 significantly decreased cellular glycolysis but increased the glycolytic reserve (the difference between the maximum glycolytic capacity and the glycolytic rate of cells). On the other hand, inhibiting eEF2K via A484954 only increased the glycolytic reserve. Considering that there were no significant differences between WT and eEF2K-KO cell glycolysis, this could potentially mean these inhibitors have some off-target effects that affect rate-limiting proteins in glycolysis, such as PFK1. However, since the XFp Seahorse instrument only allows 6 samples per experiment, the variability was rather high. Therefore, the comparison between WT and eEF2K-KO cells had to be confirmed using the 96-well instrument. In this case, MDA-MB-231, A549 and PC3 cells were used and both the Glyco

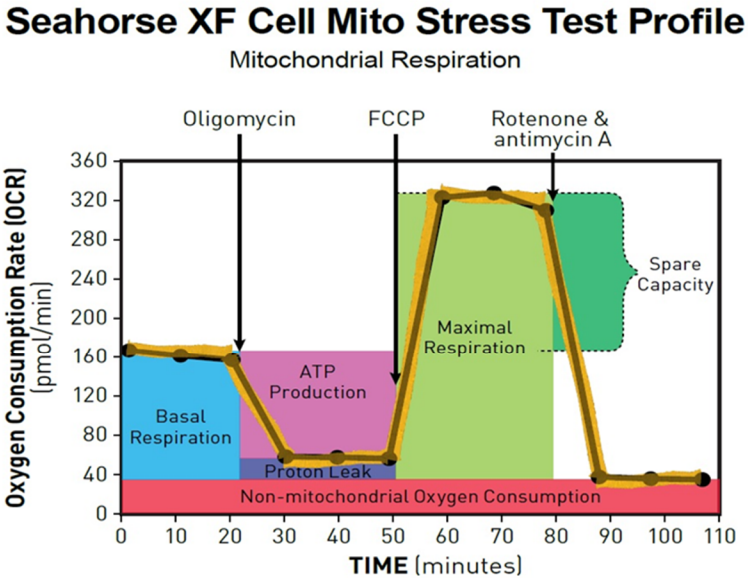
and Mito Stress tests were performed (**Figures 3.44-3.49**). As these experiments allowed a lot more replicates in each experiment, the data were more reliable.

Overall, both the Glyco Stress Test and the Mito Stress Test showed no change in cell glycolysis or mitochondrial respiration rate when eEF2K was either knocked out or silenced, except for the change in the proton leak (the basal respiration that is not coupled to ATP production) between WT and KO clones of MDA-MB-231 cells (**Figure 3.47**). In this case the data suggested a decrease in this basal respiration when comparing WT and KO #1 or KO #2 to KO #1 cells. Considering the KO clones behave differently in this regard, no conclusion can be reached about eEF2K's affect on the proton leakage of these cells. A similar issue can be seen with PC3 cells in regard to the proton leak and the spare respiratory capacity (the ability of the cells to respond to increased energy demand) of the cells. It can be seen that that the spare respiratory capacity of PC3 KO #1 cells is lower than either the WT or KO #2 cells. The proton leak of KO #1 cells is also significantly lower than that of WT cells. Once again, as the KO clones behave differently in this experiment, no conclusion can be reached about the effect of eEF2K on these processes. However, this also points out that these clones may be different from each other in some regards, possibly due to off-target CRISPR-Cas9 cuts.

The data overall further supports the evidence that targeting eEF2K has varying effects on different cell lines, as these data differ from what was found for MCF-7 and N2A cells[207, 208]. It also shows that silencing eEF2K has a different effect to knocking it out, as there was no conclusive change in cell metabolism in these cells from knocking-out eEF2K compared to the inhibition of glycolysis seen in siRNA silenced MDA-MB-231 cells from Cheng *et al.*'s study[207].

Figure 3.41

(A)



(B)

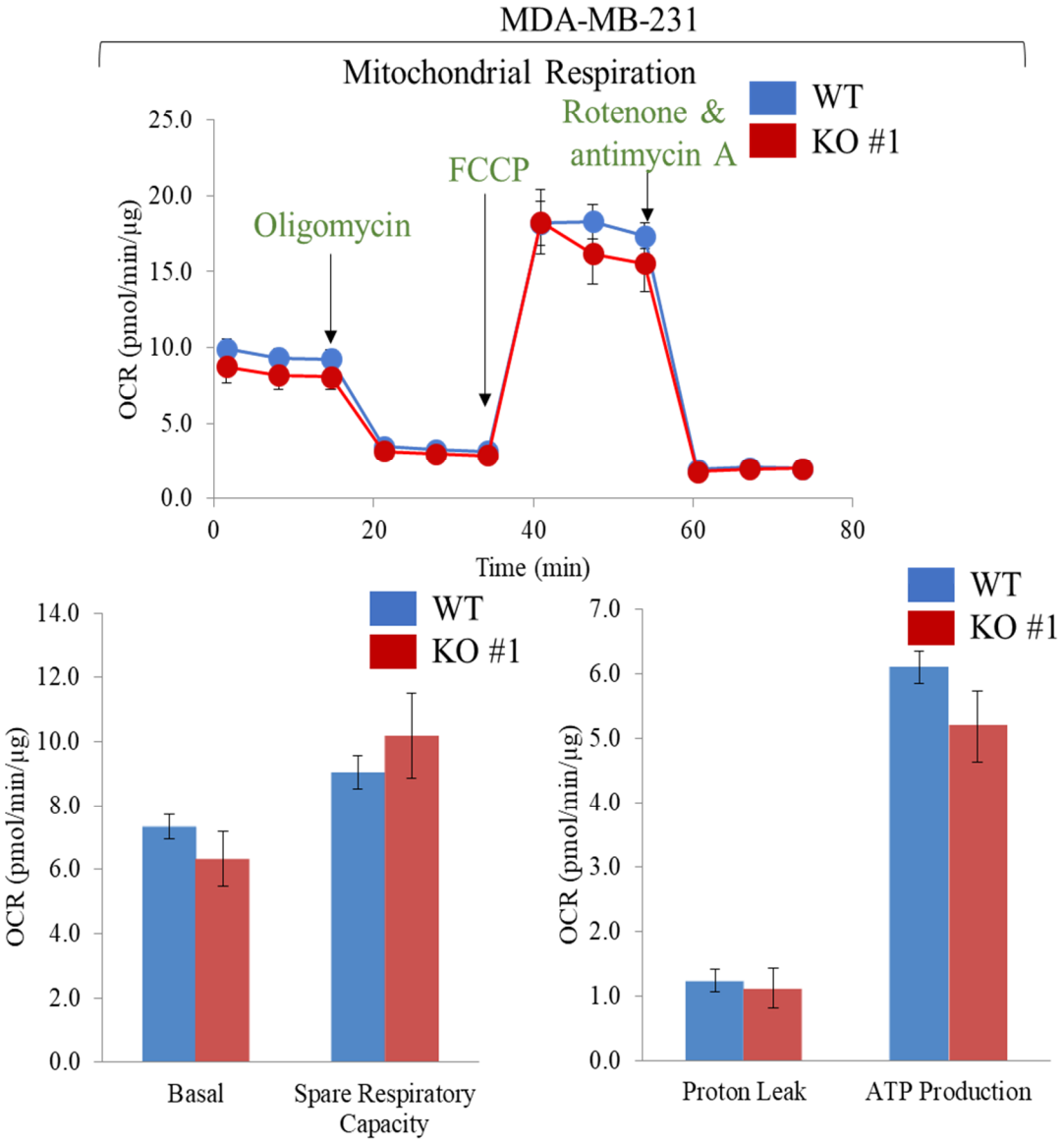


Figure 3.41: Knocking out eEF2K does not affect the mitochondrial respiration of MDA-MB-231 cells. A: Schematic of the Xfp Glyco Stress Test Kit showing the features of glycolysis measured. The diagram was taken from the assay manual[142]. **B:** MDA-MB-231 cells were grown in fully supplemented medium for 24 h prior to performing the XFp Mito Stress Test. Arrows indicate the time point at which compounds were injected into the wells. Error bars represent S.D. (n=3). The assay was normalised to total protein content.

Figure 3.42

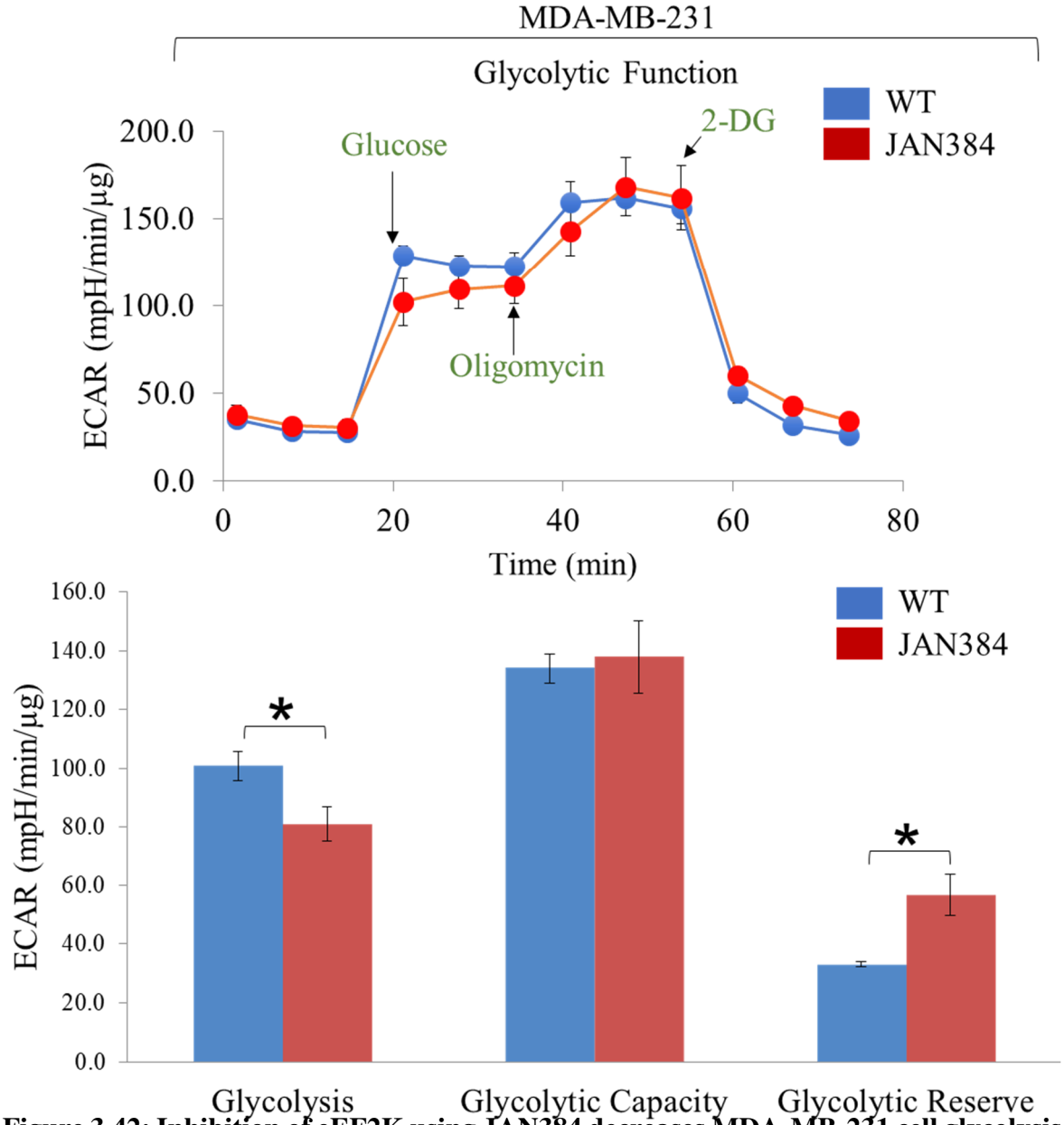


Figure 3.42: Inhibition of eEF2K using JAN384 decreases MDA-MB-231 cell glycolysis but increases the glycolytic reserve. MDA-MB-231 cells were grown in fully supplemented medium and treated with 6 µM JAN384 for 24 h prior to performing the XFp Glyco Stress Test. Arrows indicate the time point at which compounds were injected into the wells. The p-values were calculated using an unpaired, parametric, two-tailed T-test with Welch's correction. P-value: *≤0.05. Error bars represent S.D. (n=3). The assay was normalised to total protein content.

Figure 3.43

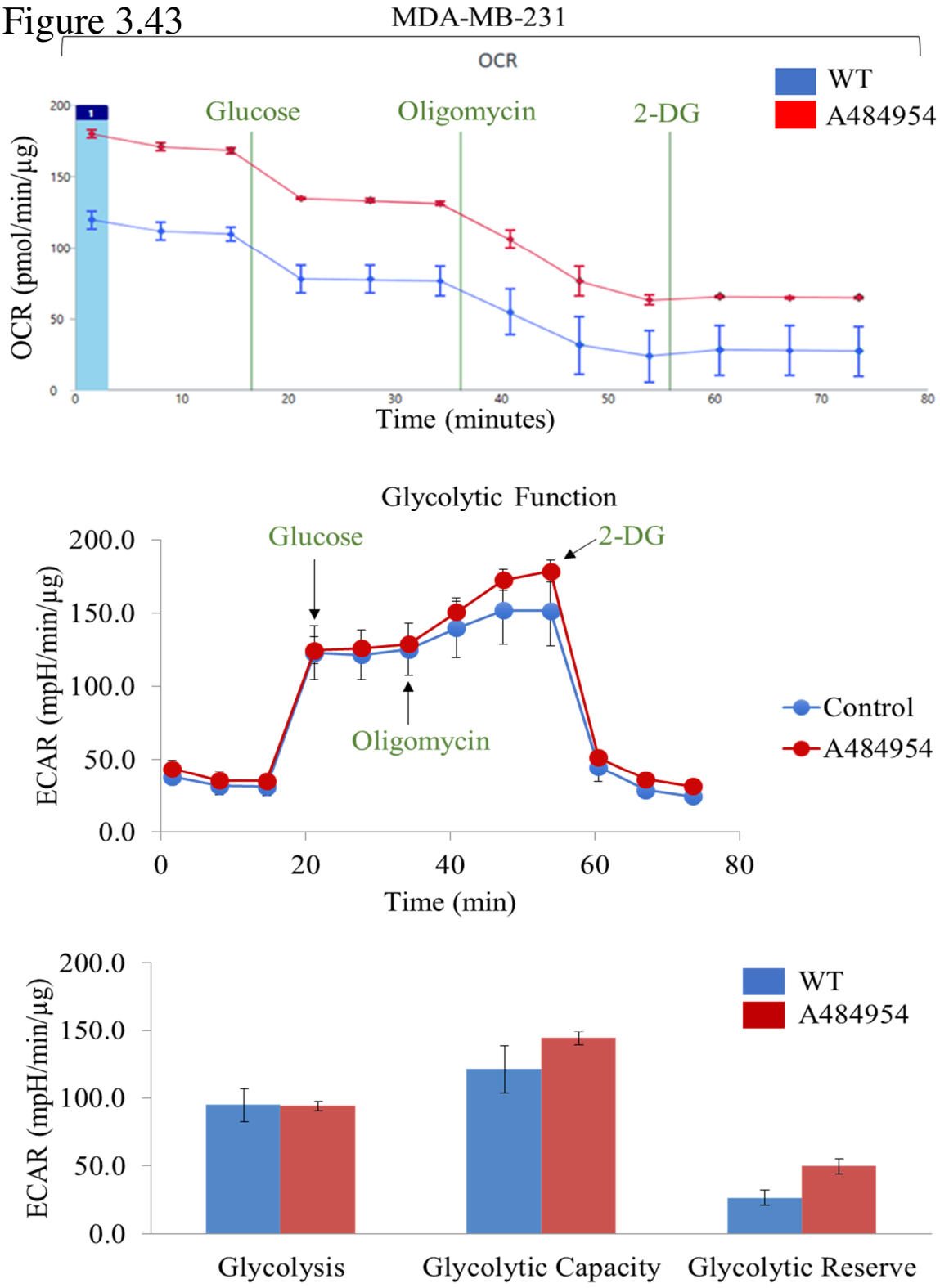

MDA-MB-231
OCR
WT
A484954
Glucose
Oligomycin
2-DG
OCR (pmol/min/µg)
Time (minutes)
Glycolytic Function
Glucose
2-DG
Oligomycin
ECAR (mpH/min/µg)
Time (min)
Control
A484954
WT
A484954
ECAR (mpH/min/µg)
Glycolysis
Glycolytic Capacity
Glycolytic Reserve

Figure 3.43: Inhibition of eEF2K using A484954 increases MDA-MB-231 cell glycolytic reserve. MDA-MB-231 cells were grown in fully supplemented medium and treated with 30 μM A484954 for 24 h prior to performing the XFp Glyco Stress Test. Arrows indicate the time point at which compounds were injected into the wells. Error bars represent S.D. (n=3). The assay was normalised to total protein content.

Figure 3.44

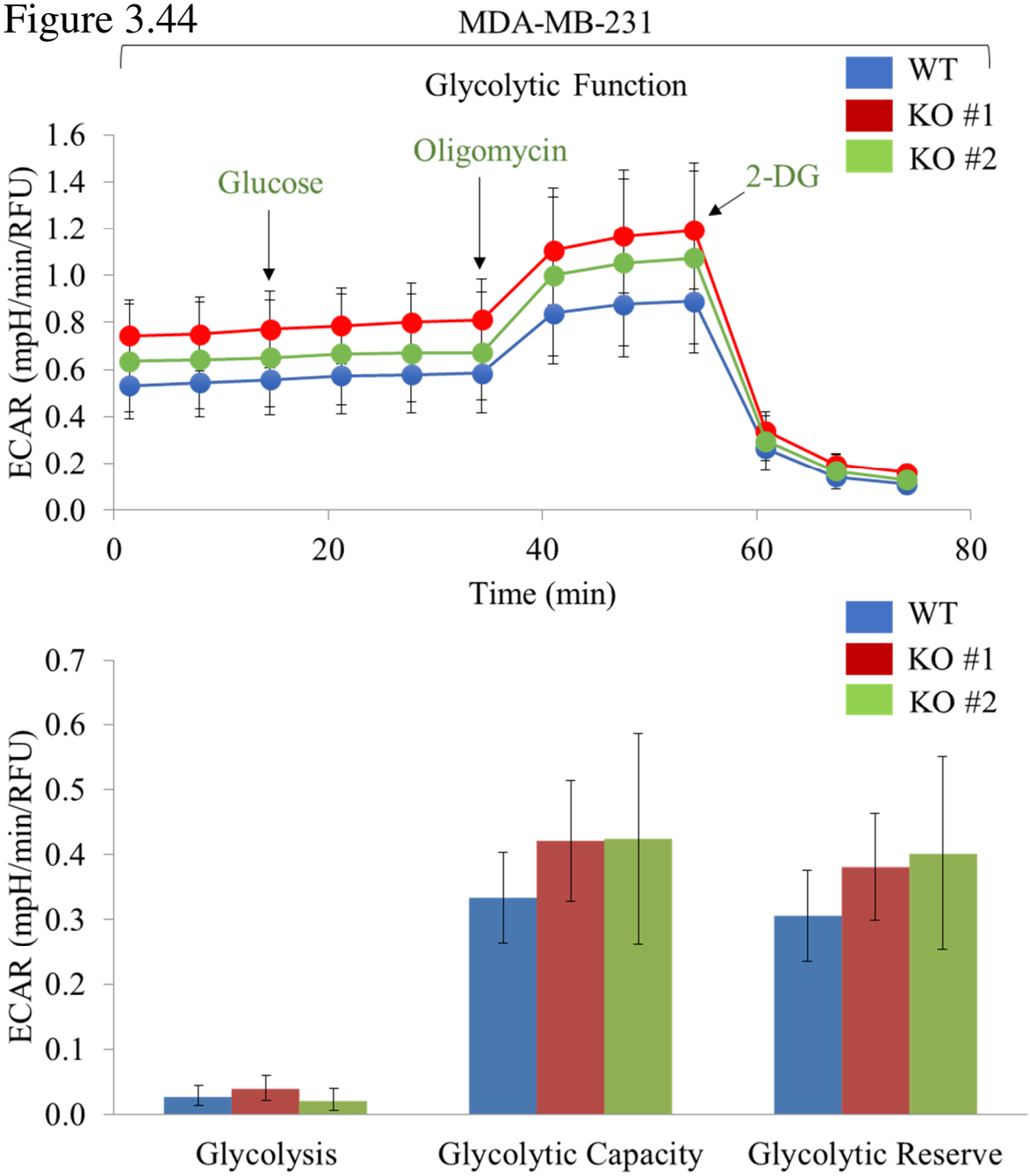


Figure 3.44: Knocking out eEF2K does not affect MDA-MB-231 cell glycolysis. MDA-MB-231 WT and eEF2K-KO cells were grown in fully supplemented medium for 24 h prior to performing the XF Glyco Stress Test. Arrows indicate the time point at which compounds were injected into the wells. Error bars represent S.D. (n=3). The assay was normalised to total Hoescht33342 signal (RFU) which is proportional to cell number.

Figure 3.45

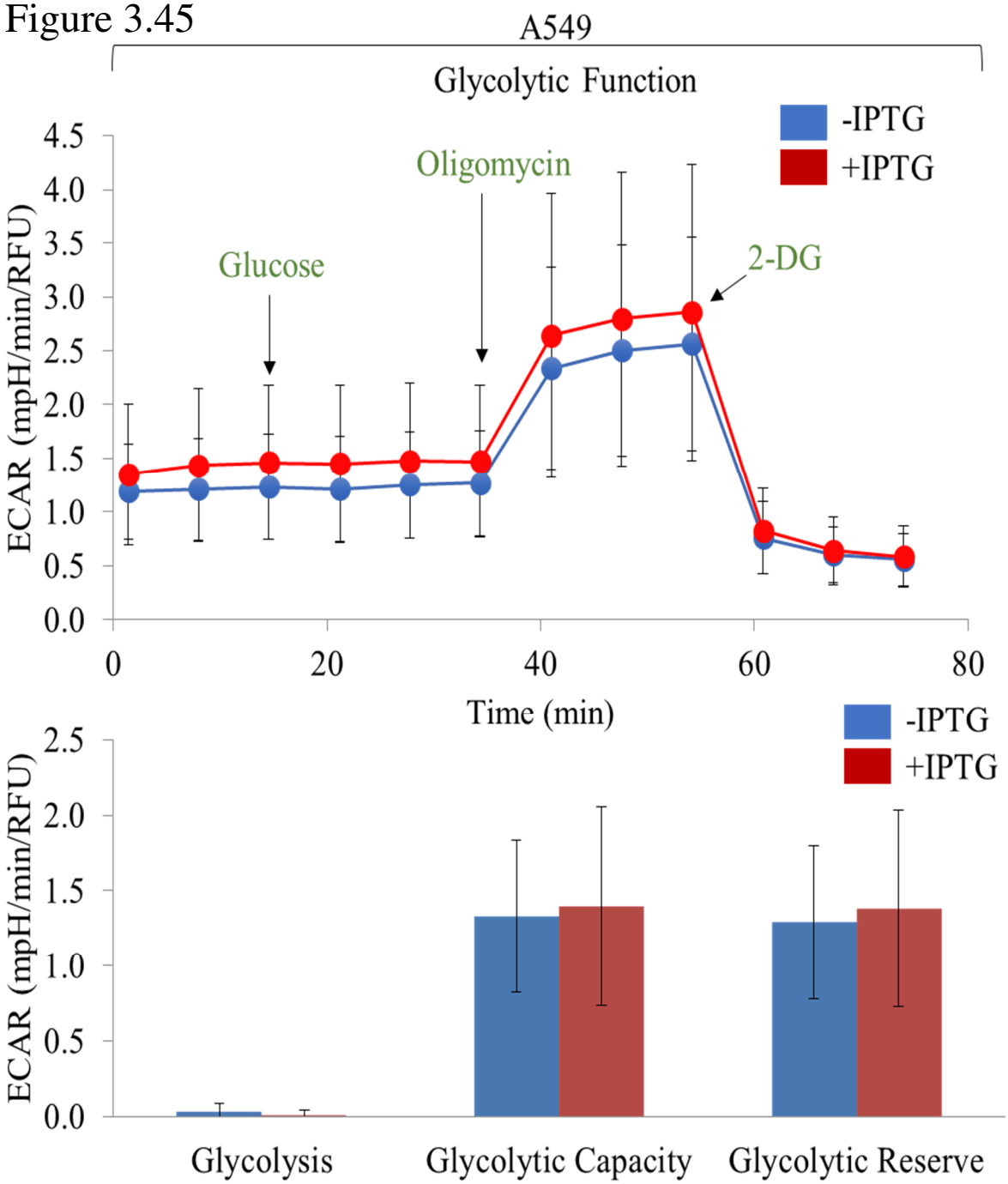


Figure 3.45: Silencing eEF2K does not affect A549 cell glycolysis. A549 cells were grown in fully supplemented medium for 24 h prior to performing the XF Glyco Stress Test. eEF2K silencing was induced with 1 mM IPTG for 5 days prior to the experiment. Arrows indicate the time point at which compounds were injected into the wells. Error bars represent S.D. (n=3). The assay was normalised to total Hoescht33342 signal (RFU) which is proportional to cell number.

Figure 3.46

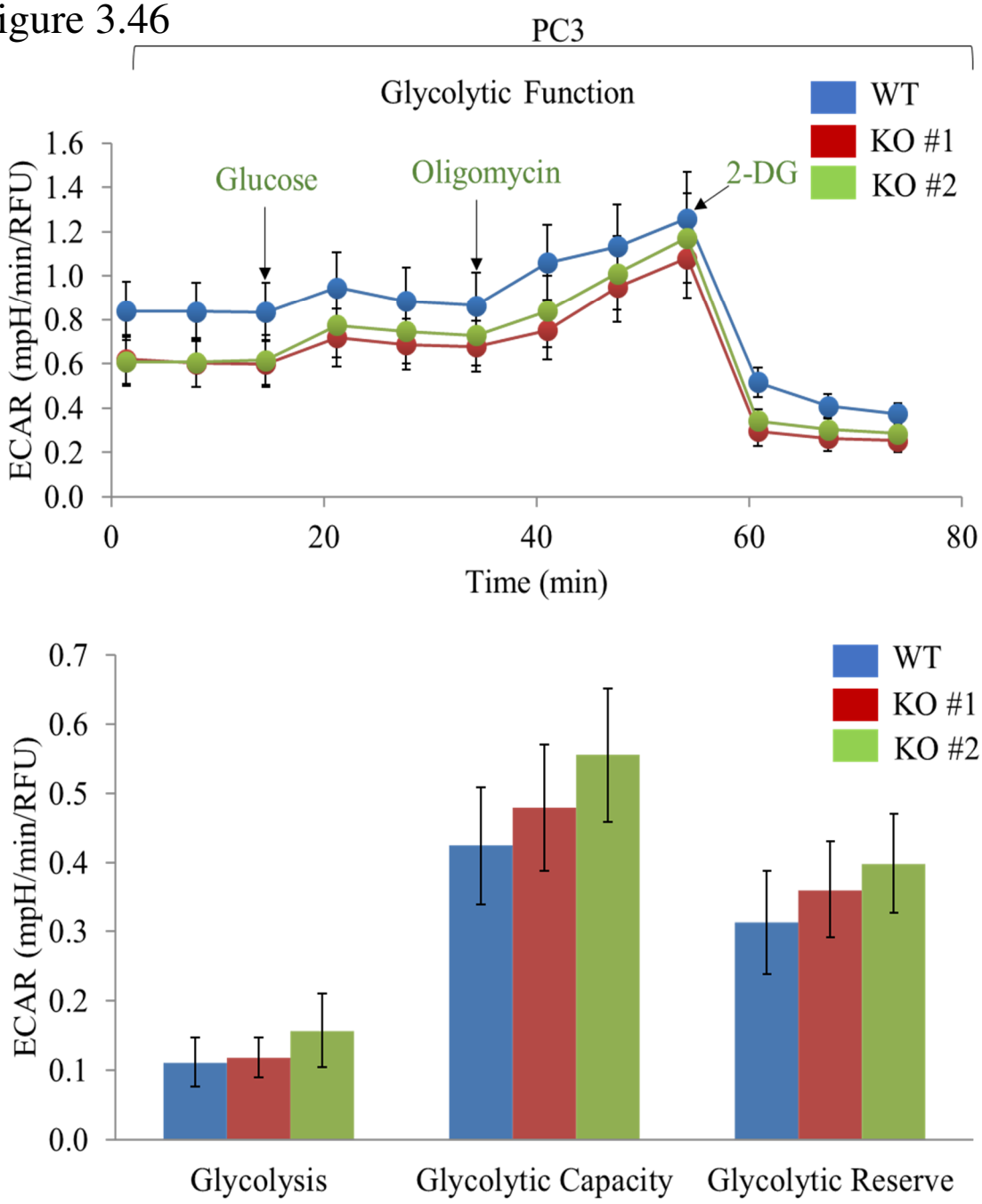


Figure 3.46: Knocking out eEF2K does not affect PC3 cell glycolysis. PC3 WT and eEFK2-KO cells were grown in fully supplemented medium for 24 h prior to performing the XF Glyco Stress Test. Arrows indicate the time point at which compounds were injected into the wells. Error bars represent S.D. (n=3). The assay was normalised to total Hoescht33342 signal (RFU) which is proportional to cell number.

Figure 3.47

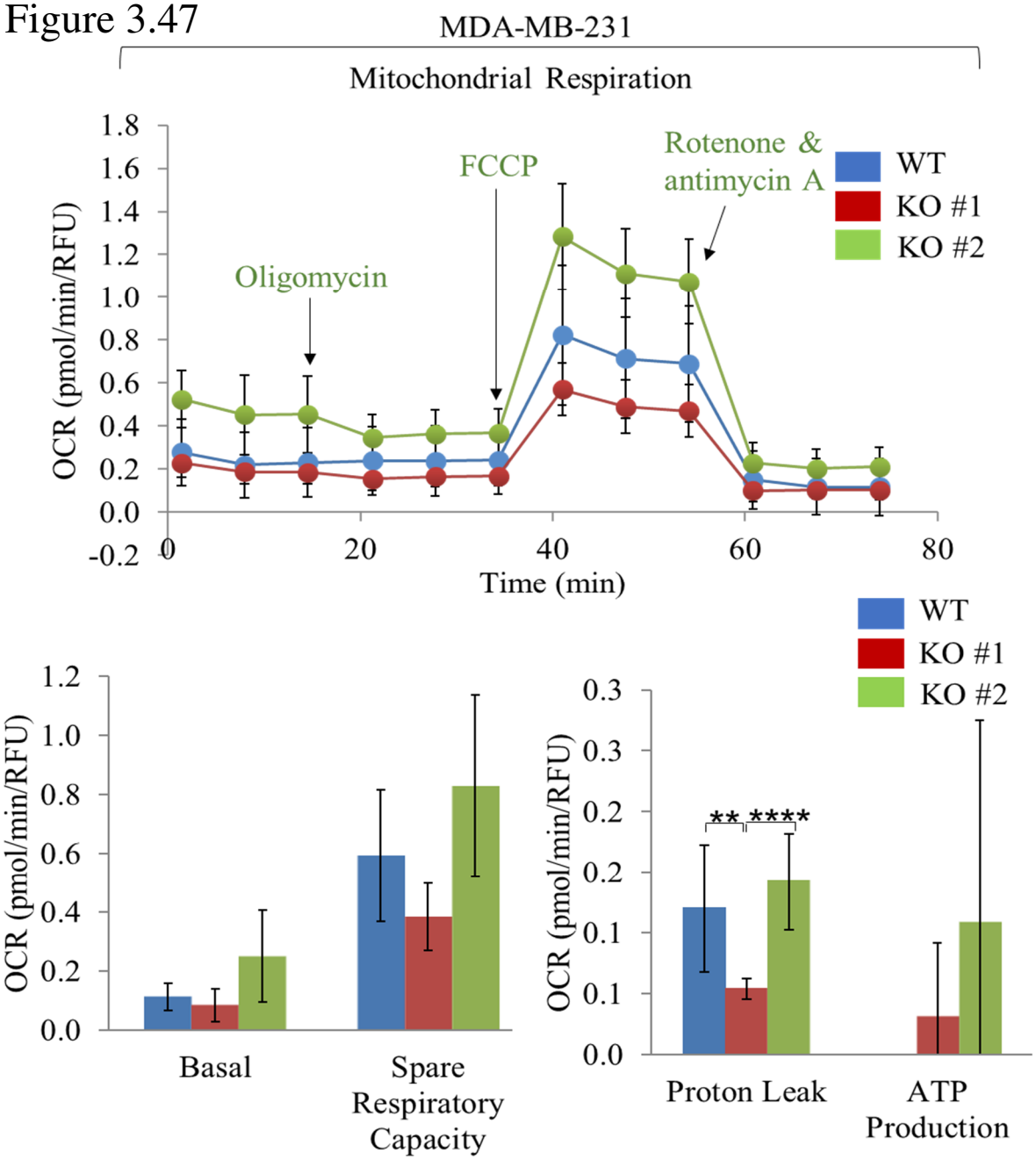


Figure 3.47: Knocking out eEF2K does not affect MDA-MB-231 cell mitochondrial respiration. MDA-MB-231 WT and eEF2K-KO cells were grown in fully supplemented medium for 24 h prior to performing the XF Mito Stress Test. Arrows indicate the time point at which compounds were injected into the wells. Error bars represent S.D. (n=3). The p-values were calculated using One-Way ANOVA Brown-Forsythe and Welch ANOVA tests. P-values: **≤0.01. The assay was normalised to total Hoescht33342 signal (RFU) which is proportional to cell number.

Figure 3.48

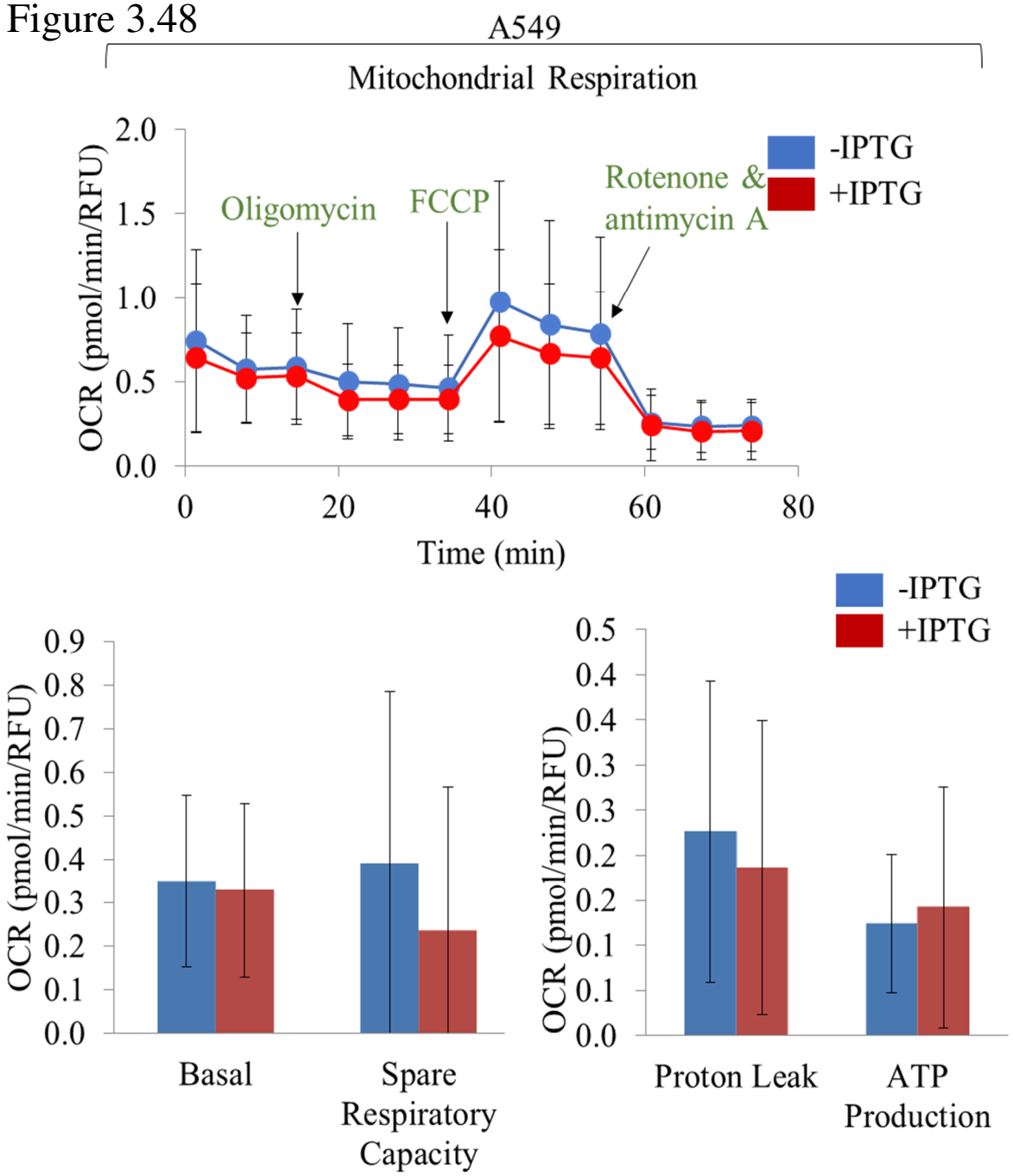


Figure 3.48: Silencing eEF2K does not affect A549 cell mitochondrial respiration. A549 cells were grown in fully supplemented medium for 24 h prior to performing the XF Mito Stress Test. eEF2K silencing was induced with 1 mM IPTG for 5 days prior to the experiment. Arrows indicate the time point at which compounds were injected into the wells. Error bars represent S.D. (n=3). The assay was normalised to total Hoescht33342 signal (RFU) which is proportional to cell number.

Figure 3.49

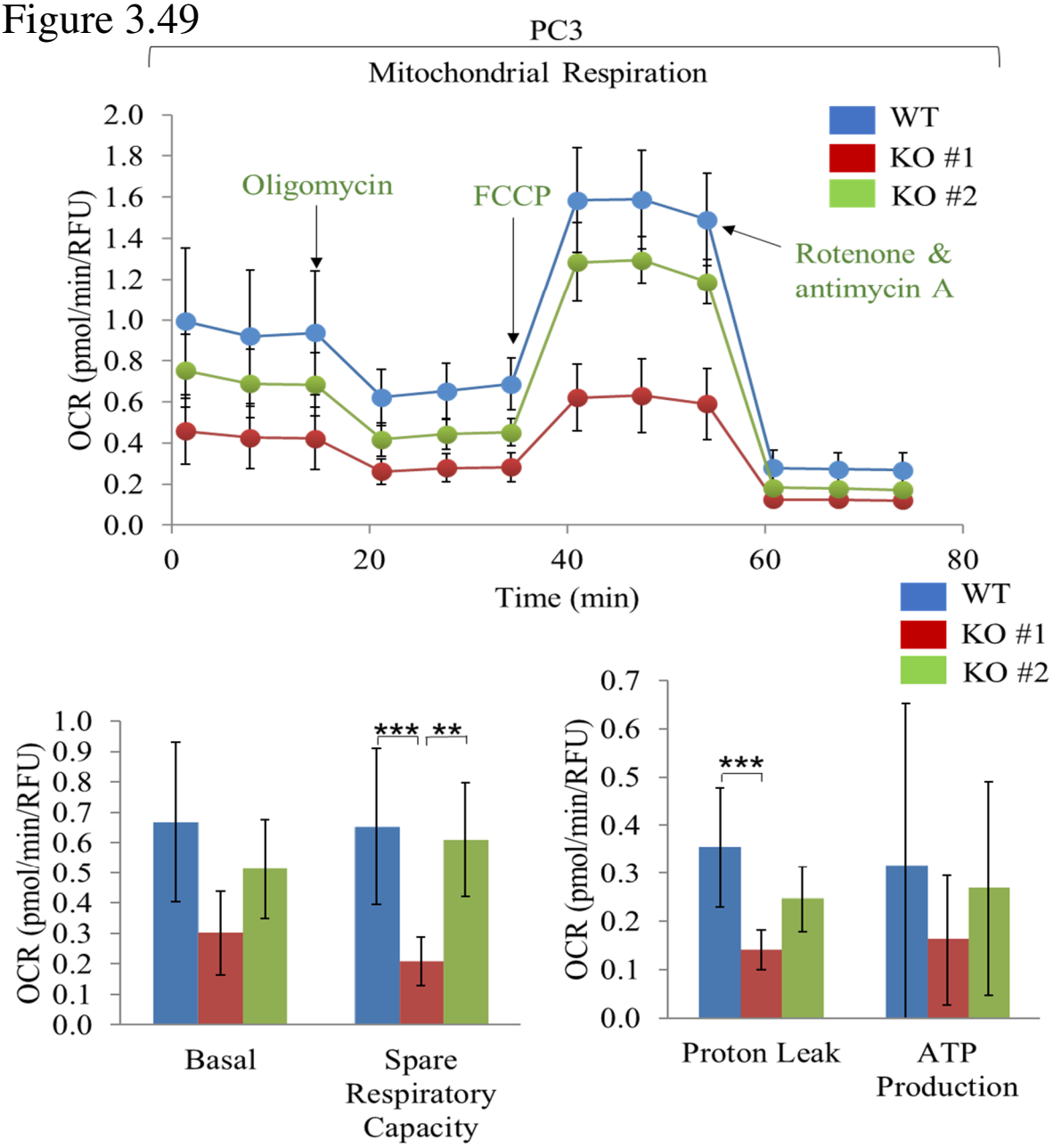


Figure 3.49: Knocking out eEF2K does not affect PC3 cell mitochondrial respiration. PC3 WT and eEFK2-KO cells were grown in fully supplemented medium for 24 h prior to performing the XF Mito Stress Test. Arrows indicate the time point at which compounds were injected into the wells. Error bars represent S.D. (n=3). The p-values were calculated using One-Way ANOVA Brown-Forsythe and Welch ANOVA tests. P-values: **≤0.01; ***≤0.001. The assay was normalised to total Hoescht33342 signal (RFU) which is proportional to cell number.

3.3 Discussion

A major study on the role of eEF2K in cell survival was published by Leprivier in 2013[57]. The study showed that, in NIH 3T3 MSCV with constitutively active Ras, eEF2K protects cells under nutrient deprived conditions through its phosphorylation and inhibition of eEF2. That study also showed that MG63 osteosarcoma cells' resistance to nutrient deprivation was directly related to their high levels of eEF2K protein. Importantly, the study also showed that MSCV cells overexpressing eEF2K survived better than control MSCV cells when injected into *nu/nu* mice on a caloric restriction diet. Another important finding was that in patients which had glioblastoma multiforme, high eEF2K mRNA levels correlated with significantly lower survival rates. This study opened an interesting possibility of using eEF2K as a potential therapeutic target in solid tumours.

I have shown in this Chapter that eEF2K affects the survival of MDA-MB-231, A549 and PC3 cells in different ways and that targeting eEF2K by itself would probably not be a very effective treatment against breast, lung and prostate cancers. Targeting autophagy at the same time as eEF2K on the other hand proved more promising in MDA-MB-231 and A549 cells.

The contrasting reports about eEF2K positively or negatively regulating autophagy[58, 115-119, 158] in different cell lines introduced confusion into this area and this chapter further showed that each cell line behaves differently when either of these two pathways are affected. The summary of the main findings in this chapter can be found in **Tables 3.1 and 3.2**.

Mechanism	Cell Lines (eEF2K-KO or IPTG induced)							
	MDA-MB-231		A549			PC3		
Medium	+Glc	-Glc	+Glc	-Glc	-Gln	+Glc	-Glc	-Gln
Cell Cytotoxicity	*	*	*	*	+	*	-	-
Cell Viability	*	*	*	*	-	*	+	+
Caspase 3/7 Activity	+	+	*	*	*	N/A		
Caspase 8 Activity	+	+	*	*	+	N/A		
Cellular ATP level	*	-	*	*	*	+	*	+
Glycolysis	*	N/A	*	N/A	N/A	*	N/A	N/A
Mitochondrial Respiration	*	N/A	*	N/A	N/A	*	N/A	N/A

Table 3.1: Summary of the changes in cellular processes under control conditions. The changes are in comparison to eEF2K-WT cells. **+**: higher than WT; **-**: lower than WT; *****: no significant difference.

Mechanism	Cell Lines (eEF2K-KO or IPTG induced)							
	MDA-MB-231		A549			PC3		
Medium	+Glc	-Glc	+Glc	-Glc	-Gln	+Glc	-Glc	-Gln
Cell Cytotoxicity	+	+	*	+	+	*	-	-
Cell Viability	-	-	*	-	-	*	+	+
Caspase 3/7 Activity	+	+	+	*	*	N/A		
Caspase 8 Activity	+	+	*	+	+	N/A		
Cellular ATP level	-	-	*	-	*	+	*	+

Table 3.2: Summary of the changes in cellular processes when autophagy was inhibited. The changes are of eEF2K-KO or IPTG induced cells treated with BafA in comparison to eEF2K-WT cells treated with BafA alone. **+**: higher than WT; **-**: lower than WT; *****: no significant difference.

One of the major findings of this chapter was that when both eEF2K and autophagy are inhibited in MDA-MB-231 and A549 cells under nutrient deprived conditions, cell death was greatly increased compared to when either pathway was blocked separately. This suggests that eEF2K and autophagy are both used by the cells under nutrient deprived conditions to survive and in a complementary manner. Thus, when one pathway is turned off, the other pathway is still active, allowing the cells to either save their energy reserves or scavenge their own proteins. However, when both pathways are turned off, the cells can no longer control their protein synthesis and have no way to regain lost energy. Thus, these cells die far quicker. This is supported by data for cell death, viability and partially caspase 3/7 and 8 activity. This opens a possibility of using a combination therapy of eEF2K and autophagy inhibitors. It has previously been shown that autophagy is triggered by some tumour cells to mitigate the cellular stress induced by anti-cancer drugs. These studies were done in esophageal squamous cell carcinoma, glioblastoma and colon cancer cells. These cells were then sensitised to anti-cancer drugs by inhibiting autophagy[164-168]. As there is now evidence that autophagy and eEF2K each play important roles in cancer cell survival, a combination treatment therapy should be tested on *in vivo* xenograft models of breast and lung cancer, when suitable inhibitors of eEF2K become available.

On the other hand, the data for PC3 cells strongly suggest that inhibiting eEF2K in prostate cancer would give a worse prognosis. Cell cytotoxicity and viability assays showed that inhibiting eEF2K in these cells led to lower cytotoxicity and higher viability. The inhibition of autophagy in eEF2K-KO PC3 cells did not further affect cell survival. This shows that eEF2K or autophagy inhibition leads to differing effects on cell survival in different cell

lines. This combination of autophagy and eEF2K inhibition needs to be tested on other breast, lung, and prostate cancer cell lines to confirm these trends.

Interestingly, I also found that eEF2K knock-out or silencing alone lowered cellular ATP levels in MDA-MB-231 cells under-Glc conditions, while in PC3 cells these levels were unexpectedly increased under +Glc and -Gln conditions. This suggested that PC3 cells upregulate glycolysis or respiration related proteins to metabolise the nutrients provided by the medium more efficiently, building up larger stores of ATP that they are then able to use when put in nutrient deprived conditions.

Treatment with BafA also caused a drop in ATP under +Glc conditions for MDA-MB-231 cells and -Glc conditions for A549 cells. These data suggested that eEF2K inhibition altered cell metabolism which would be a possible explanation as to why eEF2K altered cell viability in such ways. However, experiments using the Seahorse instrument showed no significant change in glycolysis or mitochondrial oxidation in any of the three tested cell lines. It is important to understand the mechanisms behind how eEF2K and autophagy act to protect MDA-MB-231 and A549 cells. For this, a proteomics experiment to study cellular protein changes in eEF2K-WT and KO cells under nutrient deprived conditions could be informative. This proteomics study was performed and is described in detail in **Chapter 4**.

4.1 Introduction

4.1.1 Creation of cells resistant to chemotherapy drugs

Cancer cell lines resistant to various chemotherapy drugs have been artificially developed in laboratories since the 1990's with the aim of understanding the potential mechanisms by which these cells were able to survive the effects of these agents. For example, cisplatin is a major chemotherapeutic agent that has been used to treat various types of cancer, including lung, ovarian, bladder and cervical cancers. However, as with any anti-cancer drug, tumours show resistance to cisplatin, eventually making the treatment ineffective. One of the earliest studies was done by Shen *et al*.[211] in 1995, who isolated a variety of cisplatin resistant cancer cell lines and grew cell lines that showed strong resistance to cisplatin from the isolates. This method involved selecting surviving cells from colonies grown in stepwise increases in cisplatin concentration from 300 ng/ml to 20 μg/ml. This proceeded over a period of 24 months. The group was then able to show common features between cisplatin resistant human adenocarcinoma and liver carcinoma cell lines, such as cross-resistance to methotrexate (another anti-cancer drug) and heightened expression of hsp60, advancing understanding of how these cancers acquire resistance to this drug.

The above study was an example of how high-level resistance cell lines were created. These types of models involve growing cells continuously in the presence of the drug and increasing its concentration over time. Surviving clones are then selected from the mixed population. These types of models typically retain their resistance and are easier to maintain in cell culture without losing it. As these types of cells have high levels of resistance,

molecular changes associated with the mechanism of this resistance are greater and easier to identify[212]. These types of resistance cells have also been created for cervical, leukemia and lung cancer cell lines with resistance against diverse anti-tumour agents such as cisplatin, erubicin, taxane and verapamil[211, 213-217].

The other type of resistant cell lines are created with a pulsed dosing of the chemotherapy compounds. Cells are typically treated with a lower dose of the drug and the survivors are left to recover in drug-free medium. This mimics the chemotherapy cycles a patient receives, making these types of resistant models more clinically relevant. However, potential disadvantages are lower degrees of resistance to the drugs, unstable resistance and smaller molecular changes that can be detected and analysed. Such cell lines have been created to become resistant to cisplatin, oxaliplatin, paclitaxel, verapamil and idarubicin[213-215, 218-223]. A major advantage of the pulsed method is also that it takes far less time to create resistant cells. While the changes may be smaller than for high-level resistant cells, for initial studies it is a good first step.

4.1.2 Aims of this Chapter

It is important to find out more information on how cells are able to obtain resistance to adverse conditions. In the case of this project, these conditions are nutrient deprivation and inhibition of autophagy. To that end, the first aim of this chapter was to create eEF2K-WT and KO MDA-MB-231 cells that are resistant to deprivation of glucose and pyruvate as well as concurrent lack of eEF2K and inhibition of autophagy via the pulsed dosing method. The second aim is to perform a comparative proteomics study between resistant and non-resistant cells that have been treated in nutrient-deprived conditions and autophagy has been inhibited.

A proteomics experiment that looks at total protein abundance could point in the direction of how these cells had become resistant to lack of eEF2K and autophagy. A secondary goal was to perform a phospho-proteomics study to seek potential phosphorylation targets of eEF2K other than its only known target, eEF2.

Please note that the majority of the data shown in this chapter is in a currently submitted manuscript which is attached as an Appendix to this thesis.

4.2 Results

4.2.1 Creation of MDA-MB-231 WT and eEF2K-KO cells that are resistant to glucose deprivation and inhibition of autophagy

To create resistant cells, the approach shown in **Figure 4.1** was followed. MDA-MB-231 eEF2K-WT and both eEF2K-KO clones were treated for 48 h in -Glc medium with 125 nM BafA once they had reached 90% confluency in 6-well plates. The medium was removed, and the cells were washed three times with PBS to remove dead cells, replacing the final wash with +Glc medium. This medium was changed each day to remove any dead or dying cells. After the survivors reach 90% confluency, this process was repeated. This treatment was also done on non-resistant cell lines for comparison after the resistant cells had undergone 10 pulsed cycles. Once there was a significant visual increase in the number of 'resistant' cells still attached to the plate after treatment compared to parental cells the resistant cells were grown up in T75 flasks and seeded into 96-well plates for cytotoxicity measurements, as well as into 6-well plates for western blotting. The eEF2K-WT and KO resistant cells were then treated for 48 h in ±Glc medium with 125 nM BafA or 25 μM

chloroquine (CQ) alongside non-resistant cells. Cell cytotoxicity measurements and western blots are shown in **Figures 4.2 and 4.3**, respectively. CellTox Green fluorescence images are shown in **Figures 4.4-4.6**. Chloroquine, a weak base, accumulates within the lysosome, raising its pH by binding protons, preventing the function of the hydrolases within, so that the contents of the autophagosome cannot be degraded[224]. It was used to ensure whether the cells were truly resistant to autophagy inhibition or only to the effect that BafA has on the V-ATPase. If the cells were only resistant to BafA, CQ treatment would still lead to increased cell death. However, if the cells were resistant to the inhibition of the autophagic process overall, they would also be resistant to the effects of CQ.

As seen in **Figure 4.2**, MDA-MB-231 WT and both eEF2K-KO clones had become partially resistant to nutrient deprivation and inhibition of autophagy. Interestingly, in +Glc conditions, CQ treatment did not increase cell death compared to control, unlike BafA, even though it successfully inhibited autophagy (**Figure 4.3**). This suggests that BafA may be a more potent inhibitor of autophagy, i.e., cells that have had their autophagy inhibited earlier will run out of nutrients and thus die faster. Another possibility is that BafA targets another pathway that results in higher cell death when disrupted, such as mitochondrial respiration, as has been previously suggested to be the case in primary rat cortical neurons[206] . Under -Glc conditions, both WT and eEF2K-KO resistant cells showed approximately a 4.4-fold decrease in cell cytotoxicity under control, CQ and BafA treatment conditions compared to non-resistant cells. This shows that these cells are partially resistant to nutrient deprivation and inhibition of autophagy. Since the resistance was comparable whether treated with CQ or BafA, these data also show that the cells did not become resistant only to BafA's ability to inhibit of autophagy but to the inhibition of the overall process, i.e., their survival becomes independent of autophagy.

Figure 4.1 **Generation of MDA-MB-231 Resistant Cells**

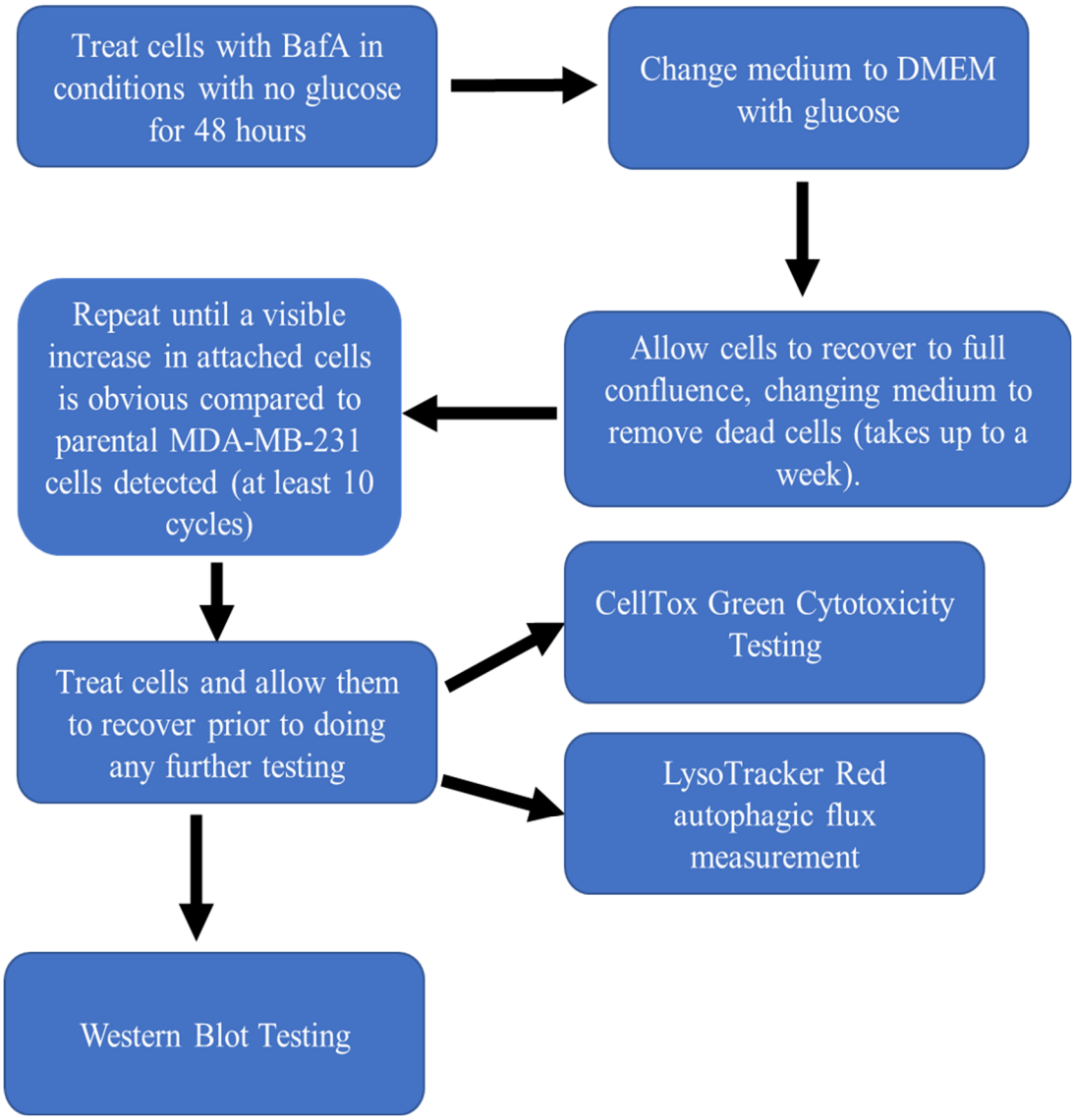


Figure 4.1: Schematic of the process used to create cells resistant to nutrient deprivation, lack of eEF2K and autophagy inhibition. MDA-MB-231 cells were treated in medium without Glc/Pyr and 125 nM BafA for 48 h. Medium was changed to +Glc and the survivors were allowed to recuperate with media changes removing dead cells every day. This pulsed treatment was repeated until a visible change in survival between non-resistant and resistant cells. Resistant cells were then compared to non-resistant cells using CellTox Green to measure cell viability. LysoTracker Red was used to measure autophagic flux while western blotting was performed to check for protein levels and correct inhibition of eEF2K and autophagic pathways.

Figure 4.2

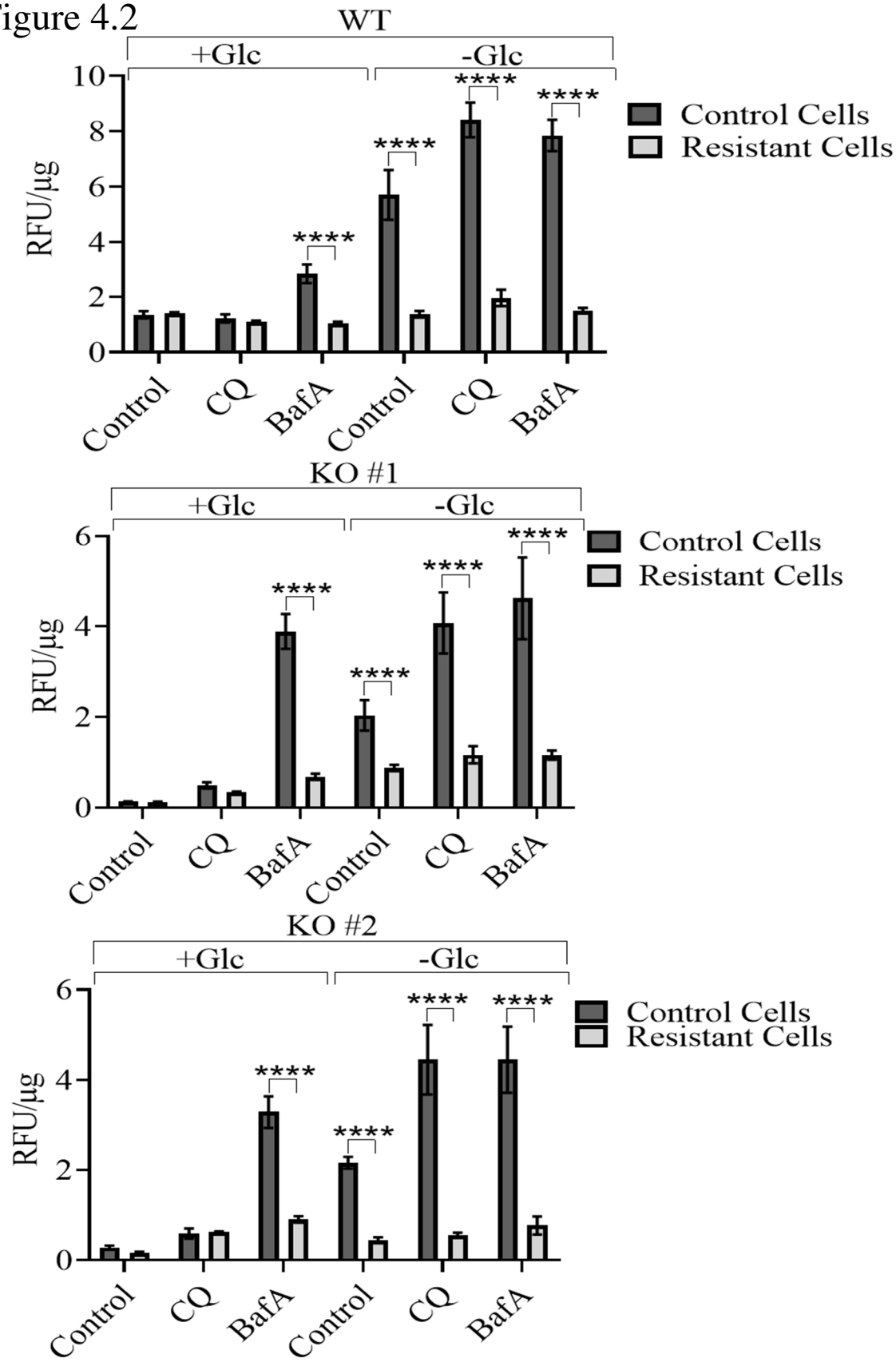

WT
+Glc
-Glc
RFU/µg
Control Cells
Resistant Cells
****
Control
CQ
BafA
KO #1
KO #2

Figure 4.2: Resistant cells are partially resistant to cell death under nutrient deprived conditions and autophagy inhibition. CellTox Green Assays of MDA-MB-231 eEF2K-WT and KO non-resistant and resistant cells treated in medium with or without Glc/Pyr and with or without CQ (25 μM) or BafA (125 nM) for 48 h. Error bars represent S.D. (n=3). The p-values were calculated using Two-Way ANOVA with the Turkey multiple comparisons test. P-values: ****≤0.0001. RFU was normalised to total protein content.

Figure 4.3

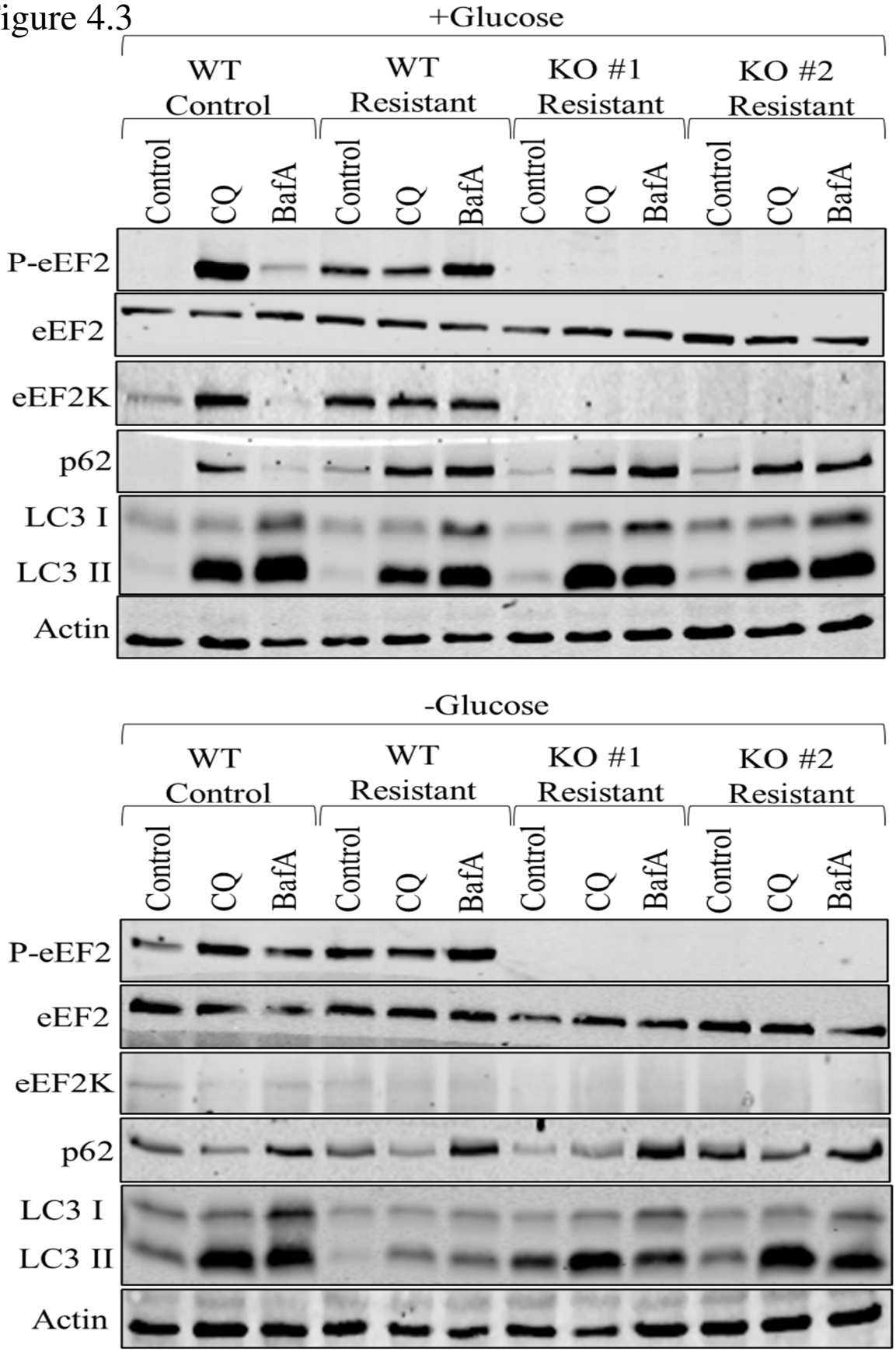

+Glucose
WT Control
WT Resistant
KO #1 Resistant
KO #2 Resistant
Control
CQ
BafA
P-eEF2
eEF2
eEF2K
p62
LC3 I
LC3 II
Actin
-Glucose
WT Control
WT Resistant
KO #1 Resistant
KO #2 Resistant
Control
CQ
BafA
P-eEF2
eEF2
eEF2K
p62
LC3 I
LC3 II
Actin

Figure 4.3: Chloroquine and Bafilomycin A successfully inhibit autophagy in WT and eEF2K KO MDA-MB-231 resistant cells. MDA-MB-231 eEF2K-WT and KO cells were treated in medium with or without Glc/Pyr and with or without CQ (25 μM) or BafA (125 nM) for 48 h. The cells were lysed, and the lysates were run on (16%) SDS-PAGE for low molecular weight proteins and (12.5%) for others. Images are representative of n=3.

Figure 4.4

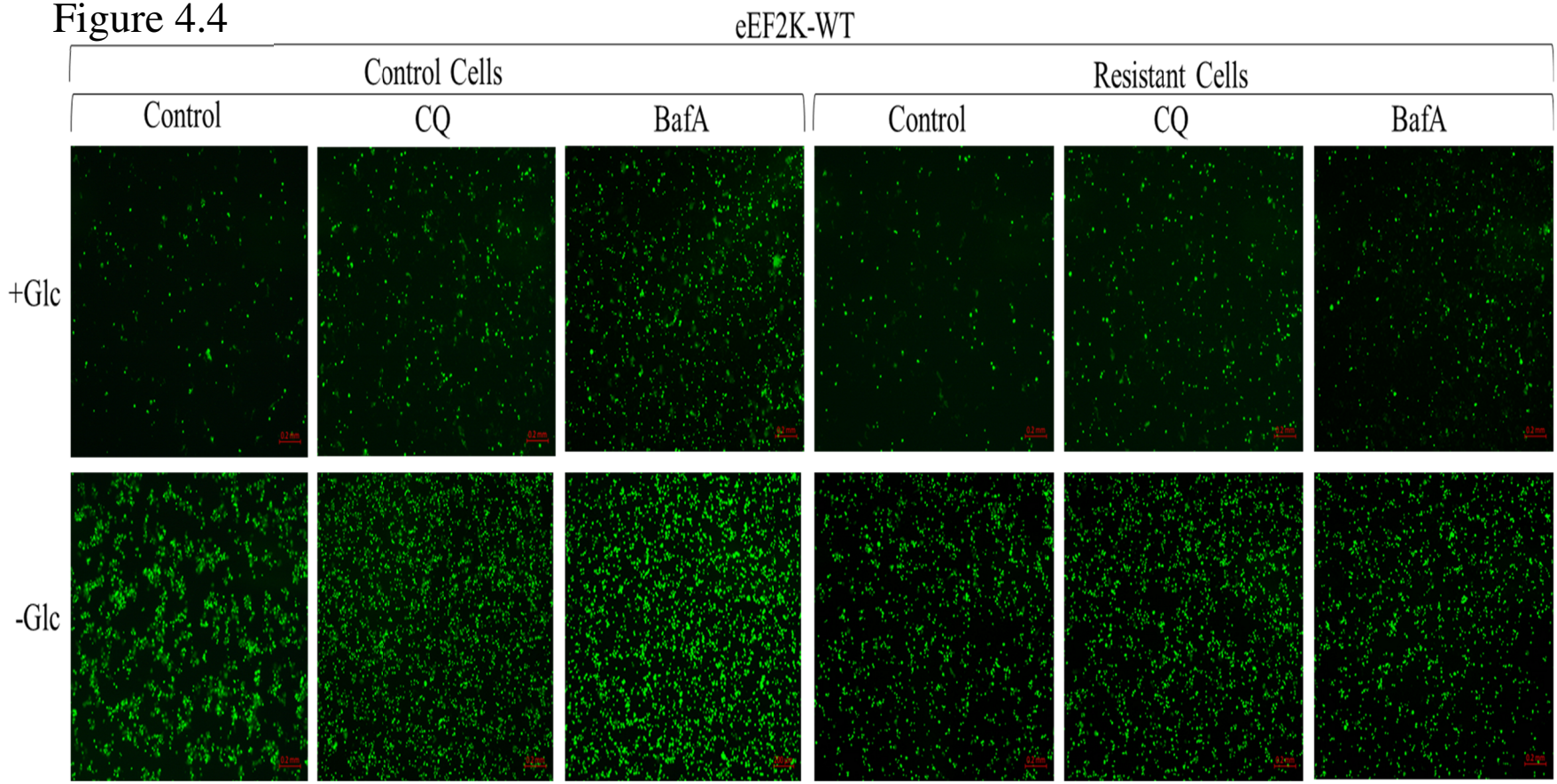


Figure 4.4: eEF2K-WT resistant cells are partially resistant to cell death under nutrient deprived conditions and autophagy inhibition. CellTox Green Assay images of MDA-MB-231 eEF2K-WT non-resistant and resistant cells treated under ±Glc conditions with or without CQ (25 μM) or BafA (125 nM) for 48 h. Images were taken using Zeiss Axiovert 200 microscope with the 4X magnifying lens. Each image is representative of 15 images total from 3 biological replicates.

Figure 4.5

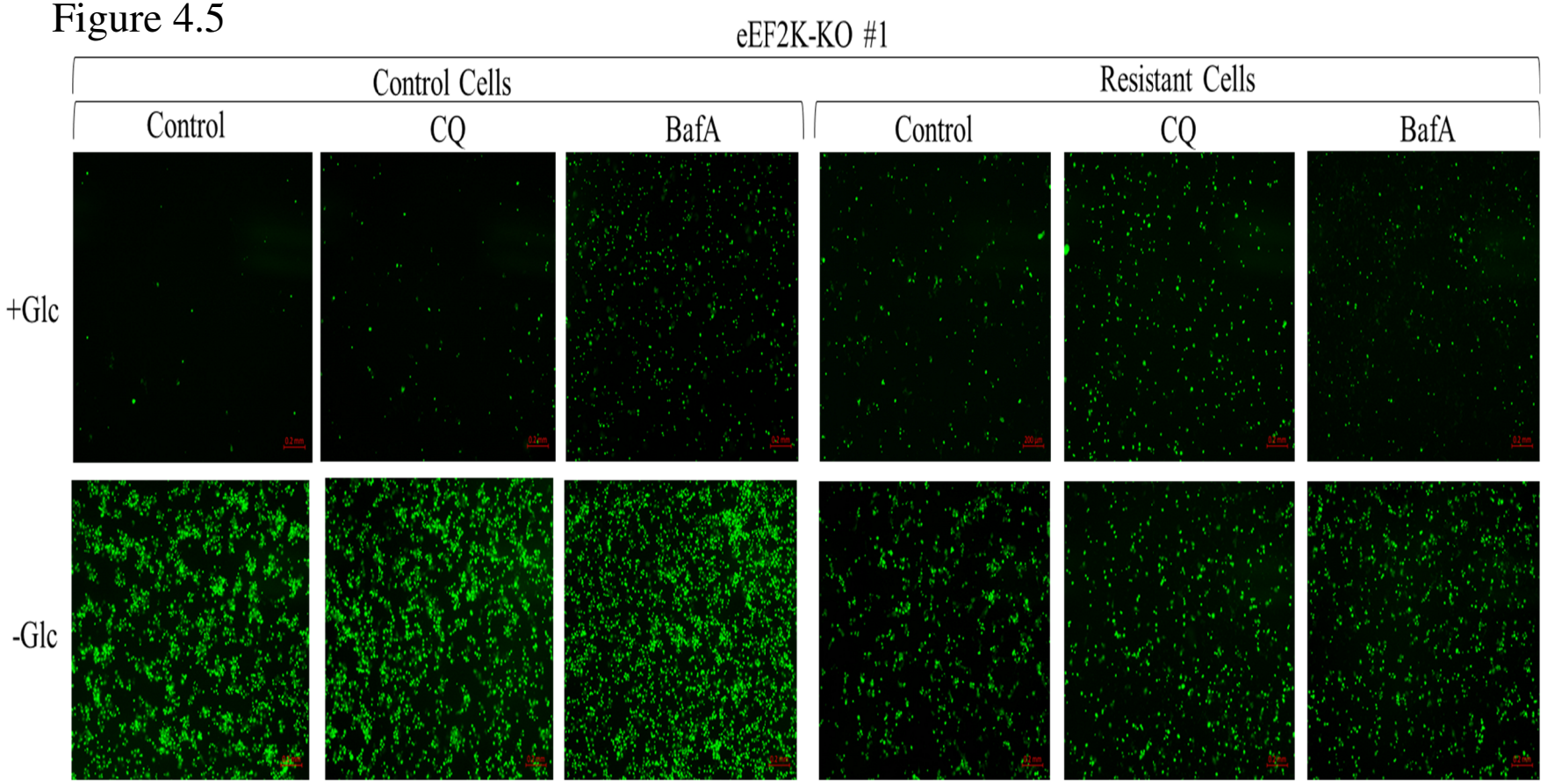


Figure 4.5: eEF2K-KO #1 resistant cells are partially resistant to cell death under nutrient deprived conditions and autophagy inhibition. CellTox Green Assay images of MDA-MB-231 eEF2K-KO #1 non-resistant and resistant cells treated under ±Glc conditions with or without CQ (25 μM) or BafA (125 nM) for 48 h. Images were taken using Zeiss Axiovert 200 microscope with the 4X magnifying lens. Each image is representative of 15 images total from 3 biological replicates.

Figure 4.6

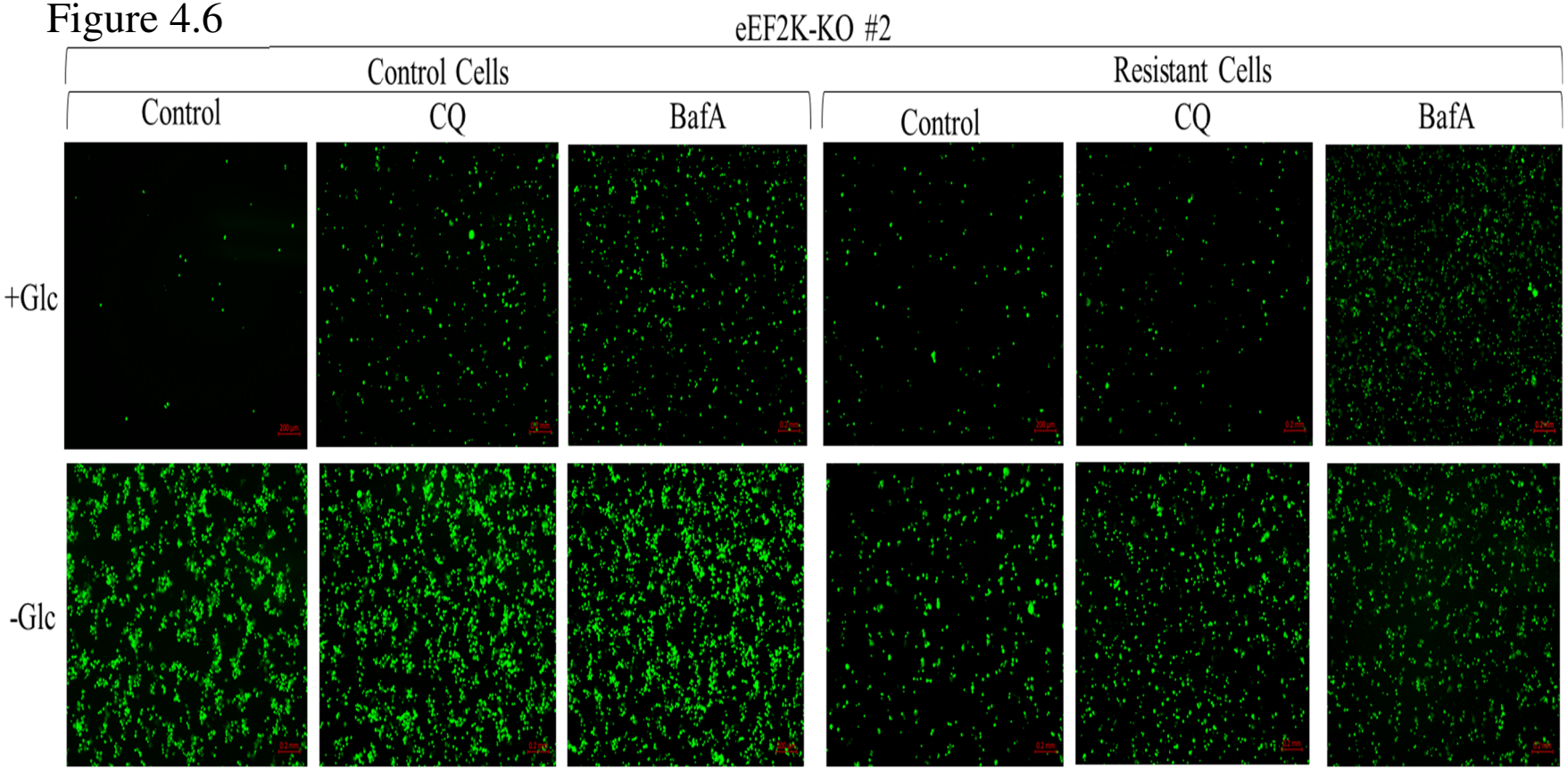


Figure 4.6: eEF2K-KO #2 resistant cells are partially resistant to cell death under nutrient deprived conditions and autophagy inhibition. CellTox Green Assay images of MDA-MB-231 eEF2K-KO #2 non-resistant and resistant cells treated under ±Glc conditions with or without CQ (25 μM) or BafA (125 nM) for 48 h. Images were taken using Zeiss Axiovert 200 microscope with the 4X magnifying lens. Each image is representative of 15 images total from 3 biological replicates.

Looking at **Figure 4.3**, both CQ and BafA effectively inhibit autophagy in both non-resistant and resistant cells in ±Glc conditions. As expected, p62 and LC3-II levels greatly increased when the cells were treated with CQ or BafA, showing that autophagy cannot break down these two proteins, confirming that it is inhibited. Interestingly, in +Glc control conditions, the resistant eEF2K-WT and KO cells showed higher levels of p62 and LC3-II, suggesting these cells have higher levels of basal autophagic flux (under these conditions, where no inhibitor of lysosomal function has been added).

Another experiment to confirm that CQ and BafA worked successfully was performed using a LysoTracker Red probe[136]. This probe accumulates in the acidic lysosome which relieves the quenching of the dye by its weak base side chain. The dye then fluoresces at a much higher intensity. This allows for the measurement of autophagic flux. Using BafA or CQ on cells should prevent the dye from accumulating inside the lysosomes as the autophagic process is inhibited, thus little Lysotracker signal would be measured. MDA-MB-231 eEF2K-WT and KO non-resistant and resistant cells were treated in -Glc conditions for 2 h with or without CQ or BafA (**Figure 4.7**). The signal was normalised to total cell signal via Hoechst33342 staining. According to the LysoTracker Red signal, both BafA and CQ effectively inhibited autophagic flux within 2 h, as the level of signal was very low compared to control. Interestingly, autophagic flux was higher in BafA resistant WT and eEF2K-KO cells compared to their non-resistant counterparts under control conditions. WT and KO #1 resistant lines showed a small increase of approximately 1.3-fold. However, eEF2K-KO #2 resistant clone showed a much larger increase of approximately 3-fold. This increase in flux can also be seen when cells were treated with CQ and BafA. Compared to non-resistant KO #2 cells, the flux was higher by 3.5-fold and 2.6-fold when treated with BafA and CQ

respectively. This suggests that the KO #2 resistant cell lines could be able to utilise autophagy to build up a metabolite reserve that is then used to assist them in surviving nutrient deprivation and autophagy inhibition. WT and KO #1 resistant cells could also be able to use their higher autophagic flux to build up a metabolite reserve, albeit to a lesser degree than KO #2 resistant cells. Importantly, the differences in autophagic flux between the different resistant cell lines also suggests that the mechanisms by which these cells have gained resistance to nutrient deprivation and autophagy inhibition are different.

4.2.2 The resistance to nutrient deprivation and autophagy inhibition is lost over time

The method for creating these resistant cells involved dosing the cells with BafA under nutrient deprivation and allowing them to recover prior to dosing them again. A disadvantage of this method is that the resistance gained is not stable. Resistant cells were grown in optimal growth conditions for 1, 2 or 3 weeks, followed by cell death measurements after treatment in -Glc conditions with or without BafA or CQ and compared against non-resistant (control) cells treated in the same manner. **Figures 4.8-4.10** show that by the second week of growth without any stresses, the resistance was halved and by the third week there was no significant difference between the non-resistant and resistant cells. This means that the cells must be treated in -Glc conditions with BafA and allowed to recover for up to a week prior to performing any further experiments. This will ensure the cells retain their resistance.

Figure 4.7

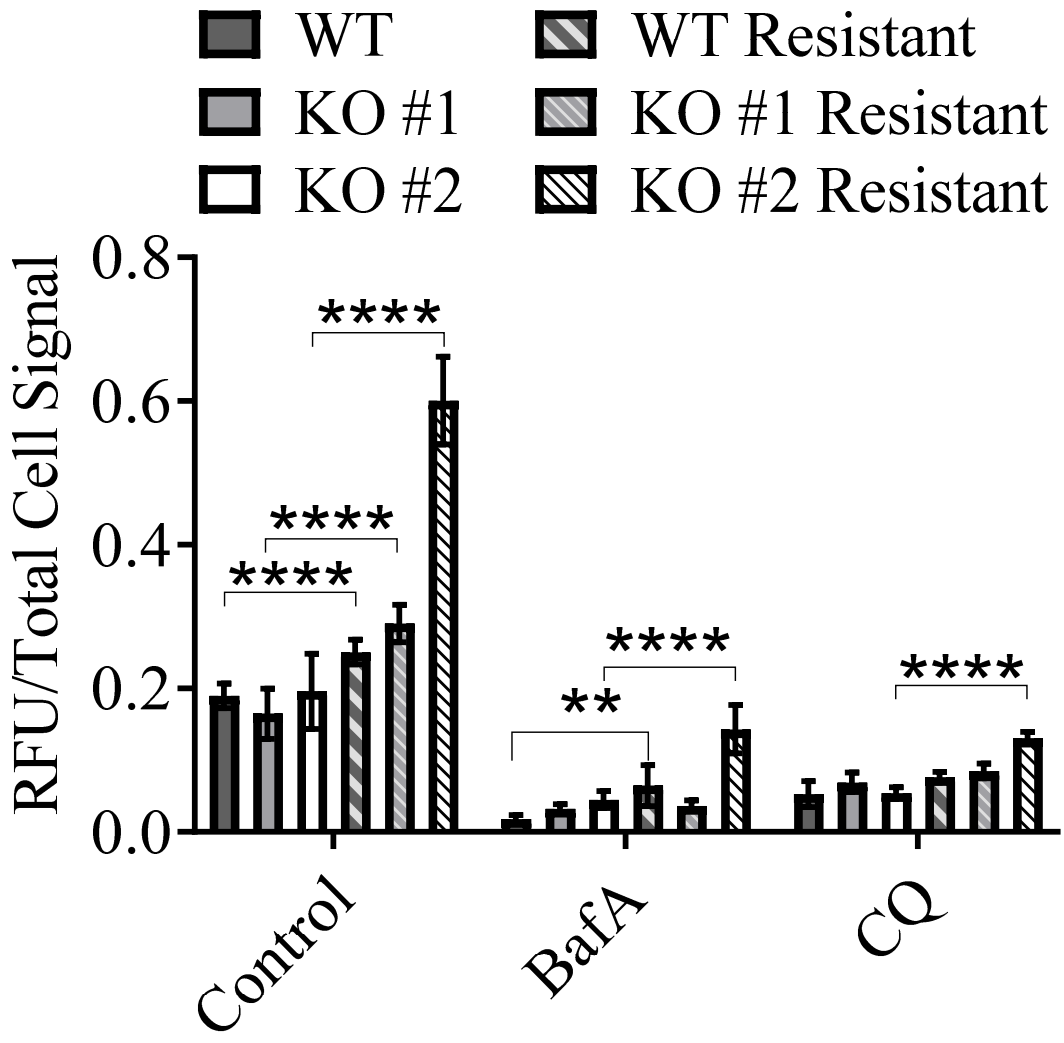
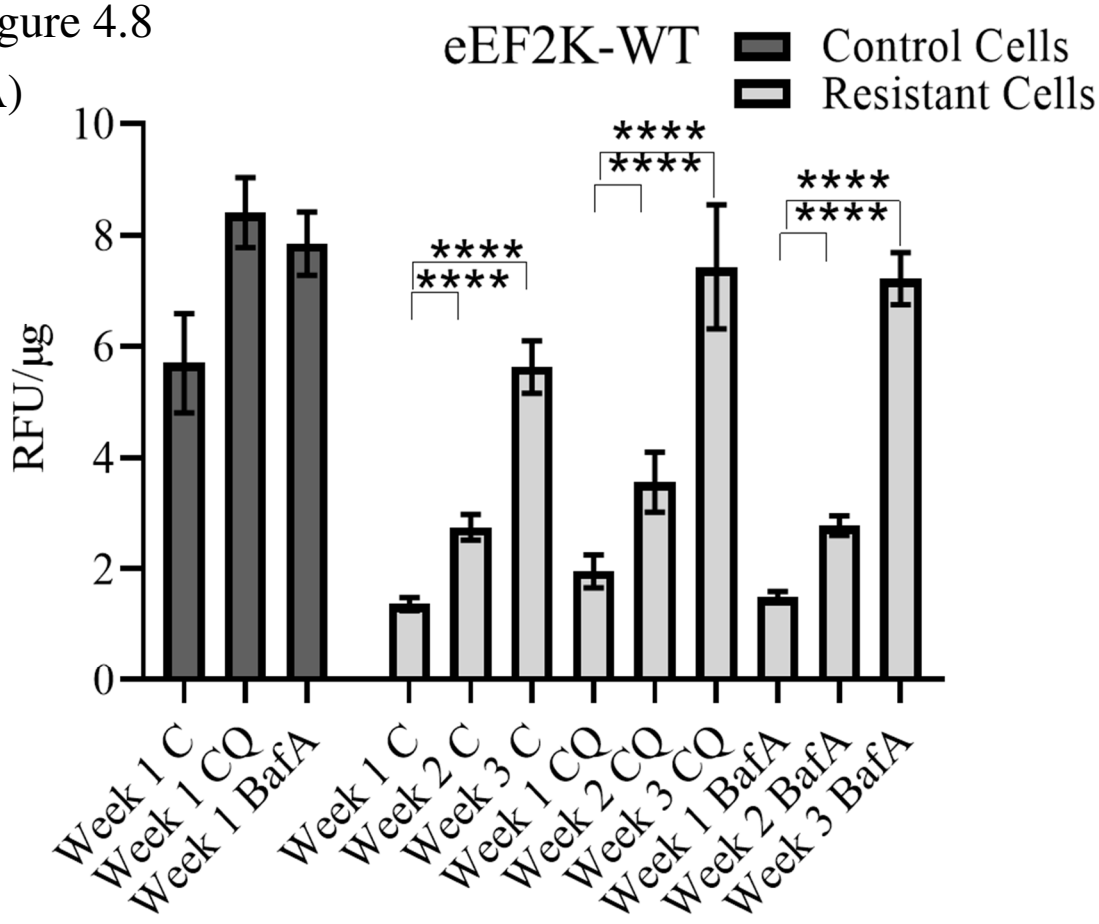


Figure 4.7: CQ and Baf A successfully inhibit autophagic flux. Resistant cells have higher levels of autophagic flux. LysoTracker Red Assay of MDA-MB-231 eEF2K-WT and KO resistant and non-resistant cells treated with 125 nM BafA for 2 h in medium without Glc/Pyr. Error bars represent S.D. (n=3). The p-values were calculated using Two-Way ANOVA with the Tukey multiple comparisons test. P-values: **≤0.01; ****≤0.0001. RFU was normalised to Hoesscht33342 signal (Total Cell Signal)

Figure 4.8

(A)


eEF2K-WT
Control Cells
Resistant Cells
RFU/µg
10
8
6
4
2
0
****
****
****
****
****
****
Week 1 C
Week 1 CQ
Week 1 BafA
Week 1 C
Week 2 C
Week 3 C
Week 1 CQ
Week 2 CQ
Week 3 CQ
Week 1 BafA
Week 2 BafA
Week 3 BafA

(B)

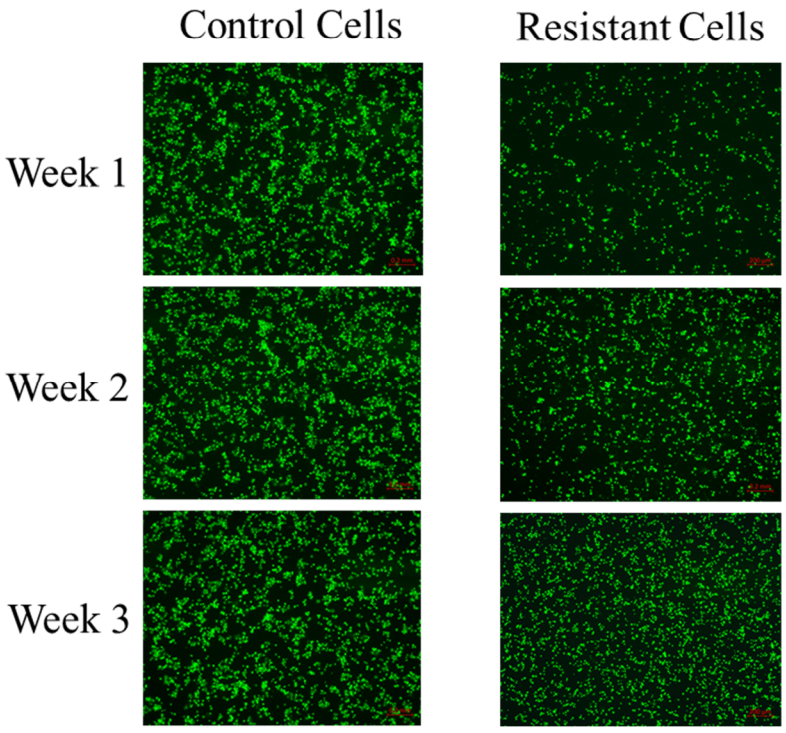
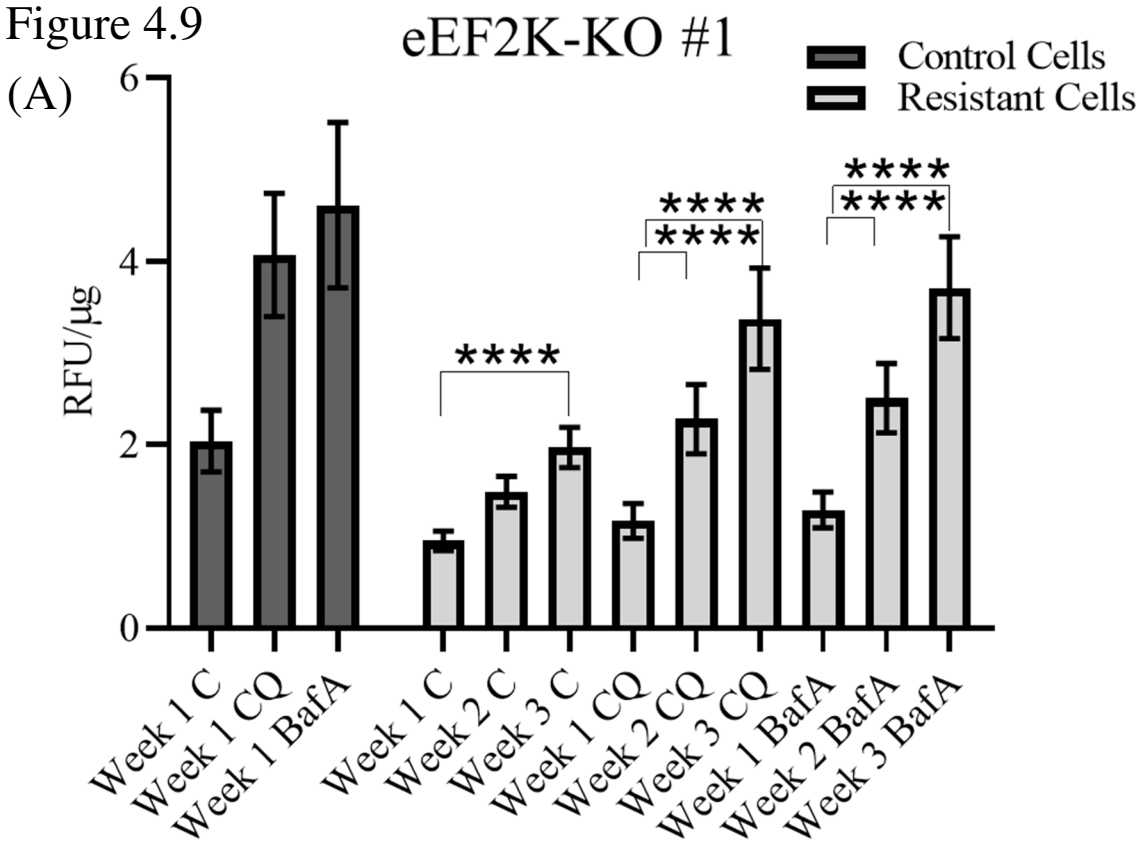

Control Cells
Resistant Cells
Week 1
Week 2
Week 3

Figure 4.8: MDA-MB-231 WT Resistant cells lose their resistance to stress over time. **A:** CellTox Green Assays of MDA-MB-231 WT resistant cells comparing to control cells treated in medium without Glc/Pyr and with or without 125 nM BafA or 25 μM CQ for 48 h after 1, 2 or 3 weeks spent growing under optimal conditions. **B:** CellTox Green images of MDA-MB-231 WT control and resistant cells treated in medium without Glc/Pyr and with 125 nM BafA for 48 h after 1, 2 or 3 weeks spent growing in optimal conditions. Images of CellTox Green fluorescence were taken using the GFP filter on a Zeiss Axio Vert.A1 200 microscope with the 4X magnifying lens. Each image is representative of 15 images total from 3 biological replicates. Error bars represent S.D. (n=3). The p-values were calculated using Two-Way ANOVA with the Tukey multiple comparisons test. P-values: ****≤0.0001. RFU was normalised to total protein content.

Figure 4.9


(A)
eEF2K-KO #1
Control Cells
Resistant Cells
RFU/µg
6
4
2
0
****
****
****
****
****
Week 1 C
Week 1 CQ
Week 1 BafA
Week 1 C
Week 2 C
Week 3 C
Week 1 CQ
Week 2 CQ
Week 3 CQ
Week 1 BafA
Week 2 BafA
Week 3 BafA

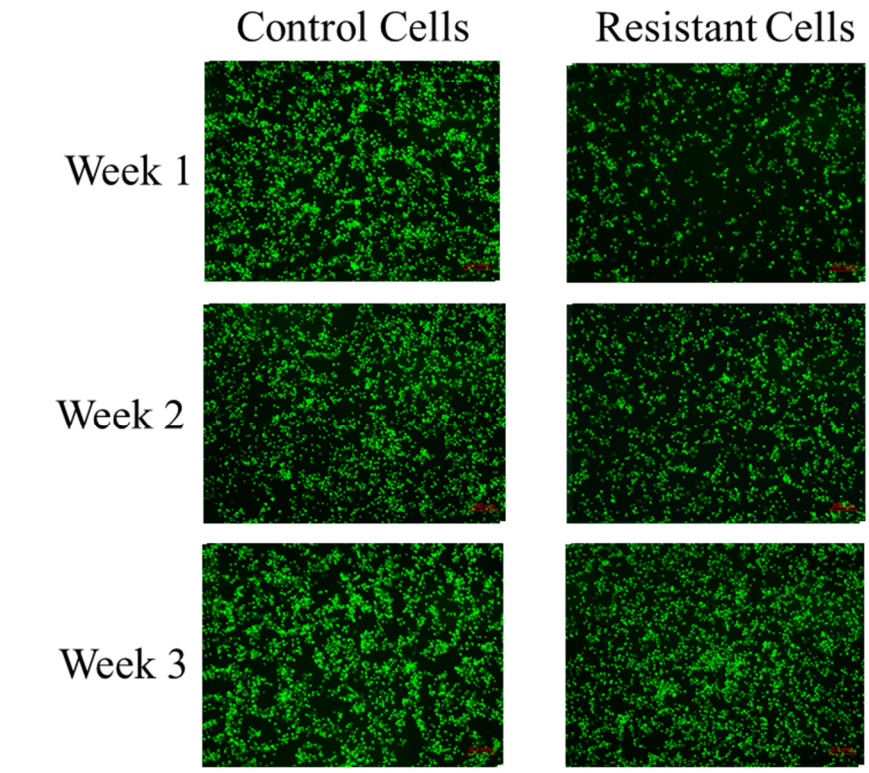
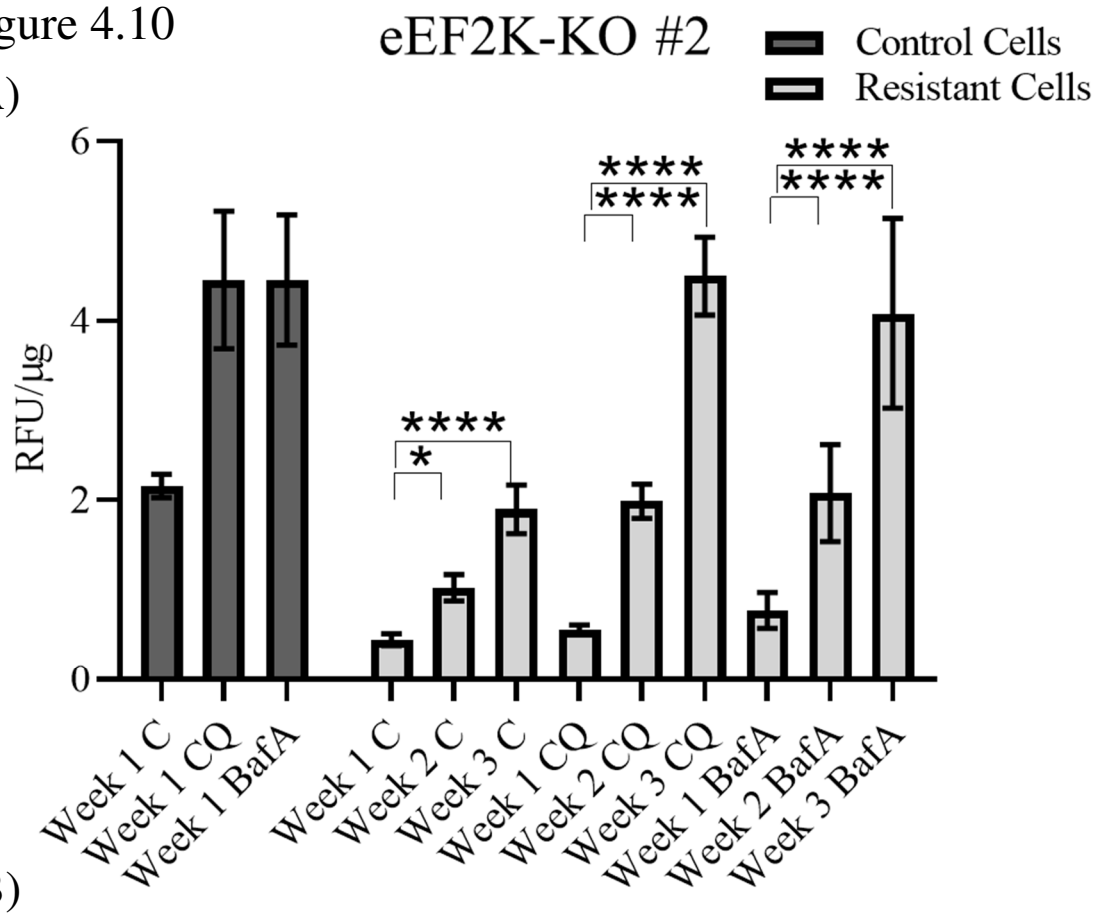

(B)
Control Cells
Resistant Cells
Week 1
Week 2
Week 3

Figure 4.9: MDA-MB-231 eEF2K KO #1 Resistant cells lose their resistance to stress over time. A: CellTox Green Assays of MDA-MB-231 eEF2K-KO #1 resistant cells comparing to control cells treated in –Glc +125 nM BafA or 25 μM CQ for 48 h after 1, 2 or 3 weeks spent growing under optimal conditions. **B:** CellTox Green images of MDA-MB-231 eEF2K KO #1 control and resistant cells treated in medium without Glc/Pyr and with 125 nM BafA for 48 h after 1, 2 or 3 weeks spent growing in optimal conditions. Images of CellTox Green fluorescence were taken using the GFP filter on a Zeiss Axio Vert.A1 200 microscope with the 4X magnifying lens. Each image is representative of 15 images total from 3 biological replicates. Error bars represent S.D. (n=3). The p-values were calculated using Two-Way ANOVA with the Tukey multiple comparisons test. P-values: ****≤0.0001. RFU was normalised to total protein content.

Figure 4.10

(A)



(B)

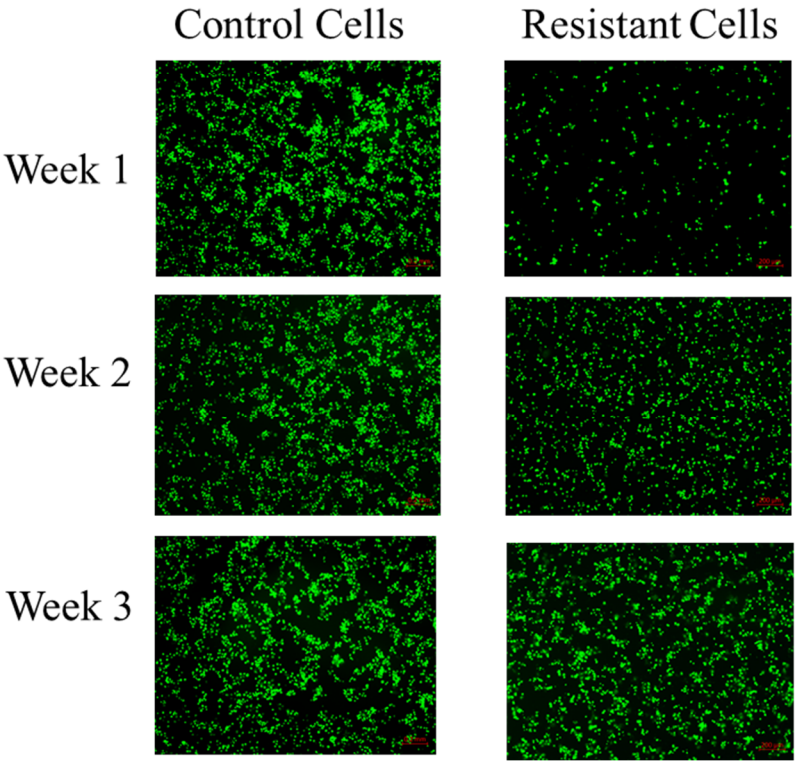


Figure 4.10: MDA-MB-231 eEF2K KO #2 Resistant cells lose their resistance to stress over time. A: CellTox Green Assays of MDA-MB-231 eEF2K-KO #2 resistant cells comparing to control cells treated in –Glc +125 nM BafA or 25 μM CQ for 48 h after 1, 2 or 3 weeks spent growing under optimal conditions. **B:** CellTox Green images of MDA-MB-231 eEF2K KO #2 control and resistant cells treated in medium without Glc/Pyr and with 125 nM BafA for 48 h after 1, 2 or 3 weeks spent growing in optimal conditions. Images of CellTox Green fluorescence were taken using the GFP filter on a Zeiss Axio Vert.A1 200 microscope with the 4X magnifying lens. Each image is representative of 15 images total from 3 biological replicates. Error bars represent S.D. (n=3). The p-values were calculated using Two-Way ANOVA with the Tukey multiple comparisons test. P-values: *≤0.05; ****≤0.0001. RFU was normalised to total protein content.

4.2.3 Protein abundance and phospho-proteomic analysis of 'resistant and sensitive' cells

The proteomics data analyses were performed by Dr. Sushma Rao from the Proteomics, Metabolomics and MS-Imaging Facility at the South Australian Health and Medical Research Institute, Adelaide, SA, 5000, Australia. Please note that the raw data is available by using the following URL: https://www.ebi.ac.uk/pride/login
(Username: reviewer_pxd022528@ebi.ac.uk; Password: Ewd2cAve).
The Appendix tables and figures are available by using the following link:
https://universityofadelaide.box.com/s/qrodwr56kv6zgkr8mzqyw8ebzsnud9mf

To explore the mechanisms by which the cells obtained resistance to nutrient deprivation and inhibition of autophagy, a label-free proteomics approach was used to quantify relative protein abundance between cell lines. Non-resistant (sensitive) and resistant cells were treated for 24 h in -Glc medium with 125 nM BafA prior to being lysed. The protein extracts then underwent LC-MS/MS (liquid chromatography with tandem mass spectrometry). A total of 3804 proteins were detected within the MDA-MB-231 proteome (**Appendix Table 1**). 622 of these proteins showed statistically significant differences (false discovery rate - FDR<0.01) in their protein abundance when comparing at least one pair of cell lines, e.g., WT sensitive vs WT resistant cells (**Appendix Table 2**). The significant changes that are discussed in this chapter are listed in **Table 4.1** and shown in **Figures 4.11 and 4.12**.

It was found in all three of the BafA resistant cell lines (WT, KO #1 and KO #2) that the amounts of several proteins that require cellular energy to function are decreased. Five aminoacyl tRNA synthetases were downregulated in all the resistant lines, although in some

cases the downregulation was not statistically significant. The enzymes catalyse a two-step ATP-requiring reaction which adds amino acids specific to that enzyme to their cognate tRNAs. This reaction requires the equivalent of two ATP molecules[225] (**Figure 4.11A**). Several translation factors, as well as proteins linked to RNA transport, were also decreased (**Figure 4.11B**). These proteins are essential for protein synthesis, which is a process that consumes a large amount of energy and amino acids[1]. The levels of ribosomal proteins RPS3 and RPS8 (40S ribosomal protein S3, 40S ribosomal protein S8) were also decreased. HSPA5 (also known as BiP and grp78) aids protein folding in the endoplasmic reticulum (ER) and was downregulated in all resistant cell lines (**Appendix Figure 1, western blots in Figure 4.13A, B**). DNAJB1 (DnaJ homolog subfamily b member 1), another chaperone that also aids protein folding, was also decreased.

FASN (fatty acid synthase), an enzyme which catalyses a key step in the energy intensive process of fatty acid synthesis, was greatly reduced in all three of the resistant cell lines[225] (**Figure 4.12**). This was confirmed by western blotting of the same samples that were used for mass spectrometry, with a trending decrease in FASN in all three resistant lines (**Figure 4.13A, B**). ACAT2 (cytosolic acetyl-CoA acetyltransferase) was also decreased in all three resistant cell lines. This protein catalyses the conversion of two molecules of acetyl-CoA into acetoacetyl-CoA which is the first step required for cholesterol synthesis[226]. Conversely, ACADVL (mitochondrial very long-chain specific acyl-CoA dehydrogenase) was increased in all three cell lines. This enzyme plays a key role in fatty acid oxidation, which leads to fatty acid breakdown, thus being the 'opposite' of FASN in function[227].

Figure 4.11

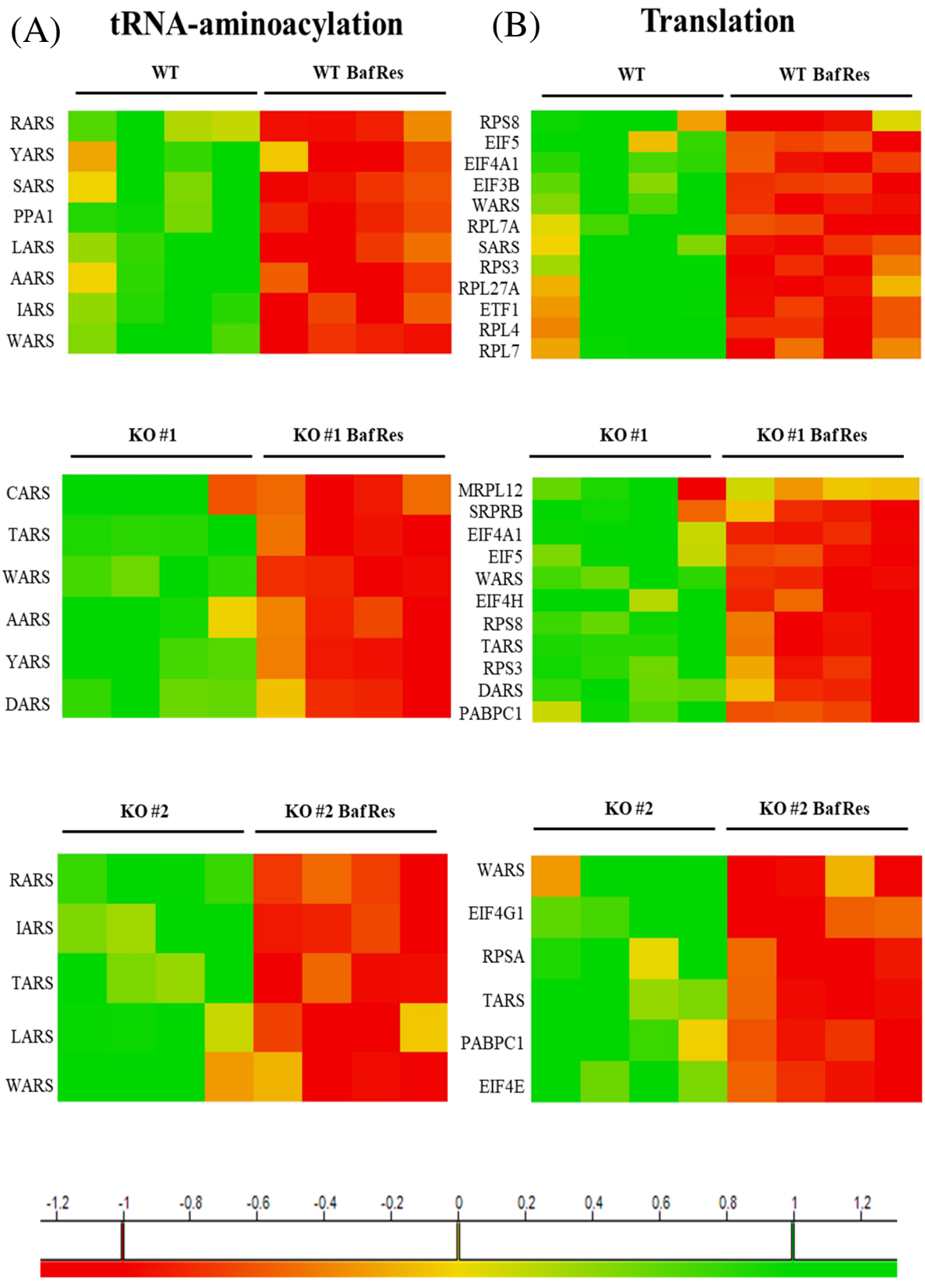

(A) tRNA-aminoacylation
(B) Translation
WT
WT BafRes
RARS
YARS
SARS
PPA1
LARS
AARS
IARS
WARS
RPS8
EIF5
EIF4A1
EIF3B
WARS
RPL7A
SARS
RPS3
RPL27A
ETF1
RPL4
RPL7
KO #1
KO #1 BafRes
CARS
TARS
WARS
AARS
YARS
DARS
MRPL12
SRPRB
EIF4A1
EIF5
WARS
EIF4H
RPS8
TARS
RPS3
DARS
PABPC1
KO #2
KO #2 BafRes
RARS
IARS
TARS
LARS
WARS
WARS
EIF4G1
RPSA
TARS
PABPC1
EIF4E
-1.2
-1
-0.8
-0.6
-0.4
-0.2
0
0.2
0.4
0.6
0.8
1
1.2

Figure 4.11: Heatmap of significantly altered proteins between MDA-MB-231 resistant and non-resistant cell lysates. Significantly altered proteins ($p < 0.01$) quantified by LC-MS/MS were grouped according to their parent Gene Ontology (GO) biological process (BP). Heatmaps showing proteins involved in: **A**. tRNA aminoacylation and **B**. Translation are depicted. Each node of the hierarchical cluster depicts a biological replicate corresponding to the non-resistant and resistant cells. Top panel = changes between WT and BafA resistant WT, middle panel =KO#1 and BafA resistant KO#1 cells, bottom panel = KO#2 and BafA resistant KO#2 cells. Protein abundance changes were calculated using Multi-sample ANOVA (FDR<0.01) followed by Post-hoc Tukey test (FDR<0.01). The values represent a $\log_2$ fold change. This figure was generated by Dr. Sushma Rao.

Figure 4.12 **Fatty acid metabolism**

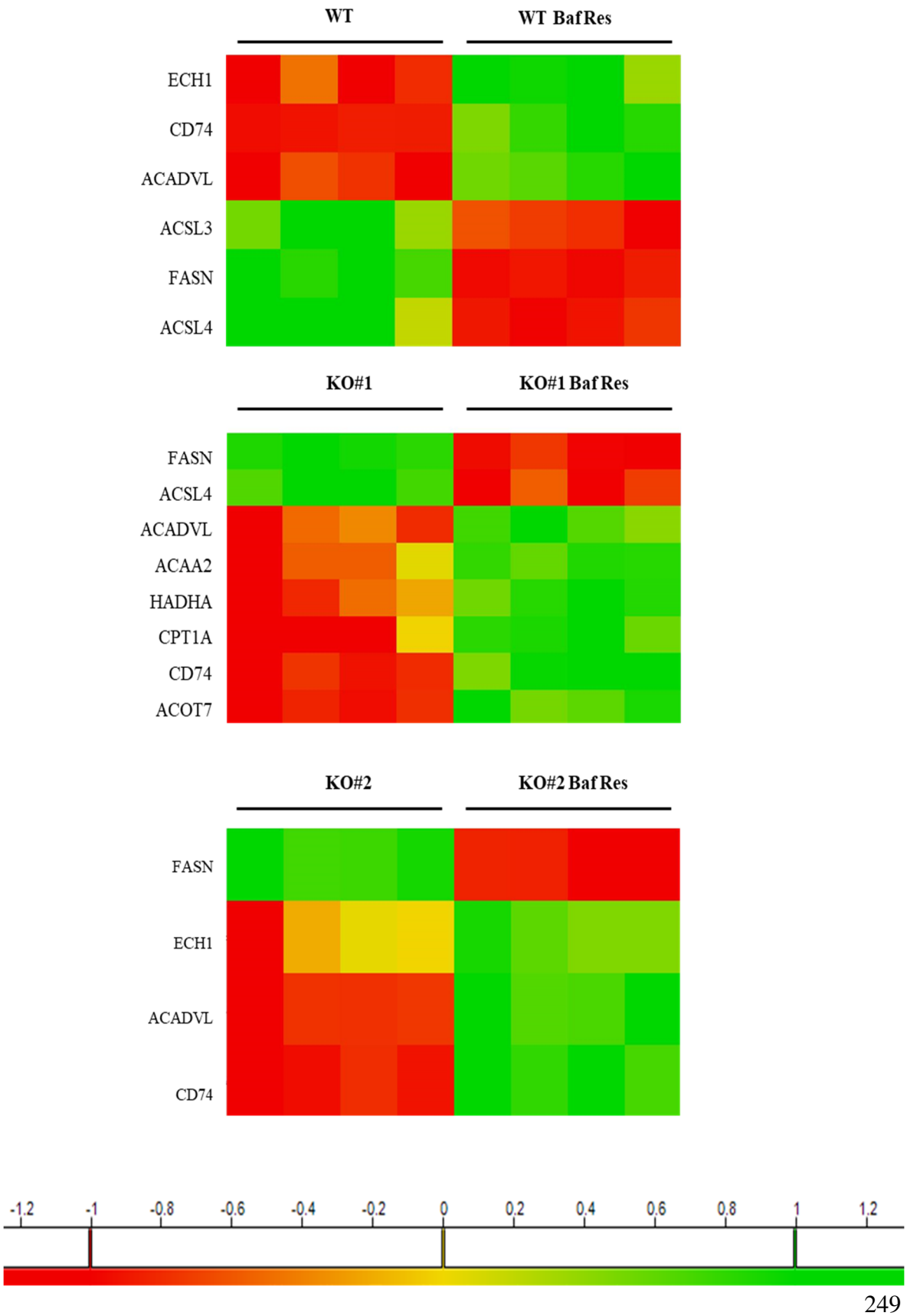
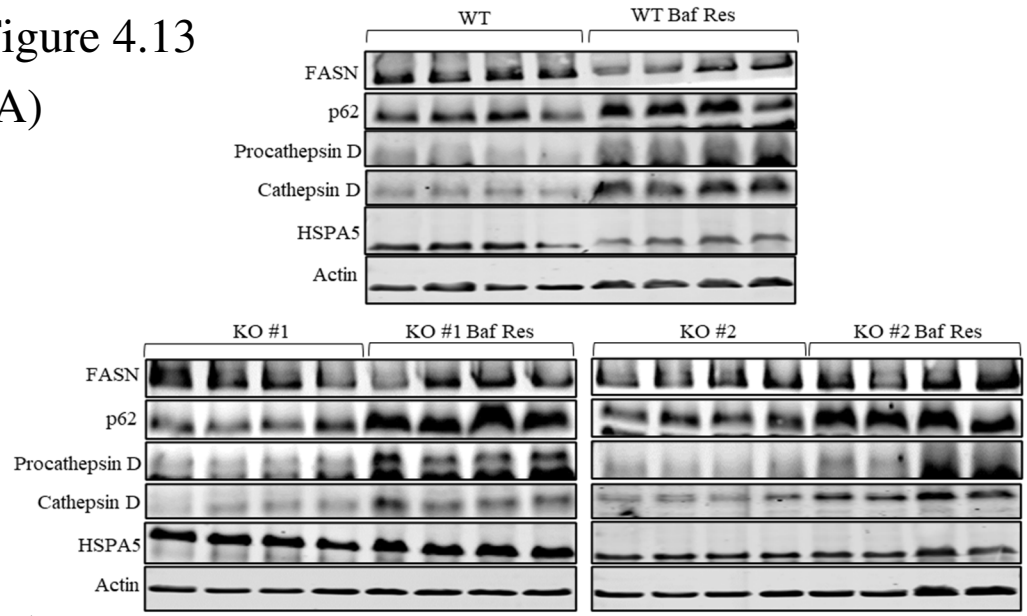


Figure 4.12. Fatty acid metabolism heatmap. Significantly altered proteins involved in fatty acid metabolism between MDA-MB-231 non-resistant and resistant cell lysates are shown. Each node of the hierarchical cluster depicts a biological replicate corresponding to the non-resistant and resistant cells. Top panel = changes between WT and BafA resistant WT, middle panel =KO#1 and BafA resistant KO#1 cells, bottom panel = KO#2 and BafA resistant KO#2 cells. Protein abundance changes were calculated using Multi-sample ANOVA (FDR<0.01) followed by Post-hoc Tukey test (FDR<0.01). The values represent a $\log_2$ fold change. This figure was generated by Dr. Sushma Rao.

Figure 4.13

(A)



(B)

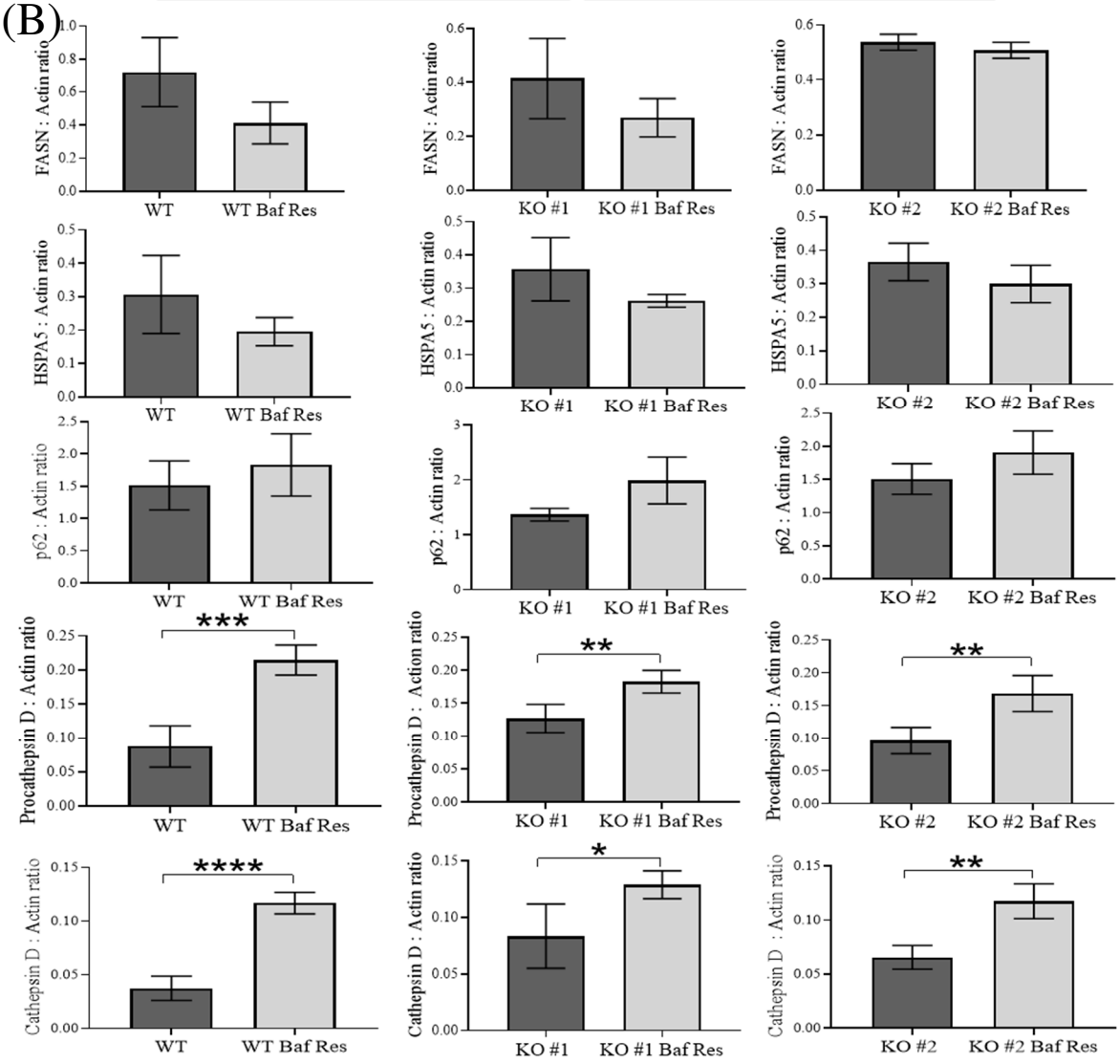


Figure 4.13: Protein changes in MDA-MB-231resistant cell lysates compared to non-resistant cell lysates followed the same trend as in the proteomics data. A: Cell lysates that were used for the proteomics experiment were run on 10% (for FASN) and 12.5% (for all other proteins) SDS-PAGE, followed by analysis via immunoblot. The four samples of each group correspond to the replicates used for the proteomics experiment (n=4). **B**: Quantification of **A** normalised to β-actin. Error bars represent S.D. (n=4). The p-values were calculated using an unpaired, parametric, two-tailed T-test with Welch's correction. P-values: *≤0.05; **≤0.01; ***≤0.001 ****≤0.0001.

The levels of some proteins that are related to autophagy through being necessary for the function of lysosomes were also upregulated in resistant cells, e.g., AP1B1 (AP-1 complex subunit beta-1), NPC1 (Niemann-Pick disease, type C1) and CTSD (cathepsin D) [**Appendix Figure 1**]. The western blots performed on the lysates ysed for proteomic analysis also showed statistically significant increases in both procathepsin D (the immature form of cathepsin D) and cathepsin D itself. The western data also showed a trending increase in p62 in all three cell lines, although it was not significant (**Figure 4.13A, B**).

Certain proteins related to glucose metabolism were either up or down-regulated in resistant cells. This is discussed in detail in section **4.3 – Discussion**.

Phosphopeptide enrichment followed by phosphoproteomic analysis by LC-MS/MS was also performed on the WT and eEF2K-KO sensitive and resistant cell lines. A total of 19,506 phosphopeptides were detected, of which 12,702 were class I sites (site probability score > 0.75) (**Appendix Table 3**). This also provided an opportunity to search for potential eEF2K substrates other than Thr56 on eEF2, i.e., whether the deletion of eEF2K causes a loss of phosphorylation of a site of other proteins. This analysis confirmed the complete absence in eEF2K-KO cells of the phosphopeptide AGETRFTDTR corresponding to Thr56 on eEF2[7] (**Appendix Table 4**). Another 31 sites were found to be phosphorylated only in WT cells and not in either of the eEF2K-KO cell lines (**Appendix Table 5**). These could be potential eEF2K substrates, although further experiments are required to confirm this, which were outside the scope of this project. It is important to note that there is currently no consensus motif for phosphorylation of substrates by eEF2K, as eEF2 is its only known target. Also of note is that none of these sites corresponded to the sites found to be phosphorylated in a study, by Lazarus *et al*. in 2017[228], that looked for new substrates of eEF2K using a very

different chemical biology approach. A comparison of the relative change in phosphopeptide abundance between cells of the same phenotype (e.g., WT sensitive vs WT resistant cells) revealed the following changes: 2 significantly altered sites between WT and WT BafA-resistant cells; 25 significantly altered sites between KO #1 and KO#1 BafA-resistant cells; and 56 significantly altered sites between KO #2 and KO#2 BafA-resistant cells (**Appendix Figure 2**).

The relevant phosphopeptide changes between sensitive and resistant cells are shown in **Table 4.2**. These changes differed between the various cell lines, again supporting the hypothesis that they had gained resistance in differing ways. A major trend is the decreased phosphorylation of sites in proteins related to the mTORC1 pathway. 4E-BP1 (eukaryotic translation initiation factor 4E-binding protein 1), a protein whose phosphorylation on Ser 65 and Thr 70 by mTORC1 de-represses translation initiation was decreased in KO #1 resistant cells[229]. eIF4G1 (eukaryotic translation initiation factor 4 gamma 1) is required for the recruitment of mRNAs to the ribosome[230]. Ser 1187 phosphorylation, which was reported to be linked to the binding of eIF4G1 to MNK1 (MAP kinase interacting serine/threonine-protein kinase 1, which phosphorylates eIF4E) was also decreased in KO #1 resistant cells, again suggesting a decrease in translation[231]. The phosphorylation of sites on eIF5B (functioning late in translation initiation[232]) and NPM1 (nucleophosmin 1, involved in ribosome biogenesis[233]) that are critical to their function was decreased in both KO #1 and KO #2 resistant cells. Importantly, the phosphorylation of the mTORC1 component RAPTOR at Ser887 (which leads to mTORC1 inhibition) was increased[234]. Overall, this suggests that mTORC1 signalling is diminished in resistant KO #1 and KO #2 cells. This suggests that cells are trying to downregulate the nutrient-consuming anabolic pathways that

are promoted by mTORC1 to reduce their demand for energy, which may contribute to these cells' resistance.

The phosphorylation of DNAJC2 (DnaJ homolog subfamily C member 2, also known as ZRF1) at Ser47 was reduced in KO #2 resistant cells. This is a substrate for S6 kinase, which is downstream of mTORC1. This site is known to increase DNAJC2's ability to induce p16, a protein that is involved in cell senescence[235]. A reduction in this phosphorylation site is expected to limit the ability of these resistant cells to senesce.

A decrease in the activating site (Ser14) of DHCR7 (7-dehydrocholesterol reductase), an enzyme which regulates cholesterol synthesis, was observed in KO #1 resistant cells, further supporting the idea that fatty acid synthesis was decreased in the resistant cell lines[236].

Also of note is the decreased phosphorylation of GFPT1 (glutamine-fructose-6-phosphate transaminase) at Ser261 in both KO#1 and KO#2 resistant cells, which is modulated by AMPK. This phosphorylation is required for activation of GFPT1 which then positively regulates the flux of glucose into the hexosamine pathway. As this phosphorylation is decreased, it follows that the hexosamine pathway might be downregulated in these cells, likely as a response to the lack of glucose[237].

Furthermore, a decrease in the phosphorylation of FAK/PTK2 at Ser910 was observed in WT and KO#2 resistant cells. This phosphorylation is needed for PTK2 to dissociate from focal adhesions, allowing for their degradation. The decrease in this phosphorylation suggests that the cells are trying to more strongly attach to the surface and thus survive[238].

		Log$_2$ fold change		
Process	**Protein**	**WT Res/WT**	**KO #1 Res/KO #1**	**KO #2 Res/ KO #2**
Aminoacyl tRNA synthesis	AARS	-0.3907	-0.489	0.0503*
	YARS	-0.364	-0.638	-0.223*
	LARS	-0.377	-0.167*	-0.268
	WARS	-0.543	-0.606	-0.299
	TARS	-0.461*	-0.477	-0.478
Translation factors	PABPC1	-0.258*	-0.466	-0.378
	eIF3B	-0.429	-0.189	-0.142
	eIF4A1	-0.479	-0.46	-0.541
	eIF4A3	-0.543	-0.513	-0.367
	eIF4G1	-0.107*	-0.156	-0.216
	eIF5	-0.544	-0.555	-0.134*
RNA transport	RAN	-0.377	-0.332	-0.235*
	RANGAP1	-0.255	-0.374	-0.26*
Fatty acid metabolism	FASN	-1.672	-1.157	-1.107
	ACAT2	-0.038*	-0.833	-0.567
	ADH5	-0.535	-0.159*	-0.588
	ACSL4	-0.98	-2.983	-0.323*
	ACADVL	0.833	0.594	0.774
Lysosome	CTSD	0.644	0.617	0.314*
	AP1B1	0.723	0.799	0.416*
Protein folding	HSPA5	-0.435	-0.311	-0.264
	DNAJB1	-0.57	-0.354	-0.83
	HSPA4L	-0.985	-0.006*	-0.961
	ERO1L	0.475	0.444*	0.512
Ribosomes	RPS8	-0.431	-0.455	-0.322*
	RPS3	-0.633	-0.48	-0.3*
Glucose metabolism	DLAT	-0.076*	-0.819	-0.627
	AKR1A1	0.623	0.828	0.611
	PKM	0.412	0.34	0.247*
	PGK1	0.282	-0.508	0.341
	TPI1	0.453	0.333*	0.394
	LDHA	0.204	0.407	0.296
	ALDH2	0.48*	-0.977	-0.71

Table 4.1: Log$_2$ fold changes of select groups of proteins between resistant and non-resistant cells. * indicates a statistically non-significant change, as analysed by post-hoc Tukey's test (FDR<0.1).

Protein	Phospho-site log_2 fold change (Res/non-Res)	Function
FAK/PTK2	Ser910 -1.15 (WT Res/WT) -1.96 (KO #2 Res/KO #2)	Controls focal adhesions. Necessary for cell attachment to surfaces.
RAPTOR	Ser877 3.06 (KO #1 Res/ KO #1)	Inhibits mTORC1, leading to lower protein synthesis.
4E-BP1	Ser65; -1.864 Thr70; -1.864 (KO #1 Res/ KO #1)	Indication of lower mTORC1 signalling and slower mRNA translation.
eIF5B	Ser214, -1.29 (KO #1 Baf Res/ KO #1) -5.76 (KO #2 Res/ KO #2)	This site promotes eIF5B binding to RNA-binding and processing proteins. Regulated by mTORC1, suggesting lower mTORC1 activity and mRNA translation.
eIF4G1	Ser1187 -2.31 (KO #1 Res/ KO #1)	This site promotes the binding of eIF4G1 to MNK1, suggesting a decrease in this site could result in a decrease in translation.
DHCR7	Ser14 -1.28 (KO #1 Res/KO #1)	This site is necessary for protein activity which is involved in cholesterol synthesis.
GFPT1	Ser261 -2.07 (KO #1 Res/ KO #1) -2.95 (KO #2 Res/ KO #2)	This site is phosphorylated by AMPK, activating the protein which positively regulates the flux of glucose into the hexosamine pathway.
DNAJC2/ZRF1	Ser47 -3.2 (KO#2 Res/KO #2)	This site is phosphorylated by S6K and leads to an increase in p16 expression, leading to cell senescence.
NPM1	Ser70 -3.35 (KO #2 Res/KO #2)	This site is necessary for NPM1 to SENP3 (Sentrin-specific protease 3) binding, leading to ribosome biogenesis.

Table 4.2: Phosphorylation site changes between non-resistant and resistant cells. R: indicates cells resistant to glucose deprivation and autophagy inhibition.

4.3 Discussion

A major issue in the area of cancer therapy is that cancers can acquire resistance to therapeutic agents and to the conditions they find themselves in such as low nutrient availability, hypoxia and acidity[239-241]. **Chapter 3** of this thesis has shown that eEF2K and autophagy are pathways that are both vital to survival of some kinds of cancer cells under nutrient-deprived conditions yet act independently of each other in the cells tested. This implies eEF2K does not regulate autophagy in these cells. To determine how cells could obtain resistance to a lack of nutrients, eEF2K and inhibition of autophagy, MDA-MB-231 cells underwent repeated, pulsed treatments in -Glc conditions with BafA over months. Eventually, the cells obtained a significant level of resistance to these conditions, although evidence gathered indicates that the resistance mechanisms differed between the WT, eEF2K-KO #1 and KO #2 lines. Importantly, even though the cells gained resistance following treatment with BafA, they were also resistant to the effects of CQ, showing that they are resistant to the inhibition of autophagy and not just to the effects of BafA (which might arise, e.g., to a mutation in the v-ATPase).

Interestingly, it was found that the cells lose their resistance over time when grown in fully supplemented medium without stresses. This suggests that the cells do not undergo mutations that would allow stable resistance but increase or decrease the expression of certain genes to help them cope with the adverse conditions. This is consistent with the pulsed approach to generating resistant cells[213-215, 218-223].

A proteomics approach was used to measure relative protein abundance between ‘sensitive’ and ‘resistant’ cells in conjunction with a phosphoproteomics screen. Importantly, the

phosphoproteomics screen for novel eEF2K substrates showed 21 sites that were absent in the KO cells compared to WT. This raises the possibility that at least some of these sites represent novel eEF2K substrates. However, further testing with antibodies relating to those sites is required to confirm this observation followed by biochemical studies to determine whether the corresponding protein is indeed a substrate for eEF2K. Notably, none of these sites corresponded to a previous study that screened for eEF2K substrates[228]. It is important to note that the approach used in that study was different to what was used in this Thesis. Their approach involved using a mutated eEF2K that could accept a bulky analogue of ATP that cannot be used efficiently by other kinases, allowing for the ATP analogue to transfer thiophosphates instead of phosphates to its substrates, thereby pinpointing proteins phosphorylated by eEF2K HeLa cell lysates were then incubated with this mutant eEF2K alongside the ATP analogue prior to analysis via mass-spectrometry. This approach did not use eEF2K-KO cells, which presents clearer data of potential substrates.

When comparing sensitive to resistant cells, it was observed that a number of amino-acyl tRNA synthetases, as well as a tRNA ligase were downregulated – AARS (alanyl tRNA ligase), YARS, LARS, WARS and TARS (tyrosyl, leucyl, seryl, tryptophanyl and threonyl tRNA synthetases). PABPC1 (polyadenylate-binding protein 1, a partner for eIF4G), and the translation factors eIF3B, eIF4A1, eIF4A3, eIF4G1 and eIF5 were also decreased in resistant cells. RAN (GTP-binding nuclear protein Ran) and RANGAP (Ran GTPase-activating protein), proteins that are involved in RNA transport, were downregulated. Ribosomal proteins RPS3 and RPS8 were also decreased. Considering that protein synthesis and ribosome biogenesis use up a large proportion of the cell's energy, it is possible that these resistant cells downregulate these processes to conserve energy, allowing them to survive longer under nutrient-deprived conditions[1].

Proteins involved in the folding of proteins were also decreased in all of the resistant cell lines (chaperone proteins HSPA5, HSPA4L [heat shock 70 kDa protein 4L], DNAJB1, ERO1L [ERO1-like protein alpha]). This is in line with the finding that the cells likely had lower rates of protein synthesis, thus requiring less chaperones to help fold proteins. Considering that heat shock proteins consume ATP, this could be another way for cells to save energy.

Furthermore, proteins involved in fatty acid synthesis, another energy-consuming process, were downregulated in resistant cells (FASN, ACAT2). Conversely, levels of the rate-limiting enzyme of fatty acid oxidation (the inverse of synthesis), ACADVL were increased in resistant cells[227]. Furthermore, ACSL4 (long chain fatty acid-CoA ligase 4) levels were decreased. This enzyme catalyses the conversion of fatty acids to acyl-CoA for lipid synthesis or for their degradation via beta-oxidation[242]. ADH5 (alcohol dehydrogenase 5), an enzyme that is involved in the oxidation of hydroxy-fatty acids was also downregulated in resistant cells[243]. The decreases in ADH5 and ACSL4 could be explained by the lack of need for these proteins if the cells have downregulated fatty acid synthesis overall. This decrease in fatty acid synthesis could potentially save the cells a lot of energy as it is not a process that is necessary for cells during nutrient deprivation.

Several enzymes that are involved in glucose metabolism were either up or down-regulated in resistant cells with several differences between the cell lines, highlighting that these cells gained their resistance in different ways. PKM (pyruvate kinase PKM) was increased in all three lines. This enzyme catalyses the conversion of phosphoenolpyruvate to pyruvate, the last step in glycolysis. LDHA (lactate dehydrogenase A) was also increased. This enzyme

converts pyruvate to lactate, which is necessary for continued anaerobic glycolysis as it regenerates NAD^+. This process does not require the carbon atoms from the breakdown of glucose to enter the Krebs cycle, and they are therefore saved instead of being lost through becoming CO_2. This resembles the 'Warburg effect' which is a feature of many cancer cells[244, 245], and may help glucose-deprived cells conserve carbon atoms. Furthermore, the levels of ALDH2 (mitochondrial aldehyde dehydrogenase) were decrease in both KO resistant lines. This enzyme oxidises acetalaldehyde to acetate which is then converted to acetyl-CoA by acetyl-CoA synthetase, a process which requires ATP, further suggesting that the resistant cells are trying to reduce ATP consumption. Notably, DLAT (mitochondrial dihydrolipoyllysine-residue acetyltransferase component of pyruvate dehydrogenase complex) levels were also reduced. This enzyme catalyses the final step of the conversion of pyruvate to acetyl-CoA[246], to allow carbon atoms from glucose to enter the Krebs cycle. As the cells are adapting to using anaerobic glycolysis, they would have less requirement for acetyl-CoA, thereby they could save energy by reducing the levels of proteins that convert acetate to acetyl-CoA, which would in turn slow down this process. This may complement the increase in LDHA by decreasing the flux of carbon atoms into the TCA cycle where they would be lost, suggesting that the cells are shuttling available carbon towards anaerobic glycolysis.

Interestingly, the levels of PGK1 (phosphoglycerate kinase 1) were increased in WT and KO #2 resistant cells but decreased in KO #1 resistant cells, further adding to the idea that these cells gain resistance in varying ways. PGK1 catalyses the conversion of glycerate-1,$3P_2$ to glycerate-3P[247], which is eventually converted to pyruvate. For WT and KO #2 resistant cells, this could potentially mean more pyruvate for the anaerobic glycolysis. On the other

hand, KO #1 resistant cells may be trying to slow down the process of glycolysis overall, to save carbon.

Furthermore, it was also shown by western blots that procathepsin D, cathepsin D and p62 levels were increased (**Figure 4.13**). This might explain the higher levels of basal autophagic flux observed in all of the resistant cell lines, according to the LysoTracker Red assay (**Figure 4.7**). The cells may have used this higher autophagic flux to their advantage as soon as they were placed in glucose-free medium to generate amino acids and molecules from which they can generate ATP from unnecessary proteins, prior to BafA being able to block autophagy. Furthermore, the LysoTracker Red assay showed that even with BafA and CQ treatment, KO #2 and WT resistant cells still showed higher levels of flux than 'sensitive' cells, suggesting that autophagy in these cells is more active under these conditions, perhaps because their basal rates of autophagy are higher.

The phosphoproteomic data indicate an overall decrease in mTORC1 signalling in resistant eEF2K-KO cells. These changes suggest that the ribosome biogenesis and protein synthesis are downregulated in them, these being processes which use a large proportion of the cell's energy. This 'response' could help cells save nutrients, as mTORC1 promotes multiple energy-demanding anabolic pathways. A downregulation of these pathways could reduce the energy demand on these cells and thus help them survive nutrient deprivation for longer periods of time. These changes to mTORC1 signalling were not seen in WT resistant cells, suggesting that their ability to use eEF2K in these conditions is what assists them in slowing down translation elongation and thus decreasing their energy use. As the activation of eEF2K occurs through AMPK independently of mTORC1 (which is inhibited in nutrient-deprived

conditions), perhaps these cells had no need to downregulate mTORC1 signalling as well in order to gain resistance[47, 48].

This phosphoproteomic data could explain why treating solid tumours with mTORC1 inhibiting compounds such as rapamycin has not been effective in treating cancer, as cells might use this inhibition of mTORC1 signalling to their advantage, e.g., by activating autophagy and/or alleviating the inhibition of eEF2K by mTORC1. Several studies have shown that mTORC1 inhibition through rapamycin or other compounds helps cancer cells to survive. One study showed that rapamycin assisted certain tumour cells in withstanding amino acid deprivation, through activating autophagy[248]. Another study showed that mTORC1 inhibition in cells that are experiencing glutamine deficiency enhanced autophagy and prevented PKB degradation (an enzyme which promotes cell survival), which in turn helped cells survive[249]. A different study showed that mTORC1 inhibition increased cell viability under ER stress (induced by thapsigargin treatment) by maintaining autophagy[250]. Furthermore, my data showed that resistant cells eventually lose their resistance over time, suggesting that treatment of cancer with intermittent dosing may be more effective than continuous dosing treatments. This is because tumour cells may become resistant to the drug used if they are dosed continuously but if they are left without treatment for a time, they may revert to their original state, allowing the drug to become effective in treating the cancer once more.

5.1 Introduction

5.1.1 eEF2K and its role in cell migration and invasion

Secondary tumours that are created by cancer cell metastasis are the cause of mortality for most cancer patients, accounting for approximately 90% of all cancer-related deaths[251]. According to the US National Cancer Institute Surveillance, Epidemiology and End Results (SEER) Program, the Centers for Disease Control and Prevention and the North American Association of Cancer Registries, the average survival rate of patients with metastatic tumours is 25% or lower[252, 253]. A key aspect in the ability of cancer cells to metastasise is their capacity to invade through barriers, which is driven by cell motility[254]. Cell motility, in turn is dependent on the changes in cancer cell morphology, driven by modifications in the polymerisation of actin which in turn alters the cell cytoskeleton[255, 256]. The changes in cell morphology are directly linked to a process known as epithelial-to-mesenchymal transition (EMT). This transition leads to morphological changes, loss of tight junctions, cytoskeletal remodelling and enhanced migratory and invasive capabilities[257].

A typical cancer therapy approach would be to target cancer cell proliferation at the primary site[258]. However, to treat cancer cells more effectively, inhibiting migration which is associated with metastasis might be a more effective tool. Combining both approaches might prove to be a more potent therapy against cancer. Recent research has shown that cancer cells use molecular signalling pathways to control protein synthesis and drive metastasis. Considering eEF2K's role in controlling translation elongation, it became an interesting target to look at in terms of cancer cell metastasis. Recently, Forkhead box M1 (FOXM1), miR-603 and mIR-877 were found to play roles in tumour growth and were connected to eEF2K expression levels[259-261]. In MDA-MB-231 and BT-20 triple negative breast cancer cells, it was found that silencing FOXM1 decreases the migratory and invasive capabilities of these cells, as well as lowering

eEF2K levels[259]. miR-603 was found to bind to the 3'-UTR of eEF2K, suppressing its expression and inhibiting the migration of, and invasion by, MDA-MB-231 and MDA-MB-436 cells. miR-877 was also found to bind the 3'-UTR of eEF2K, downregulating its expression and inhibiting the ability of renal cell carcinoma cells to migrate[261]. However, there was still no explanation as to why modulating translation elongation affected cell migration and invasion.

A study by our group published in 2017 investigated eEF2K's effect on cell migration and invasion in MDA-MB-231 and A549 cells, as well as in A549 tumours *in vivo*[123]. Importantly, this study found that when eEF2K was knocked down in A549 cells, the levels of 34 proteins involved in cell migration were decreased, including some integrins. Integrins are vital for cell migration, regulating the interactions between the extracellular matrix (ECM) and the actin cytoskeleton[262]. eEF2K was also found to promote the association of integrin mRNAs with actively translating polysomes, suggesting a reason as to why it increased their cellular protein levels. Inhibiting or knocking down eEF2K also decreased cell migration and invasion in MDA-MB-231 and A549 cells, as well as preventing A549 'tumour spread' *in vivo*. This Chapter uses the opportunity provided by MDA-MB-231 eEF2K-KO cells to provide further support for the findings in that study.

5.1.2 eEF2K and translation fidelity

Production of properly folded and correctly made proteins is vital for cell survival. The build-up of incorrectly folded proteins can lead to various diseases, including neurodegenerative illnesses[263]. It is important for cells to maintain accuracy during mRNA translation to properly decode and synthesise proteins.

It is known that translational accuracy correlates with longer lifespan in mammals[264, 265]. For example, a study by Zhonghe Ke, *et al*.[264] published in 2017 looked at translational accuracy (termed fidelity) across 17 different rodent species with diverse lifespans. The study used

luciferase-based reporter constructs with mutations in an amino acid residue critical to luciferase function such that when an amino acid is mis-incorporated into the mutated codon, luciferase activity is restored. Mistranslation of the first and second codons was found to negatively correlate with maximum lifespan in 16 different rodent species. As translation fidelity is so important for proper cell function, it follows that cells must have mechanisms in place to ensure efficient protein synthesis while maintaining accuracy. One major pathway that is associated with accelerated aging in eukaryotic organisms is the target of rapamycin complex 1 (TORC1), which has a major role in activating protein synthesis[266, 267]. A study by Conn and Qian published in 2016 showed that activated mammalian (m)TORC1 decreases translational fidelity in HEK293 and MEF cells[268]. Since almost all the amino acids are incorporated into new proteins during translation elongation, this is the stage where most translation errors take place[269].

When mRNA translation begins, aminoacyl-tRNAs are recruited to the ribosomal A site by eukaryotic elongation factor 1A (eEF1A). Once the correct codon:anticodon match occurs, the amino acid is added to the growing polypeptide chain which is also transferred to the tRNA in the ribosomal A site. The ribosome then undergoes translocation, moving one codon along the mRNA, and bringing the peptidyl-tRNA to the P site and the next codon into the A site. This is the step where eEF2 is required. mTORC1 keeps eEF2K inactive (via multiple phosphorylation events on eEF2K), thus stopping it from phosphorylating and inactivating eEF2, allowing the translocation process to proceed[270]. It is known that TSC2 KO cells (when mTORC1 is constitutively active) have earlier ribosomal runoff which indicates a faster rate of translation elongation (eEF2 is active)[271]. On the other hand, inhibiting mTORC1 with rapamycin slowed down translation elongation in CHO cells[270], presumably by causing disinhibition (activation) of eEF2K and phosphorylation/inactivation of eEF2.

Considering that mTORC1 controls eEF2K and. through it, the rate of elongation, a study by our group asked whether mTORC1 signalling affects translation fidelity by regulating eEF2

through eEF2K[128]. The study found that even though eEF2 is not involved in selecting amino-acyl tRNAs, activating eEF2K nevertheless increases translational accuracy.

It is known that caloric restriction, a dietary modification that impairs mTORC1 signalling, extends the lifespan of a variety of organisms such as yeast, worms and flies[266]. It was also found in the translation fidelity study that deleting eEF2K increased the lifespan of *C. elegans*[128].

This part of the Chapter adds extra data to this study by looking at translation fidelity in eEF2K-WT and KO MDA-MB-231 cells.

5.1.3 eEF2K and hypoxia

Generally, cells need aerobic metabolism to generate the large amount of energy necessary for important processes, such as protein synthesis. Protein synthesis is one of the most energy consuming processes in the cell (using approximately 34% of the cells' available energy)[2]. It uses both ATP and GTP during the process. ATP is used for aminoacylation of tRNAs (tRNA charging). GTP is necessary for energising the translation factors necessary for polypeptide synthesis (eukaryotic initiation factor 2 [eIF2], elongation factor 1 alpha 1 [eEF1A1] and eEF2)[272-274].

When cells are stressed, thy eEF2K is activated, thus slowing down translation elongation, allowing the cells to conserve ATP, GTP and amino acids. One such stress is hypoxia, which impairs ATP production in cells. Hypoxia is very important for highly oxidative tissues such as brain and heart during stroke or cardiac ischemia. One mechanism by which cells can respond to hypoxia is via proline hydroxylases (PHDs). PHDs require oxygen as a co-substrate[55]. HIF1α (hypoxia inducible factor 1α) is the best-known example of a protein regulated by proline hydroxylation. During normoxia, proline hydroxylation of HIF1α marks it as a substrate for the E3 ubiquitin ligase Von-Hippel Lindau (VHL), leading to HIF1α's rapid degradation by the

proteasome[55]. During hypoxia, proline hydroxylation of HIF1α is impaired, allowing it to remain present and to upregulate its target genes which help cells withstand hypoxia, such as the Glut1 glucose transporter[275]. As proline hydroxylation is a vital regulatory mechanism for the cells, it is important to identify other targets of this mechanism. Until a study by Moore *et al.*[78] published in 2015, there were no targets found regulated by PHDs that controlled energy demanding processes. It has been previously shown that eEF2 phosphorylation was increased during hypoxia and assists survival of cardiomyocytes and breast cancer cells [76, 77]. It was also shown that inhibition of prolyl hydroxylases increased p-eEF2 in HeLa, Mlp9, PC12 and Huh7 cells[54]. However, no mechanism was discovered as to why this occurs.

The study by Moore *et al.*[78] investigated eEF2K's role in hypoxia within MEFs, and A549, HCT116 and HEK293 cells, as well as in mouse primary cortical neurons. The study found that eEF2 phosphorylation gradually increased in HCT116, HeLa, MEF and cortical neuron cells during 16 h of hypoxic (0.1% O_2) conditions. There was no significant change to eEF2K protein levels under these conditions. Interestingly, it was found that the increase in eEF2 phosphorylation in hypoxia was independent of AMPK (which is turned on under poor energy conditions) as this increased phosphorylation was still evident in AMPKα1/α2 double KO MEFs. The proline hydroxylase inhibitor dimethyloxallyl glycine (DMOG) was found to increase eEF2 phosphorylation in Hela, HCT116, MEF and A549 cells without any changes to eEF2K protein levels. It was found that inhibition of PHDs altered eEF2 phosphorylation independently of changes in mTORC1 or AMPK signalling by using AZD8055 and MRT199665 to block each pathway respectively. MRT199665 failed to block increases in p-eEF2 in HCT116 cells, further showing that the increase is independent of AMPK. AZD8055 increased p-eEF2 faster than DMOG did, suggesting that the effect of DMOG on eEF2 is not due to impaired mTORC1 signalling. It was confirmed that DMOG increased eEF2K activity itself by immunoprecipitating MEF lysates in conditions with calcium ions present, meaning calmodulin (CaM) remains associated with eEF2K[49]. In this case, higher activity of eEF2K was

observed in DMOG treated cells, suggesting that proline hydroxylation affects the binding of eEF2K to CaM.

Mass-spectrometric analysis was performed on immunoprecipitated eEF2K from cells under normoxic conditions. A peptide with a shift of mass equivalent to two additional oxygen atoms was found meaning this peptide was hydroxylated. The non-hydroxylated peptide was no observed under the same conditions. The peptide identified corresponded to a region between the CaM-binding motif and the catalytic domain of eEF2K[18, 19]. It was found that this region contained a hydroxyproline (at Pro98). It was then found that even in the presence of excess CaM, eEF2K from DMOG-treated cells had higher activity than eEF2K from control cells. This shows that CaM does not stimulate eEF2K from control cells as well as from DMOG treated cells due to the Pro98 hydroxylation. The data showed that hydroxylation of Pro98 weakened the binding of CaM to eEF2K as well as its ability to activate eEF2K. A schematic of the relationship between hypoxia and eEF2K is shown in **Figure 1.2**. Finally, the study showed that cortical neurons from eEF2K-KO mice could not withstand hypoxia as well as eEF2K-WT cells, as shown by lower ATP levels and higher PARP cleavage in eEF2K-KO cells.

In regard to hypoxia, my goal in the work described in this chapter was to test various hypoxic oxygen concentrations and their effect on eEF2 phosphorylation in MDA-MB-231, A549 and HCT116 cells. The study by Moore *et al.*[78] tested only 0.1% O_2 hypoxia which is not as biologically relevant as higher concentrations[276].

5.1.4 eEF2K and Nrf2

Alzheimer's disease (AD) is the most common cause of dementia in the world. As of 2016, more than 47 million people are affected by this disease, according to the Alzheimer's Disease International organisation[277]. The molecular hallmarks of AD are amyloid-β (Aβ) plaques and neurofibrillary tangles made of hyperphosphorylated tau[278, 279].

Soluble Aβ oligomers have been shown to play a role in the pathogenesis of AD[280]. They have been shown to cause cell death in neuronal cultures as well as impair long term potentiation (LTP) which is important for strengthening synapses[281-284]. They have also been shown to induce long term depression (LTD)[285, 286]. Memory, as well as long term synaptic plasticity require protein synthesis[287]. Disruption of energy metabolism may cause the loss of synapses which leads to memory impairment and cognitive problems in AD[288].

It has been previously shown that eEF2K activity (p-eEF2 phosphorylation) and expression are increased in the temporal cortices of AD brains[289, 290]. Increased eEF2K activity has also been shown in the hippocampi of $APP_{swe}/PS1_{dE9}$ (amyloid precursor protein/presenilin 1) mice. These are double transgenic mice overexpressing the Swedish mutated form of APP and the dE9 mutated for of PS1, with both mutations associated with early onset AD, which itself leads to defective protein synthesis[289]. Treatment of neuronal cultures with synthetic Aβ oligomers and brain extracts from AD patients led to increased eEF2 phosphorylation as well as loss of dendritic spines[291]. This seems to point to eEF2K regulating Aβ oligomer neurotoxicity through altering protein synthesis due to its effect on p-eEF2. If eEF2K activity is increased, protein synthesis is inhibited, which in turn could affect long term synaptic plasticity in AD patients.

A study by Jan *et al.*[292] in 2016 showed that eEF2K activity is increased in the cortex and hippocampi of AD patients as well as AD mice. Aβo (Aβ oligomers) induce the degradation of post-synaptic density-95 (PSD-95) protein which is crucial for synaptic maturation and dendrite stability at synapses[293]. The study showed that inhibiting eEF2K in N2A neuroblastoma cells via A484954 or with shRNA in the presence of Aβo restored the PSD-95 levels to those of control cells. It was also found that eEF2K knockdown slightly increased ATP levels and significantly increased cell viability in the presence of Aβo. Importantly, it was found that eEF2K knockdown increased the expression of nuclear Nrf2, a transcription factor that is important in cellular antioxidant responses. It was observed that eEF2K knockdown reduced

reactive oxygen species (ROS) levels in N2A neuroblastoma cells under oxidative stress (using H_2O_2). Furthermore, the deletion of *efk-1* in *C. elegans* worms that also expressed Aβo significantly reduced ROS levels as well as improving neuronal function compared to worms that only expressed Aβo.

In this section of the Chapter, I investigate the effects of eEF2K inhibition or knock-out on Nrf2 levels in MDA-MB-231 and A549 cells.

5.1.5 eEF2K and PD-L1

It has now been firmly established that immunotherapy can be a good approach to cancer treatment[294]. However, cancer resistance to immune system attack through immune checkpoints can be a hindrance to this approach. The two most widely studied checkpoints are programmed cell death protein 1 (PD-1) and cytotoxic T lymphocyte protein 4 (CTLA-4)[294-296]. PD-1 is expressed on the surface of T lymphocytes and binds to ligands on the surfaces of other cells. This allows the cells to repress the activity of these T lymphocytes through PD-1, leaving them unharmed. PD-ligand 1 (PD-L1, also known as CD274 or B7-H1) is one of these ligands and its expression can be stimulated by interferon-γ, a cytokine that is critical for the immune system's response to foreign organisms. Recent studies have shown that countering these immune checkpoints increases the immune response against cancer[294]. Blocking these immune checkpoints has shown to elicit antitumour response in mice that had myeloma or mastocytoma[297-300]. It has also been shown that blocking the interaction between PD-1 and PD-L1 via antibodies elicited good clinical responses in patients with a wide range of cancers, both solid and haematologic[301]. Thus, 'immunotherapies' have emerged as an attractive and effective addition to our armoury of anti-cancer treatments.

It is important to understand the regulation of PD-L1 expression in cancer cells and how it enables them to suppress the immune response. It is known that PD-L1 expression is controlled at multiple stages, including mRNA stability, microRNAs and transcription[294, 302]

A recently published study (attached in the appendix) by Wu *et al.*[188] working closely with our group has established that eEF2K promotes the expression of PD-L1. eEF2K does this by suppressing the effect of an inhibitory upstream open reading-frame (uORF). This part of the chapter explores this study.

5.1.6 eEF2K and IRS-1

In Chapter 3, the potential of eEF2K to affect glycolysis and respiration was discussed. Previously, a study by Y. Cheng *et al.*[207] suggested that eEF2K regulated glycolysis in MDA-MB-231 and MCF-7 cells. The study found that a lack of eEF2K in these cells reduced their glucose uptake, production of lactate and ATP, as well as showing a decrease in the OCR of these cells. Another study by Jen *et al.*[208] showed that in N2A neuroblastoma cells' mitochondrial respiration actually increased upon eEF2K knockdown, suggesting eEF2K negatively regulates mitochondrial respiration in these cells. This could be because of increased protein synthesis due to eEF2K's inactivity increasing the consumption of ATP and GTP, thus forcing the cell to increase its metabolism to compensate.

In Chapter 3, I found that both glycolysis and mitochondrial respiration were not affected upon eEF2K-KO in MDA-MB-231 and PC3 cells or upon eEF2K knockdown in A549 cells. However, data from a phospho-proteomics study performed by Dr. Antigoni Manousopoulou from Professor Spiros D. Garbis' group using MDA-MB-231 eEF2K-WT and KO cells suggested that eEF2K may phosphorylate insulin receptor substrate 1 (IRS-1; Proud group, unpublished findings).

IRS-1 mediates the cell's responses to insulin by regulating the transmission of signals from the insulin-like growth factor-1 (IGF-1) receptors to the PI3K/PKB and ERK (MAP kinase) pathways. For example, tyrosine phosphorylation of IRS-1 by the insulin receptor allows for proteins bearing an SH-2 domain to bind, bringing PI3K to the inner face of the plasma membrane, where it generates phosphatidylinositol 3,4-bisphosphate (PIP_2). This in turn allows for the recruitment of PKB to the membrane which becomes activate upon phosphorylation of Thr308 by the kinase PDK1. This cascade of signalling events is followed by glucose uptake[303, 304]. This part of the chapter investigated the effect of eEF2K on glucose uptake and on IRS-1, as well as providing an overview of the steady state proteomics and phospho-proteomics data from studies performed on MDA-MB-231 eEF2K-WT and KO cells.

5.2 Results

Please note that sections of this chapter will refer to figures in studies attached to the Appendix. The data and figures provided in the text of this chapter were generated by me, with some of these figures used in the attached studies with different formatting.

5.2.1 eEF2K positively regulates cell migration and invasion

This part of the chapter directly refers to the study performed by Xie *et al.*[123] looking into eEF2K's effect on MDA-MB-231 and A549 cell migration and invasion. Please see the Appendix for a copy of this study. Some of the data presented were published in that article. The experiments in MDA-MB-231 cells were performed by me, while the A549 experiments were performed by Dr. Jianling Xie (then at the South Australian Health and Medical Research Institute). The A549 experiments will be referenced by the figure numbers in the attached paper.

All migration and invasion experiments were performed in the presence of mitomycin C to halt cell proliferation. After overnight starvation, a wound-healing assay was performed on MDA-MB-231 WT cells pre-treated with the eEF2K inhibitor JAN384. JAN384 was present in the medium throughout the 48 h of the experiment. **Figure 5.1A** shows that JAN384 did inhibit eEF2K throughout the experiment as shown by the absence of p-eEF2. **Figure 5.1B** from this chapter and **Figure 2A-C** from the published study[123] clearly shows that cells treated with JAN384 closed the wound much more slowly than untreated cells, suggesting that eEF2K promotes cell migration. **Figures 1D, E, F** from the study show that JAN384 has the same effect on the migration of A549 cells. To confirm that this is not just a 'side effect' of JAN384, the same wound healing assays were performed with two other eEF2K inhibitors, NH125 and A484954, in the presence of 2-DG in low glucose medium (5.55 mM) to activate eEF2K. NH125 has been known to possess off-target effects[176, 177], which is why A484954 was used as a comparison. **Figures 5.2A and B** (**shown as Supp. Figure 10E, F in the published study**[123]) show that A484954 and NH125 each effectively inhibited eEF2K up to 48 h. **Figure 5.3** (**supported by Supp. Figure 2E, F in the published study**[123]) showed that inhibition of eEF2K by either of these two inhibitors significantly slowed wound healing in studies on MDA-MB-231 cells. The same effect was seen for A549 cells (**Supp. Figure 2A-D** from the published paper[123]).

To support these data further, wound-healing assays were performed on eEF2K-WT and KO cells with or without JAN384 (**Figures 5.4 and 5.5A, western blots shown in 5.5B**). These data show that knocking out eEF2K slowed wound-healing in MDA-MB-231 cells. It is of note that JAN384 further slowed wound-healing in eEF2K-KO cells. This strongly suggests that the inhibitor has an off-target effect(s) that affects cell migration or other related processes.

To further expand on this, transwell migration and invasion assays were used. The transwell is a porous membrane through which cells must change shape and squeeze through in order to migrate to the other side and reach the chemoattractant such as FBS. For invasion assays, this transwell is coated with Matrigel. This gelatinous mixture resembles a biological barrier and

cells need to digest it in order to reach the transwell membrane and get to the other side of the membrane. This is close to what occurs during cell metastasis[305]. Transwell migration assays were performed with JAN384 treatments on cells migrating towards Type I bovine collagen as a chemoattractant. **Figure 5.6** shows a very similar trend to the wound-healing data. eEF2K-KO MDA-MB-231 cells migrated approximately half as fast as WT cells across the transwell membrane but not as slowly as when they were treated with JAN384. **Figures 1G, H, and 2D, E from the published paper[123]** complement these data in A549 and MDA-MB-231 cells, respectively. However, silencing eEF2K in A549 cells led to the same decrease in migration capability as when A549 cells were treated with JAN384.

Figure 5.1

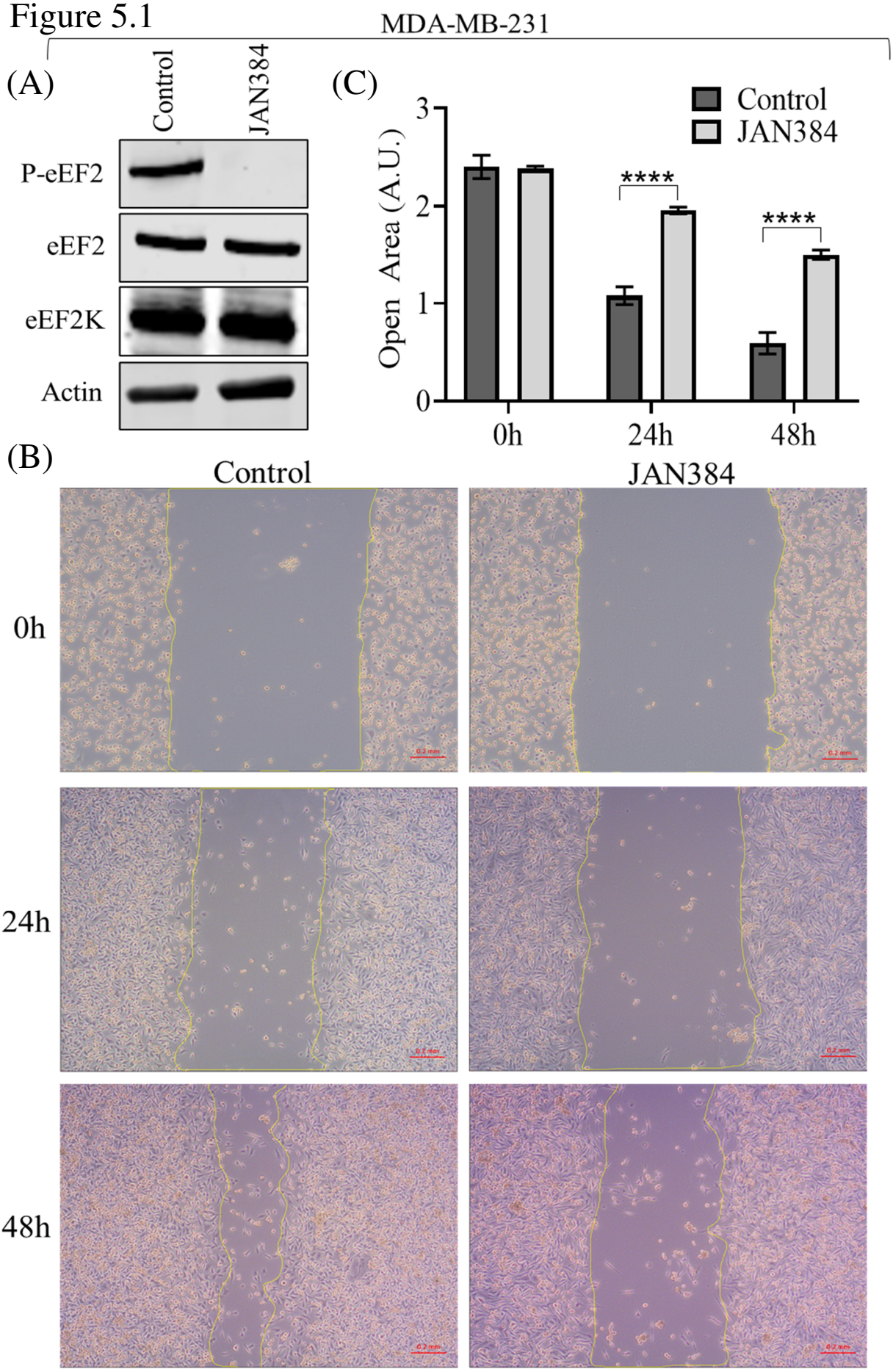

MDA-MB-231
(A)
Control
JAN384
P-eEF2
eEF2
eEF2K
Actin
(C)
Control
JAN384
Open Area (A.U.)
0
1
2
3
****
****
0h
24h
48h
(B)
Control
JAN384
0h
24h
48h

Figure 5.1: Inhibiting eEF2K with JAN384 slows wound healing of MDA-MB-231 cells. **A:** MDA-MB-231 cells were lysed after the scratch wound-healing assay shown in **B**. The lysates were run on (12.5%) SDS-PAGE and analysed by immunoblot. Image is representative of n=3. **B:** Scratch wound-healing assays were performed on cells after overnight serum starvation and pre-treatment with 6 μM JAN384 with the inhibitor being present for the duration of the assay. All cells were also treated with 0.5 μg/μl mitomycin C. Images were taken using Zeiss Axiovert 200 microscope with the 4X magnifying lens at the indicated times. Each image is representative of 15 images total from 3 biological replicates. **C:** Quantification of data in **A**. Error bars represent S.D. (n=3). The p-values were calculated using Two-Way ANOVA with the Tukey multiple comparisons test. P-values: ****≤0.0001.

Figure 5.2

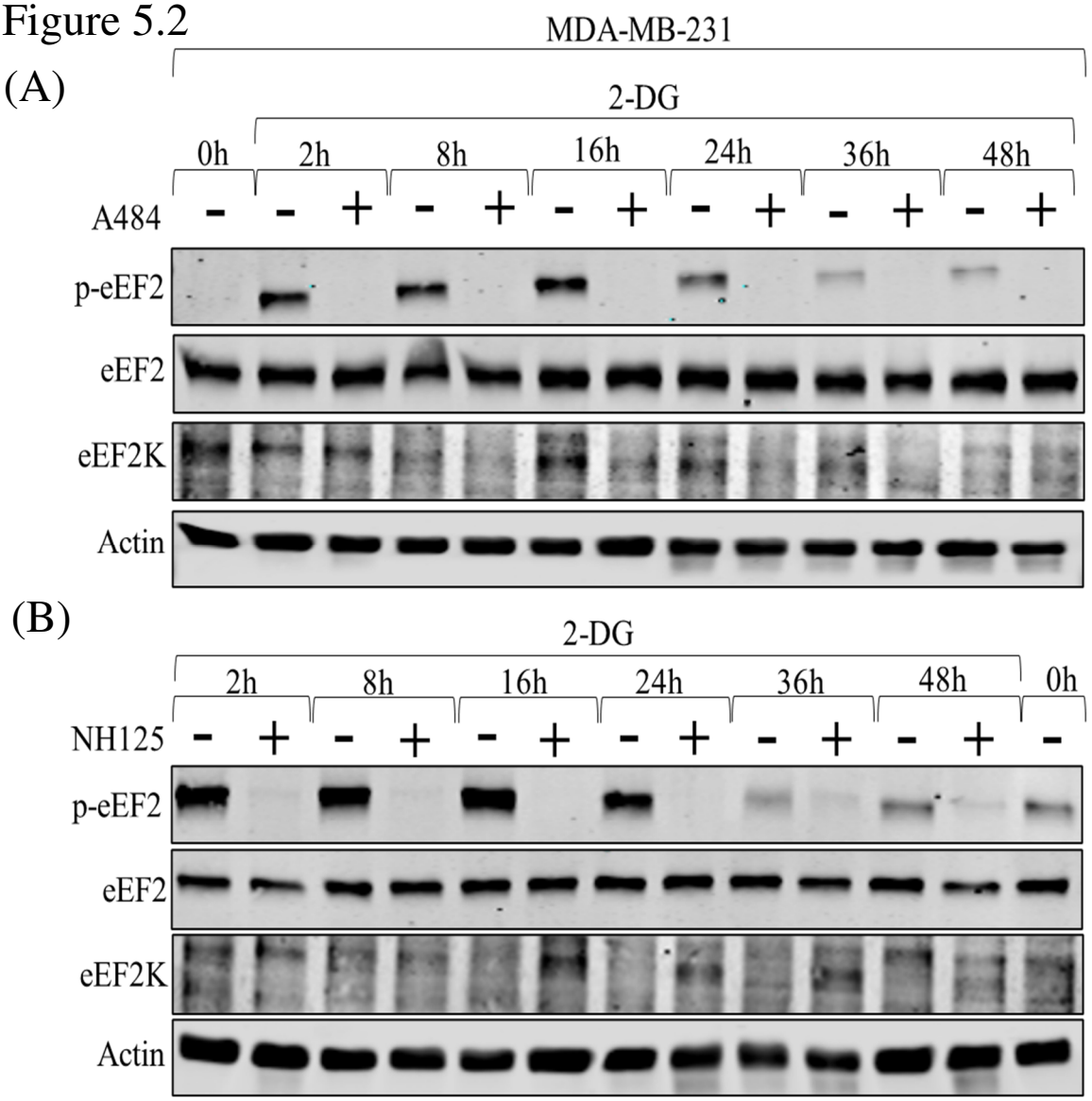


Figure 5.2: NH125 and A484954 successfully inhibit eEF2K in MDA-MB-231 cells. MDA-MB-231 cells were cultured in low glucose (5.55 mM) DMEM for 1 h prior to treatment with 10 mM 2-DG for the indicated times, alongside either 30 μM A484954 (**A**) or 1 μM NH125 (**B**). Cells were lysed and the lysates were run on (12.5%) SDS-PAGE, followed by immunoblot analysis. Images are representative of n=3.

Figure 5.3

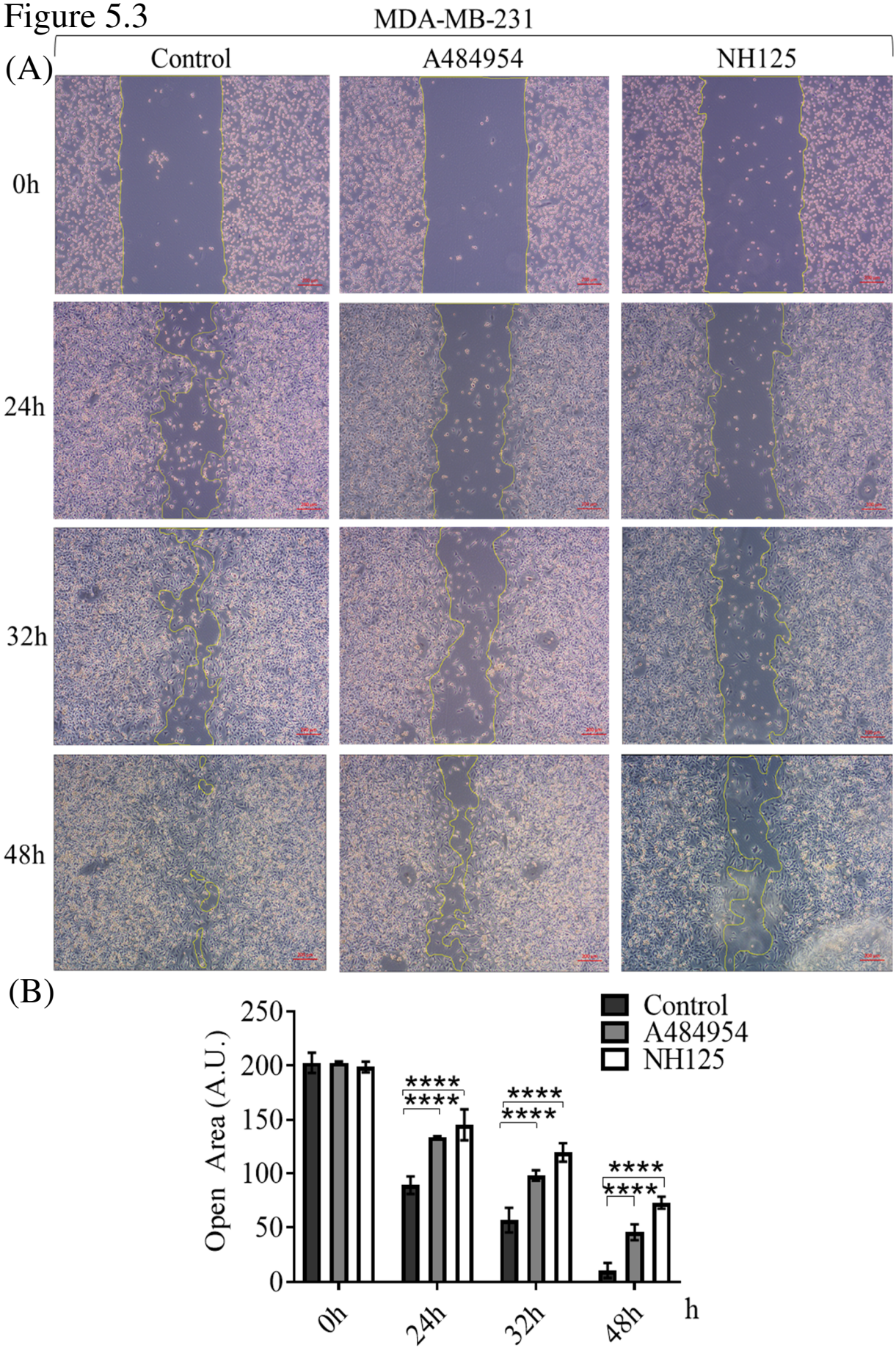

MDA-MB-231
(A)
Control
A484954
NH125
0h
24h
32h
48h
(B)
Control
A484954
NH125
Open Area (A.U.)
250
200
150
100
50
0
****
****
****
****
****
****
0h
24h
32h
48h
h

Figure 5.3: Inhibiting eEF2K with A484954 or NH125 slows down healing of MDA-MB-231 cells. A: After overnight serum starvation MDA-MB-231 cells were cultured in low glucose (5.55 mM) DMEM for 1 h prior to treatment with 10 mM 2-DG. 30 µM A484954 or 1 µM NH125 were then added. All cells were treated with 0.5 µg/µl mitomycin C. Images were taken using Zeiss Axiovert 200 microscope with the 4X magnifying lens at the indicated times. Each image is representative of 15 images total from 3 biological replicates. **B:** Quantification of data in **A**. Error bars represent S.D. (n=3). The p-values were calculated using Two-Way ANOVA with the Tukey multiple comparisons test. P-values: ****≤0.0001.

Figure 5.4

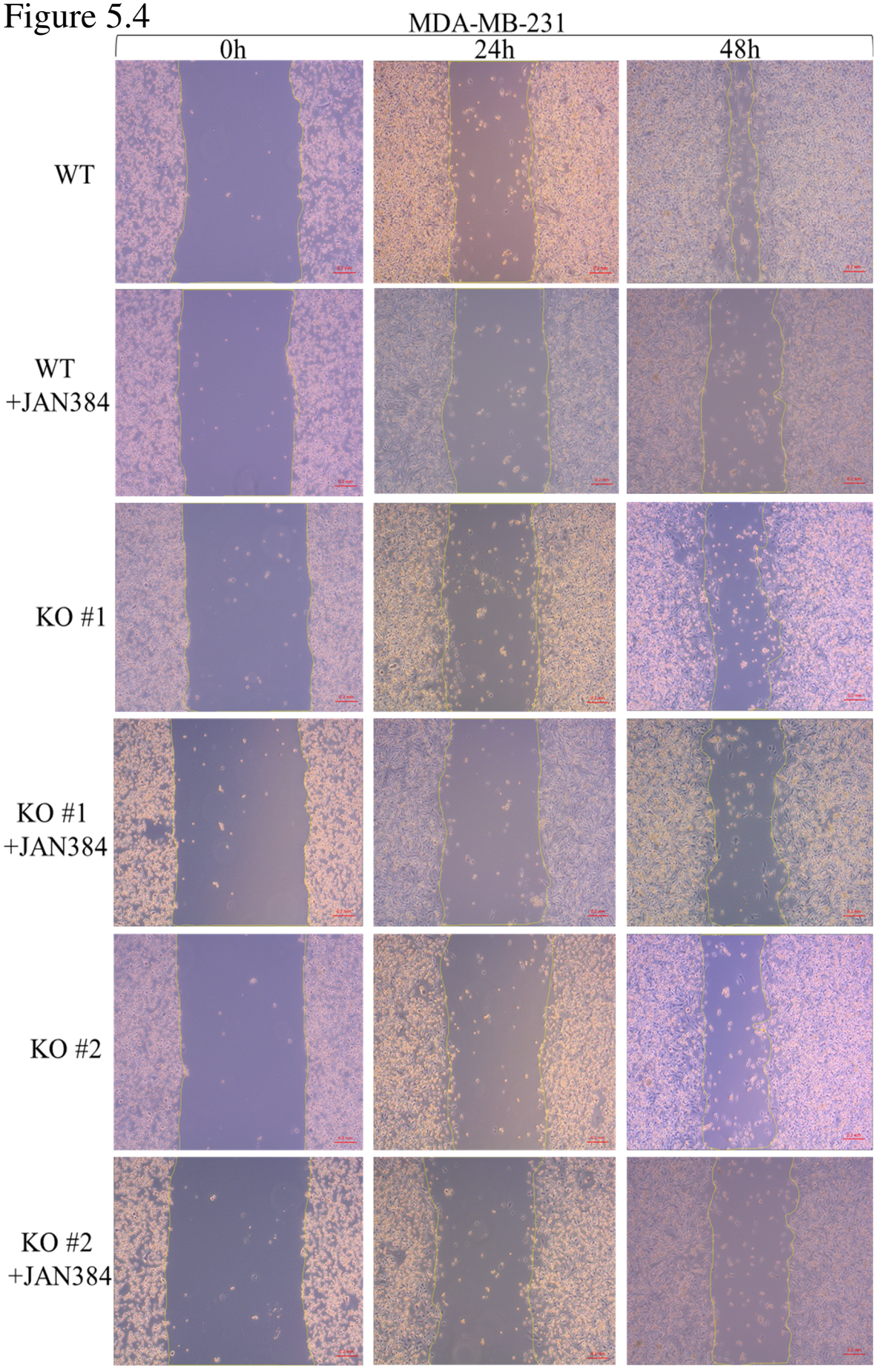

MDA-MB-231
0h
24h
48h
WT
WT
+JAN384
KO #1
KO #1
+JAN384
KO #2
KO #2
+JAN384

Figure 5.4: Lack of eEF2K slows wound healing of MDA-MB-231 cells, with JAN384 slowing wound healing further. After overnight serum starvation, scratch wound-healing assays were performed on MDA-MB-231 WT and eEF2K-KO cells with or without 5 μM JAN384. All cells were treated with 0.5 μg/μl mitomycin C. Images were taken using Zeiss Axiovert 200 microscope with the 4X magnifying lens at the indicated times. Each image is representative of 15 images total from 3 biological replicates.

Figure 5.5

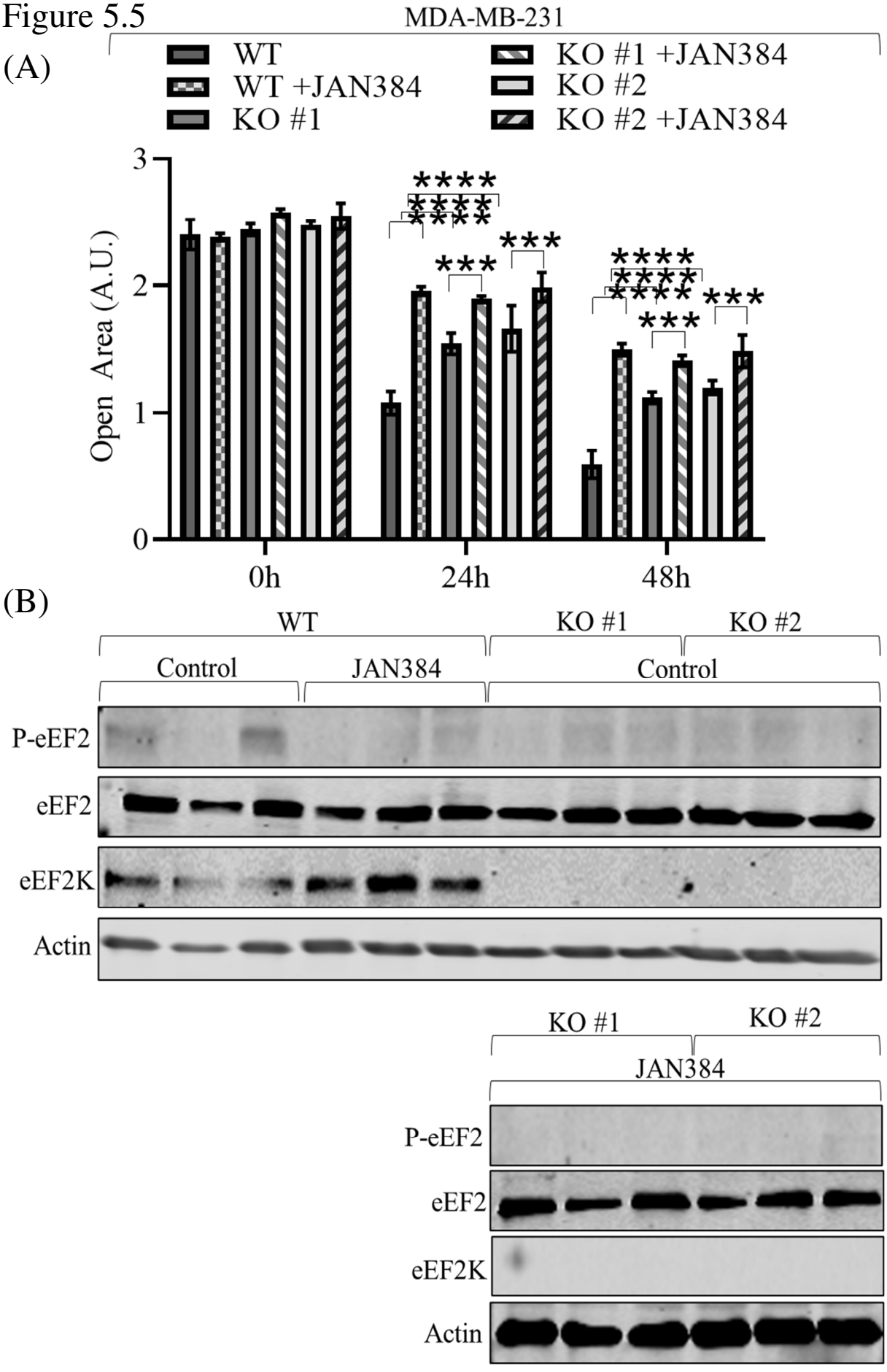

(A)
MDA-MB-231
WT
WT +JAN384
KO #1
KO #1 +JAN384
KO #2
KO #2 +JAN384
Open Area (A.U.)
0
1
2
3
0h
24h
48h
****
****
****
***
***
****
****
****
***
***
(B)
WT
KO #1
KO #2
Control
JAN384
Control
P-eEF2
eEF2
eEF2K
Actin
KO #1
KO #2
JAN384
P-eEF2
eEF2
eEF2K
Actin

Figure 5.5: Lack of eEF2K slows wound healing of MDA-MB-231 cells, with JAN384 slowing wound healing further. A: Quantification of data in **Figure 5.4**. Error bars represent S.D. (n=3). The p-values were calculated using Two-Way ANOVA with the Tukey multiple comparisons test. P-valuse: ****≤0.0001 **B:** After the completion of the wound-healing assay, MDA-MB231 cells were lysed and the lysates were run on (12.5%) SDS-PAGE, followed by analysis via immunoblotting. Images are representative of n=3. Error bars represent S.D. (n=3). The p-values were calculated using Two-Way ANOVA with the Tukey multiple comparisons test. P-value: *** ≤ 0.001; ****≤0.0001.

Figure 5.6

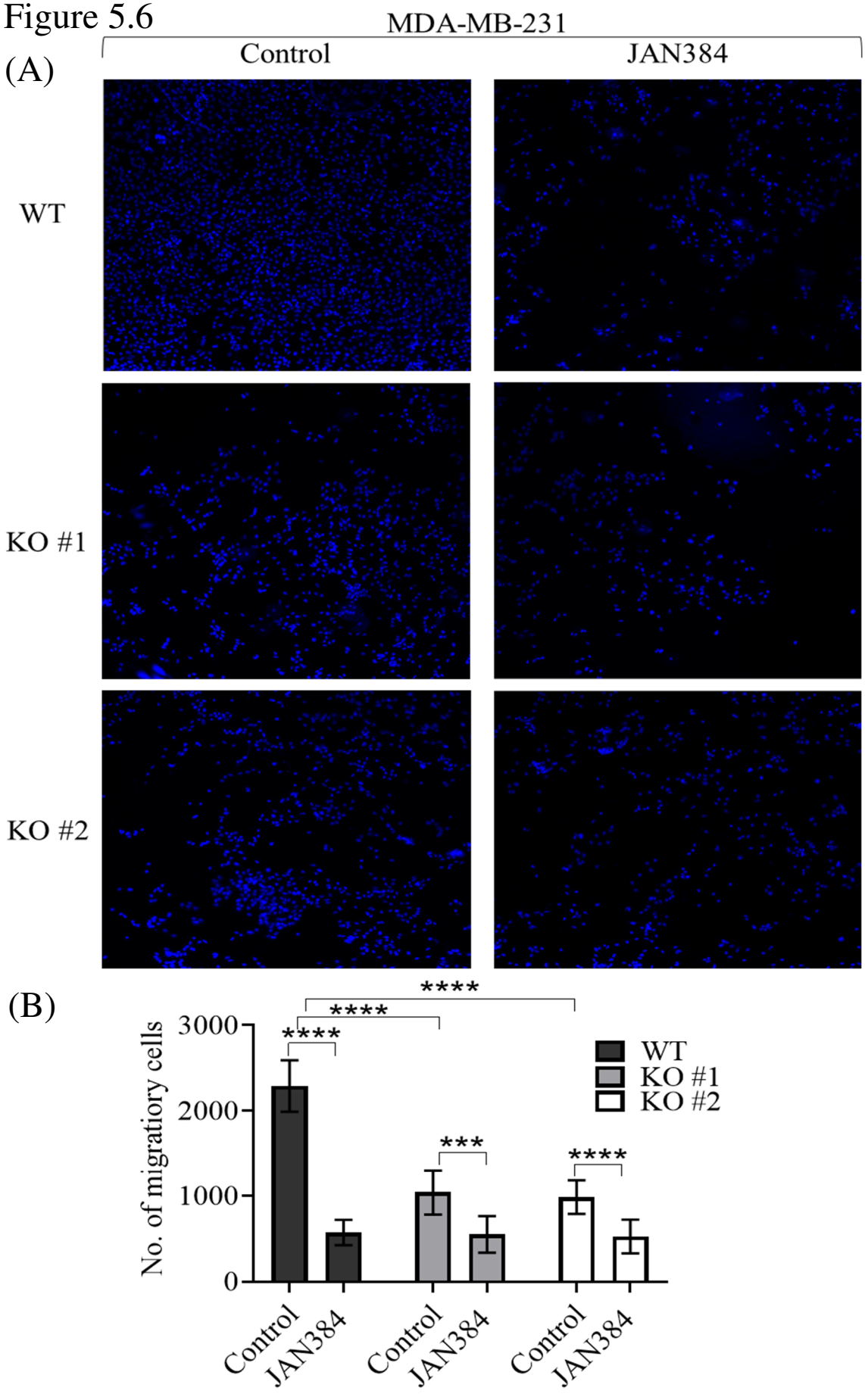

(A)
MDA-MB-231
Control
JAN384
WT
KO #1
KO #2
(B)
No. of migratiory cells
3000
2000
1000
0
****
****
****
***
****
WT
KO #1
KO #2
Control
JAN384
Control
JAN384
Control
JAN384

Figure 5.6: Lack of eEF2K slows migration of MDA-MB-231 cells, with JAN384 slowing migration further. A: Transwell migration assay of MDA-MB-231 WT and eEF2K-KO cells with or without 5 μM JAN384. All cells were treated with 0.5 μg/μl mitomycin C. Cells migrated towards 10 μg/mL collagen for 48 h. Images were taken with the Nikon Eclipse Ni microscope (10x magnification, DAPI filter). Each image is representative of 15 images total from 3 biological replicates. **B:** Quantification of data in **A**. Error bars represent S.D. (n=3). The p-values were calculated using Two-Way ANOVA with the Tukey multiple comparisons test. P-values: ****≤0.0001.

Invasion assays were then performed on MDA-MB-231 cells treated with JAN384, A484954 and NH125. **Figure 5.7 (shown as Figure 2 F, G in the published paper[123])** clearly shows that inhibition of eEF2K with any of the three inhibitors greatly decreased the invasion capability of MDA-MB-231 cells. This is also seen in A549 cells with IPTG-induced eEF2K silencing or treatment with either A484954 or NH125 greatly decreasing A549 cell invasion capability (**Figure 1I, J in the published paper[123]**). I then tested the effect of knocking out eEF2K on MDA-MB-231 invasion with or without JAN384 treatment (**Figure 5.8**). eEF2K-KO cells invaded through the Matrigel and across the membrane approximately half as fast as WT cells but treatment with JAN384 slowed down invasion even further in both WT and KO cells, further supporting the conclusion that JAN384 has an off-target effect. To determine why eEF2K affects migration, adhesion assays were performed on non-coated surfaces or surfaces coated with gelatin, poly-L-lysine, or Type I bovine collagen. Cells were allowed to attach to the surface for 30 min after which point all unattached cells were removed and the attached cells were stained with Calcein-AM dye to quantify the adhesion capacity of these cells. **Figure 1K and L** from the published study[123] show that silencing eEF2K in A549 cells or inhibiting it with A484954 or NH125 significantly reduced cell adhesion on gelatin and poly-L-lysine. **Figure 5.9A** (**shown as Figure 2H in the published study[123]**) shows that NH125 significantly lowered adhesion of MDA-MB-231 cells to gelatin, while JAN384 and A484954 did not statistically significantly alter it, although three was trend to a decrease. The adhesion assay was then performed on MDA-MB-231 eEF2K-WT and KO cells on non-coated and collagen coated surfaces (**Figure 5.9B, C, Figure 5.10**). These assays showed no significant change in adhesion between WT and eEF2K-KO cells, suggesting the eEF2K inhibitors have an off-target effect that affects cell adhesion.

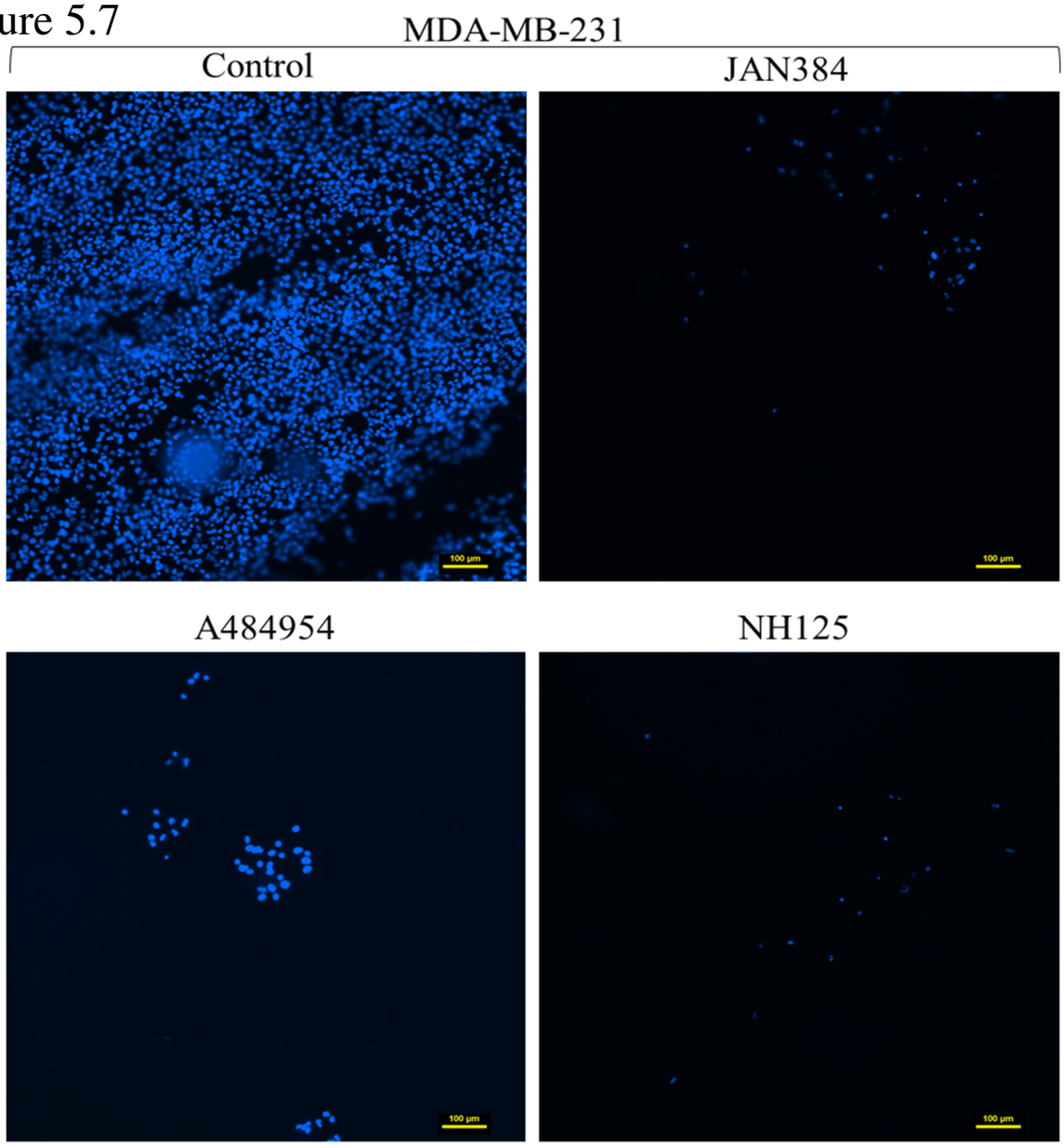
To confirm that migration and invasion was affected by eEF2K, FLAG-tagged eEF2K was overexpressed and compared to the overexpressed K170M kinase dead mutant in a wound-healing experiment. Overexpressing eEF2K in MDA-MB-231 and A549 cells greatly increased the speed of the wound-healing, while the cells with overexpressed K170M migrated at the

same speed as empty vector control cells (**Figures 5.11, 5.12, Figure 3 from the published study**[123]). To check whether this is due to eEF2K's effect on eEF2, the wound-healing experiment was done with si-RNA against eEF2 (**Figure 5.12**, **Figure 3 from the published study**[123]). Fully or strongly silencing eEF2 leads to cell death (as eEF2 is an essential protein), hence an siRNA that leads to approximately 50% reduction in eEF2 protein was used. As expected, a reduction in eEF2 protein (i.e., active eEF2) led to an increase in wound-healing, similar to what is seen when WT eEF2K was overexpressed.

Finally, eEF2K's effect on cell proliferation was investigated using propidium iodide flow cytometry (FACS) and a 5-bromo-2'-deoxyuridine (BrdU) incorporation assay. Propidium iodide (PI) binds DNA and does so in proportion to the amount of DNA present in the cell. As the DNA amount is different at each stage of the cell cycle, FACS using PI can be used to quantify the proportion of cells in each stage of the cell cycle[306]. BrdU is incorporated into newly synthesised DNA of proliferating cells during S-phase and this incorporation can then be detected with an anti-BrdU antibody to quantify cell proliferation[129]. According to the BrdU assay, there was no significant change in proliferation between MDA-MB-231 eEF2K-WT and KO cells or A549 WT and eEF2K silenced cells (**Figure 5.13**). The propidium iodide FACS assay showed that there was no significant change to the percentages of cells in the G0/G1, S or G2/M phases of the cell cycle between MDA-MB-231 eEF2K-WT and KO cells (**Figures 5.14 and 5.15**). This further confirms that eEF2K's effect on cell migration and invasion was not due to differences in cell proliferation or cell number.

Figure 5.7

(A)


MDA-MB-231
Control
JAN384
A484954
NH125
100 µm

(B)

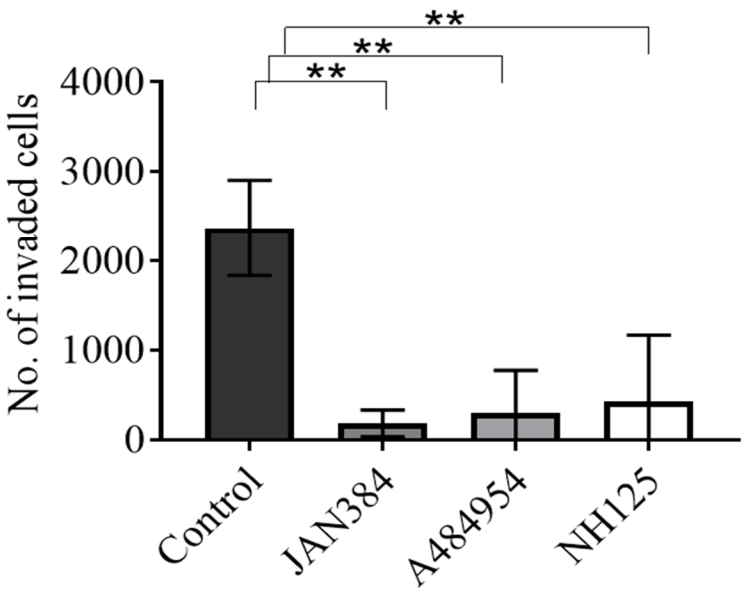

**
**
**
4000
3000
2000
1000
0
No. of invaded cells
Control
JAN384
A484954
NH125

Figure 5.7: Inhibition of eEF2K slows invasion of MDA-MB-231 cells through Matrigel. **A:** Transwell invasion assay of MDA-MB-231 WT with or without 5 μM JAN384, 30 μM A484954, 1 μM NH125. All cells were treated with 0.5 μg/μl mitomycin C. Cells migrated towards 10% FBS for 72 h. Images were taken with the Nikon Eclipse Ni microscope (10x magnification, DAPI filter). Each image is representative of 15 images total from 3 biological replicates. **B:** Quantification of data in **A**. Error bars represent S.D. (n=3). The p-values were calculated using Two-Way ANOVA with the Tukey multiple comparisons test. P-values: ****≤0.0001.

Figure 5.8

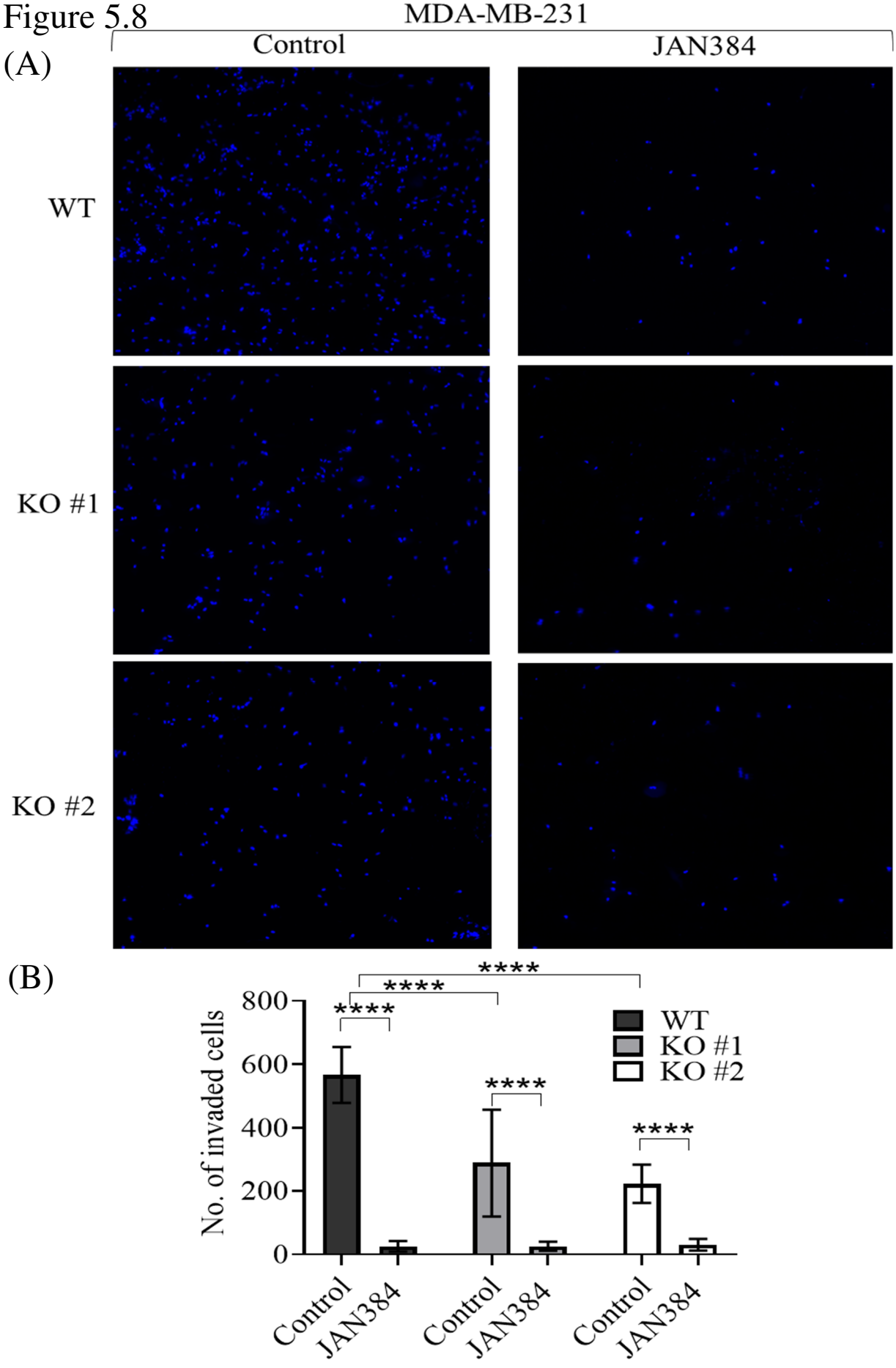
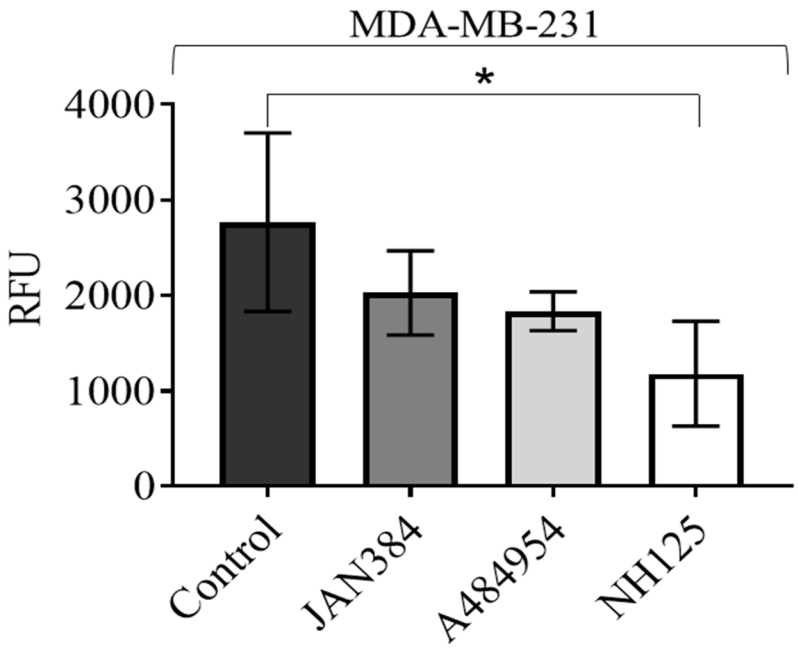

(A)
MDA-MB-231
Control
JAN384
WT
KO #1
KO #2
(B)
No. of invaded cells
800
600
400
200
0
****
****
****
****
****
WT
KO #1
KO #2
Control
JAN384
Control
JAN384
Control
JAN384

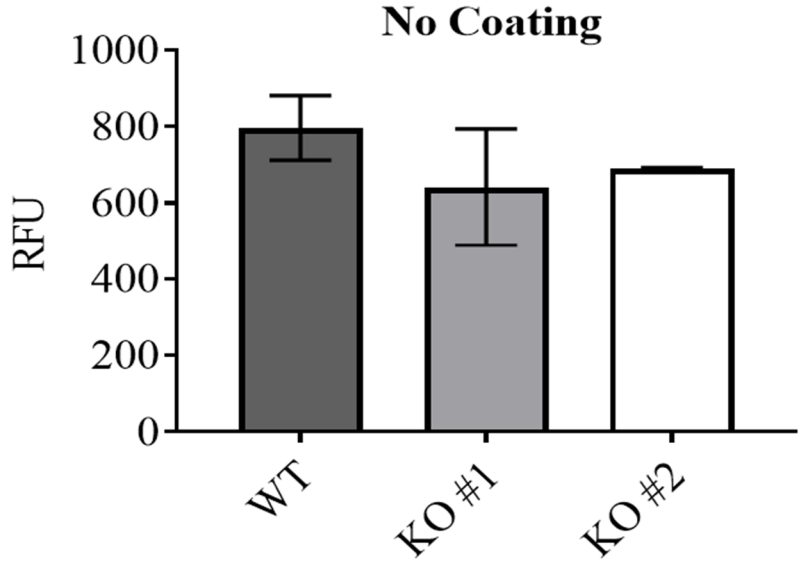
Figure 5.8: Lack of eEF2K slows invasion of MDA-MB-231 cells, with JAN384 slowing invasion further. A: Transwell invasion assay of MDA-MB-231 eEF2K WT and KO cells with or without 5 μM JAN384. All cells were treated with 0.5 μg/μl mitomycin C. Cells migrated towards 20% FBS for 24 h. Images were taken with the Nikon Eclipse Ni microscope (10x magnification, DAPI filter). Each image is representative of 15 images total from 3 biological replicates. **B:** Quantification of data in **A**. Error bars represent S.D. (n=3). The p-values were calculated using Two-Way ANOVA with the Tukey multiple comparisons test. P-values: ****≤0.0001

Figure 5.9

(A)



(B)



(C)

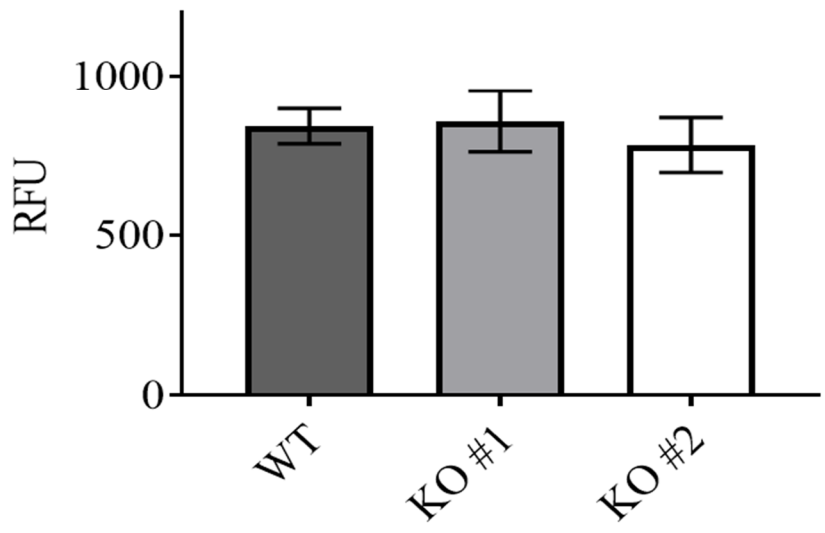


Figure 5.9: Inhibition of eEF2K with NH125 decreases adhesion of MDA-MB-231 cells, while knocking it out has no effect. A: Adhesions assays performed on MDA-MB-231 eEF2K WT cells with or without 5 µM JAN384, 30 µM A484954 or 1 µM NH125. The well surface was coated with 20 µg/mL gelatin and the cells were allowed to attach for 30 min. **B, C:** Adhesion assays of MDA-MB-231 eEF2K WT and KO cells on surfaces with no coating or coated with bovine Type I collagen at 10 µg/mL. Attached cells were stained with 1 µM Calcein-AM for 1h and the signal measured using the GloMax Discover instrument. Error bars represent S.D. (n=3). The p-values were calculated using One-Way ANOVA with Brown-Forsythe and Welch ANOVA tests. P-values: *≤0.05.

Figure 5.10

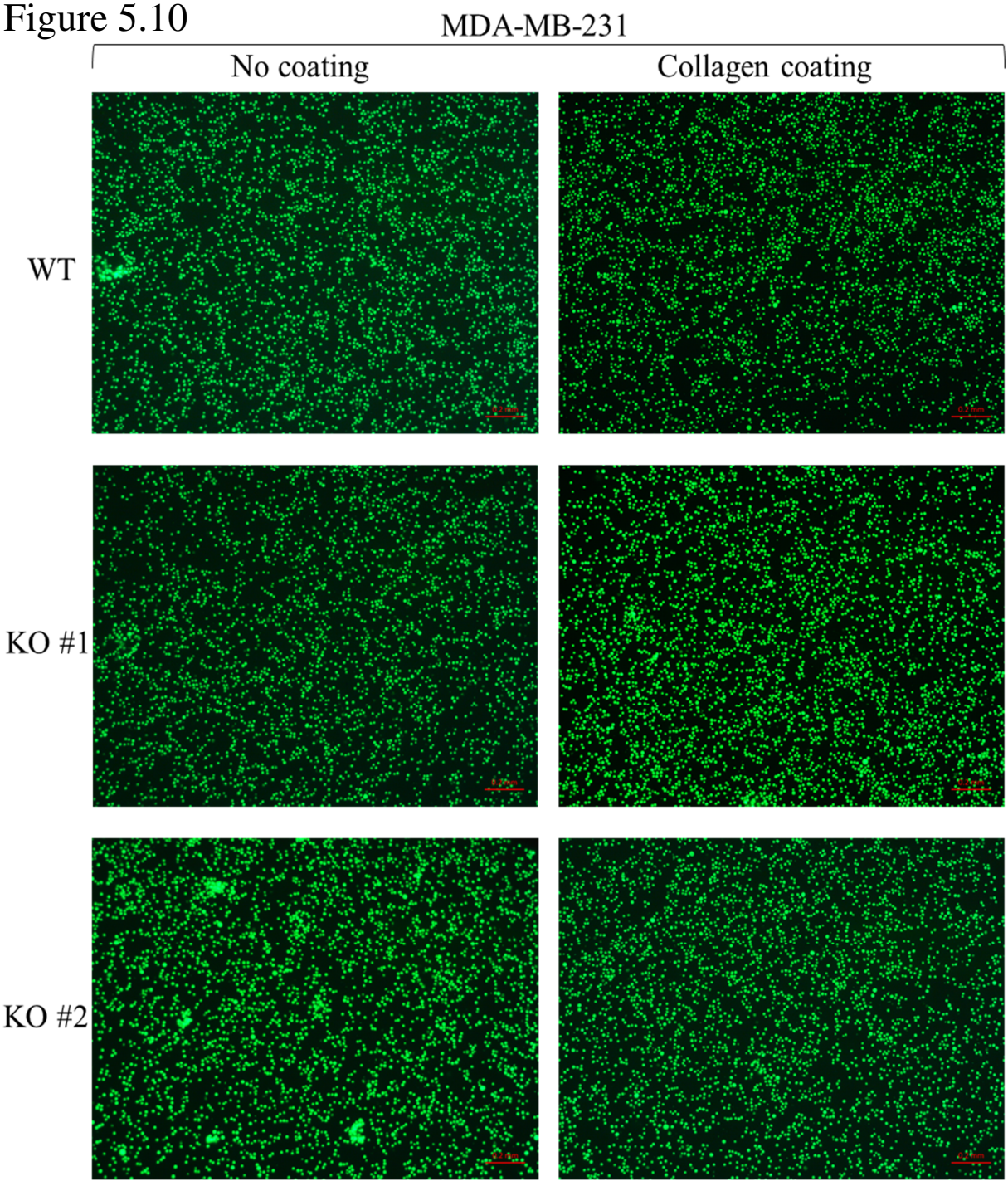


Figure 5.10: Knocking out eEF2K in MDA-MB-231 cells has no effect on cell adhesion. Images of the cell adhesion assay performed in **Figure 5.9 B and C**. Images were taken using Zeiss Axiovert 200 microscope with the 4X magnifying lens and GFP filter after Calcein-AM staining. Each image is representative of 15 images total from 3 biological replicates.

The published study goes on to show that silencing eEF2K reduced the expression of several proteins relevant to cell migration and invasion (in particular, integrins α2 and α3 [ITGA2 and ITGA3])[307] via analysis of the steady state proteome (**Figure 4 in the published study**[123]). It was then found that eEF2K controls the translation of the mRNAs for such proteins as shown by analysing ribosomal and polyribosomal fractions collected after resolving them through sucrose density gradients (**Figure 5 in the published study**[123]). Upon eEF2K knockdown in A549 cells, the amounts of mRNAs encoding integrins α2 and α3 that were associated with translationally active polysomes decreased, while the amount found in non-translationally active sub-polysomal fractions increased. This shows that eEF2K positively controls the association of these migration-related mRNAs with ribosomes. i.e., promotes their translation.

Overall, my work complemented the published study by confirming the migration and invasion data obtained in it via inhibiting eEF2K chemically or silencing it by comparing it to stable MDA-MB-231 eEF2K-KO cells. It is important to note that the eEF2K inhibitor JAN384 had a larger effect on migration and invasion than what was observed in the KO cells. However, eEF2K-KO cells still migrated and invaded approximately half as quickly as WT cells. This shows that eEF2K does indeed regulate migration and invasion, but it is important to take note of the off-target effects of JAN384 on these processes.

Figure 5.11

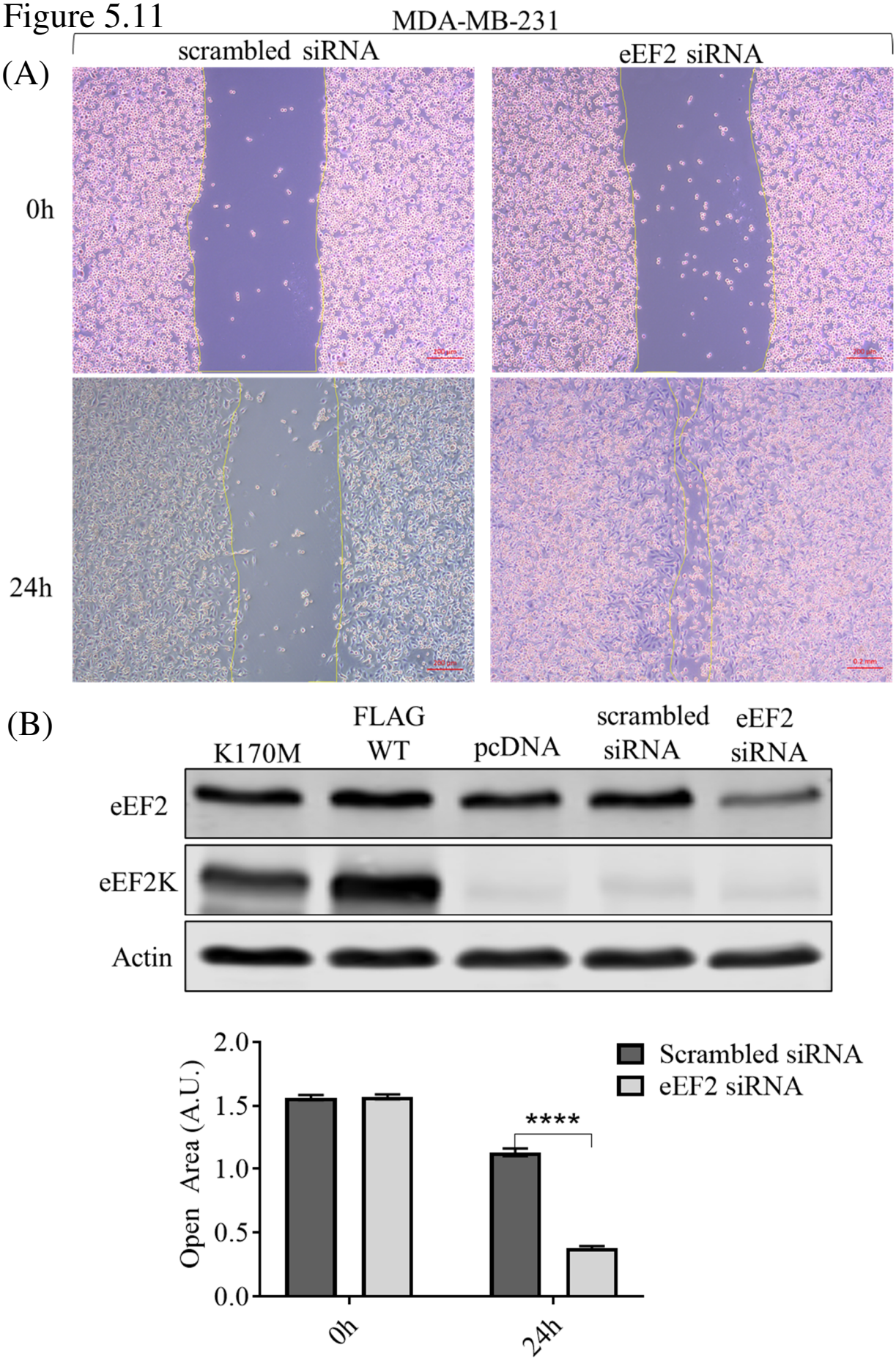

MDA-MB-231
(A)
scrambled siRNA
eEF2 siRNA
0h
24h
(B)
K170M
FLAG WT
pcDNA
scrambled siRNA
eEF2 siRNA
eEF2
eEF2K
Actin
Scrambled siRNA
eEF2 siRNA
Open Area (A.U.)
2.0
1.5
1.0
0.5
0.0
****
0h
24h

Figure 5.11: Overexpressing eEF2K accelerates wound-healing of MDA-MB-231 cells. A: MDA-MB-231 cells were transfected with empty vector (pcDNA) or vectors overexpressing FLAG-eEF2K-WT or K170M for 24 h. Wound-healing assays were then performed, and images were taken at the indicated times using the Zeiss Axiovert 200 microscope with the 4X magnifying lens. Each image is representative of 15 images total from 3 biological replicates. **B:** After the conclusion of the wound-healing assay, the cells were lysed and the lysates were run on (12.5%) SDS-PAGE, followed by analysis via immunoblot. The image is representative of n=3**. C:** Quantification of data in **A**. Error bars represent S.D. (n=3). The p-values were calculated using Two-Way ANOVA with the Tukey multiple comparisons test. P-values: ****≤0.0001.

Figure 5.12

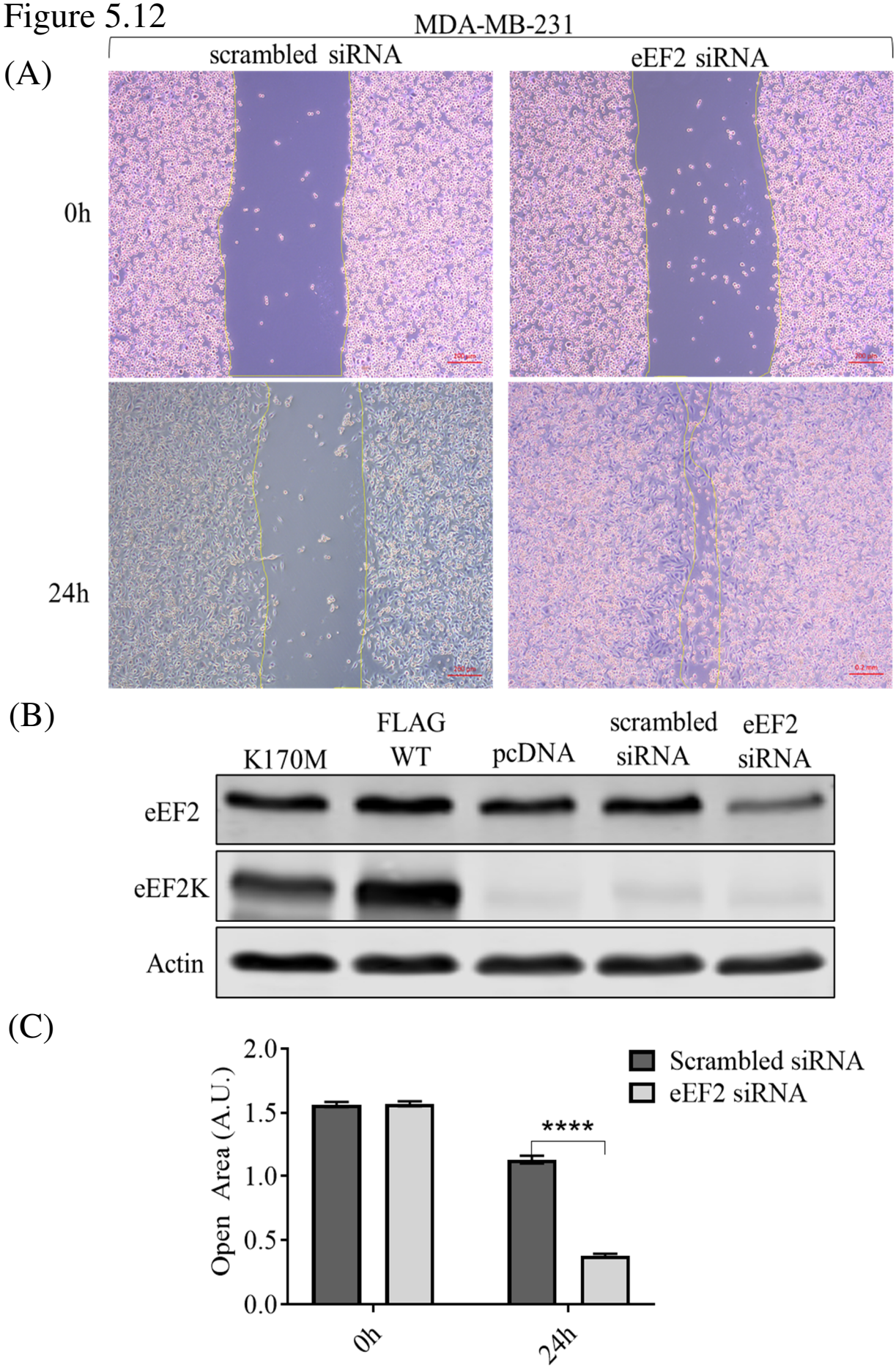

(A)
MDA-MB-231
scrambled siRNA
eEF2 siRNA
0h
24h
(B)
K170M
FLAG WT
pcDNA
scrambled siRNA
eEF2 siRNA
eEF2
eEF2K
Actin
(C)
Scrambled siRNA
eEF2 siRNA
Open Area (A.U.)
2.0
1.5
1.0
0.5
0.0
****
0h
24h

Figure 5.12: Partially silencing eEF2 accelerates wound-healing of MDA-MB-231 cells. A: MDA-MB-231 cells were transfected with scrambled siRNA or siRNA against eEF2 for 24 h. Wound-healing assays were then performed, and images were taken at the indicated times using the Zeiss Axiovert 200 microscope with the 4X magnifying lens. Each image is representative of 15 images total from 3 biological replicates. **B:** After the conclusion of the wound-healing assay, samples were lysed and the lysates were run on (12.5%) SDS-PAGE, followed by analysis with immunoblot. The image is representative of n=3. **C:** Quantification of data in **A**. Error bars represent S.D. (n=3). The p-values were calculated using Two-Way ANOVA with the Tukey multiple comparisons test. P-value: ****≤0.0001.

Figure 5.13

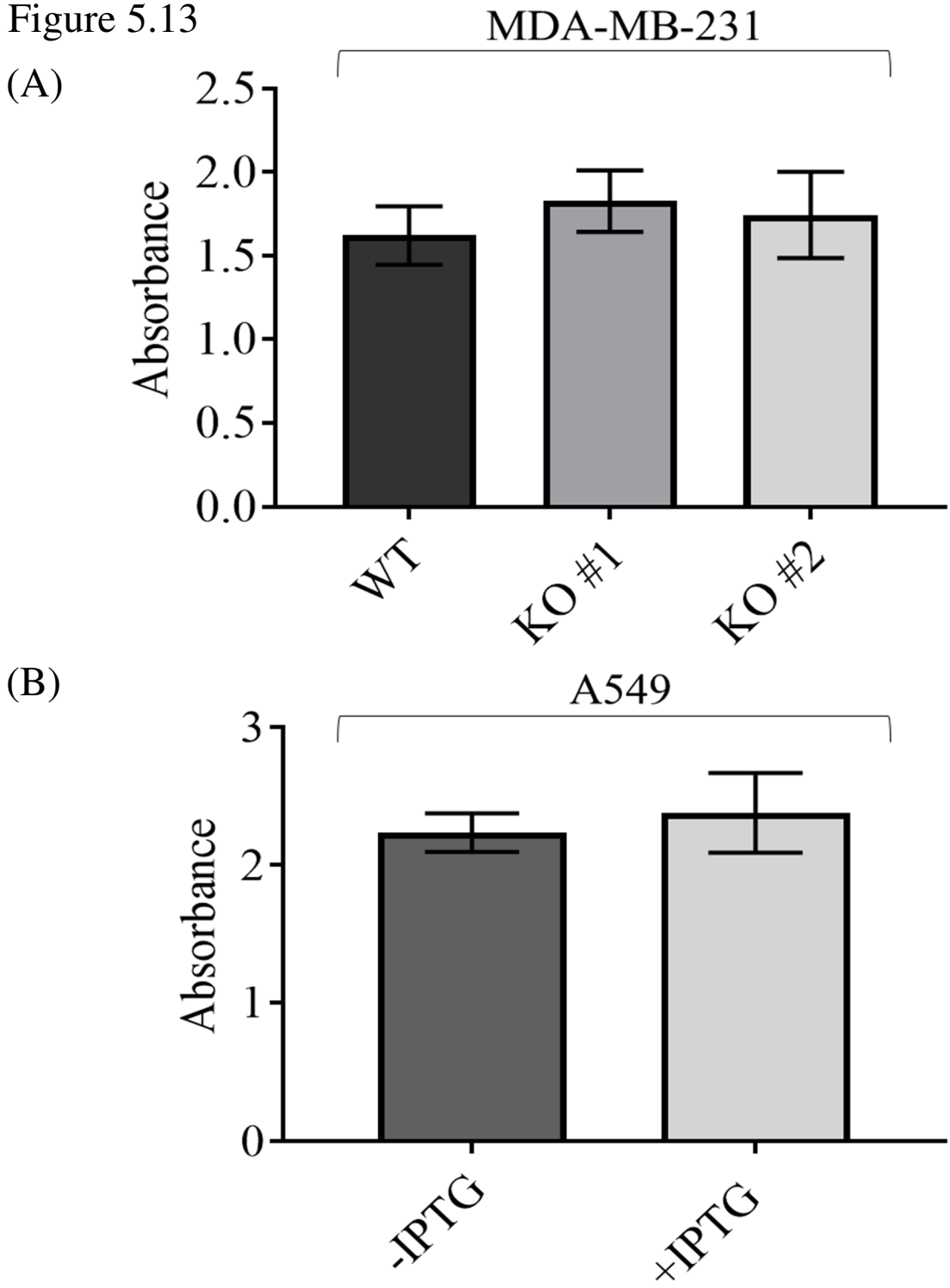


Figure 5.13: Knocking out eEF2K in MDA-MB-231 cells or silencing it in A549 cells does not affect cell proliferation. A, B: MDA-MB-231 or A549 cells respectively were serum starved overnight prior to performing the BrdU assay. The endpoint measurement was performed at 24 h post addition of BrdU. Error bars represent S.D. (n=3). The p-values were calculated using One-Way ANOVA with Brown-Forsythe and Welch ANOVA tests.

Figure 5.14

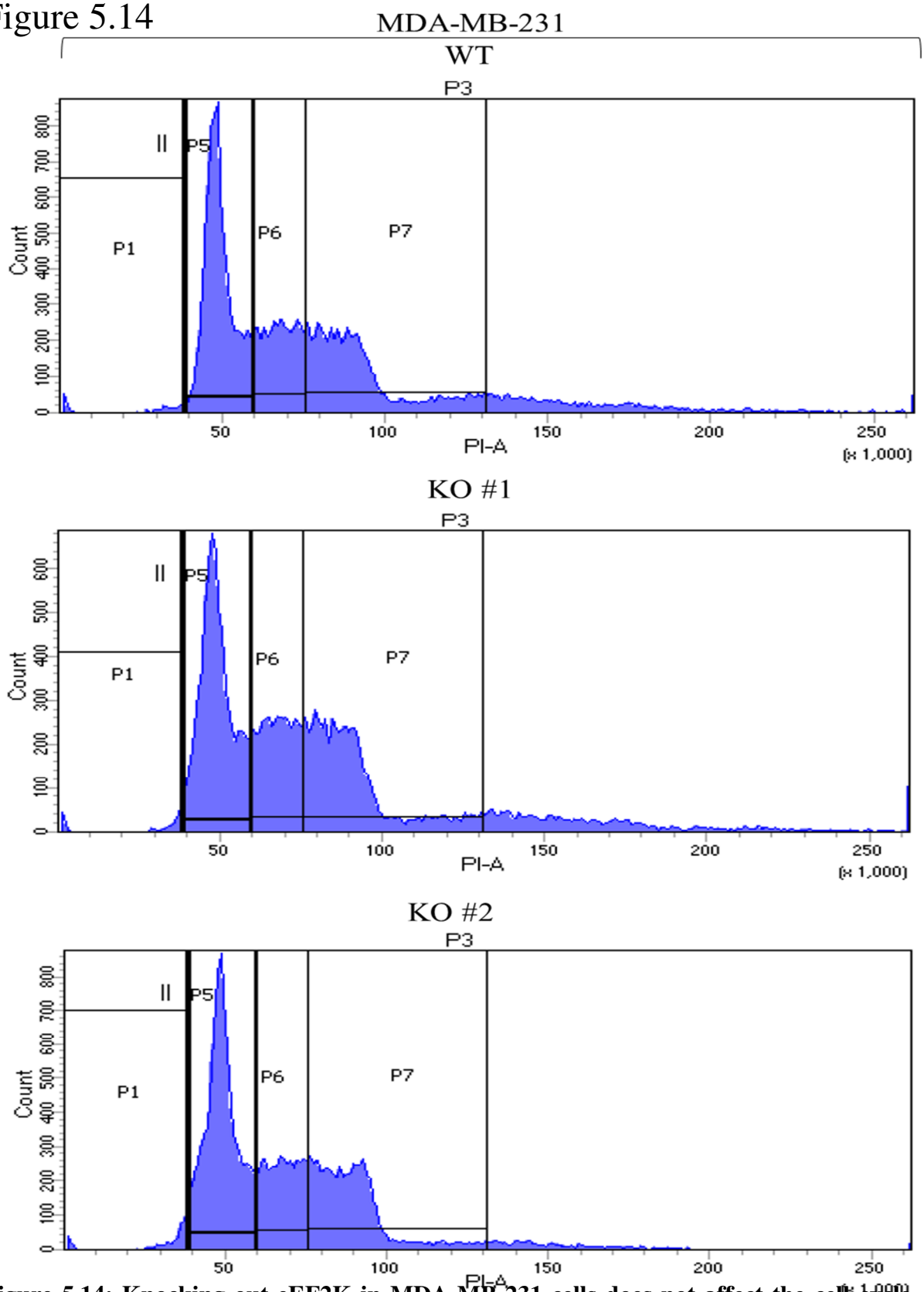


Figure 5.14: Knocking out eEF2K in MDA-MB-231 cells does not affect the cell cycle. MDA-MB-231 cells were serum starved overnight and allowed to proliferate for 24 h prior to fixation and staining with propidium iodide. The BD FACS CantoTM II system was used to gate the single cell population and quantify the fluorescence. Each image is representative of n=3 from 3 technical replicates each.

Figure 5.15

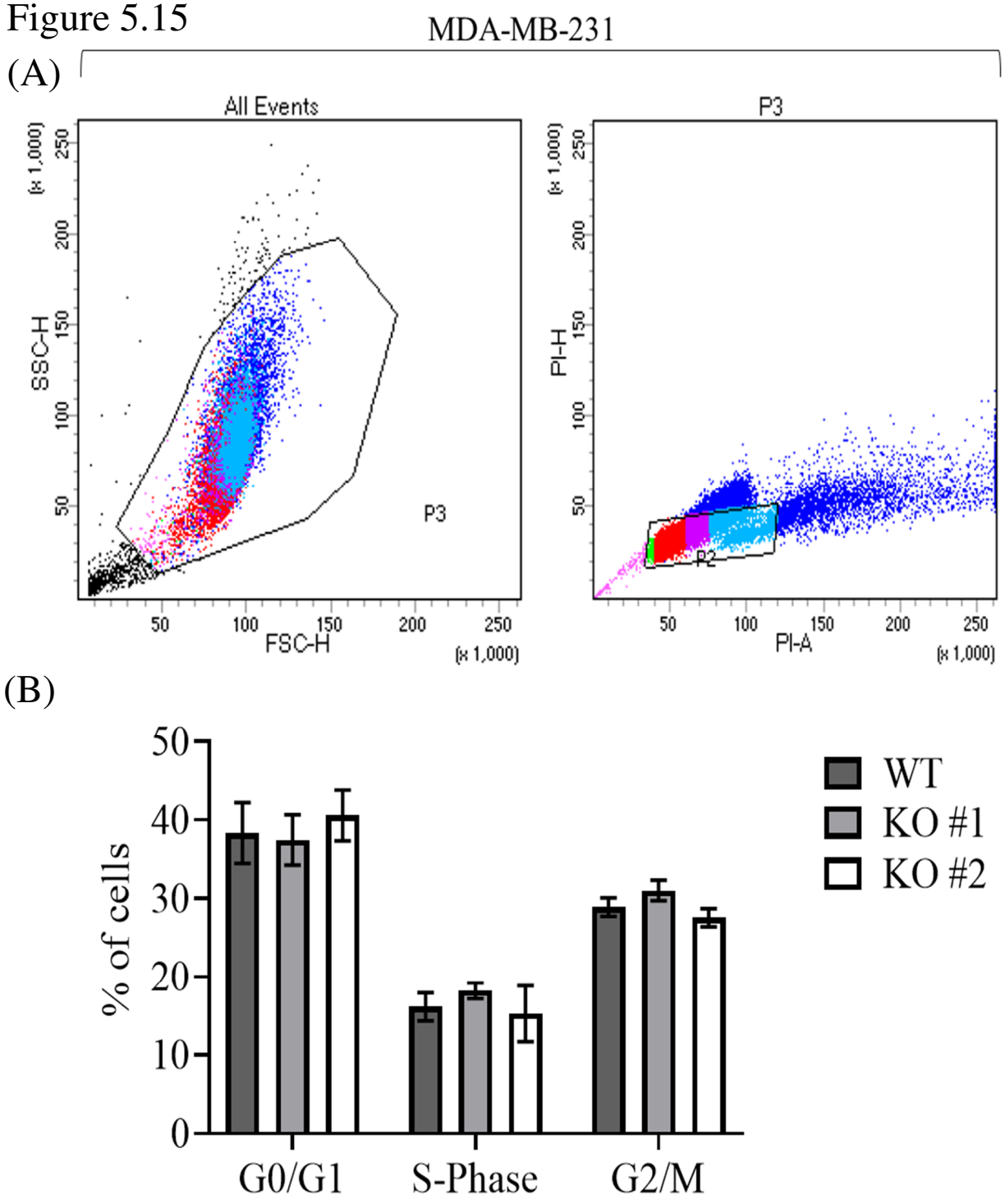


Figure 5.15: Knocking out eEF2K in MDA-MB-231 cells does not affect the cell cycle. A: An example of the gating strategy used to gate single cells for analysis. **B:** Percentages of MDA-MB-231cells in each phase of the cell cycle. Error bars represent S.D. (n=3). The p-values were calculated using Two-Way ANOVA with the Tukey multiple comparisons test.

5.2.2 eEF2K increases the accuracy of translation elongation

The results in this section complement the study by Dr. Jianling Xie from our group and others (the results were also in the published study)[128]. Please see the appendix for a copy of that published study, which used a variety of luciferase constructs to test translation fidelity as shown in **Table 1 of the study**[128]. MaxCFluc, StaCFluc and MinCFluc constructs indicate the luciferase constructs designed to have the fastest, WT and slowest decoding times (elongation rates), based on codon and tRNA frequencies in human cells. The R218S mutation indicates an arginine to serine mutation at position 218. Arg218 is a key residue for the binding of substrate to luciferase, thus correct decoding of the mutant would generate a catalytically inactive protein[308]. If this codon is incorrectly decoded as a serine, it would generate active luciferase, thus implying a lack of fidelity during translation[309]. The STOP construct indicated a mutation of a leucine at 210 to a STOP codon (TGA). This allowed the detection of read-through errors, i.e., if the STOP codon was ignored, active luciferase would be produced. The PEST motif was used to ensure the destabilisation and rapid degradation of newly synthesised luciferase, so that luciferase protein levels reflect newly made protein, rather than enzyme that already existed in the cells before treatment began. This allows for more accurate assessment of Fluc synthesis, as there is much less interference from pre-existing Fluc. In both cases (R218S and STOP), higher luciferase levels indicate greater error rates during translation.

The most important finding of this study was the eEF2K promotes translational fidelity. A549 cells were transfected with WT or mutant StaCFluc or MaxCFluc (R218S or STOP) prior to culturing them with or without 2-DG (used to increase the levels of p-eEF2). IPTG induced knockdown of eEF2K in these cells was also tested under these conditions. Looking at **Figure 1E, F** of the study[128], eEF2K knockdown did not affect the Firefly luciferase/Renilla luciferase ratio of WT transfected cells. However, eEF2K knockdown did increase the Fluc/Rluc ratio in cells transfected with the R218S or STOP mutants of both StaCFluc and MaxCFluc with or without 2-DG. It can be seen in cells treated with 2-DG that the ratio is decreased, suggesting

eEF2K is active and slowing down translation. This effect likely accounts for the enhanced fidelity of translation seen in cells where eEF2K is more active.

To re-examine these findings of the study in MDA-MB-231 KO cells, I transfected both eEF2K-KO clones with the StaCFluc R218S vectors. Following this, some plates of cells were treated with 2-DG (**Figure 5.16, Figure S5A-C in the published study[128]**). As expected, treatment of WT with 2-DG decreased protein synthesis while treatment of eEF2K-KO cells with 2-DG increased it. This further confirms that eEF2K modulates translation fidelity.

Treatment with AZD8055 or rapamycin to inhibit mTORC1 activity in A549 or MEF cells showed expected reduction of Fluc/Rluc ratio in cells transfected with the R218S or STOP vectors, further showing that mTORC1 likely increases global protein synthesis but also decreases fidelity. As expected, knockdown of eEF2K in combination with the mTOR inhibitors significantly increased Fluc/Rluc ratio compared to WT cells. This shows that mTORC1 modulates translational error rates at least partially via eEF2K (**Figure 2 in the published study[128]**).

It was also tested whether eEF2K was able to maintain the accuracy of translation in stress conditions such as low pH, DPBS or hypoxia where eEF2K is activated (**Figure 2 in the published study[128]**). Incubation of cells in DPBS modestly decreased the levels of active Fluc from the StaCFluc vector, while hypoxic conditions greatly decreased Fluc levels. In each of the conditions, it was shown that a lack of eEF2K led to an increase in mistranslated Fluc, further confirming eEF2K as a general modulator of translation fidelity under stressed conditions. Furthermore, it was shown that eEF2K knockdown A549 cells had a higher proportion of translationally inactive monosomes, with a decrease in translationally-active polysomes, according to sucrose density gradients (**Figure 3 in the published study[128]**).

Figure 5.16

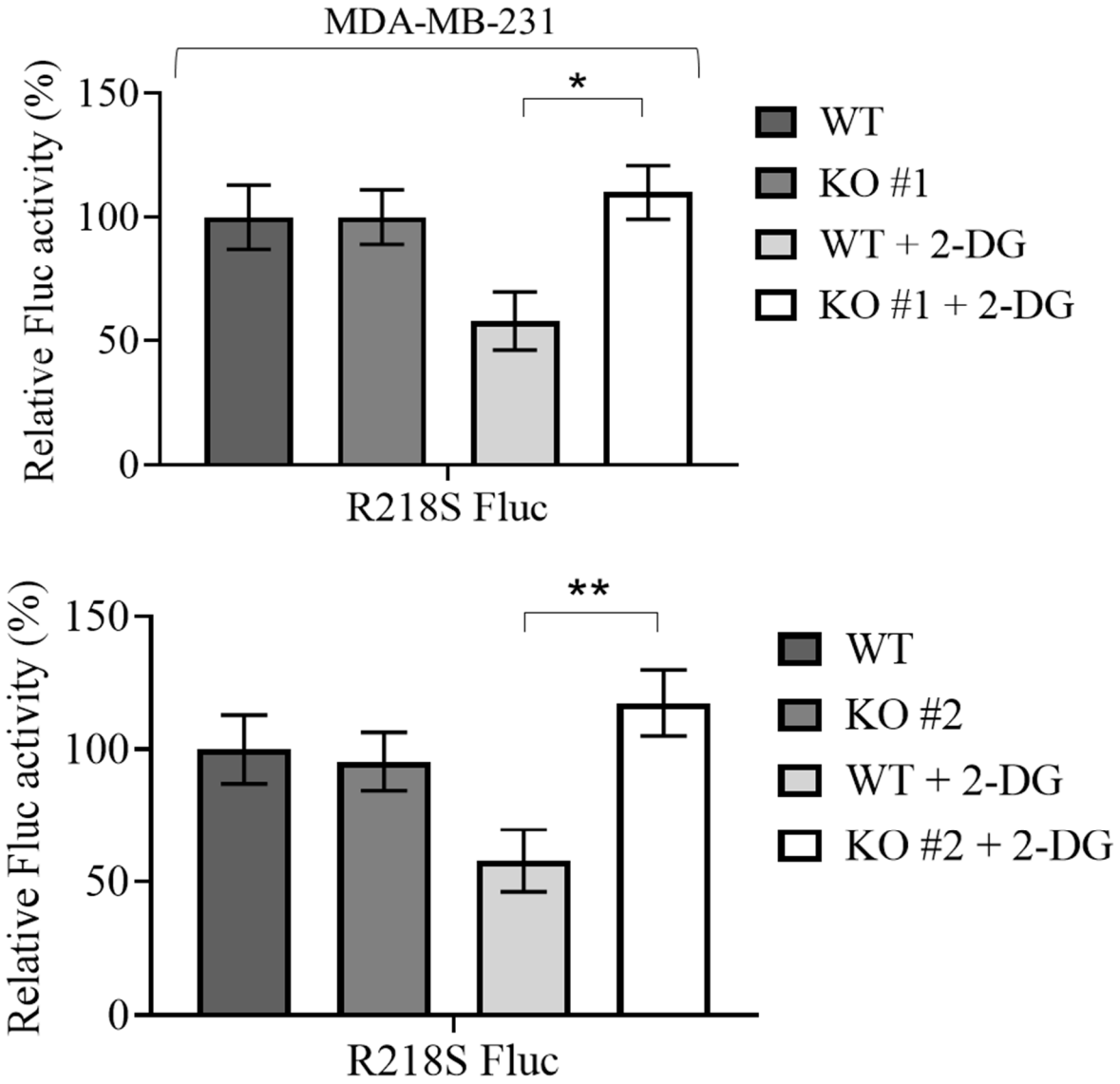


Figure 5.16: eEF2K positively regulates translation fidelity. MDA-MB-231 WT and eEF2K-KO cells were transfected with the StaCFluc R218S constructs for 24 h. Cells were then cultured in low glucose (5.5 mM) medium for 1 h prior to treatment with 10 mM 2-DG for 24 h. Fluc activity was measured via luciferase assay and normalised to non-treated control. Error bars represent S.D. (n=5). The p-values were calculated using Two-Way ANOVA with the Tukey multiple comparisons test. P-values: *≤0.05; **≤0.01.

As AMPK is an activator of eEF2K[47], it was tested whether AMPK is involved in modulating translation fidelity. AMPK-null MEFS exhibited lower overall eEF2K levels, as well as lower eEF2 phosphorylation in 2-DG conditions. AMPK-null MEFs also exhibit higher Fluc/Rluc ratios than WT when using the R218S and STOP StaCFluc constructs, but not the WT construct (**Figure 4 in the published study**[128]). This indicates that AMPK helps ensure translational accuracy under stress conditions. It was also shown that partial silencing of eEF2 (another way of reducing its activity) led to reduced luciferase activity for the R218S and STOP constructs, confirming that the AMPK-eEF2K-eEF2 pathway is important for maintaining translational accuracy.

It was reported by Chu *et al*.[310] that, in yeast, when rare codons are positioned after the start codon, slow translation elongation can restrict the 40S subunit's liberation and the positioning of the next 40S subunit. Thus, elongation is able to affect the initiation process. As eEF2K regulates the rate of elongation, it was asked whether eEF2K can also affect the start-site selection in mammalian cells. Previously developed dual luciferase reporters with non-AUG start codons (GUG or CUG) and non-optimal Kozak sequences were used for this[311]. These 'inferior' reporters produced 7.7% and 17.3% of luciferase activity compared to the WT (AUG start codon) construct in A549 cells. 2-DG was used to increase eEF2 phosphorylation, which in turn reduced Fluc levels. Knocking down eEF2K caused a significant increase in expression of Fluc from the constructs with GUG and CUG start codons but did not significantly alter Fluc expression in cells with the WT AUG start codon construct (**Figure 5 in the published study**[128]). From this, it could be inferred that increased eEF2 phosphorylation also increases the fidelity of the start site recognition by helping the ribosome to distinguish between AUG or non-AUG start codons, perhaps through slowing down protein synthesis (restricting the release and positioning of the ribosomal subunits), thus allowing the ribosome to select the correct start codon during initiation.

It was then tested whether eEF2K affects 'chaperoning' of proteins or their degradation via the proteasome, as a downregulation of these processes could contribute to increased Fluc levels when eEF2K is knocked down. A refolding assay was used to test whether chaperoning was affected by eEF2K knockdown. Denatured luciferase was added to A549 cells which could then use chaperones to refold the protein to form active luciferase. The cells were treated with 2-DG, AZD8055 or in low pH (6.7) medium to increase p-eEF2. It was found that eEF2K knockdown cells had slightly lower refolding capability than cells with normal levels of eEF2K, which suggests higher levels of misfolded proteins present in these cells due to decreased translation fidelity (**Figure S5K-S5N in the published study[128]**). This means that the increase Fluc levels in eEF2K knockdown cells in R218S or STOP construct transfected cells cannot be explained by decreased chaperone activity and protein folding. To determine whether differing levels of eEF2K affect the proteosome, A549 or HCT116 cells were treated with MG-132 (a proteasome inhibitor). Increasing MG-132 concentrations led to higher levels of p-eEF2, as well as an increase in polyubiquitinated proteins. Knocking down eEF2K did not lead to any changes in polyubiquitinated proteins or expressed WT StaCFluc (**Figure S6A-C in the published study[128]**). Using an assay to measure the 'trypsin-like' activity of the proteasomes, it was found that 2-DG treatment decreased this activity while DPBS increased it. However, in all of the conditions tested, eEF2K knockdown did not lead to further changes in proteasome activity, meaning any change in Fluc ratios were not due to changes in proteasome activity (**Figure S6D-G in the published study[128]**).

Looking to test whether eEF2K affects lifespan, *C.elegans* was used as it is a short-lived organism, widely used in such studies. *C.elegans* has an eEF2K ortholog, *efk-1*. Caloric restriction diet alone extended the lifespan of WT (N2) worms. Knocking out *efk-1* resulted in only a small reduction in lifespan on a normal diet, however caloric restriction did not lead to an increase in lifespan of these worms (**Figure 6B in the published study[128]**). This indicates that eEF2K is necessary for extending the lifespan of these worms on a caloric restriction diet. Interestingly, knocking down the aminoacyl tRNA synthetases *lrs-1*, *kars-1*, *nrs-1* did not lead

to a change in lifespan. However, knocking down *mrs-1* further reduced the lifespan of *efk1*-KO worms, perhaps because this tRNA is necessary for initiation as well as elongation, unlike the others which are only necessary for elongation (**Figure 6C in the published study[128]**).

Overall, this study showed that eEF2K positively correlates with translational accuracy in MDA-MB-231, A549 and HCT116 cells, and extends the lifespan of nematodes.

5.2.3 eEF2K activity is increased in hypoxic conditions in MDA-MB-231, A549 and HCT116 cells

To test more biologically relevant hypoxic conditions than the 0.1% O_2 used in the Moore *et al.*[78] study, oxygen concentrations ranging from 8.5% to 0.1% O_2 were employed here[312]. The effects of glucose and pyruvate deprivation were also investigated under these conditions. MDA-MB-231, A549 and HCT116 cells in ±Glc medium were put into a sealed hypoxic chamber and treated for 16 h with 8.5, 5, 1.5, 1 or 0.1% O_2 at 37°C. Normoxic controls at approximately 21% O_2 were used as a comparison (**Figure 5.17**). Interestingly, p-eEF2 did not change at any of the oxygen concentrations in +Glc conditions for MDA-MB-231 cells, while there was a clear increase in A549 cells at 5% O_2. HCT116 cells showed that as the oxygen concentration decreased from 5%, p-eEF2 decreased with it. In -Glc conditions, hypoxia clearly increased p-eEF2 in MDA-MB-231 cells at 8.5% O_2 which peaked at 5% O_2. It then decreased at lower oxygen concentrations until it became undetectable. A549 cells also showed increases in p-eEF2 at 8.5% and 5% O_2 concentrations compared to its normoxic controls, as well as an increase at 0.1% O_2. The increase in p-eEF2 in +Glc conditions at 0.1% O_2 was not observed in A549 cells, unlike in the Moore *et al.*[78] study. However, the data are from cells treated for 16 h, rather than the 8 h used in that paper. HCT116 cells also exhibited an increase in p-eEF2 at 5% O_2 compared to the normoxic control, with p-eEF2 gradually decreasing at lower O_2 concentrations. These data suggest that eEF2K might be most active at 8.5 and 5% O_2

concentrations in these cells, specifically MDA-MB-231 cells, when glucose is also lacking. However, it cannot be ruled out that eEF2K activity is increased at oxygen concentrations less than 5% at earlier time points prior to decreasing (e.g., due to degradation of the activated eEF2K).

Figure 5.17

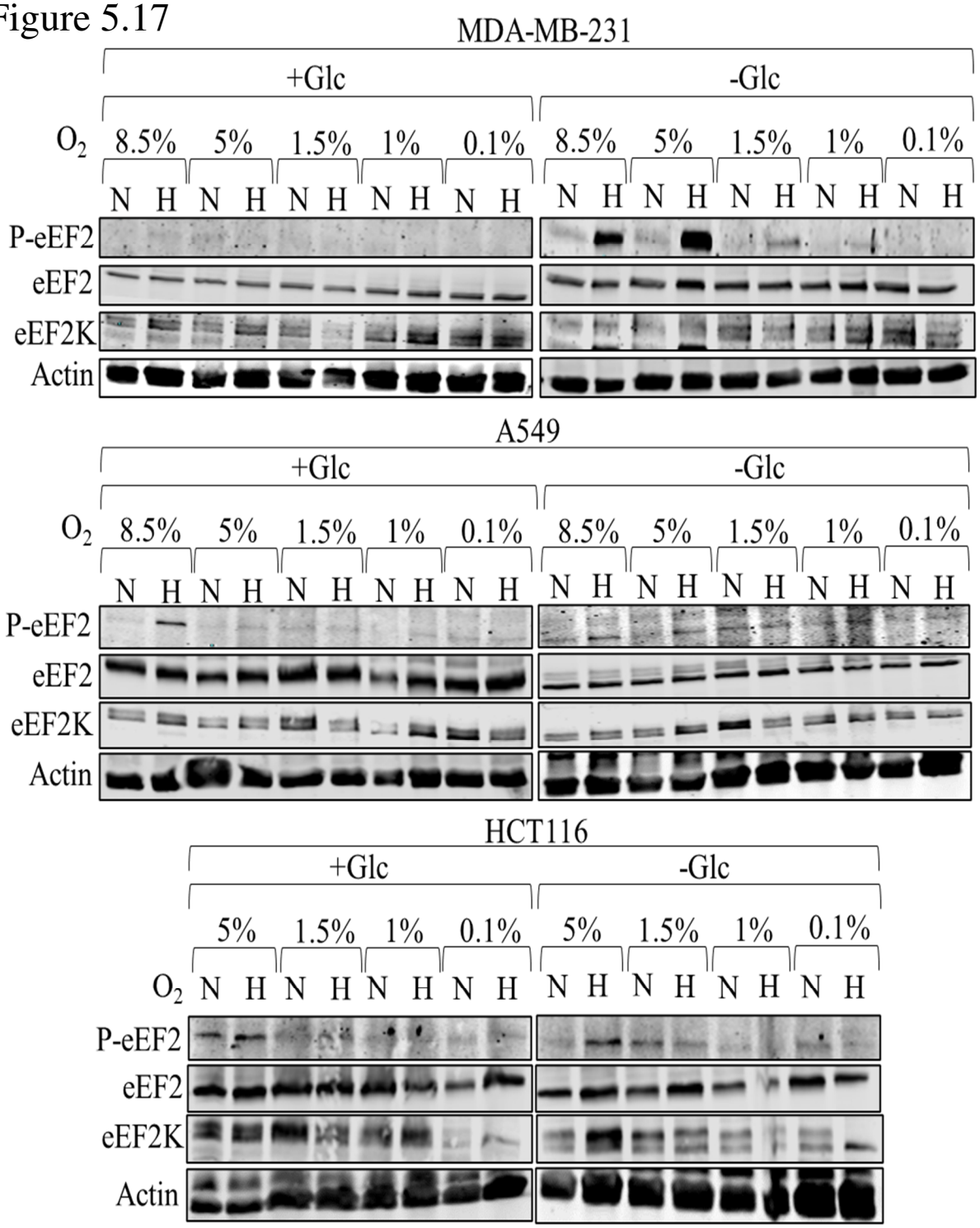


Figure 5.17: eEF2K activity is increased under hypoxic conditions in MDA-MB-231, A549 and HCT116 cells. MDA-MB-231, A549 or HCT116 cells were treated for 16 h in either normoxic (21% O_2) or hypoxic (ranging from 8.5% to 0.1% O_2) conditions at 37 °C. Hypoxic cells were lysed inside the hypoxic chamber while normoxic cells were lysed outside of it. The lysates were then run on (12.5%) SDS-PAGE, followed by analysis via immunoblotting. Images are representative of n=3. N: Normoxia; H: Hypoxia.

5.2.4 Inhibition or knock-out/knock-down of eEF2K does not affect Nrf2 levels in MDA-MsB-231 and A549 cells

To check whether the findings in the study by Jan *et al.*[292] in 2016 worked in MDA-MB-231 and A549 cells, I investigated the Nrf2 levels of these cells after treatment with JAN384 or when eEF2K was knocked down by shRNA or knocked out by CRISPR. The cells were 'stressed' with H_2O_2 or 2-DG to activate eEF2K, while MG132 was used as a control to activate Nrf2 (it is known that cells upregulate Nrf2 to increase proteosome subunit gene expression to compensate for proteosomeal inhibiton by MG132)[313, 314]. **Figure 5.18** shows MDA-MB-231 and A549 cells treated for 6 h with a combination of H_2O_2, 2-DG, MG-132 and IPTG (to induce eEF2K knockdown). Phosphorylation of eIF2α at Ser51 was used as a positive control to confirm the H_2O_2 had caused oxidative stress on the cells. The phosphorylation of eIF2α on Ser51 increases as a response to oxidative stress, helping cells to resist this stress[315]. As expected, p-eIF2α increased in cells treated with H_2O_2. eEF2 phosphorylation was also increased in cells treated with 2-DG and H_2O_2. However, the only significant change to Nrf2 levels occurred when cells were treated with MG-132, showing that eEF2K inhibition with JAN384 or its knock-down did not influence Nrf2 protein levels at this time point.

Once eEF2K-KO MDA-MB-231 cells had been made, I was able to confirm the results obtained with the inhibitor and the knockdown. eEF2K-WT and KO cells were treated with MG132 and H_2O_2 to use as a control for detection of Nrf2 and to activate eEF2K, respectively. These treatments were done for 16 h to allow for Nrf2 build up in the nucleus. **Figure 5.19** shows no significant change in the WT cells stressed with DPBS, 2-DG or H_2O_2. eEF2K-KO cells did not have significantly altered levels of Nrf2 compared to WT cells. It appeared that Nrf2 was slightly lower in the KO cells treated with H_2O_2 or MG132, but it was not a significant change. To conclude, Nrf2 levels did not increase in MDA-MB-231 and A549 cells in which eeF2K was inhibited or knockout/down. This suggests eEF2K does not specifically regulate Nrf2 in these cells as it has been reported to do in N2A neuroblastoma cells[292].

Figure 5.18

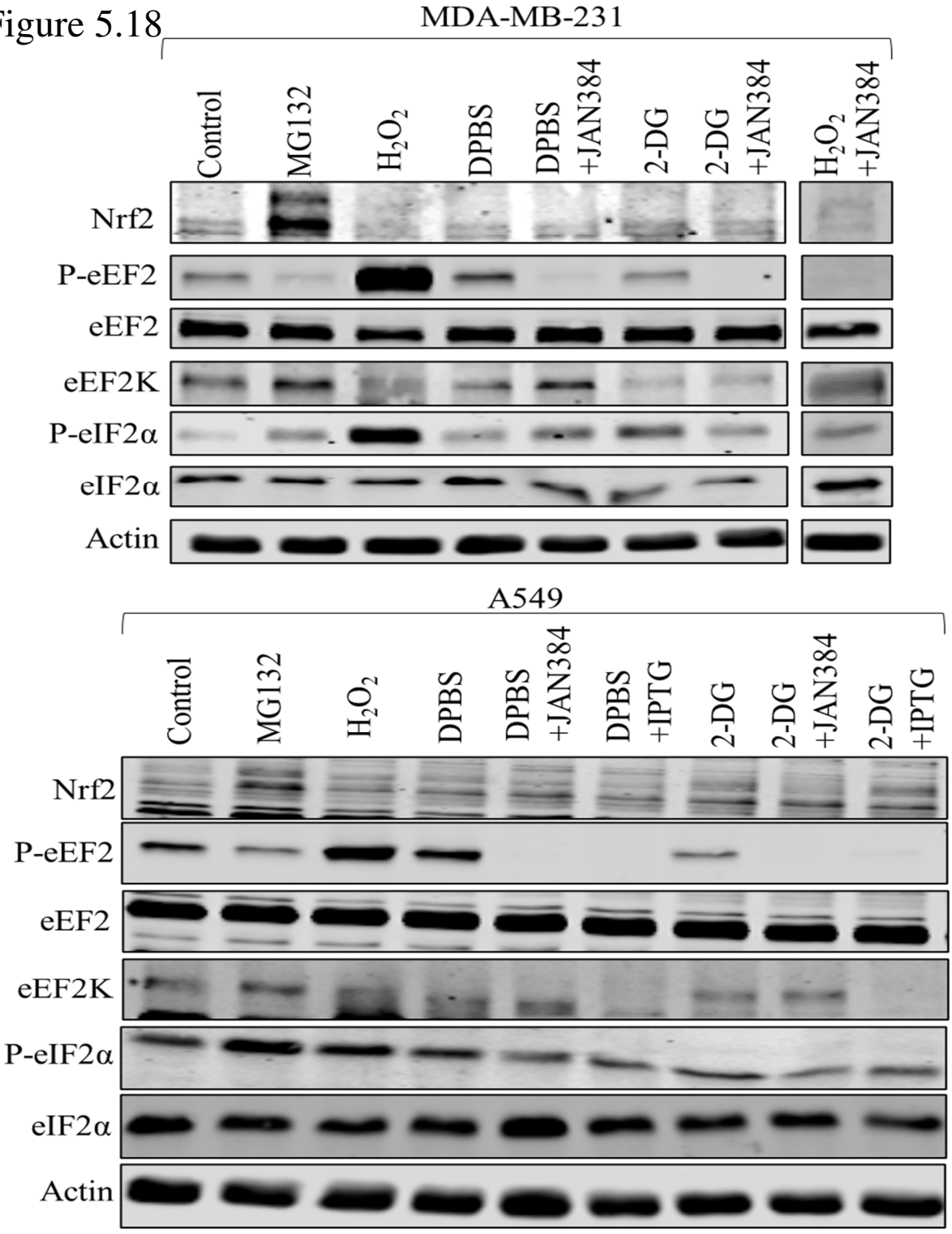


Figure 5.18: Inhibition or knockdown of eEF2K does not alter Nrf2 levels in MDA-MB-231 or A549 cells. MDA-MB-231 or A549 cells were treated for 6 h with the listed combination of the following compounds: 25 μM MG132, 3 mM H_2O_2, 5 μM JAN384, 10 mM 2-DG. Prior to 2-DG treatment, cells were left in 5.5 mM D-Glucose medium for 1 h. A549 cells were pre-treated with 1 mM IPTG for 5 days to induce eEF2K shRNA. After treatment, the cells were lysed in high-salt lysis buffer to extract nuclear proteins. The lysates were then run on (12.5%) SDS-PAGE, followed by analysis via immunoblotting. Images are representative of n=3.

Figure 5.19

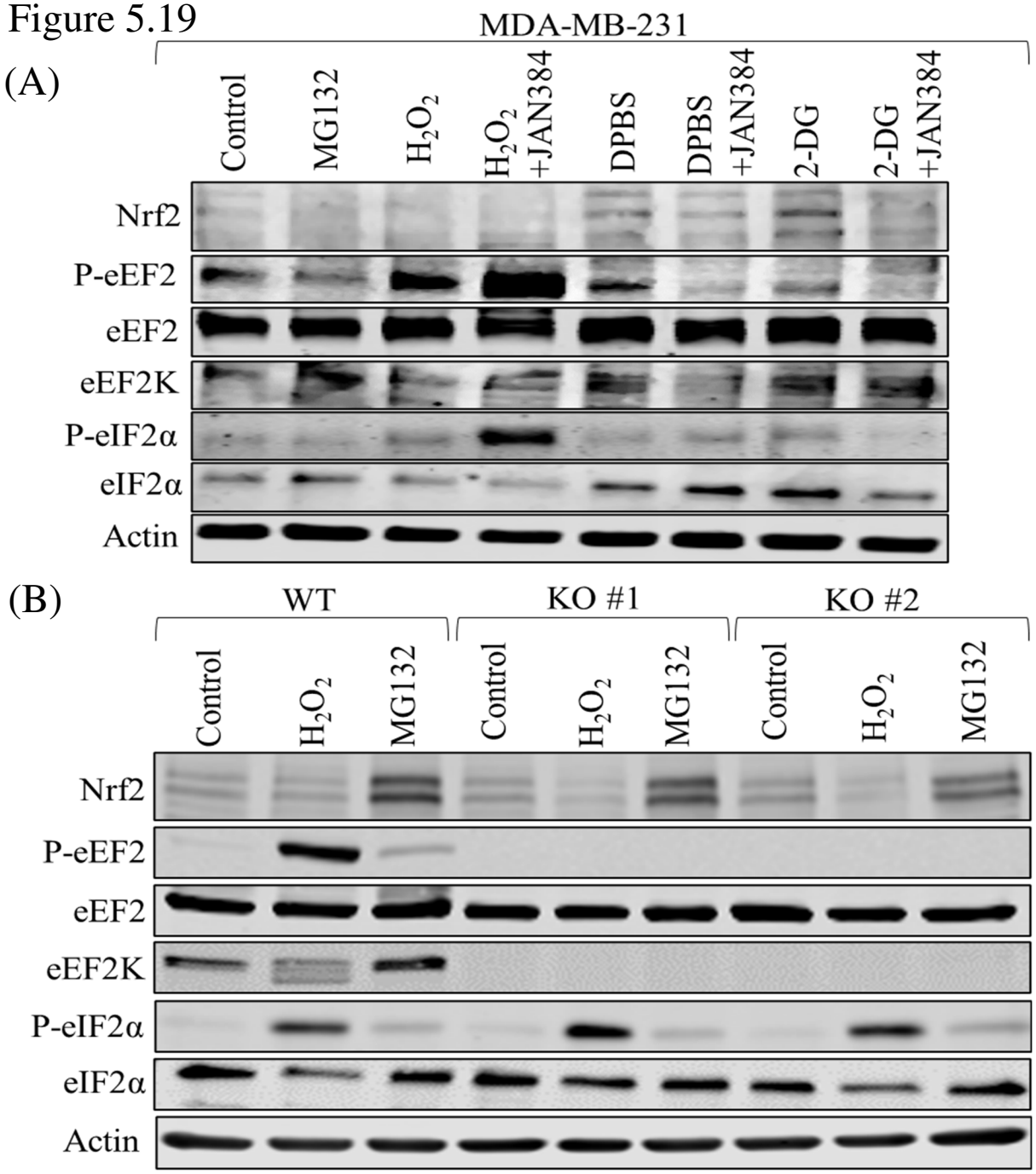


Figure 5.19: Inhibition or knocking out of eEF2K does not alter Nrf2 levels in MDA-MB-231 cells. A: MDA-MB-231 WT cells were treated for 16 h with the listed combination of the following compounds: 25 μM MG132, 3 mM H_2O_2, 5 μM JAN384, 10 mM 2-DG. Prior to 2-DG treatment, cells were left in 5.5 mM D-Glucose medium for 1 h. **B:** eEF2K-WT and KO cells were treated with either 3 mM H_2O_2 or 25 μM MG132 for 16 h. After treatment, the cells were lysed in high-salt lysis buffer to extract nuclear proteins. The lysates were then run on (12.5%) SDS-PAGE, followed by analysis via immunoblotting. Images are representative of n=3.

5.2.5 eEF2K promotes PD-L1 expression and assists cancer cells to escape immune surveillance

This part of the chapter discusses the results from the recently study to which I contributed by Mr. Yu Wu working closely with Dr. Jianling Xie and others from our group, including myself[188].

It has been shown that IFNγ induces PD-L1 expression in some types of cancer cells, such as ovarian and glioma cell lines[298, 316-318]. Indeed, treatment with IFNγ increased PD-L1 levels in human prostate cancer PC3 cells (**Figure 1A, B in the published study**[188]). In the same experiment, it can also be seen that eEF2-KO PC3 cells had far lower PD-L1 protein levels than eEF2K-WT cells. IFNγ treatment of eEF2K-KO cells did not significantly increase PD-L1 levels. This suggests that eEF2K promotes the expression of PD-L1 in PC3 cells. It was also important to investigate the amount of PD-L1 expressed on the cell surface, to which PD-1 on T lymphocytes binds. This was assessed by FACS analysis, which showed similar results to the western blot. PD-L1 was markedly decreased in eEF2K-KO cells with or without IFNγ treatment (**Figure 1C, D in the published study**[188]**, 5.20A**). Interestingly, I found that if H_2O_2 was used to stress cells (and activate eEF2K[59]), PD-L1 levels increased in both WT and KO cells. An increase in surface PD-L1 was also evident in eEF2K-KO cells treated with IFNγ. This is in line with a recent study by Dr. Tiara Bunga Mayang Permata *et al*.[319] that showed H_2O_2 increased PD-L1 levels in U2OS, H1299 and MCF7 cells. That study suggested that PD-L1 can be regulated by DNA damage through oxidative stress. Importantly, **Figures 1E and F in the published study**[188] showed that overexpressing WT eEF2K but not the kinase dead (K170M) version increased PD-L1 expression in A549 and PC3 cells, indicating that eEF2K is necessary for PD-L1 expression in these cells.

A549 and MDA-MB-231 cells were tested under conditions where eEF2K is active – no serum, no glucose, acidosis, H_2O_2 or rapamycin treatment (inhibition of mTORC) were used. It was

found that PD-L1 levels were higher in A549 cells treated with H_2O_2 or during acidosis. Conversely, A549 eEF2K knockdown cells tended to have lower PD-L1 protein levels with significantly lowers levels in cells treated with H_2O_2 or in acidosis than in the corresponding controls (**Figure S2A, B in the published study[188]**). Similarly, PD-L1 levels were reduced in MDA-MB-231 eEF2K-KO cells upon treatments with rapamycin, H_2O_2 or acidosis (**Figure S2C, D in the published study[188]**). Conversely, overexpressing FLAG-tagged eEF2K in A549 cells, increased protein expression of PD-L1 (**Figure 1F in the published study[188])**. However, under the same conditions no significant differences in levels of *PD-L1* mRNA were observed in the knock-out or knockdown MDA-MB-231 and A549 cells, respectively (**Figure S2F in the published study[188], Figure 5.21 in the thesis**).

Separating lysates from IFNγ-treated eEF2K-WT and KO PC3 cells on a sucrose gradient showed no difference in the proportion of ribosomes in polysomes (**Figure 2A, B in the published study[188]**). β_2-microglobulin control mRNA's distribution was also not significantly altered (**Figure 2E, F in the published study[188]**). However, it was found that 30% less of PD-L1 mRNA was associated with active polysomes in eEF2K-KO cells (**Figure 2C, D in the published study[188]**), with significantly more of the mRNA associated with non-polysomal fractions. Interestingly, while knocking down eEF2K in A549 cells did not affect the amount of ribosomes in polysomes, it did show that there was almost no *PD-L1* mRNA associated with polysomes in the knockdown cells (**Figure 3S in the published study[188]**). This suggests that eEF2K promotes the association of *PD-L1* mRNA with active polysomes in both A549 and PC3 cells to increase its protein level, further supporting the western blot data.

Figure 5.20

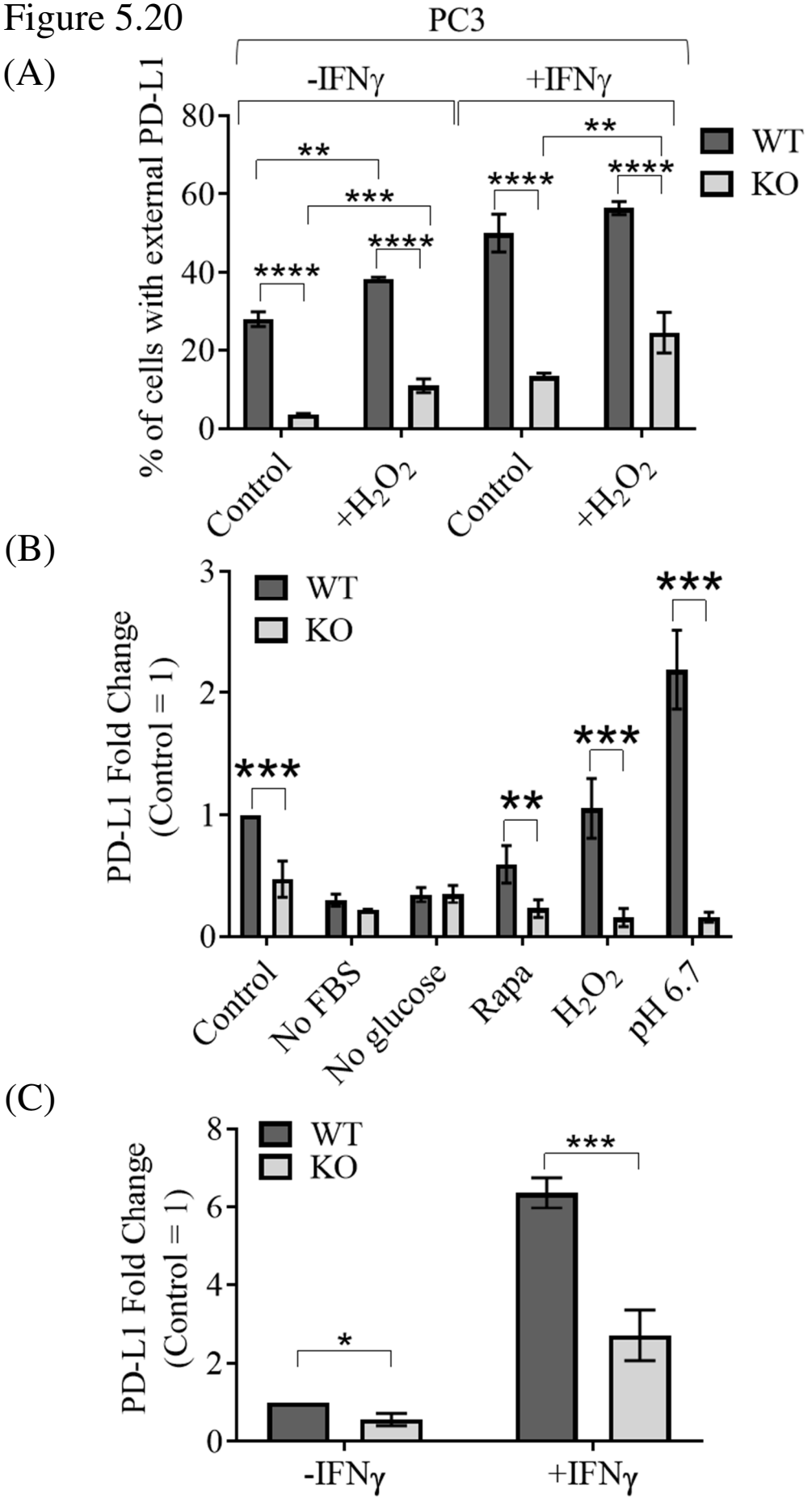
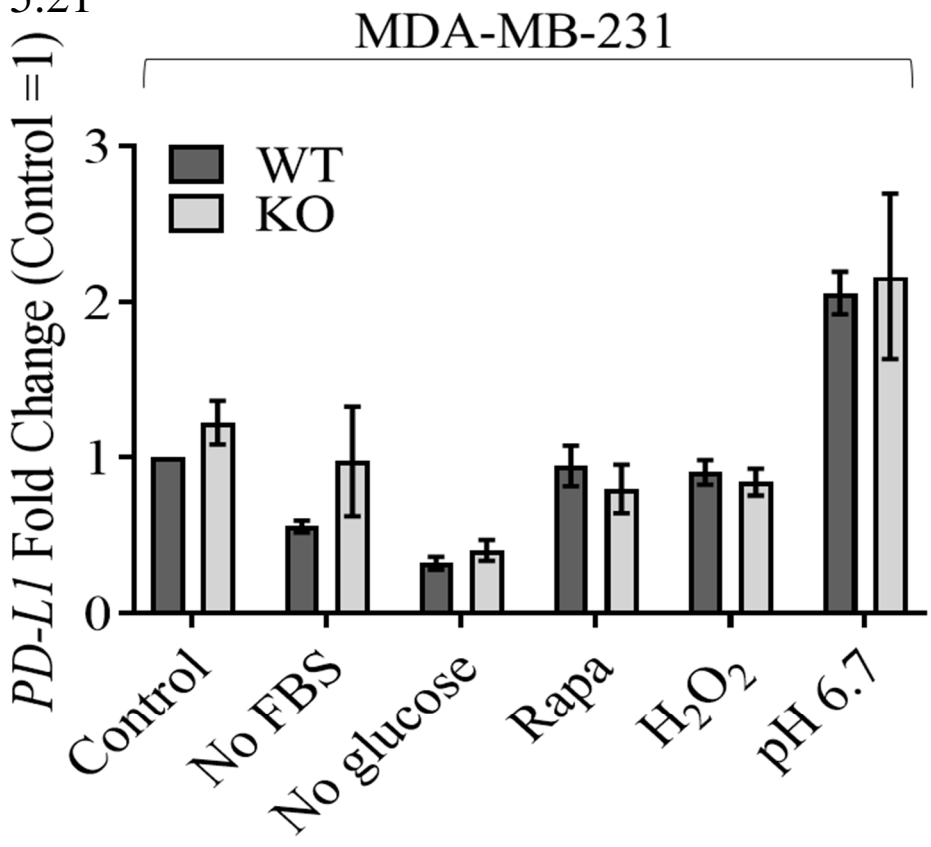

(A)
PC3
-IFNγ
+IFNγ
% of cells with external PD-L1
80
60
40
20
0
**
***
****
****
**
****
WT
KO
Control
+H2O2
Control
+H2O2
(B)
PD-L1 Fold Change
(Control = 1)
3
2
1
0
WT
KO
***
**
***
***
Control
No FBS
No glucose
Rapa
H2O2
pH 6.7
(C)
PD-L1 Fold Change
(Control = 1)
8
6
4
2
0
WT
KO
*
***
-IFNγ
+IFNγ

Figure 5.20: Knocking out eEF2K decreases PD-L1 protein and mRNA levels in PC3 cells. **A:** PC3 eEF2K WT and KO cells were treated with or without 20 ng/mL IFNγ and with or without 3 mM H_2O_2 for 24 h. Cells were then trypsinized, stained with PD-L1 antibody and subjected to flow cytometry to analyse surface level PD-L1. **B:** PC3 eEF2K WT and KO cells were treated in in growth medium (control), or in medium without serum (no FBS) or in medium with glucose, or in growth medium in the presence of 200 nM rapamycin or 3 mM H_2O_2, or medium at pH of 6.7 for 24 h. **C:** PC3 eEF2K WT and KO cells were treated with or without 20 ng/mL IFNγ for 24 h. Cells from **B and C** had their RNA extracted, followed by cDNA synthesis and RT-qPCR. Error bars represent S.D. (n=3). The p-values were calculated using Two-Way ANOVA with the Tukey multiple comparisons test. P-values: *≤0.05; **≤0.01; ***≤0.001 ****≤0.0001.

Figure 5.21

(A)



(B)

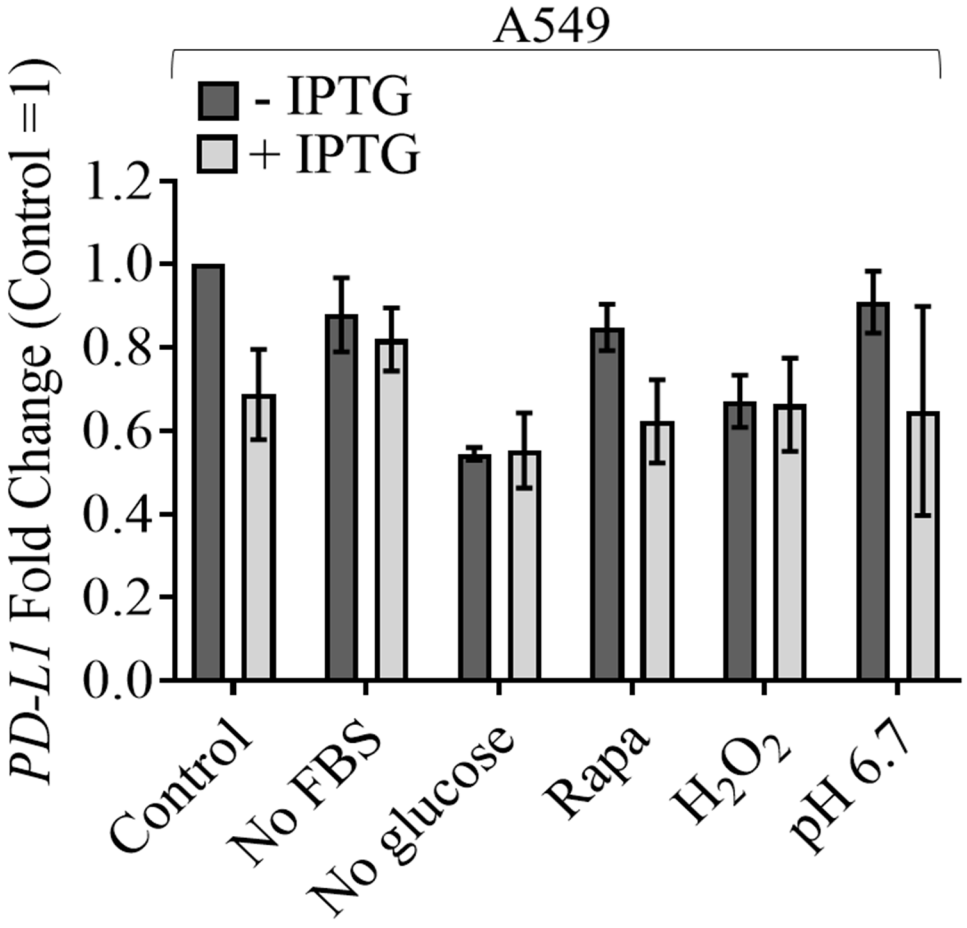


Figure 5.21: Knockdown or knock-out of eEF2K in A549 and MDA-MB-231 cells respectively does not change *PD-L1* mRNA level. A, B: MDA-MB-231 eEF2K-WT and KO cells or A549 cells respectively were treated in growth medium (control), or in medium without serum (no FBS) or in medium with glucose, or in growth medium in the presence of 200 nM rapamycin or 3 mM H_2O_2, or medium at pH of 6.7 for 24 h. A549 cells were pre-treated with 1 mM IPTG for 5 days prior to the experiment for eEF2K knockdown. RNA was then extracted from the cells, followed by cDNA synthesis and RT-qPCR to assess the levels of *PD-L1* mRNA. Error bars represent S.D. (n=5). The p-values were calculated using Two-Way ANOVA with the Tukey multiple comparisons test.

It was noted that PC3 cells had lower *PD-L1* mRNA levels in basal, acidosis, rapamycin or H_2O_2 treated conditions or following IFNγ treatment (**Figure 3A, B in the published study[188], Figure 5.20B, C in the thesis**). To assess the half-life of the *PD-L1* mRNA this parameter was measured, using actinomycin D to block new mRNA transcription. The *PD-L1* mRNA level decreased faster in eEF2K-KO PC3 cells, suggesting it is less stable when cells lack eEF2K and this mRNA is translated less efficiently (**Figure 3C, D in the published study[188]**). The overall PD-L1 protein levels were lower in PC3 eEF2K-KO cells compared to WT due to a combination of lower mRNA levels and weaker translation of the mRNAs that are available.

The control of specific mRNAs is often regulated through their 5'-untranslated region (5'-UTR)[320]. Upstream open reading frames (uORFs) can repress the expression of the protein encoded by the main open reading frame (ORF) through the regulating the downstream reinitiation at the start of the ORF. The human *PD-L1* mRNA has a single uORF that begins with a CUG start codon and partially overlaps the main ORF. This means that if the uORF is translated, PD-L1 expression would be repressed as the ribosomes would stop translating the uORF after the start of the main ORF. As reported in the translation fidelity study[128], eEF2K favours the selection of the canonical AUG start codon over non-canonical start codons such as CUG. Previously made "pICtest2" dual-luciferase reporters with CUG or AUG start codons were transfected into PC3 eEF2K-WT and KO cells[311]. The cells were treated with IFNγ and it was found that eEF2K-KO cells containing the vector with the CUG start codon exhibited 2-3 fold higher Fluc activity compared to WT cells transfected with the same vector (**Figure 4B in the published study[188]**). In contrast, there was no difference in Fluc levels measured from eEF2K-KO and WT cells when they were transfected with the Fluc construct with AUG as a start codon (**Figure S4A in the published study[188]**).

Next, a pICtest2 vector containing the full-length human *PD-L1* 5'-UTR was transfected into PC3 cells and it was found that following IFNγ treatment, or acidosis, H_2O_2 or glucose starvation stresses enhanced Fluc activity in WT but not eEF2K-KO cells (**Figure 4C in the**

study). WT and eEF2K-KO PC3 cells exhibited similar levels of Fluc when transfected with a construct that had the uCUG mutated to a CUC codon which is not a start codon. This confirms that the uCUG impairs the translation of the main *PD-L1* ORF. This showed that eEF2K favours slowing down translation elongation, enhancing selection of the AUG start codon and hence translation of the main *PD-L1* ORF.

To investigate the effect of eEF2K knockdown or knockout on cancer immune cell mediated death, immune killing assays were performed. A549 and PC3 were infected with sh-NC (lentiviral non-targeting control) or sh-eEF2K, followed by transfection with either empty vector (E.V) or FLAG-eEF2K-WT, followed by co-culture with NK-92 cells. The percentage of cancer cell survival was determined by normalising the number of surviving cells with NK cells by the total remaining cells without NK cells. The PD-1/PD-L1 inhibitor 3 was used as a positive control for this assay[321]. A549 and PC3 cells, which express lower PD-L1 levels due to ablation of eEF2K, were more susceptible to NK-92 immune cell killing compared to cells expressing sh-NC (**Figure 5A, 5S in the published study**[188]). Conversely, overexpressing eEF2K by transfecting cells with a vector encoding FLAG-eEF2K alleviated the cell death-inducing effects of NK-92 cells towards both A549 and PC3 cells (**Figure 5B, 5S in the published study**[188]). The levels of granzyme B, IFNγ and perforin (markers of NK-92 cell activity)[322] in the medium was also lower for PC3 cells transfected with FLAG-eEF2K, while being significantly higher in medium with cells that had ablated eEF2K (**Figure 5C-E in the published study**[188]).

Additionally, gene expression profiles from TCGA and Grasso databases showed that *eEF2K* and *CD-274* (*PD-L1*) expression levels correlate positively in tumour samples from prostate cancer patients[323, 324] (**Figure 6A, B in the published study**[188]). High levels of eEF2K expression correlated with lower survival rates for patients with prostate cancer while high levels of PD-L1 expression correlated with lower survival rates for patients with lung cancer (**Figure 6C, D in the published study**[188]).

Overall, this study showed that eEF2K positively regulates PD-L1 expression which allows prostate and lung cancer cells to escape immune mediated killing.

5.2.6 eEF2K does not affect glucose uptake but may regulate IRS-1 levels

eEF2 is currently the only known substrate for eEF2K. Unpublished screens for another substrate of eEF2K did not reveal any new targets. A study by Lazarus *et al*.[228] identified potential eEF2K substrates such as NDRG1 (Protein NDRG1). However, experiments performed by Dr. Shuye Tian from our group could not confirm this. Therefore, the Lazarus *et* al.[228] data from that study should be confirmed by others prior to considering the proteins identified in it as genuine eEF2K substrates. Considering eEF2K plays such a key role in regulating translation elongation, it is important to find out whether it can directly phosphorylate proteins other than eEF2, as well the changes in protein levels that occur from a lack of eEF2K in cells. To that end, a proteomics and phosphoproteomics study was conducted by our group in collaboration with Dr. Antigoni Manousopoulou from Dr. Spiros D. Garbis' group (then at the University of Southampton, UK).

The study used the isobaric tag for relative and absolute quantitation (iTRAQ) method to identify possible new phospho-targets of eEF2K, as well as to detect steady-state protein levels. First of all, it was important to ensure that eEF2K was active in WT cells for a good comparison against eEF2K-KO cells. To that end, I incubated cells in low glucose DMEM (5.55mM) for 1 h, prior to treatment with 2-DG for 1 h. Treatment with 2-DG quickly stimulated eEF2K, as evident by the increased p-eEF2 levels compared to the low glucose control (**Figure 5.22**). This condition was used to treat WT and eEF2K-KO cells, prior to cell lysis and iTRAQ labelling. This was followed by enrichment of the proteins and mass-spectrometry on an Orbitrap Elite (Thermo Scientific) instrument (**Appendix Table 6** for full steady-state protein level data set;

Appendix Table 7 for list of proteins up or down-regulated in both KO #1 and KO #2; **Appendix Table 8** for phosphorylation sites up or down-regulated in eEF2K-KO cells; **Appendix Table 9** for phosphorylation sites missing in eEF2K-KO cells compared to WT).

Figure 5.22

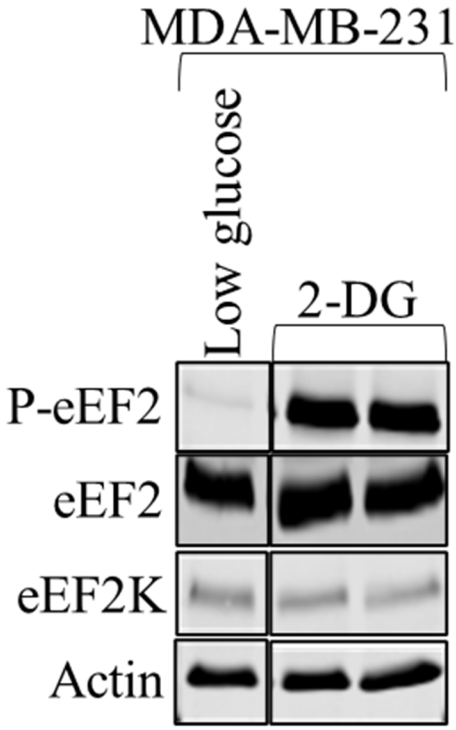


Figure 5.22: 2-DG treatment quickly stimulates eEF2K activity. MDA-MB-231 cells were treated in the following conditions - low glucose: 5.5 mM D-glucose in DMEM for 1 h. 2-DG: 1 h in low glucose DMEM, followed by 10 mM 2-DG treatment for 1 hour. After treatment, the cells were lysed and the lysates were run on (12.5%) SDS-PAGE, followed by analysis via immunoblotting. Images represent n=3. Cells were treated in duplicate for 2-DG treatment.

Interestingly, the data showed an almost doubling of Acyl CoA Synthetase Short Chain Family Member 3 (ACSS3) in the eEF2K-KO cells compared to WT (**Appendix Table 7**). This protein catalyses the synthesis of acetyl-CoA from short-chain fatty acids[325]. This suggested that eEF2K-KO cells utilised a more efficient citric acid cycle. Furthermore, the phospho-proteomics showed an increase in the phosphorylation of insulin receptor substrate 1 (IRS-1) at Ser330 (**Appendix Table 9**). There is little information about this phosphorylation site. However, unpublished data generated by Dr. Claire Moore from our group had also suggested that eEF2K may phosphorylate IRS-1. Considering IRS-1 is crucial in activating the signalling cascade which allows cells to uptake glucose, this was investigated further.

Insulin stimulates glucose uptake into cells by GLUT4, going through the IRS-1 pathway to do so[326]. To assess whether eEF2K affected MDA-MB-231 cell responses to insulin, eEF2K-WT and KO cells were starved of serum overnight and then treated with 100 nM insulin. Samples were taken at 5, 15, 30, 45- and 60-min time points for immunoblot analysis. The phosphorylation of PKB was analysed at Ser473. While Thr308 is the main activation phosphorylation site of PKB, it is difficult to detect and no signal was seen. Phosphorylation of Ser473 can be used as another indicator of PKB activation. The phosphorylation of ERK1/2 at Thr202/Tyr204 was also analysed, as it is another pathway downstream of IRS-1. Interestingly, it appeared that IRS-1 protein levels were slightly increased in KO cells compared to WT under control conditions and at 5 min after insulin treatment (**Figure 5.23**). However, there was no obvious change at the later time points. Furthermore, IRS-1 levels decreased over time in all three cell lines following prolonged insulin treatment. It has previously been shown that insulin treatment can decrease IRS-1 protein levels in 3T3-L1 adipocytes and MCF-7 cells[327, 328], through increasing its degradation, which could be a sign of cells being desensitised to insulin. Another possibility is that IRS1 translocated to the cell membrane at those time points and was lost in the cell pellet upon centrifugation of the lysate.

Figure 5.23

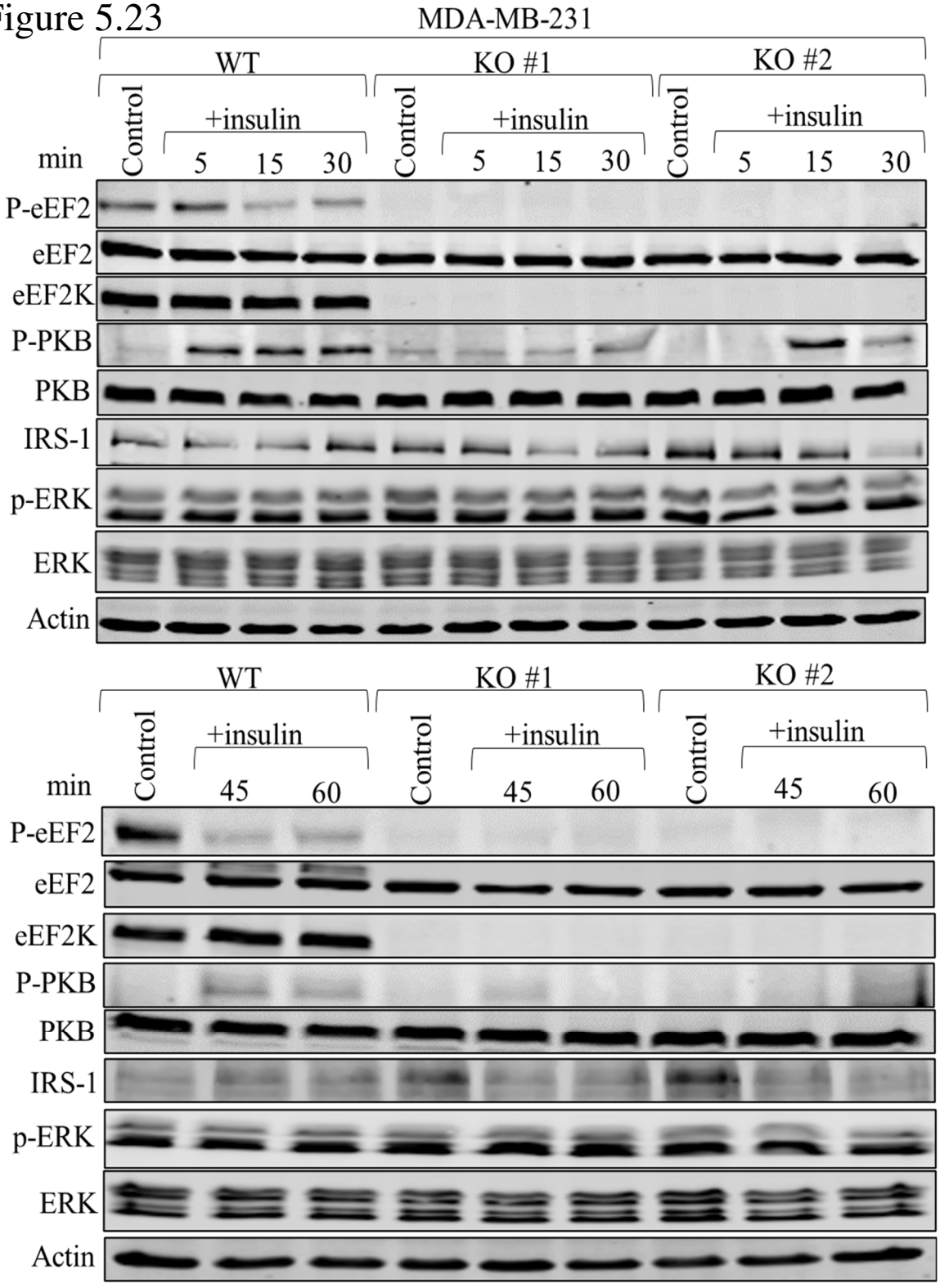


Figure 5.23: Lack of eEF2K increases IRS-1 under control conditions and early after insulin treatment. MDA-MB-231 eEF2K WT and KO cells were serum starved overnight. The cells were then treated with or without 100 nM insulin for the indicated time points (in minutes). The control sample indicates cells left in serum free medium without insulin for 60 min. After treatment, the cells were lysed and the lysates were run on (12.5%) SDS-PAGE, followed by analysis via immunoblotting. Images represent n=3.

Finally, while the phosphorylation of ERK was not affected, PKB phosphorylation at Ser743 appeared to be lower in both KO clones at most time points, which is in contrast the higher IRS-1 levels.

To further investigate this, low pH medium was used to activate eEF2K and the same pathways were probed for after insulin treatment. For this experiment, the same conditions as in the previous experiment were used, except the cells were treated in DMEM without serum that was buffered to 6.7. These low pH conditions activated eEF2K in WT cells (**Figure 5.24**). The phosphorylation of PKB was increased with insulin treatment as expected. At the early time points of 5-30 min, it appeared that p-PKB was increased in KO #1 but to a lesser extent than in KO #2 and WT cells. This suggests that these two KO clones are not identical when it comes to the IRS-1 pathway. As in the previous experiment, insulin does not affect p-ERK in these cells. IRS-1 levels appeared to be slightly higher in both KO clones under the control conditions. The IRS-1 and p-PKB data appear to conflict with each other, hence it was determined that directly measuring the glucose uptake of these cells would shine more light on any changes in the overall pathway.

Figure 5.24

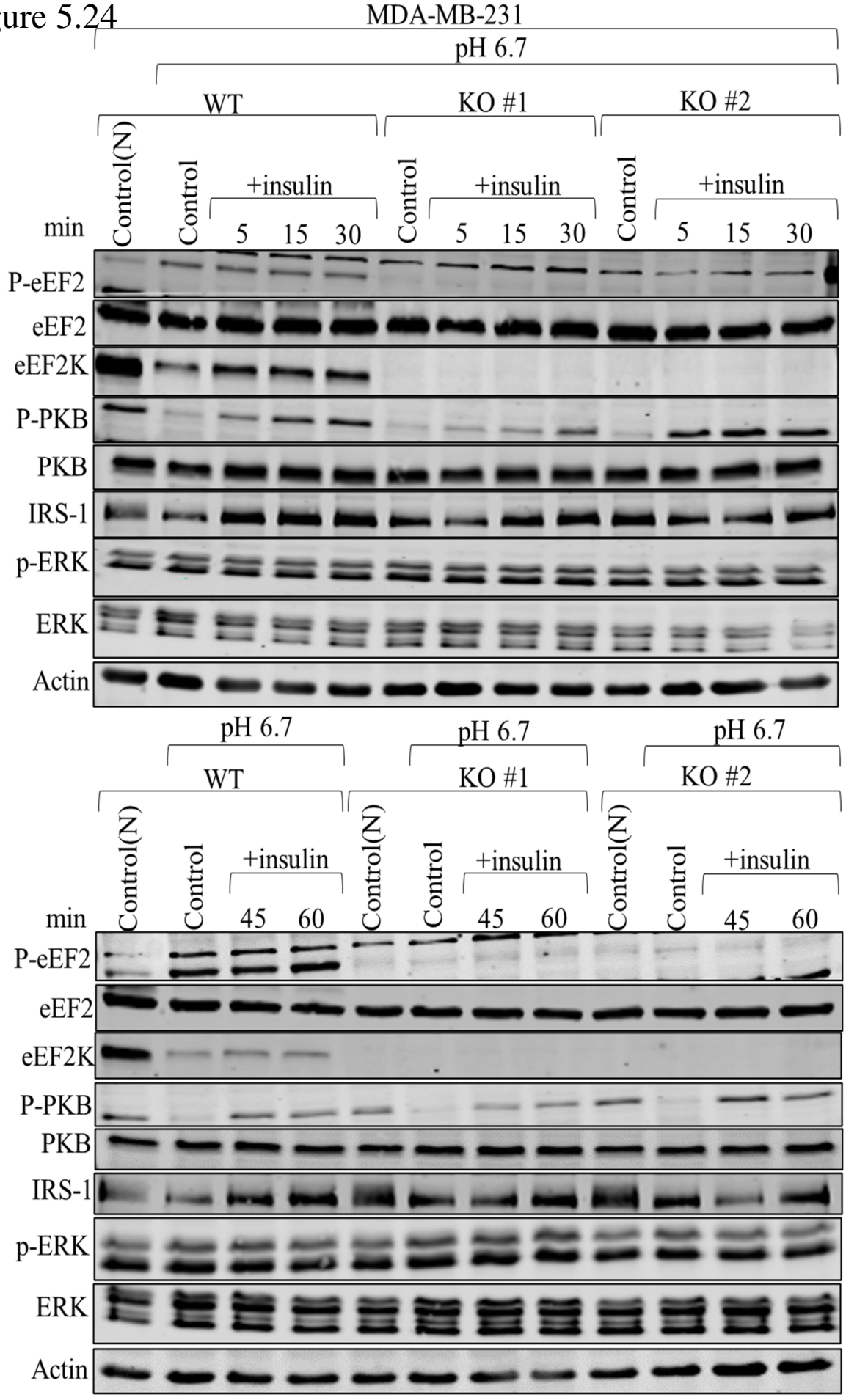

MDA-MB-231
pH 6.7
WT
KO #1
KO #2
Control(N)
Control
+insulin
min
5
15
30
P-eEF2
eEF2
eEF2K
P-PKB
PKB
IRS-1
p-ERK
ERK
Actin
pH 6.7
WT
KO #1
KO #2
Control(N)
Control
+insulin
min
45
60
P-eEF2
eEF2
eEF2K
P-PKB
PKB
IRS-1
p-ERK
ERK
Actin

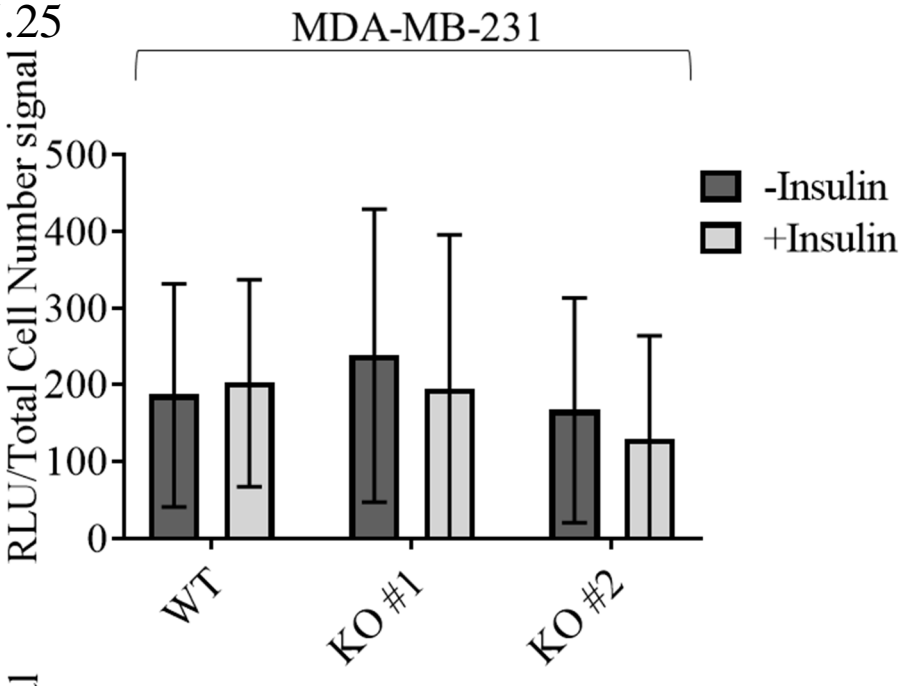
Figure 5.24: Lack of eEF2K in low pH medium does not significantly alter IRS-1 levels but may affect PKB signalling. MDA-MB-231 eEF2K-WT and KO cells were serum starved overnight. The medium was then changed to DMEM without serum that was buffered to pH 6.7 and the cells were treated with or without 100 nM insulin for the indicated time points (in minutes). The control sample indicates cells left in medium without insulin for 60 min. After treatment, the cells were lysed and the lysates were run on (12.5%) SDS-PAGE, followed by analysis via immunoblotting. Images represent n=3. All samples were treated in DMEM buffered to pH 6.7 except those labelled. Control (N): Standard DMEM; Control: pH 6.7 DMEM without insulin.

The Glucose Uptake-Glo Assay from Promega was used to measure glucose uptake into MDA-MB-231, A549 and PC3 eEF2K-WT and KO or knockdown cells, following overnight serum starvation and 1 h of insulin treatment[126]. The CellTox Green Assay was used to normalise the glucose uptake assay signal to cell number. According to this assay, there was no significant change in glucose uptake between eEF2K-WT and KO (or knockdown) MDA-MB-231, PC3 and A549 cells (**Figure 5.25**). Unexpectedly, insulin treatment did not significantly stimulate glucose uptake. This is a surprising result, as all three of these cell lines express GLUT4[329, 330]. It has also been shown that GLUT4 plays a role in MDA-MB-231 cells' basal glucose uptake[314]. However, it is possible that GLUT4 is only a minor contributor to these cells' overall glucose uptake. These cells may use the insulin independent transporter GLUT1 as their main method of glucose uptake as it has been previously shown to be important for glucose uptake in all three cell lines[331-333]. It is also worth mentioning that this assay has a significant number of steps during which cells might be removed from areas of the wells which might affect the luminescence measurement.

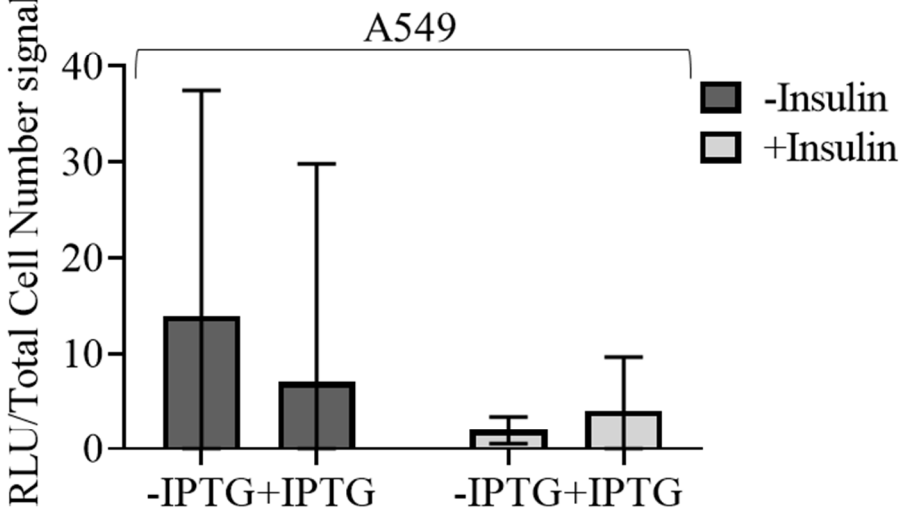
Overall, this section of the chapter showed that eEF2K does not seem to alter basal glucose uptake and ERK signalling but might affect IRS-1 protein levels. The Seahorse assays showed no significant changes in glycolysis in MDA-MB-231, A549 and PC3 cells may indicate that even if eEF2K phosphorylates IRS-1 at Ser330, that phosphorylation may not be functionally significant.

Figure 5.25

(A)



(B)



(C)

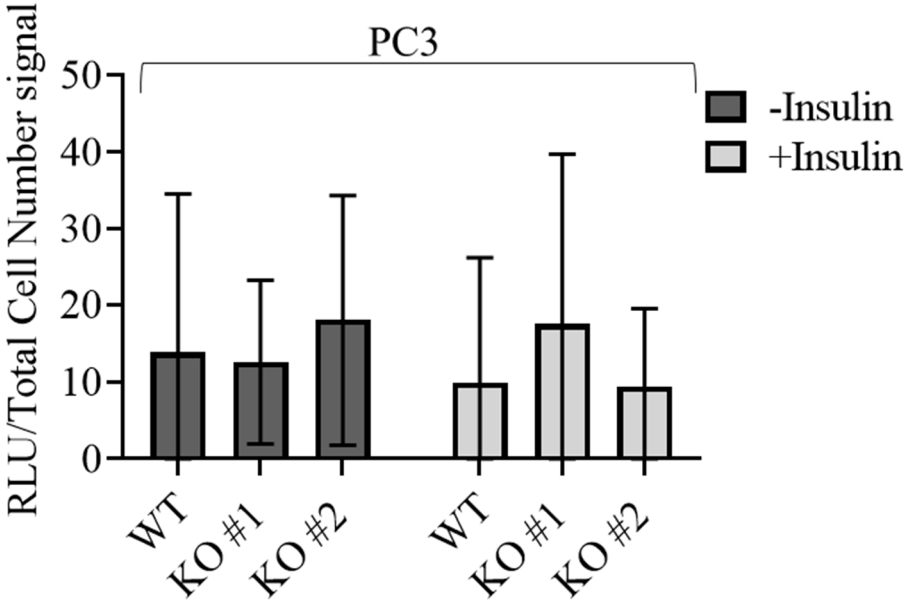


Figure 5.25: Knock out or knockdown of eEF2K does not affect glucose uptake in MDA-MB-231, A549 or PC3 cells. MDA-MB-231 **(A),** PC3 **(C)** eEF2K-WT and KO cells and A549 **(B)** eEF2K-WT and knockdown cells were serum starved overnight in 96-well plates. The medium was changed to fully supplemented medium with or without 100 nM insulin for 1 h. Following this treatment, the Glucose Uptake Glo kit instructions from Promega were followed. The luminescence was measured on the GloMax Discover instrument. Cell-Tox Green Assay dye was then added to each well to normalise the luminescence signal to the total cell signal. Error bars represent S.D. (n=3). The p-values were calculated using Two-Way ANOVA with the Tukey multiple comparisons test.

5.3 Discussion

This chapter looked at a range of possible links between eEF2K and cellular pathways – migration/invasion, translational accuracy, Nrf2, hypoxia, PD-L1-linked immune evasion and insulin signalling/glucose uptake.

Cell migration and invasion

Cancer metastasis is the hallmark of aggressive cancers and most deaths that are due to cancers are due to metastatic disease[251-253]. Targeting cancer cell migration could be a good way to slow down the cancer from spreading into other areas of the body. Until recently, it was not known whether control of translation elongation could affect cell migration. The study by Dr. Jianling Xie *et al*.[123] about eEF2K's role in cancer cell migration and invasion delves into this. This part of the chapter discussed this study, as well as further adding to its data by using eEF2K-KO MDA-MB-231 cells.

Importantly, the study found that inhibiting eEF2K pharmacologically (through use of the eeF2K inhibitors JAN384, NH125 and A484954) as well as by knockdown of eEF2K (in A549 cells) slowed down the rate of wound healing in both MDA-MB-231 and A549 cells. This was confirmed through transwell migration and invasion assays, which showed significantly lower numbers of cells migrated or invaded through to the other side of the membrane when eEF2K was inhibited or silenced. To further validate this result, eEF2K was overexpressed or eEF2 was partially silenced; under these conditions, it was observed that wound healing speed significantly increased, further confirming eEF2K as a positive regulator of cell migration. A proteomics experiment also showed that in A549 cells in which eEF2K was silenced, levels of proteins (such as integrins α2 and α3) related to cell migration are decreased. Importantly, knocking down eEF2K in A549 cells caused a shift of the *ITGA2* and *ITGA3* mRNAs from the polysomal to the non-polysomal fractions, indicating that eEF2K positively controls the

association of these migration-related mRNAs with polysomes. It was also observed that eEF2K silencing blocked lung cancer metastasis *in vivo*.

MDA-MB-231 eEF2K-KO cells were also used in the same kinds of wound-healing and transwell migration/invasion assays described in the study by Xie *et al.*[123] from our group, showing a decrease in wound-healing speed and cells that have migrated or invaded through transwells. eEF2K-KO did not affect the cell cycle in both A549 and MDA-MB-231 cells, further supporting the evidence that eEF2K's effect on migration was not due to an effect on cell proliferation. These findings complement the data presented in the paper. However, it is of note that JAN384 causes a further decrease in migration and invasion speed of eEF2K-KO cells, strongly suggesting it has an off-target effect that affects these processes. Nevertheless, this does not take away the importance of eEF2K in regulation migration and invasion, further showing that eEF2K could be a good potential therapeutic target to slow down the spread of, for example, breast and lung tumours in the body.

Translational accuracy

Maintaining translational accuracy (otherwise known as fidelity) is crucial for cells to create properly folded proteins. In this Chapter, I discussed the study by Xie *et* al.'s[128] study which linked eEF2K to translation fidelity, as well as showing my contributions to it. . This study made use of dual luciferase reporter constructs with the fastest, WT and slowest decoding times (elongation rates) based on codon and tRNA frequences in human cells, resulting in varying yields of functional luciferase. By transfecting these constructs into A549 cells, it was found that increased translational speed results in lower translational fidelity (lower yield of luciferase). Silencing eEF2K in A549 cells led to a decrease in translational fidelity, showing that eEF2K regulates this process. I also confirmed this using MDA-MB-231 eEF2K-KO cells. The study moved on to show that eEF2K knockdown led to a reduction in the polysome/monosome ratio in A549 cells (while not affecting protein synthesis in any of the conditions tested), likely indicating faster elongation in eEF2K knockdown cells through

ribosomal 'run-off'. This part of the study concluded that eEF2K's positive effect on translation fidelity is due to it causing a slower rate of translation elongation, rather than overall protein synthesis. Importantly, it was found that eEF2K assists the ribosome in the selection of canonical AUG start codons, rather than the non-canonical CUG start codons in cells. Finally, it was shown that *C. elegans* worms knocked out for *efk-1* (the eEF2K homolog) survived for a shorter period of time than WT N2 worms, potentially because of the decrease in translation fidelity due to a lack of *efk-1*, linking translation fidelity to longer lifespan. Overall, this study showed that eEF2K promotes fidelity during translation elongation and, indirectly, initiation, as well as providing a mechanism as to why mTORC1's inhibition leads to increased translational accuracy.

Hypoxia

Cells in the centre of solid tumours are typically under hypoxic conditions due to the mass of cells surrounding them and blocking access to oxygen. Moore *et al*.[78], investigated how eEF2K could be regulated under hypoxic conditions. The study found that eEF2K is hydroxylated at Pro98 under normoxic conditions, reducing calmodulin's ability to bind, as well as activate eEF2K. Under hypoxia, this does not take place, allowing eEF2K to become activated. Importantly, the study also found that the loss of eEF2K compromises the ability of primary neuronal cells to withstand hypoxia. Due to this data, I looked into a range of hypoxic conditions (different oxygen concentrations below 21% O_2) and their effect on eEF2K activation in MDA-MB-231, A549 and HCT116 cells. Interestingly, I found that the phosphorylation of eEF2 was highest at 8.5% and 5% O_2, with it decreasing at lower oxygen concentrations, possibly because of degradation of eEF2K (which is linked to its activation[59]. These oxygen concentrations are more relevant 8.5% and 5% than the 0.1% O_2 used in the earlier study[312] as cells are unlikely to have such low percentage of oxygen [276]. The finding that eEF2K becomes more active at these lower oxygen concentrations needs to be further explored with cell death studies. If cancer cells lack eEF2K at these oxygen concentrations, they could potentially undergo death. If this is indeed the case, eEF2K could be a good target for solid tumours with poor vascularisation.

Nrf2

eEF2K has been linked to synaptic plasticity and various neurological diseases. A study by Jan *et al.*[292] showed that eEF2K inhibition increased Nrf2 levels which is critical for cell's antioxidant response and to the cell survival of primary neurons which were exposed to Aβ oligomers. I investigated whether this increase in Nrf2 also occurs in eEF2K-KO MDA-MB-231 and eEF2K knockdown A549 cells. eEF2K did not appear to play a role in regulating Nrf2 protein levels in these cells under stress associated with reactive oxygen species. However, this could be important to investigate in brain-related cancers, such as medulloblastoma.

PD-L1

This part of the chapter investigated eEF2K's link to PD-L1 by discussing a recently published study by Wu *et al.*[188] working closely with our group. This study showed that eEF2K promotes the translation of PD-L1, thus allowing cancer cells to 'hide' from the body's immune response. This was shown in A549, MDA-MB-231 and PC3 cells. The greatest effect was observed for surface and total PD-L1 in PC3 cells (which will bind to the immune cells) levels greatly reduced. eEF2K promoted the association of *PD-L1* mRNAs with polysomes and enhanced *PD-L1* mRNA translation by bypassing the uORF in the 5'-UTR that typically represses its translation. It was then shown that a lack of eEF2K led to higher cell death mediated by immune cells (NK cells) in both A549 and PC3 cells. This further supports the idea that eEF2K could be a very good therapeutic target to augment immune-based therapies against these types of cancers.

IRS-1 and glucose uptake

Previously unpublished data by Dr. Claire Moore from our group showed that eEF2K might phosphorylate IRS-1, a major component of the insulin-stimulated glucose uptake pathway. Our more recent phospho-proteomics data further supported this idea with a possible phosphorylation by eEF2K at Ser330 on IRS-1. My experiments showed that IRS-1 levels may be slightly upregulated upon eEF2K-KO, however, the ERK signalling and insulin-stimulated

PKB signalling pathways were largely unaffected. It was also found that eEF2K did not affect glucose uptake upon insulin treatment of cells, further supporting data shown in Chapter 3 – i.e., that the lack eEF2K did not affect the glycolysis or mitochondrial respiration of MDA-MB-231, A549 and PC3 cells.

Key findings and future work

This original reasoning for this project was that while eEF2K has been shown to be important for cell or tumour survival[57-60], other studies have shown the opposite in different cells[61, 62]. This suggested that eEF2K's effect on cell survival may differ depending on the cell type, and thus any treatment developed that targeted eEF2K would need to be carefully tested in each cancer type. Unpublished data from Dr. Marina Kochetkova (University of South Australia) showed that eEF2 was highly phosphorylated in breast tumour tissue, suggesting that breast cancer cells utilise eEF2K to help them survive. Thus, it was decided to use an aggressive and metastatic breast cancer cell model (MDA-MB-231) to investigate whether eEF2K can assist these cells to survive glucose and pyruvate deprivation. Using the custom-made eEF2K inhibitor JAN384, kindly provided by Janssen Pharmaceutica, I was able to show that inhibiting eEF2K alone did not significantly change cell death due to nutrient deprivation (**Figure 3.3**). This led to the investigation of another pathway which has been previously – but controversially - linked to eEF2K – autophagy[58, 113-119, 158].

Using the autophagy inhibitor BafA, I was able to show that individual treatments with JAN384 or BafA did not significantly increase cell death (via the CellTox Green Assay), but concurrent treatments led to a large increase (**Figure 3.6A, 3.9A**). To confirm this and rule out potential off-target effects of JAN384, lung carcinoma A549 cells with an inducible shRNA against eEF2K were used. The same pattern was shown in those cells (**Figure 3.6B, 3.9B**). By analysing western blots, it was observed that the silencing of eEF2K in A549 cells did not significantly alter p62 or LC3-II levels (markers of autophagy), while the inhibition of eEF2K by JAN384 in MDA-MB-231 cells did increase both p62 and LC3-II (**Figure 3.5**).

This suggested that JAN384 potentially has a off-target effect that affected the autophagic pathway.

To deal with the need to use inhibitors of eEF2K, I designed a CRISPR-Cas9 strategy to knock-out eEF2K in MDA-MB-231 cells, with the assistance of Dr. Kirk Jensen from our group. Following clonal selection and testing, I successfully generated two clones of eEF2K-KO cells (**Figures 3.11-3.17**). I found that knocking-out eEF2K did not lead to the increase in p62 and LC3-II seen when cells were treated with JAN384, confirming this to be an off-target effect of the inhibitor (**Figure 3.20C**).

Instead of JAN384, I also used the less potent eEF2K inhibitor A484954 (A484 for short) on WT cells, showing that it did not have the same off-target effect on p62 and LC3-II (**Figure 3.20C**). Using a combination treatment of A484 and BafA, I confirmed the findings found with JAN384 and BafA, i.e., that simultaneous inhibition of eEF2K and autophagy increased cell death compared to when each pathway was inhibited separately in nutrient-deprived conditions. The eEF2K-KO cells showed a significant increase in cell death when treated with BafA, confirming this observation (**Figure 3.22A**). These findings were further supported by propidium iodide and Calcein-AM data (**Figures 3.22B, 3.24**).

Interestingly, when testing A549 cells in media lacking glutamine, glucose, and pyruvate, it was found that eEF2K did assist the survival of A549 cells under -Gln conditions, but not in -Glc medium. MDA-MB-231 cells could not survive -Gln conditions for long periods of time, so no tests could be performed in these conditions. This again highlighted the different effects of eEF2K between cell lines. Nevertheless, this data overall suggests that eEF2K and

autophagic pathways act independently of each other to assist survival of MDA-MB-231 and A549 cells to during nutrient deprivation.

To test further these observations about eEF2K and autophagy, an androgen receptor negative prostate cancer cell line, PC3, was chosen. Ms. Danielle Fang generated eEF2K-KO cells using the same methodology I used, creating two distinct clones of PC3 eEF2K-KO cells (**Figures 3.11-3.14, 3.18, 3.19**). Surprisingly, it was found that the absence of eEF2K in PC3 cells assisted cell survival in -Glc and -Gln conditions (**Figures 3.31, 3.33**). Treatment with BafA did not significantly affect cell death in eEF2K-KO cells. While this is surprising, these data do match studies that reported eEF2K activity as being detrimental to cancer progression[61, 62]. It is possible that in the case of PC3 cells, eEF2K activation alters the translation machinery to downregulate factors that affect cell survival, although other explanations are also possible. This once more highlights the importance of testing the effects of disrupting eEF2K in a variety of cells.

Importantly, my data show that eEF2K does not regulate autophagy in these cells, as its silencing or knock-out has no effect on LC3-II or p62 levels.

Knowing eEF2K's ability to regulate protein synthesis, a major energy-consuming process, I then looked into the changes in ATP levels in the same conditions that the previous experiments were carried out. I found that in both MDA-MB-231 and A549 cells, a lack of eEF2K led to a decrease in ATP levels in nutrient deprived conditions, which was further exacerbated when the cells were treated with BafA (**Figure 3.37A, B**). This suggests that when both eEF2K and autophagy are turned off, the cells end up with lower levels of energy, causing them to die quicker due to lack of nutrients. Interestingly, in PC3 eEF2K-KO cells,

I observed an unexpected increase in ATP levels in nutrient deprived conditions, perhaps explaining their ability to survive those conditions for longer (**Figure 3.38**). PC3 eEF2K-KO cells could use their potentially higher rates of protein synthesis to generate larger stores of ATP (possibly through the upregulation of proteins related to generating energy) when they are growing in +Glc conditions, thus allowing them to use these larger amounts of ATP to survive for longer in -Glc/-Gln medium.

Following the above finding, I investigated whether eEF2K affected glycolysis or mitochondrial respiration, as a study by Cheng *et al*.[306] in 2016 suggested, by using the Agilent XFp Seahorse Analyzer. Unexpectedly, I found that eEF2K does not affect either of these processes in all three cell lines; thus, the changes in ATP levels cannot be explained in this way.

Future work: It is important to test the effects of concurrent eEF2K and autophagy inhibition in other types of cancer cells. eEF2K-KO mice have no obvious phenotype under standard husbandry conditions[70], while autophagy inhibition through hydroxychloroquine has been tested and found to lead to better outcomes for cancer patients[97-100]. Thus, a potential treatment by inhibiting both eEF2K and autophagy at the same time could be a good way to fight certain types of cancers.

It is important to note that the results found in cell culture may not fully reflect what happens in mouse models. It would be important to test xenografts of WT and knock-out or knockdown MDA-MB-231, A549 and PC3 cells in mouse models, alongside autophagy inhibition. Chloroquine, BafA and the dual AMPK/ULK1 inhibitor SBI-0206965[334] could be used to inhibit autophagy to compare the effects of the different inhibitors on cell death.

Monitoring the sizes of the resulting tumours and their metastasis would give a good indication of whether the results obtained from cell culture would be similar in a whole organism. As a further step, it could also be interesting to test the effects of inhibiting eEF2K and/or autophagy inhibition on patient-derived tumour organoids.

Chapter 4 of this thesis focused on the ability of cancer cells to become resistant to therapeutic agents[212, 335]. Due to the potential of eEF2K and autophagy inhibition as a therapy, it was relevant to examine the ways cancer cells could gain resistance to this treatment. To that end, I created MDA-MB-231 WT and eEF2K-KO cells that were resistant to a lack of glucose and pyruvate, as well as autophagy inhibition through pulsed treatment in -Glc medium with BafA. After a year of treatment, the cells were able to survive in these conditions significantly better than the parental 'sensitive' cells (**Figure 4.2**). Interestingly, it was then found that all three of the resistant cell lines showed higher levels of autophagic flux compared to their 'sensitive' counterparts, with the flux being particularly greatly increased in KO #2 cells (**Figure 4.7**). This was the first piece of evidence showing that cells obtain resistance to the same conditions in varying ways. Importantly, it was then shown that the resistant cells lose their resistance over time if not faced with constant adverse conditions (**Figures 4.8-4.10**). Furthermore, this assay also confirmed that there was no significant difference in autophagic flux between sensitive WT and eEF2K-KO cells, further supporting the evidence that eEF2K does not regulate autophagy in these cells.

To examine the process by which these cells obtained their resistance, relative abundance proteomic and phospho-proteomic analyses were performed on these cells (**Figures 4.11-4.13, Appendix Figures 1-2, Appendix Tables 1-5**). These data provided further evidence that cells gained resistance in varying ways, through the modification of levels of different

proteins in various pathways and processes. However, there were pathways that were affected in all three resistant lines. Importantly, it was found that levels of amino-acyl tRNA synthetases and a ligase were decreased in all resistant cell lines. Levels of proteins related to RNA transport, ribosome biogenesis and fatty acid synthesis were also decreased. All of these processes use a substantial amount of cellular energy; therefore, it makes sense for resistant cells to downregulate them under stressed conditions to save this energy and allow them to survive for longer. It would have been interesting to confirm some of these protein changes by measuring cell cholesterol synthesis and lipid biogenesis.

The phosphoproteomic analysis also showed a general downregulation in mTORC1 signalling in both KO cell lines, suggesting a downregulation of protein synthesis and other energy-consuming anabolic processes, thus saving the cells a substantial amount of energy. This was not evident in WT cells; likely due to the fact they are still able to use eEF2K to regulate protein synthesis rates.

Importantly, the phosphoproteomic data also showed 21 phosphosites that were present in WT 'sensitive' cells and absent in both KO 'sensitive' cell lines, suggesting them as potential new substrates of eEF2K. Notably, none of them correlated with candidates identified in a screen for eEF2K substrates performed by Lazarus *et al*. in 2017[228]. The Lazarus *et al*.[228] study showed the possibility of eEF2K being able to phosphorylate AMPK on Thr482. While the function of this phosphorylation site is unknown, it is interesting to consider why eEF2K would phosphorylate AMPK. A possible function of the Thr482 phosphorylation by eEF2K could be to try to increase AMPK activity under nutrient stress conditions, which would in turn increase eEF2K activity through AMPK phosphorylating Ser398, leading to a positive feedforward loop. However, more phosphoproteomics screens (e.g. from WT and eEF2K-

KO cells) and *in vitro* phosphorylation data are needed to confirm whether AMPK is an authentic *in vivo* substrate for eEF2K substrate, as the data in this thesis did not show this to be the case.

Future work: It would be important to confirm more of the relative proteome data via western blotting. However, the limitation of this method is that, as the cells gain resistance in different ways, there is no guarantee that if new samples were generated, the cells would have undergone the same changes as the samples that were analysed here by mass spectrometry. Therefore, it would be important to ensure the remaining samples are used carefully, since they cannot be generated again.

Furthermore, looking at the general trends seen in all the resistant cell lines, it would be interesting to see the effect of disrupting pathways such as fatty acid oxidation would have on the resistance of these cells. For example, if ACADVL was inhibited, it could be expected that, as cells would no longer oxidise their fatty acids as efficiently, they would die quicker.

Finally, the list of potential eEF2K substrates needs to be tested by western blot with phospho-specific antibodies or through the incubation of purified proteins with active eEF2K and ^{32}P-labelled ATP. So far, no new confirmed substrates of eEF2K have been found in previous screens. This is also what adds to the potential of eEF2K to be used as a therapeutic target, due to a lack of on-target 'side-effects'. If new substrates are confirmed, this would drastically change the field of eEF2K research.

Chapter 5 of this thesis investigated a variety of pathways that have been linked to eEF2K. Some of this data has been published in papers that have been attached in the **Appendix**.

The first pathway investigated was that of cell migration and invasion, which is a key aspect of the cancer cell's ability to metastastise[254]. Proteomics data from our study showed that a number of migration related proteins were downregulated in A549 eEF2K silenced cells[123]. I was able to show that pharmacological inhibition of eEF2K slowed down wound-healing (**Figures 5.1, 5.3**). Importantly, testing this on eEF2K-KO cells confirmed this finding, although also showing that JAN384 treatment significantly decreased the wound-healing abilities of eEF2K-KO cells, suggesting it has an off-target effect that affects cell migration (**Figure 5.4**). I also showed that eEF2K regulates cell migration and invasion by using 3D migration assays through transwells, followed by invasion assays through matrigel (**Figures 5.6-5.8**). I was also able to show that knocking-out eEF2K had no effect on cell adhesion (**Figures 5.9, 5.10**). Importantly, the lack of, or silencing of, eEF2K had no effect on cell proliferation or the cell cycle (**Figures 5.13-5.15**), meaning that any changes in migration and invasion are due to eEF2K's regulation of the processes and not cell division.

Furthermore, I added my findings to a publication from our group concerning eEF2K's role in translation fidelity[128]. I confirmed the findings in A549 cells that eEF2K regulates translation fidelity by using the MDA-MB-231 eEF2K-KO cells in a similar experiment, showing that a lack of eEF2K leads to faster translation and reduced translation fidelity. (**Figure 5.16**).

Further pursuing a study on the effects of hypoxia on eEF2K that was started by Moore *et al*. in 2015[78], I tested the effects of a variety of oxygen concentrations on the phosphorylation of eEF2 in MDA-MB-231, A549 and HCT116 cells (**Figure 5.17**). I found that the phosphorylation of eEF2 is highest when the cells are in 8.5% or 5% O_2 in -Glc conditions, which is more physiologically relevant than the 0.1% tested in the study[312]. It cannot be ruled

out that eEF2K activity was also increased at the lower oxygen concentrations that were tested, prior to a decrease in activity due to degradation of activated eEF2K. Thus, it would be important to test a variety of time points at the lower oxygen concentrations. Furthermore, it would be interesting to investigate whether inhibition or knock out of eEF2K, and perhaps autophagy as well would affect cell survival at the tested oxygen concentrations.

Due to the claims by Jan *et al*.[292] in 2017 that eEF2K inhibition increased the levels of Nrf2 in N2A neuroblastoma cells (an important antioxidant response protein), I tested whether eEF2K inhibition or knock-out affected Nrf2 levels in MDA-MB-231 cells, finding no link between the two (**Figure 5.19**). This suggests the effect of eEF2K on Nrf2 differs depending on the cell type; more cell types should clearly be investigated.

Next, I investigated whether eEF2K regulated the expression of PD-L1 protein together with Dr. Jianling Xie from our group and others in a study published in 2020[188]. I was able to show that knocking out eEF2K in PC3 cells significantly decreased total and external PD-L1 protein (through western blot and flow cytometry respectively) and mRNA levels (**Figure 5.20**). This needs further investigation in different cell types as such a large decrease was not seen in A549 and MDA-MB-231 cells.

Lastly, I investigated the effects of eEF2K on glucose uptake, following phospho-proteomic analysis of eEF2K-WT and KO samples by Dr. Antigoni Manousopoulou, which showed that the eEF2K-KO samples were missing a phosphorylation of IRS-1 at Ser330. This suggested that site might be a target for eEF2K. Unpublished data by Dr. Claire Moore also suggested that eEF2K may phosphorylate IRS-1, although on different sites. Due to IRS-1's importance in the insulin signalling cascade and glucose uptake, it was important to examine

if the lack of eEF2K affected its function[303, 304]. I showed that a lack of eEF2K in normal and low pH conditions (where eEF2K is more active) led to an increase in IRS-1 protein levels in eEF2K-KO cells (**Figures 5.23, 5.24**). Interestingly, I also found that IRS-1 levels eventually decrease at later time points of insulin treatment, perhaps indicative of its degradation or loss in the cell pellet upon the spinning of the lysate due to insulin-induced translocation of IRS-1 to the plasma membrane.

Examining basal glucose uptake itself, I found no significant change between MDA-MB-231, A549 or PC3 cells with or without eEF2K (**Figure 5.25**); lack of effect of insulin precluded me drawing conclusions about the role of eEF2K, if any, in insulin signalling. This suggested that the phosphorylation of IRS-1 at Ser330 is not important for its function and that eEF2K does not affect glucose uptake. However, the glucose uptake assay has limitations, as it is easy to dislodge cells during the process, resulting in erroneous data. Therefore, another assay might be worth pursuing before ruling that eEF2K has no effect on this process.

Overall, this thesis has examined a variety of pathways linked to eEF2K and importantly, showed the importance of eEF2K and autophagy in cell survival. This Thesis has made a substantial headway into investigating the effects these pathways have on cells and their mechanisms, but further study in a wider variety of cell lines is required.

Appendices

The proteomics data analyses were performed by Dr. Sushma Rao from the Proteomics, Metabolomics and MS-Imaging Facility at the South Australian Health and Medical Research Institute, Adelaide, SA, 5000, Australia. The raw data is available by using the following URL: https://www.ebi.ac.uk/pride/login

(Username: reviewer_pxd022528@ebi.ac.uk; Password: Ewd2cAve).

The Appendix tables, figures and articles are available by using the following link (including data from the iTRAQ proteomics experiment performed by Dr. Antigoni Manousopoulou and the original resolution images of microscopy figures):

https://universityofadelaide.box.com/s/qrodwr56kv6zgkr8mzqyw8ebzsnud9mf

References

1. Buttgereit F, Brand MD. 1995. *A hierarchy of ATP-consuming processes in mammalian cells*. Biochem J 312 (Pt 1): 163-7. 10.1042/bj3120163

2. Princiotta MF, Finzi D, Qian SB, Gibbs J, Schuchmann S, et al. 2003. *Quantitating protein synthesis, degradation, and endogenous antigen processing*. Immunity 18: 343-54. 10.1016/s1074-7613(03)00051-7

3. Le Quesne JP, Spriggs KA, Bushell M, Willis AE. 2010. *Dysregulation of protein synthesis and disease*. J Pathol 220: 140-51. 10.1002/path.2627

4. Willis M JH, Stone J. 2014. *Cellular and Molecular Pathobiology of Cardiovascular Disease 1st Edition*: Elsevier. 46-7 pp.

5. Nairn AC, Bhagat B, Palfrey HC. 1985. *Identification of calmodulin-dependent protein kinase III and its major Mr 100,000 substrate in mammalian tissues*. Proc Natl Acad Sci U S A 82: 7939-43. 10.1073/pnas.82.23.7939

6. Ryazanov AG, Shestakova EA, Natapov PG. 1988. *Phosphorylation of elongation factor 2 by EF-2 kinase affects rate of translation*. Nature 334: 170-3. 10.1038/334170a0

7. Price NT, Redpath NT, Severinov KV, Campbell DG, Russell JM, Proud CG. 1991. *Identification of the phosphorylation sites in elongation factor-2 from rabbit reticulocytes*. FEBS Lett 282: 253-8. 10.1016/0014-5793(91)80489-p

8. Carlberg U, Nilsson A, Nygård O. 1990. *Functional properties of phosphorylated elongation factor 2*. Eur J Biochem 191: 639-45. 10.1111/j.1432-1033.1990.tb19169.x

9. Ryazanov AG, Spirin AS. 1990. *Phosphorylation of elongation factor 2: a key mechanism regulating gene expression in vertebrates*. New Biol 2: 843-50.

10. Hanks SK, Hunter T. 1995. *Protein kinases 6. The eukaryotic protein kinase superfamily: kinase (catalytic) domain structure and classification*. Faseb j 9: 576-96.

11. Redpath NT, Price NT, Proud CG. 1996. *Cloning and expression of cDNA encoding protein synthesis elongation factor-2 kinase*. J Biol Chem 271: 17547-54.

12. Ryazanov AG, Ward MD, Mendola CE, Pavur KS, Dorovkov MV, et al. 1997. *Identification of a new class of protein kinases represented by eukaryotic elongation factor-2 kinase*. Proc Natl Acad Sci U S A 94: 4884-9. 10.1073/pnas.94.10.4884

13. Ryazanov AG, Pavur KS, Dorovkov MV. 1999. *Alpha-kinases: a new class of protein kinases with a novel catalytic domain*. Curr Biol 9: R43-5. 10.1016/s0960-9822(99)80006-2

14. Middelbeek J, Clark K, Venselaar H, Huynen MA, van Leeuwen FN. 2010. *The alpha-kinase family: an exceptional branch on the protein kinase tree*. Cell Mol Life Sci 67: 875-90. 10.1007/s00018-009-0215-z

15. Ye Q, Crawley SW, Yang Y, Côté GP, Jia Z. 2010. *Crystal structure of the alpha-kinase domain of Dictyostelium myosin heavy chain kinase A*. Sci Signal 3: ra17. 10.1126/scisignal.2000525

16. Yamaguchi H, Matsushita M, Nairn AC, Kuriyan J. 2001. *Crystal structure of the atypical protein kinase domain of a TRP channel with phosphotransferase activity*. Mol Cell 7: 1047-57. 10.1016/s1097-2765(01)00256-8

17. Fawaz MV, Topper ME, Firestine SM. 2011. *The ATP-grasp enzymes*. Bioorg Chem 39: 185-91. 10.1016/j.bioorg.2011.08.004

18. Pavur KS, Petrov AN, Ryazanov AG. 2000. *Mapping the functional domains of elongation factor-2 kinase*. Biochemistry 39: 12216-24. 10.1021/bi0007270

19. Diggle TA, Seehra CK, Hase S, Redpath NT. 1999. *Analysis of the domain structure of elongation factor-2 kinase by mutagenesis*. FEBS Lett 457: 189-92. 10.1016/s0014-5793(99)01034-0

20. Drennan D, Ryazanov AG. 2004. *Alpha-kinases: analysis of the family and comparison with conventional protein kinases*. Prog Biophys Mol Biol 85: 1-32. 10.1016/s0079-6107(03)00060-9

21. Mittl PR, Schneider-Brachert W. 2007. *Sel1-like repeat proteins in signal transduction*. Cell Signal 19: 20-31. 10.1016/j.cellsig.2006.05.034

22. Will N, Piserchio A, Snyder I, Ferguson SB, Giles DH, et al. 2016. *Structure of the C-Terminal Helical Repeat Domain of Eukaryotic Elongation Factor 2 Kinase*. Biochemistry 55: 5377-86. 10.1021/acs.biochem.6b00711

23. Pigott CR, Mikolajek H, Moore CE, Finn SJ, Phippen CW, et al. 2012. *Insights into the regulation of eukaryotic elongation factor 2 kinase and the interplay between its domains*. Biochem J 442: 105-18. 10.1042/bj20111536

24. Tavares CD, Ferguson SB, Giles DH, Wang Q, Wellmann RM, et al. 2014. *The molecular mechanism of eukaryotic elongation factor 2 kinase activation*. J Biol Chem 289: 23901-16. 10.1074/jbc.M114.577148

25. Redpath NT, Proud CG. 1993. *Purification and phosphorylation of elongation factor-2 kinase from rabbit reticulocytes*. Eur J Biochem 212: 511-20. 10.1111/j.1432-1033.1993.tb17688.x

26. Pyr Dit Ruys S, Wang X, Smith EM, Herinckx G, Hussain N, et al. 2012. *Identification of autophosphorylation sites in eukaryotic elongation factor-2 kinase*. Biochem J 442: 681-92. 10.1042/bj20111530

27. Crawley SW, Gharaei MS, Ye Q, Yang Y, Raveh B, et al. 2011. *Autophosphorylation activates Dictyostelium myosin II heavy chain kinase A by providing a ligand for an allosteric binding site in the alpha-kinase domain*. J Biol Chem 286: 2607-16. 10.1074/jbc.M110.177014

28. Frias MA, Thoreen CC, Jaffe JD, Schroder W, Sculley T, et al. 2006. *mSin1 is necessary for Akt/PKB phosphorylation, and its isoforms define three distinct mTORC2s*. Curr Biol 16: 1865-70. 10.1016/j.cub.2006.08.001

29. Yadav RB, Burgos P, Parker AW, Iadevaia V, Proud CG, et al. 2013. *mTOR direct interactions with Rheb-GTPase and raptor: sub-cellular localization using fluorescence lifetime imaging*. BMC Cell Biol 14: 3. 10.1186/1471-2121-14-3

30. Pópulo H, Lopes JM, Soares P. 2012. *The mTOR signalling pathway in human cancer*. Int J Mol Sci 13: 1886-918. 10.3390/ijms13021886

31. Brunn GJ, Hudson CC, Sekulić A, Williams JM, Hosoi H, et al. 1997. *Phosphorylation of the translational repressor PHAS-I by the mammalian target of rapamycin*. Science 277: 99-101. 10.1126/science.277.5322.99

32. Gunn RM, Hailes HC. 2008. *Insights into the PI3-K-PKB-mTOR signalling pathway from small molecules*. J Chem Biol 1: 49-62. 10.1007/s12154-008-0008-0

33. Biever A, Valjent E, Puighermanal E. 2015. *Ribosomal Protein S6 Phosphorylation in the Nervous System: From Regulation to Function*. Front Mol Neurosci 8: 75. 10.3389/fnmol.2015.00075

34. Chauvin C, Koka V, Nouschi A, Mieulet V, Hoareau-Aveilla C, et al. 2014. *Ribosomal protein S6 kinase activity controls the ribosome biogenesis transcriptional program*. Oncogene 33: 474-83. 10.1038/onc.2012.606

35. Curatolo P, Moavero R. 2012. *mTOR Inhibitors in Tuberous Sclerosis Complex*. Curr Neuropharmacol 10: 404-15. 10.2174/157015912804143595

36. Gao Y, Gao J, Li M, Zheng Y, Wang Y, et al. 2016. *Rheb1 promotes tumor progression through mTORC1 in MLL-AF9-initiated murine acute myeloid leukemia*. J Hematol Oncol 9: 36. 10.1186/s13045-016-0264-3

37. Hua H, Kong Q, Zhang H, Wang J, Luo T, Jiang Y. 2019. *Targeting mTOR for cancer therapy*. J Hematol Oncol 12: 71. 10.1186/s13045-019-0754-1

38. Vara-Ciruelos D, Russell FM, Hardie DG. 2019. *The strange case of AMPK and cancer: Dr Jekyll or Mr Hyde? (†)*. Open Biol 9: 190099. 10.1098/rsob.190099

39. Gwinn DM, Shackelford DB, Egan DF, Mihaylova MM, Mery A, et al. 2008. *AMPK phosphorylation of raptor mediates a metabolic checkpoint*. Mol Cell 30: 214-26. 10.1016/j.molcel.2008.03.003

40. Luo Z, Zang M, Guo W. 2010. *AMPK as a metabolic tumor suppressor: control of metabolism and cell growth*. Future Oncol 6: 457-70. 10.2217/fon.09.174

41. Russell FM, Hardie DG. 2020. *AMP-Activated Protein Kinase: Do We Need Activators or Inhibitors to Treat or Prevent Cancer?* Int J Mol Sci 2210.3390/ijms22010186

42. Eichner LJ, Brun SN, Herzig S, Young NP, Curtis SD, et al. 2019. *Genetic Analysis Reveals AMPK Is Required to Support Tumor Growth in Murine Kras-Dependent Lung Cancer Models*. Cell Metab 29: 285-302.e7. 10.1016/j.cmet.2018.10.005

43. Carrière A, Cargnello M, Julien LA, Gao H, Bonneil E, et al. 2008. *Oncogenic MAPK signaling stimulates mTORC1 activity by promoting RSK-mediated raptor phosphorylation*. Curr Biol 18: 1269-77. 10.1016/j.cub.2008.07.078

44. Salaroglio IC, Mungo E, Gazzano E, Kopecka J, Riganti C. 2019. *ERK is a Pivotal Player of Chemo-Immune-Resistance in Cancer*. Int J Mol Sci 2010.3390/ijms20102505

45. Wang X, Xie J, Proud CG. 2017. *Eukaryotic Elongation Factor 2 Kinase (eEF2K) in Cancer*. Cancers (Basel) 910.3390/cancers9120162

46. Wang X, Regufe da Mota S, Liu R, Moore CE, Xie J, et al. 2014. *Eukaryotic elongation factor 2 kinase activity is controlled by multiple inputs from oncogenic signaling*. Mol Cell Biol 34: 4088-103. 10.1128/mcb.01035-14

47. Horman S, Browne G, Krause U, Patel J, Vertommen D, et al. 2002. *Activation of AMP-activated protein kinase leads to the phosphorylation of elongation factor 2 and an inhibition of protein synthesis*. Curr Biol 12: 1419-23. 10.1016/s0960-9822(02)01077-1

48. Browne GJ, Finn SG, Proud CG. 2004. *Stimulation of the AMP-activated protein kinase leads to activation of eukaryotic elongation factor 2 kinase and to its phosphorylation at a novel site, serine 398*. J Biol Chem 279: 12220-31. 10.1074/jbc.M309773200

49. Browne GJ, Proud CG. 2004. *A novel mTOR-regulated phosphorylation site in elongation factor 2 kinase modulates the activity of the kinase and its binding to calmodulin*. Mol Cell Biol 24: 2986-97. 10.1128/mcb.24.7.2986-2997.2004

50. Smith EM, Proud CG. 2008. *cdc2-cyclin B regulates eEF2 kinase activity in a cell cycle- and amino acid-dependent manner*. Embo j 27: 1005-16. 10.1038/emboj.2008.39

51. Wang X, Li W, Williams M, Terada N, Alessi DR, Proud CG. 2001. *Regulation of elongation factor 2 kinase by p90(RSK1) and p70 S6 kinase*. Embo j 20: 4370-9. 10.1093/emboj/20.16.4370

52. Beurel E, Grieco SF, Jope RS. 2015. *Glycogen synthase kinase-3 (GSK3): regulation, actions, and diseases*. Pharmacol Ther 148: 114-31. 10.1016/j.pharmthera.2014.11.016

53. Johanns M, Pyr Dit Ruys S, Houddane A, Vertommen D, Herinckx G, et al. 2017. *Direct and indirect activation of eukaryotic elongation factor 2 kinase by AMP-activated protein kinase*. Cell Signal 36: 212-21. 10.1016/j.cellsig.2017.05.010

54. Romero-Ruiz A, Bautista L, Navarro V, Heras-Garvín A, March-Díaz R, et al. 2012. *Prolyl hydroxylase-dependent modulation of eukaryotic elongation factor 2 activity and protein translation under acute hypoxia*. J Biol Chem 287: 9651-8. 10.1074/jbc.M111.299180

55. Kaelin WG, Jr., Ratcliffe PJ. 2008. *Oxygen sensing by metazoans: the central role of the HIF hydroxylase pathway*. Mol Cell 30: 393-402. 10.1016/j.molcel.2008.04.009

56. Liu R, Proud CG. 2016. *Eukaryotic elongation factor 2 kinase as a drug target in cancer, and in cardiovascular and neurodegenerative diseases*. Acta Pharmacol Sin 37: 285-94. 10.1038/aps.2015.123

57. Leprivier G, Remke M, Rotblat B, Dubuc A, Mateo AR, et al. 2013. *The eEF2 kinase confers resistance to nutrient deprivation by blocking translation elongation*. Cell 153: 1064-79. 10.1016/j.cell.2013.04.055

58. Moore CE, Wang X, Xie J, Pickford J, Barron J, et al. 2016. *Elongation factor 2 kinase promotes cell survival by inhibiting protein synthesis without inducing autophagy*. Cell Signal 28: 284-93. 10.1016/j.cellsig.2016.01.005

59. Xie J, Mikolajek H, Pigott CR, Hooper KJ, Mellows T, et al. 2015. *Molecular Mechanism for the Control of Eukaryotic Elongation Factor 2 Kinase by pH: Role in Cancer Cell Survival*. Mol Cell Biol 35: 1805-24. 10.1128/mcb.00012-15

60. Tekedereli I, Alpay SN, Tavares CD, Cobanoglu ZE, Kaoud TS, et al. 2012. *Targeted silencing of elongation factor 2 kinase suppresses growth and sensitizes tumors to doxorubicin in an orthotopic model of breast cancer*. PLoS One 7: e41171. 10.1371/journal.pone.0041171

61. De Gassart A, Demaria O, Panes R, Zaffalon L, Ryazanov AG, et al. 2016. *Pharmacological eEF2K activation promotes cell death and inhibits cancer progression*. EMBO Rep 17: 1471-84. 10.15252/embr.201642194

62. Faller WJ, Jackson TJ, Knight JR, Ridgway RA, Jamieson T, et al. 2015. *mTORC1-mediated translational elongation limits intestinal tumour initiation and growth*. Nature 517: 497-500. 10.1038/nature13896

63. Tognon C, Knezevich SR, Huntsman D, Roskelley CD, Melnyk N, et al. 2002. *Expression of the ETV6-NTRK3 gene fusion as a primary event in human secretory breast carcinoma*. Cancer Cell 2: 367-76. 10.1016/s1535-6108(02)00180-0

64. Hardie DG. 2011. *AMP-activated protein kinase: an energy sensor that regulates all aspects of cell function*. Genes Dev 25: 1895-908. 10.1101/gad.17420111

65. Matthews MB SN, Hershey JWB 2007. In *Translational Control in Biology and Medicine. Origins and Principles of Translational Control*, ed. SN Matthews MB, Hershey JWB pp. 1-40. Cold Spring Harbor, NY: Cold Spring Harbor Laboratory Press.

66. Liang J, Shao SH, Xu ZX, Hennessy B, Ding Z, et al. 2007. *The energy sensing LKB1-AMPK pathway regulates p27(kip1) phosphorylation mediating the decision to enter autophagy or apoptosis*. Nat Cell Biol 9: 218-24. 10.1038/ncb1537

67. Northcott PA, Korshunov A, Witt H, Hielscher T, Eberhart CG, et al. 2011. *Medulloblastoma comprises four distinct molecular variants*. J Clin Oncol 29: 1408-14. 10.1200/jco.2009.27.4324

68. Verhaak RG, Hoadley KA, Purdom E, Wang V, Qi Y, et al. 2010. *Integrated genomic analysis identifies clinically relevant subtypes of glioblastoma characterized by abnormalities in PDGFRA, IDH1, EGFR, and NF1*. Cancer Cell 17: 98-110. 10.1016/j.ccr.2009.12.020

69. Wu X, Northcott PA, Dubuc A, Dupuy AJ, Shih DJ, et al. 2012. *Clonal selection drives genetic divergence of metastatic medulloblastoma*. Nature 482: 529-33. 10.1038/nature10825

70. Chu HP, Liao Y, Novak JS, Hu Z, Merkin JJ, et al. 2014. *Germline quality control: eEF2K stands guard to eliminate defective oocytes*. Dev Cell 28: 561-72. 10.1016/j.devcel.2014.01.027

71. Neri D, Supuran CT. 2011. *Interfering with pH regulation in tumours as a therapeutic strategy*. Nat Rev Drug Discov 10: 767-77. 10.1038/nrd3554

72. Estrella V, Chen T, Lloyd M, Wojtkowiak J, Cornnell HH, et al. 2013. *Acidity generated by the tumor microenvironment drives local invasion*. Cancer Res 73: 1524-35. 10.1158/0008-5472.Can-12-2796

73. Damaghi M, Wojtkowiak JW, Gillies RJ. 2013. *pH sensing and regulation in cancer*. Front Physiol 4: 370. 10.3389/fphys.2013.00370

74. Dorovkov MV, Pavur KS, Petrov AN, Ryazanov AG. 2002. *Regulation of elongation factor-2 kinase by pH*. Biochemistry 41: 13444-50. 10.1021/bi026494p

75. Michiels C. 2004. *Physiological and pathological responses to hypoxia*. Am J Pathol 164: 1875-82. 10.1016/s0002-9440(10)63747-9

76. Connolly E, Braunstein S, Formenti S, Schneider RJ. 2006. *Hypoxia inhibits protein synthesis through a 4E-BP1 and elongation factor 2 kinase pathway controlled by mTOR and uncoupled in breast cancer cells*. Mol Cell Biol 26: 3955-65. 10.1128/mcb.26.10.3955-3965.2006

77. Terai K, Hiramoto Y, Masaki M, Sugiyama S, Kuroda T, et al. 2005. *AMP-activated protein kinase protects cardiomyocytes against hypoxic injury through attenuation of endoplasmic reticulum stress*. Mol Cell Biol 25: 9554-75. 10.1128/mcb.25.21.9554-9575.2005

78. Moore CE, Mikolajek H, Regufe da Mota S, Wang X, Kenney JW, et al. 2015. *Elongation Factor 2 Kinase Is Regulated by Proline Hydroxylation and Protects Cells during Hypoxia*. Mol Cell Biol 35: 1788-804. 10.1128/mcb.01457-14

79. Lehane C, Guelzow T, Zenker S, Erxleben A, Schwer CI, et al. 2013. *Carbimazole is an inhibitor of protein synthesis and protects from neuronal hypoxic damage in vitro*. J Pharmacol Exp Ther 347: 781-93. 10.1124/jpet.113.205989

80. Yu L, Chen Y, Tooze SA. 2018. *Autophagy pathway: Cellular and molecular mechanisms*. Autophagy 14: 207-15. 10.1080/15548627.2017.1378838

81. He C, Klionsky DJ. 2009. *Regulation mechanisms and signaling pathways of autophagy*. Annu Rev Genet 43: 67-93. 10.1146/annurev-genet-102808-114910

82. Glick D, Barth S, Macleod KF. 2010. *Autophagy: cellular and molecular mechanisms*. J Pathol 221: 3-12. 10.1002/path.2697

83. Yorimitsu T, Klionsky DJ. 2005. *Autophagy: molecular machinery for self-eating*. Cell Death Differ 12 Suppl 2: 1542-52. 10.1038/sj.cdd.4401765

84. Khandia R, Dadar M, Munjal A, Dhama K, Karthik K, et al. 2019. *A Comprehensive Review of Autophagy and Its Various Roles in Infectious, Non-Infectious, and Lifestyle Diseases: Current Knowledge and Prospects for Disease Prevention, Novel Drug Design, and Therapy*. Cells 810.3390/cells8070674

85. Levy JMM, Towers CG, Thorburn A. 2017. *Targeting autophagy in cancer*. Nat Rev Cancer 17: 528-42. 10.1038/nrc.2017.53

86. Saftig P, Beertsen W, Eskelinen EL. 2008. *LAMP-2: a control step for phagosome and autophagosome maturation*. Autophagy 4: 510-2. 10.4161/auto.5724

87. Chiang HL, Terlecky SR, Plant CP, Dice JF. 1989. *A role for a 70-kilodalton heat shock protein in lysosomal degradation of intracellular proteins*. Science 246: 382-5. 10.1126/science.2799391

88. Klionsky DJ, Abdelmohsen K, Abe A, Abedin MJ, Abeliovich H, et al. 2016. *Guidelines for the use and interpretation of assays for monitoring autophagy (3rd edition)*. Autophagy 12: 1-222. 10.1080/15548627.2015.1100356

89. Biologicals N. *FAQs - Autophagy and LC3*. Retrieved from https://www.novusbio.com/support/faqs-autophagy-and-lc3

90. Chen HY, White E. 2011. *Role of autophagy in cancer prevention*. Cancer Prev Res (Phila) 4: 973-83. 10.1158/1940-6207.Capr-10-0387

91. Briceño E, Reyes S, Sotelo J. 2003. *Therapy of glioblastoma multiforme improved by the antimutagenic chloroquine*. Neurosurg Focus 14: e3. 10.3171/foc.2003.14.2.4

92. Amaravadi RK, Yu D, Lum JJ, Bui T, Christophorou MA, et al. 2007. *Autophagy inhibition enhances therapy-induced apoptosis in a Myc-induced model of lymphoma*. J Clin Invest 117: 326-36. 10.1172/jci28833

93. Rao S, Tortola L, Perlot T, Wirnsberger G, Novatchkova M, et al. 2014. *A dual role for autophagy in a murine model of lung cancer*. Nat Commun 5: 3056. 10.1038/ncomms4056

94. Rosenfeldt MT, O'Prey J, Morton JP, Nixon C, MacKay G, et al. 2013. *p53 status determines the role of autophagy in pancreatic tumour development*. Nature 504: 296-300. 10.1038/nature12865

95. Yang A, Rajeshkumar NV, Wang X, Yabuuchi S, Alexander BM, et al. 2014. *Autophagy is critical for pancreatic tumor growth and progression in tumors with p53 alterations*. Cancer Discov 4: 905-13. 10.1158/2159-8290.Cd-14-0362

96. Karsli-Uzunbas G, Guo JY, Price S, Teng X, Laddha SV, et al. 2014. *Autophagy is required for glucose homeostasis and lung tumor maintenance*. Cancer Discov 4: 914-27. 10.1158/2159-8290.Cd-14-0363

97. Vogl DT, Stadtmauer EA, Tan KS, Heitjan DF, Davis LE, et al. 2014. *Combined autophagy and proteasome inhibition: a phase 1 trial of hydroxychloroquine and bortezomib in patients with relapsed/refractory myeloma*. Autophagy 10: 1380-90. 10.4161/auto.29264

98. Rangwala R, Leone R, Chang YC, Fecher LA, Schuchter LM, et al. 2014. *Phase I trial of hydroxychloroquine with dose-intense temozolomide in patients with advanced solid tumors and melanoma*. Autophagy 10: 1369-79. 10.4161/auto.29118

99. Rangwala R, Chang YC, Hu J, Algazy KM, Evans TL, et al. 2014. *Combined MTOR and autophagy inhibition: phase I trial of hydroxychloroquine and temsirolimus in patients with advanced solid tumors and melanoma*. Autophagy 10: 1391-402. 10.4161/auto.29119

100. Mahalingam D, Mita M, Sarantopoulos J, Wood L, Amaravadi RK, et al. 2014. *Combined autophagy and HDAC inhibition: a phase I safety, tolerability, pharmacokinetic, and pharmacodynamic analysis of hydroxychloroquine in combination with the HDAC inhibitor vorinostat in patients with advanced solid tumors*. Autophagy 10: 1403-14. 10.4161/auto.29231

101. Mulcahy Levy JM, Zahedi S, Griesinger AM, Morin A, Davies KD, et al. 2017. *Autophagy inhibition overcomes multiple mechanisms of resistance to BRAF inhibition in brain tumors*. Elife 610.7554/eLife.19671

102. Penman CL, Faulkner C, Lowis SP, Kurian KM. 2015. *Current Understanding of BRAF Alterations in Diagnosis, Prognosis, and Therapeutic Targeting in Pediatric Low-Grade Gliomas*. Front Oncol 5: 54. 10.3389/fonc.2015.00054

103. Fan QW, Cheng C, Hackett C, Feldman M, Houseman BT, et al. 2010. *Akt and autophagy cooperate to promote survival of drug-resistant glioma*. Sci Signal 3: ra81. 10.1126/scisignal.2001017

104. Ma XH, Piao SF, Dey S, McAfee Q, Karakousis G, et al. 2014. *Targeting ER stress-induced autophagy overcomes BRAF inhibitor resistance in melanoma*. J Clin Invest 124: 1406-17. 10.1172/jci70454

105. Su KH, Dai C. 2017. *mTORC1 senses stresses: Coupling stress to proteostasis*. Bioessays 3910.1002/bies.201600268

106. Rabanal-Ruiz Y, Otten EG, Korolchuk VI. 2017. *mTORC1 as the main gateway to autophagy*. Essays Biochem 61: 565-84. 10.1042/ebc20170027

107. Dossou AS, Basu A. 2019. *The Emerging Roles of mTORC1 in Macromanaging Autophagy*. Cancers (Basel) 1110.3390/cancers11101422

108. Puente C, Hendrickson RC, Jiang X. 2016. *Nutrient-regulated Phosphorylation of ATG13 Inhibits Starvation-induced Autophagy*. J Biol Chem 291: 6026-35. 10.1074/jbc.M115.689646

109. Tamargo-Gómez I, Mariño G. 2018. *AMPK: Regulation of Metabolic Dynamics in the Context of Autophagy*. Int J Mol Sci 1910.3390/ijms19123812

110. Takeuchi H, Kondo Y, Fujiwara K, Kanzawa T, Aoki H, et al. 2005. *Synergistic augmentation of rapamycin-induced autophagy in malignant glioma cells by phosphatidylinositol 3-kinase/protein kinase B inhibitors*. Cancer Res 65: 3336-46. 10.1158/0008-5472.Can-04-3640

111. Egan DF, Shackelford DB, Mihaylova MM, Gelino S, Kohnz RA, et al. 2011. *Phosphorylation of ULK1 (hATG1) by AMP-activated protein kinase connects energy sensing to mitophagy*. Science 331: 456-61. 10.1126/science.1196371

112. Ling NXY, Kaczmarek A, Hoque A, Davie E, Ngoei KRW, et al. 2020. *mTORC1 directly inhibits AMPK to promote cell proliferation under nutrient stress*. Nat Metab 2: 41-9. 10.1038/s42255-019-0157-1

113. Wu H, Zhu H, Liu DX, Niu TK, Ren X, et al. 2009. *Silencing of elongation factor-2 kinase potentiates the effect of 2-deoxy-D-glucose against human glioma cells through blunting of autophagy*. Cancer Res 69: 2453-60. 10.1158/0008-5472.Can-08-2872

114. Wu H, Yang JM, Jin S, Zhang H, Hait WN. 2006. *Elongation factor-2 kinase regulates autophagy in human glioblastoma cells*. Cancer Res 66: 3015-23. 10.1158/0008-5472.Can-05-1554

115. Py BF, Boyce M, Yuan J. 2009. *A critical role of eEF-2K in mediating autophagy in response to multiple cellular stresses*. Autophagy 5: 393-6. 10.4161/auto.5.3.7762

116. Cheng Y, Ren X, Zhang Y, Shan Y, Huber-Keener KJ, et al. 2013. *Integrated regulation of autophagy and apoptosis by EEF2K controls cellular fate and modulates the efficacy of curcumin and velcade against tumor cells*. Autophagy 9: 208-19. 10.4161/auto.22801

117. Cheng Y, Ren X, Zhang Y, Patel R, Sharma A, et al. 2011. *eEF-2 kinase dictates cross-talk between autophagy and apoptosis induced by Akt Inhibition, thereby modulating cytotoxicity of novel Akt inhibitor MK-2206*. Cancer Res 71: 2654-63. 10.1158/0008-5472.Can-10-2889

118. Cheng Y, Li H, Ren X, Niu T, Hait WN, Yang J. 2010. *Cytoprotective effect of the elongation factor-2 kinase-mediated autophagy in breast cancer cells subjected to growth factor inhibition*. PLoS One 5: e9715. 10.1371/journal.pone.0009715

119. Xie CM, Liu XY, Sham KW, Lai JM, Cheng CH. 2014. *Silencing of EEF2K (eukaryotic elongation factor-2 kinase) reveals AMPK-ULK1-dependent autophagy in colon cancer cells*. Autophagy 10: 1495-508. 10.4161/auto.29164

120. Macherey-Nagel. March 2014. *Plasmid DNA Purification*. Retrieved from https://www.takarabio.com/assets/documents/User%20Manual/NucleoBond%20Xtra%20Plasmid%20DNA%20Purification%20User%20Manual%20(PT4011-1)_Rev_12.pdf

121. Macherey-Nagel. December 2015. *Plasmid DNA Purification*. Retrieved from https://www.labunlimited.com/CAR1/CAR1-LCOM/pdf/LabUnlimited_Macherey_Nagel_NUCLEO%20PLASMID.pdf

122. Technologies L. 2014. *Lipofectamine 3000 Reagent Protocol*. Retrieved from https://www.thermofisher.com/content/dam/LifeTech/Documents/PDFs/lipofectamine3000_protocol.pdf

123. Xie J, Shen K, Lenchine RV, Gethings LA, Trim PJ, et al. 2018. *Eukaryotic elongation factor 2 kinase upregulates the expression of proteins implicated in cell migration and cancer cell metastasis*. Int J Cancer 142: 1865-77. 10.1002/ijc.31210

124. Qiagen. June 2015. *QuantiNova Reverse Transcription Kit Handbook*. Retrieved from https://www.qiagen.com/au/resources/resourcedetail?id=56fde2cb-deb6-4497-9680-edd2a3b98f72&lang=en

125. Biosystems A. July 2010. *Fast SYBR Green Master Mix*. https://assets.thermofisher.com/TFS-Assets/LSG/manuals/cms_046776.pdf

126. Promega. November 2018. *Glucose Uptake-Glo Assay*. Retrieved from https://www.promega.com.au/-/media/files/resources/protocols/technical-manuals/101/tm467-glucose-uptakeglo-assay.pdf?la=en

127. Promega. September 2015. *Dual-Glo Luciferase Assay System*. https://www.promega.com.au/-/media/files/resources/protocols/technical-manuals/0/dual-glo-luciferase-assay-system-protocol.pdf?la=en

128. Xie J, de Souza Alves V, von der Haar T, O'Keefe L, Lenchine RV, et al. 2019. *Regulation of the Elongation Phase of Protein Synthesis Enhances Translation Accuracy and Modulates Lifespan*. Curr Biol 29: 737-49.e5. 10.1016/j.cub.2019.01.029

129. Technology CS. October 2012. *BrdU Cell Proliferation Protocol*. https://www.cellsignal.com/contents/resources-protocols/brdu-cell-proliferation-protocol/6813-brdu-kit

130. Promega. August 2019. *CellTox Green Cytotoxicity Assay*. https://www.promega.com/-/media/files/resources/protocols/technical-manuals/101/celltox-green-cytotoxicity-assay-protocol.pdf

131. Promega. March 2016. *RealTime-Glo MT Cell Viability Assay*. https://www.promega.com.au/-/media/files/resources/protocols/technical-manuals/101/realtimeglo-mt-cell-viability-assay-protocol.pdf?la=en

132. Promega. January 2019. *Caspase-Glo 3/7 Assay*. https://www.promega.com/-/media/files/resources/protocols/technical-bulletins/101/caspase-glo-3-7-assay-protocol.pdf

133. Promega. March 2015. *Caspase-Glo 8 Assay*. https://www.promega.com/-/media/files/resources/protocols/technical-bulletins/101/caspase-glo-8-assay-protocol.pdf?la=en

134. Promega. October 2018. *Cell-Titre Glo 2.0 Assay*. https://www.promega.com/-/media/files/resources/protocols/technical-manuals/101/celltiterglo-2-0-assay-protocol.pdf?la=en

135. Bio-Rad. 2020. *Magic Red Cathepsin Assays*. https://immunochemistry.com/wp-content/uploads/2016/05/F18-937-14-E-Manual.pdf

136. Fischer T. January 2013. *LysoTracker® and LysoSensor™ Probes*. Retrieved from https://www.thermofisher.com/document-connect/document-connect.html?url=https%3A%2F%2Fassets.thermofisher.com%2FTFS-Assets%2FLSG%2Fmanuals%2Fmp07525.pdf&title=THlzb1RyYWNrZXIgYW5kIEx5c29TZW5zb3IgUHJvYmVz

137. Technologies L. February 2014. *GeneArt CRISPR Nuclease Vector Kit*. Retrieved from https://www.thermofisher.com/document-connect/document-connect.html?url=https%3A%2F%2Fassets.thermofisher.com%2FTFS-Assets%2FLSG%2Fmanuals%2Fgeneart_CRISPR_man.pdf&title=R2VuZUFydCBDUklTUFIgTnVjbGVhc2UgVmVjdG9yIEtpdA==

138. Scientific T. 2015. *Thermo Scientific GeneJET Gel Extraction Kit*. Retrieved from https://assets.thermofisher.com/TFS-Assets/LSG/manuals/MAN0012661_GeneJET_Gel_Extraction_UG.pdf

139. Lonza. 2017. *4-D Nucleofector Protocol for MDA-MB-231 Cells*. Retrieved from https://knowledge.lonza.com/cell?id=815

140. Lonza. 2015. *4-D Nucleofector Protocol for PC3 Cells*. https://knowledge.lonza.com/cell?id=125&search=pc3

141. Invitrogen. November 2011. *Dynabeads C4 Positive Isolation Kit*. Retrieved from https://www.thermofisher.com/document-connect/document-connect.html?url=https%3A%2F%2Fassets.thermofisher.com%2FTFS-Assets%2FLSG%2Fmanuals%2FDynabeadsCD4PositiveIsolationKit_man.pdf&title=RHluYWwgQ0Q0IFBvc2l0aXZlIElzb2xhdGlvbiBLaXQ=

142. Lucigen. Novermber 2018. *QuickExtract DNA Extraction Solution*. Retrieved from https://www.lucigen.com/docs/manuals/MA150E-QuickExtract-DNA-Solution.pdf

143. Zeidan B, Manousopoulou A, Garay-Baquero DJ, White CH, Larkin SET, et al. 2018. *Increased circulating resistin levels in early-onset breast cancer patients of normal body mass index correlate with lymph node negative involvement and longer disease free survival: a multi-center POSH cohort serum proteomics study*. Breast Cancer Res 20: 19. 10.1186/s13058-018-0938-6

144. Humphrey SJ, Karayel O, James DE, Mann M. 2018. *High-throughput and high-sensitivity phosphoproteomics with the EasyPhos platform*. Nat Protoc 13: 1897-916. 10.1038/s41596-018-0014-9

145. Tyanova S, Temu T, Cox J. 2016. *The MaxQuant computational platform for mass spectrometry-based shotgun proteomics*. Nat Protoc 11: 2301-19. 10.1038/nprot.2016.136

146. Tyanova S, Temu T, Sinitcyn P, Carlson A, Hein MY, et al. 2016. *The Perseus computational platform for comprehensive analysis of (prote)omics data*. Nat Methods 13: 731-40. 10.1038/nmeth.3901

147. Agilent. January 2018. *How to Hydrate an Agilent Seahorse XFp Sensor Cartridge*. Retrieved from https://www.agilent.com/cs/library/usermanuals/public/Hydrating_an_XFp_Sensor_Cartridge.pdf

148. Agilent. June 2017. *Seeding Adherent cells in Agilent Seahorse XFp cell Culture Miniplates*. Retrieved from https://www.agilent.com/cs/library/usermanuals/public/Seeding%20Adherent%20Cells%20in%20XFp%20Cell%20Culture%20Miniplates.pdf

149. Agilent. April 2018. *Preparation of XF Assay Media*. Retrieved from https://www.agilent.com/cs/library/usermanuals/public/XFe96_DAY_OF_MEDIA_PREP.pdf

150. Agilent. March 2017. *Agilent Seahorse XFp Cell Energy Phenotype Test Kit*. https://www.agilent.com/cs/library/usermanuals/public/XFp_Cell_Energy_Phenotype_Test_Kit_User_Guide.pdf

151. Agilent. October 2019. *Agilent Seahorse XFp Glycolysis Stress Test Kit*. Retrieved from https://www.agilent.com/cs/library/usermanuals/public/XFp_Glycolysis_Stress_Test_User_Guide%20Rev_D.pdf

152. Agilent. April 2019. *Agilent Seahorse XFp Cell Mito Stress Test Kit*. Retrieved from https://www.agilent.com/cs/library/usermanuals/public/XFp_Cell_Mito_Stress_Test_Kit_User_Guide.pdf

153. Agilent. January 2018. *How to Hydrate an Agilent Seahorse XFe96 Sensor Cartridge*. Retrieved from https://www.agilent.com/cs/library/usermanuals/public/XFe96_DAY_BEFORE_CARTRIDGE_HYDRATION.pdf

154. Agilent. April 2019. *Seeding Adherent Cells in Agilent Seahorse XF96 Tissue Culture Microplates*. https://www.agilent.com/cs/library/usermanuals/public/XFe96_DAY_BEFORE_CELL_SEEDING.pdf

155. Agilent. April 2019. *Washing Adherent Cells in Agilent Seahorse XF96 Cell Culture Microplates*. https://www.agilent.com/cs/library/usermanuals/public/XFe96_DAY_OF_WASHING_CELLS.pdf

156. Agilent. October 2019. *Agilent Seahorse XF Glycolysis Stress Test Kit*. Retrieved from https://www.agilent.com/cs/library/usermanuals/public/XF_Glycolysis_Stress_Test_Kit_User_Guide.pdf

157. Agilent. May 2019. *Agilent Seahorse XF Cell Mito Stress Test Kit*. Retrieved from https://www.agilent.com/cs/library/usermanuals/public/XF_Cell_Mito_Stress_Test_Kit_User_Guide.pdf

158. Wang RX, Xu XE, Huang L, Chen S, Shao ZM. 2019. *eEF2 kinase mediated autophagy as a potential therapeutic target for paclitaxel-resistant triple-negative breast cancer*. Ann Transl Med 7: 783. 10.21037/atm.2019.11.39

159. Pajak B, Siwiak E, Sołtyka M, Priebe A, Zieliński R, et al. 2019. *2-Deoxy-d-Glucose and Its Analogs: From Diagnostic to Therapeutic Agents*. Int J Mol Sci 2110.3390/ijms21010234

160. Tanida I, Ueno T, Kominami E. 2008. *LC3 and Autophagy*. Methods Mol Biol 445: 77-88. 10.1007/978-1-59745-157-4_4

161. Leprivier G, Rotblat B, Khan D, Jan E, Sorensen PH. 2015. *Stress-mediated translational control in cancer cells*. Biochim Biophys Acta 1849: 845-60. 10.1016/j.bbagrm.2014.11.002

162. Liu JC, Voisin V, Wang S, Wang DY, Jones RA, et al. 2014. *Combined deletion of Pten and p53 in mammary epithelium accelerates triple-negative breast cancer with dependency on eEF2K*. EMBO Mol Med 6: 1542-60. 10.15252/emmm.201404402

163. Fu LL, Xie T, Zhang SY, Liu B. 2014. *Eukaryotic elongation factor-2 kinase (eEF2K): a potential therapeutic target in cancer*. Apoptosis 19: 1527-31. 10.1007/s10495-014-1019-7

164. Shingu T, Fujiwara K, Bögler O, Akiyama Y, Moritake K, et al. 2009. *Inhibition of autophagy at a late stage enhances imatinib-induced cytotoxicity in human malignant glioma cells*. Int J Cancer 124: 1060-71. 10.1002/ijc.24030

165. Liu D, Yang Y, Liu Q, Wang J. 2011. *Inhibition of autophagy by 3-MA potentiates cisplatin-induced apoptosis in esophageal squamous cell carcinoma cells*. Med Oncol 28: 105-11. 10.1007/s12032-009-9397-3

166. Zheng L, Li H, Mo Y, Qi G, Liu B, Zhao J. 2017. *Autophagy inhibition sensitizes LY3023414-induced anti-glioma cell activity in vitro and in vivo*. Oncotarget 8: 98964-73. 10.18632/oncotarget.22147

167. Selvakumaran M, Amaravadi RK, Vasilevskaya IA, O'Dwyer PJ. 2013. *Autophagy inhibition sensitizes colon cancer cells to antiangiogenic and cytotoxic therapy*. Clin Cancer Res 19: 2995-3007. 10.1158/1078-0432.Ccr-12-1542

168. Gammoh N, Fraser J, Puente C, Syred HM, Kang H, et al. 2016. *Suppression of autophagy impedes glioblastoma development and induces senescence*. Autophagy 12: 1431-9. 10.1080/15548627.2016.1190053

169. Solomon VR, Lee H. 2009. *Chloroquine and its analogs: a new promise of an old drug for effective and safe cancer therapies*. Eur J Pharmacol 625: 220-33. 10.1016/j.ejphar.2009.06.063

170. Savarino A, Lucia MB, Giordano F, Cauda R. 2006. *Risks and benefits of chloroquine use in anticancer strategies*. Lancet Oncol 7: 792-3. 10.1016/s1470-2045(06)70875-0

171. Cailleau R, Young R, Olivé M, Reeves WJ, Jr. 1974. *Breast Tumor Cell Lines From Pleural Effusions2*. JNCI: Journal of the National Cancer Institute 53: 661-74. 10.1093/jnci/53.3.661

172. Carey LA, Perou CM, Livasy CA, Dressler LG, Cowan D, et al. 2006. *Race, breast cancer subtypes, and survival in the Carolina Breast Cancer Study*. Jama 295: 2492-502. 10.1001/jama.295.21.2492

173. Rakha EA, El-Rehim DA, Paish C, Green AR, Lee AH, et al. 2006. *Basal phenotype identifies a poor prognostic subgroup of breast cancer of clinical importance*. Eur J Cancer 42: 3149-56. 10.1016/j.ejca.2006.08.015

174. Welsh J. 2013. In *Animal Models for the Study of Human Disease*. *Chapter 40 - Animal Models for Studying Prevention and Treatment of Breast Cancer*, pp. 997-1018: Science Direct. https://doi.org/10.1016/B978-0-12-415894-8.00040-3

175. Davies SP, Reddy H, Caivano M, Cohen P. 2000. *Specificity and mechanism of action of some commonly used protein kinase inhibitors*. Biochem J 351: 95-105. 10.1042/0264-6021:3510095

176. Chen Z, Gopalakrishnan SM, Bui MH, Soni NB, Warrior U, et al. 2011. *1-Benzyl-3-cetyl-2-methylimidazolium iodide (NH125) induces phosphorylation of eukaryotic elongation factor-2 (eEF2): a cautionary note on the anticancer mechanism of an eEF2 kinase inhibitor*. J Biol Chem 286: 43951-8. 10.1074/jbc.M111.301291

177. Devkota AK, Tavares CD, Warthaka M, Abramczyk O, Marshall KD, et al. 2012. *Investigating the kinetic mechanism of inhibition of elongation factor 2 kinase by*

NH125: evidence of a common in vitro artifact. Biochemistry 51: 2100-12. 10.1021/bi201787p

178. Devkota AK, Warthaka M, Edupuganti R, Tavares CD, Johnson WH, et al. 2014. *High-throughput screens for eEF-2 kinase*. J Biomol Screen 19: 445-52. 10.1177/1087057113505204

179. Gschwendt M, Kittstein W, Marks F. 1994. *Elongation factor-2 kinase: effective inhibition by the novel protein kinase inhibitor rottlerin and relative insensitivity towards staurosporine*. FEBS Lett 338: 85-8. 10.1016/0014-5793(94)80121-5

180. Soltoff SP. 2007. *Rottlerin: an inappropriate and ineffective inhibitor of PKCdelta*. Trends Pharmacol Sci 28: 453-8. 10.1016/j.tips.2007.07.003

181. Kruiswijk F, Yuniati L, Magliozzi R, Low TY, Lim R, et al. 2012. *Coupled activation and degradation of eEF2K regulates protein synthesis in response to genotoxic stress*. Sci Signal 5: ra40. 10.1126/scisignal.2002718

182. Yamamoto A, Tagawa Y, Yoshimori T, Moriyama Y, Masaki R, Tashiro Y. 1998. *Bafilomycin A1 prevents maturation of autophagic vacuoles by inhibiting fusion between autophagosomes and lysosomes in rat hepatoma cell line, H-4-II-E cells*. Cell Struct Funct 23: 33-42. 10.1247/csf.23.33

183. Alan J. Barrett HK. 1981. In *Methods in Enzymology. [41] Cathepsin B, cathepsin H, and cathepsin L*, pp. 535-61: Elsevier. https://doi.org/10.1016/S0076-6879(81)80043-2

184. Sánchez-Martín P, Komatsu M. 2018. *p62/SQSTM1 – steering the cell through health and disease*. Journal of Cell Science 131: jcs222836. 10.1242/jcs.222836

185. Yoshii SR, Mizushima N. 2017. *Monitoring and Measuring Autophagy*. Int J Mol Sci 1810.3390/ijms18091865

186. Ichimura Y, Komatsu M. 2010. *Selective degradation of p62 by autophagy*. Semin Immunopathol 32: 431-6. 10.1007/s00281-010-0220-1

187. Tai S, Sun Y, Squires JM, Zhang H, Oh WK, et al. 2011. *PC3 is a cell line characteristic of prostatic small cell carcinoma*. Prostate 71: 1668-79. 10.1002/pros.21383

188. Wu Y, Xie J, Xin J, Lenchine RV, Wang X, et al. 2020. *eEF2K enhances expression of PD-L1 by promoting the translation of its mRNA*. Biochem J 10.1042/bcj20200697

189. Benchling. 2020. *Biology Software*. Retrieved from https://benchling.com.

190. Sanchez M, Lin Y, Yang CC, McQuary P, Rosa Campos A, et al. 2019. *Cross Talk between eIF2α and eEF2 Phosphorylation Pathways Optimizes Translational*

Arrest in Response to Oxidative Stress. iScience 20: 466-80. 10.1016/j.isci.2019.09.031

191. Genetics D. 2020. *TIDE: Tracking of Indels by DEcomposition*. Retrieved from https://tide.deskgen.com/

192. McLeod LE, Proud CG. 2002. *ATP depletion increases phosphorylation of elongation factor eEF2 in adult cardiomyocytes independently of inhibition of mTOR signalling*. FEBS Lett 531: 448-52. 10.1016/s0014-5793(02)03582-2

193. Ruvinsky I, Sharon N, Lerer T, Cohen H, Stolovich-Rain M, et al. 2005. *Ribosomal protein S6 phosphorylation is a determinant of cell size and glucose homeostasis*. Genes Dev 19: 2199-211. 10.1101/gad.351605

194. Fedele AO, Proud CG. 2020. *Chloroquine and bafilomycin A mimic lysosomal storage disorders and impair mTORC1 signalling*. Biosci Rep 4010.1042/bsr20200905

195. Fischer T. 2017. *eBioscience™ Propidium Iodide*. Retrieved from https://www.thermofisher.com/order/catalog/product/BMS500PI?SID=srch-srp-BMS500PI#/BMS500PI?SID=srch-srp-BMS500PI

196. Fischer T. March 2017. *Technical Datasheet - eBioscience Calcein™ AM Viability Dye (UltraPure Grade)*. Retrieved from https://www.thermofisher.com/order/catalog/product/65-0853-78#/65-0853-78

197. Majno G, Joris I. 1995. *Apoptosis, oncosis, and necrosis. An overview of cell death*. Am J Pathol 146: 3-15.

198. Elmore S. 2007. *Apoptosis: a review of programmed cell death*. Toxicol Pathol 35: 495-516. 10.1080/01926230701320337

199. Proskuryakov SY, Konoplyannikov AG, Gabai VL. 2003. *Necrosis: a specific form of programmed cell death?* Exp Cell Res 283: 1-16. 10.1016/s0014-4827(02)00027-7

200. Tawa P, Hell K, Giroux A, Grimm E, Han Y, et al. *Catalytic activity of caspase-3 is required for its degradation: stabilization of the active complex by synthetic inhibitors*.

201. Suzuki Y, Nakabayashi Y, Takahashi R. 2001. *Ubiquitin-protein ligase activity of X-linked inhibitor of apoptosis protein promotes proteasomal degradation of caspase-3 and enhances its anti-apoptotic effect in Fas-induced cell death*. Proc Natl Acad Sci U S A 98: 8662-7. 10.1073/pnas.161506698

202. Tummers B, Green DR. 2017. *Caspase-8: regulating life and death*. Immunol Rev 277: 76-89. 10.1111/imr.12541

203. Someda M, Kuroki S, Miyachi H, Tachibana M, Yonehara S. 2020. *Caspase-8, receptor-interacting protein kinase 1 (RIPK1), and RIPK3 regulate retinoic acid-induced cell differentiation and necroptosis*. Cell Death Differ 27: 1539-53. 10.1038/s41418-019-0434-2

204. Fritsch M, Günther SD, Schwarzer R, Albert MC, Schorn F, et al. 2019. *Caspase-8 is the molecular switch for apoptosis, necroptosis and pyroptosis*. Nature 575: 683-7. 10.1038/s41586-019-1770-6

205. Beaudouin J, Liesche C, Aschenbrenner S, Hörner M, Eils R. *Caspase-8 cleaves its substrates from the plasma membrane upon CD95-induced apoptosis*.

206. Redmann M, Benavides GA, Berryhill TF, Wani WY, Ouyang X, et al. 2017. *Inhibition of autophagy with bafilomycin and chloroquine decreases mitochondrial quality and bioenergetic function in primary neurons*. Redox Biol 11: 73-81. 10.1016/j.redox.2016.11.004

207. Cheng Y, Ren X, Yuan Y, Shan Y, Li L, et al. 2016. *eEF-2 kinase is a critical regulator of Warburg effect through controlling PP2A-A synthesis*. Oncogene 35: 6293-308. 10.1038/onc.2016.166

208. Jan A, Jansonius B, Delaidelli A, Bhanshali F, An YA, et al. 2018. *Activity of translation regulator eukaryotic elongation factor-2 kinase is increased in Parkinson disease brain and its inhibition reduces alpha synuclein toxicity*. Acta Neuropathol Commun 6: 54. 10.1186/s40478-018-0554-9

209. Yetkin-Arik B, Vogels IMC, Nowak-Sliwinska P, Weiss A, Houtkooper RH, et al. *The role of glycolysis and mitochondrial respiration in the formation and functioning of endothelial tip cells during angiogenesis*.

210. Peng F, Li Q, Sun JY, Luo Y, Chen M, Bao Y. 2018. *PFKFB3 is involved in breast cancer proliferation, migration, invasion and angiogenesis*. Int J Oncol 52: 945-54. 10.3892/ijo.2018.4257

211. Shen DW, Akiyama S, Schoenlein P, Pastan I, Gottesman MM. 1995. *Characterisation of high-level cisplatin-resistant cell lines established from a human hepatoma cell line and human KB adenocarcinoma cells: cross-resistance and protein changes*. Br J Cancer 71: 676-83. 10.1038/bjc.1995.134

212. McDermott M, Eustace AJ, Busschots S, Breen L, Crown J, et al. 2014. *In vitro Development of Chemotherapy and Targeted Therapy Drug-Resistant Cancer Cell Lines: A Practical Guide with Case Studies*. Front Oncol 4: 40. 10.3389/fonc.2014.00040

213. Breen L, Murphy L, Keenan J, Clynes M. 2008. *Development of taxane resistance in a panel of human lung cancer cell lines*. Toxicol In Vitro 22: 1234-41. 10.1016/j.tiv.2008.04.005

214. Cullen KV, Davey RA, Davey MW. 2001. *Verapamil-stimulated glutathione transport by the multidrug resistance-associated protein (MRP1) in leukaemia cells*. Biochem Pharmacol 62: 417-24. 10.1016/s0006-2952(01)00681-5

215. Davey RA, Longhurst TJ, Davey MW, Belov L, Harvie RM, et al. 1995. *Drug resistance mechanisms and MRP expression in response to epirubicin treatment in a human leukaemia cell line*. Leuk Res 19: 275-82. 10.1016/0145-2126(94)00159-8

216. Liang XJ, Shen DW, Garfield S, Gottesman MM. 2003. *Mislocalization of membrane proteins associated with multidrug resistance in cisplatin-resistant cancer cell lines*. Cancer Res 63: 5909-16.

217. Akiyama S, Fojo A, Hanover JA, Pastan I, Gottesman MM. 1985. *Isolation and genetic characterization of human KB cell lines resistant to multiple drugs*. Somat Cell Mol Genet 11: 117-26. 10.1007/bf01534700

218. Barr MP, Gray SG, Hoffmann AC, Hilger RA, Thomale J, et al. 2013. *Generation and characterisation of cisplatin-resistant non-small cell lung cancer cell lines displaying a stem-like signature*. PLoS One 8: e54193. 10.1371/journal.pone.0054193

219. Sherman-Baust CA, Becker KG, Wood Iii WH, Zhang Y, Morin PJ. *Gene expression and pathway analysis of ovarian cancer cells selected for resistance to cisplatin, paclitaxel, or doxorubicin*.

220. Locke VL, Davey RA, Davey MW. 1999. *Altered drug sensitivity in response to idarubicin treatment in K562 human leukaemia cells*. Br J Haematol 106: 86-91. 10.1046/j.1365-2141.1999.01494.x

221. Stordal BK, Davey MW, Davey RA. 2006. *Oxaliplatin induces drug resistance more rapidly than cisplatin in H69 small cell lung cancer cells*. Cancer Chemother Pharmacol 58: 256-65. 10.1007/s00280-005-0148-7

222. Stordal B, Peters G, Davey R. 2006. *Similar chromosomal changes in cisplatin and oxaliplatin-resistant sublines of the H69 SCLC cell line are not associated with platinum resistance*. Genes Chromosomes Cancer 45: 1094-105. 10.1002/gcc.20373

223. Ma J, Maliepaard M, Kolker HJ, Verweij J, Schellens JH. 1998. *Abrogated energy-dependent uptake of cisplatin in a cisplatin-resistant subline of the human ovarian cancer cell line IGROV-1*. Cancer Chemother Pharmacol 41: 186-92. 10.1007/s002800050727

224. Poole B, Ohkuma S. 1981. *Effect of weak bases on the intralysosomal pH in mouse peritoneal macrophages*. J Cell Biol 90: 665-9. 10.1083/jcb.90.3.665

225. Berg JM TJ, Stryer L. 2002. *Section 22.4, Fatty Acids Are Synthesized and Degraded by Different Pathways*: W H Freeman.

226. Kursula P, Sikkilä H, Fukao T, Kondo N, Wierenga RK. 2005. *High resolution crystal structures of human cytosolic thiolase (CT): a comparison of the active sites of human CT, bacterial thiolase, and bacterial KAS I*. J Mol Biol 347: 189-201. 10.1016/j.jmb.2005.01.018

227. McAndrew RP, Wang Y, Mohsen AW, He M, Vockley J, Kim JJ. 2008. *Structural basis for substrate fatty acyl chain specificity: crystal structure of human very-long-chain acyl-CoA dehydrogenase*. J Biol Chem 283: 9435-43. 10.1074/jbc.M709135200

228. Lazarus MB, Levin RS, Shokat KM. 2017. *Discovery of new substrates of the elongation factor-2 kinase suggests a broader role in the cellular nutrient response*. Cell Signal 29: 78-83. 10.1016/j.cellsig.2016.10.006

229. Sonenberg N, Hinnebusch AG. 2009. *Regulation of translation initiation in eukaryotes: mechanisms and biological targets*. Cell 136: 731-45. 10.1016/j.cell.2009.01.042

230. Sonenberg N, Dever TE. 2003. *Eukaryotic translation initiation factors and regulators*. Curr Opin Struct Biol 13: 56-63. 10.1016/s0959-440x(03)00009-5

231. Dobrikov M, Dobrikova E, Shveygert M, Gromeier M. 2011. *Phosphorylation of eukaryotic translation initiation factor 4G1 (eIF4G1) by protein kinase C{alpha} regulates eIF4G1 binding to Mnk1*. Mol Cell Biol 31: 2947-59. 10.1128/mcb.05589-11

232. Jiang X, Feng S, Chen Y, Feng Y, Deng H. 2016. *Proteomic analysis of mTOR inhibition-mediated phosphorylation changes in ribosomal proteins and eukaryotic translation initiation factors*. Protein Cell 7: 533-7. 10.1007/s13238-016-0279-0

233. Raman N, Nayak A, Muller S. 2014. *mTOR signaling regulates nucleolar targeting of the SUMO-specific isopeptidase SENP3*. Mol Cell Biol 34: 4474-84. 10.1128/mcb.00801-14

234. Antonia RJ, Castillo J, Herring LE, Serafin DS, Liu P, et al. 2019. *TBK1 Limits mTORC1 by Promoting Phosphorylation of Raptor Ser877*. Sci Rep 9: 13470. 10.1038/s41598-019-49707-8

235. Barilari M, Bonfils G, Treins C, Koka V, De Villeneuve D, et al. 2017. *ZRF1 is a novel S6 kinase substrate that drives the senescence programme*. Embo j 36: 736-50. 10.15252/embj.201694966

236. Prabhu AV, Luu W, Sharpe LJ, Brown AJ. 2017. *Phosphorylation regulates activity of 7-dehydrocholesterol reductase (DHCR7), a terminal enzyme of cholesterol synthesis*. J Steroid Biochem Mol Biol 165: 363-8. 10.1016/j.jsbmb.2016.08.003

237. Eguchi S, Oshiro N, Miyamoto T, Yoshino K, Okamoto S, et al. 2009. *AMP-activated protein kinase phosphorylates glutamine : fructose-6-phosphate amidotransferase 1 at Ser243 to modulate its enzymatic activity*. Genes Cells 14: 179-89. 10.1111/j.1365-2443.2008.01260.x

238. Hunger-Glaser I, Salazar EP, Sinnett-Smith J, Rozengurt E. 2003. *Bombesin, lysophosphatidic acid, and epidermal growth factor rapidly stimulate focal adhesion kinase phosphorylation at Ser-910: requirement for ERK activation*. J Biol Chem 278: 22631-43. 10.1074/jbc.M210876200

239. Wek RC, Staschke KA. 2010. *How do tumours adapt to nutrient stress?* Embo j 29: 1946-7. 10.1038/emboj.2010.110

240. Kartal-Yandim M, Adan-Gokbulut A, Baran Y. 2016. *Molecular mechanisms of drug resistance and its reversal in cancer*. Crit Rev Biotechnol 36: 716-26. 10.3109/07388551.2015.1015957

241. Ye J, Kumanova M, Hart LS, Sloane K, Zhang H, et al. 2010. *The GCN2-ATF4 pathway is critical for tumour cell survival and proliferation in response to nutrient deprivation*. Embo j 29: 2082-96. 10.1038/emboj.2010.81

242. Golej DL, Askari B, Kramer F, Barnhart S, Vivekanandan-Giri A, et al. 2011. *Long-chain acyl-CoA synthetase 4 modulates prostaglandin E_2 release from human arterial smooth muscle cells*. J Lipid Res 52: 782-93. 10.1194/jlr.M013292

243. Hur MW, Edenberg HJ. 1992. *Cloning and characterization of the ADH5 gene encoding human alcohol dehydrogenase 5, formaldehyde dehydrogenase*. Gene 121: 305-11. 10.1016/0378-1119(92)90135-c

244. Vander Heiden MG, Cantley LC, Thompson CB. 2009. *Understanding the Warburg effect: the metabolic requirements of cell proliferation*. Science 324: 1029-33. 10.1126/science.1160809

245. Warburg O, Wind F, Negelein E. 1927. *THE METABOLISM OF TUMORS IN THE BODY*. J Gen Physiol 8: 519-30. 10.1085/jgp.8.6.519

246. Coppel RL, McNeilage LJ, Surh CD, Van de Water J, Spithill TW, et al. 1988. *Primary structure of the human M2 mitochondrial autoantigen of primary biliary cirrhosis: dihydrolipoamide acetyltransferase*. Proc Natl Acad Sci U S A 85: 7317-21. 10.1073/pnas.85.19.7317

247. Rao DR, Oesper P. 1961. *Purification and properties of muscle phosphoglycerate kinase*. Biochem J 81: 405-11. 10.1042/bj0810405

248. Palm W, Park Y, Wright K, Pavlova NN, Tuveson DA, Thompson CB. 2015. *The Utilization of Extracellular Proteins as Nutrients Is Suppressed by mTORC1*. Cell 162: 259-70. 10.1016/j.cell.2015.06.017

249. Khan MW, Layden BT, Chakrabarti P. 2018. *Inhibition of mTOR complexes protects cancer cells from glutamine starvation induced cell death by restoring Akt stability*. Biochim Biophys Acta Mol Basis Dis 1864: 2040-52. 10.1016/j.bbadis.2018.03.013

250. Kapuy O, Vinod PK, Bánhegyi G. 2014. *mTOR inhibition increases cell viability via autophagy induction during endoplasmic reticulum stress - An experimental and modeling study*. FEBS Open Bio 4: 704-13. 10.1016/j.fob.2014.07.006

251. Steeg PS. *Tumor metastasis: mechanistic insights and clinical challenges*.

252. Siegel RL, Miller KD, Jemal A. 2016. *Cancer statistics, 2016*. CA Cancer J Clin 66: 7-30. 10.3322/caac.21332

253. Jemal A, Siegel R, Ward E, Murray T, Xu J, et al. 2006. *Cancer statistics, 2006*. CA Cancer J Clin 56: 106-30. 10.3322/canjclin.56.2.106

254. Le Dévédec SE, Yan K, de Bont H, Ghotra V, Truong H, et al. *Systems microscopy approaches to understand cancer cell migration and metastasis*.

255. Vignjevic D, Montagnac G. 2008. *Reorganisation of the dendritic actin network during cancer cell migration and invasion*. Semin Cancer Biol 18: 12-22. 10.1016/j.semcancer.2007.08.001

256. Tahtamouni L, Ahram M, Koblinski J, Rolfo C. *Molecular Regulation of Cancer Cell Migration, Invasion, and Metastasis*.

257. Valastyan S, Weinberg RA. 2011. *Tumor metastasis: molecular insights and evolving paradigms*. Cell 147: 275-92. 10.1016/j.cell.2011.09.024

258. Chabner BA, Roberts TG. *Chemotherapy and the war on cancer*.

259. Hamurcu Z, Ashour A, Kahraman N, Ozpolat B. 2016. *FOXM1 regulates expression of eukaryotic elongation factor 2 kinase and promotes proliferation, invasion and tumorgenesis of human triple negative breast cancer cells*. Oncotarget 7: 16619-35. 10.18632/oncotarget.7672

260. Bayraktar R, Pichler M, Kanlikilicer P, Ivan C, Bayraktar E, et al. 2017. *MicroRNA 603 acts as a tumor suppressor and inhibits triple-negative breast cancer tumorigenesis by targeting elongation factor 2 kinase*. Oncotarget 8: 11641-58. 10.18632/oncotarget.14264

261. Shi Q, Xu X, Liu Q, Luo F, Shi J, He X. 2016. *MicroRNA-877 acts as a tumor suppressor by directly targeting eEF2K in renal cell carcinoma*. Oncol Lett 11: 1474-80. 10.3892/ol.2015.4072

262. Huttenlocher A, Horwitz AR. 2011. *Integrins in cell migration*. Cold Spring Harb Perspect Biol 3: a005074. 10.1101/cshperspect.a005074

263. Kapur M, Ackerman SL. 2018. *mRNA Translation Gone Awry: Translation Fidelity and Neurological Disease*. Trends Genet 34: 218-31. 10.1016/j.tig.2017.12.007

264. Ke Z, Mallik P, Johnson AB, Luna F, Nevo E, et al. 2017. *Translation fidelity coevolves with longevity*. Aging Cell 16: 988-93. 10.1111/acel.12628

265. Drummond DA, Wilke CO. 2008. *Mistranslation-induced protein misfolding as a dominant constraint on coding-sequence evolution*. Cell 134: 341-52. 10.1016/j.cell.2008.05.042

266. Zoncu R, Efeyan A, Sabatini DM. *mTOR: from growth signal integration to cancer, diabetes and ageing*.

267. Saxton RA, Sabatini DM. 2017. *mTOR Signaling in Growth, Metabolism, and Disease*. Cell 169: 361-71. 10.1016/j.cell.2017.03.035

268. Conn CS, Qian SB. 2013. *Nutrient signaling in protein homeostasis: an increase in quantity at the expense of quality*. Sci Signal 6: ra24. 10.1126/scisignal.2003520

269. Sherman MY, Qian SB. 2013. *Less is more: improving proteostasis by translation slow down*. Trends Biochem Sci 38: 585-91. 10.1016/j.tibs.2013.09.003

270. Redpath NT, Foulstone EJ, Proud CG. 1996. *Regulation of translation elongation factor-2 by insulin via a rapamycin-sensitive signalling pathway*. Embo j 15: 2291-7.

271. Inoki K, Li Y, Zhu T, Wu J, Guan KL. 2002. *TSC2 is phosphorylated and inhibited by Akt and suppresses mTOR signalling*. Nat Cell Biol 4: 648-57. 10.1038/ncb839

272. Zavialov AV, Ehrenberg M. 2003. *Peptidyl-tRNA regulates the GTPase activity of translation factors*. Cell 114: 113-22. 10.1016/s0092-8674(03)00478-1

273. Jewett MC, Miller ML, Chen Y, Swartz JR. 2009. *Continued protein synthesis at low [ATP] and [GTP] enables cell adaptation during energy limitation*. J Bacteriol 191: 1083-91. 10.1128/jb.00852-08

274. Kaziro Y, Itoh H, Kozasa T, Nakafuku M, Satoh T. 1991. *Structure and function of signal-transducing GTP-binding proteins*. Annu Rev Biochem 60: 349-400. 10.1146/annurev.bi.60.070191.002025

275. Gorres KL, Raines RT. 2010. *Prolyl 4-hydroxylase*. Crit Rev Biochem Mol Biol 45: 106-24. 10.3109/10409231003627991

276. Vaupel P, Mayer A. 2007. *Hypoxia in cancer: significance and impact on clinical outcome*. Cancer Metastasis Rev 26: 225-39. 10.1007/s10555-007-9055-1

277. International AsD. September 2016. *World Alzheimer's Report 2016*. Retrieved from https://www.alz.co.uk/research/WorldAlzheimerReport2016.pdf

278. Selkoe DJ. 2001. *Alzheimer's disease: genes, proteins, and therapy*. Physiol Rev 81: 741-66. 10.1152/physrev.2001.81.2.741

279. Selkoe DJ, Schenk D. 2003. *Alzheimer's disease: molecular understanding predicts amyloid-based therapeutics*. Annu Rev Pharmacol Toxicol 43: 545-84. 10.1146/annurev.pharmtox.43.100901.140248

280. Haass C, Selkoe DJ. 2007. *Soluble protein oligomers in neurodegeneration: lessons from the Alzheimer's amyloid beta-peptide*. Nat Rev Mol Cell Biol 8: 101-12. 10.1038/nrm2101

281. Lambert MP, Barlow AK, Chromy BA, Edwards C, Freed R, et al. 1998. *Diffusible, nonfibrillar ligands derived from Abeta1-42 are potent central nervous system neurotoxins*. Proc Natl Acad Sci U S A 95: 6448-53. 10.1073/pnas.95.11.6448

282. Walsh DM, Hartley DM, Kusumoto Y, Fezoui Y, Condron MM, et al. 1999. *Amyloid beta-protein fibrillogenesis. Structure and biological activity of protofibrillar intermediates*. J Biol Chem 274: 25945-52. 10.1074/jbc.274.36.25945

283. Selkoe DJ. 2008. *Soluble oligomers of the amyloid beta-protein impair synaptic plasticity and behavior*. Behav Brain Res 192: 106-13. 10.1016/j.bbr.2008.02.016

284. Wang HW, Pasternak JF, Kuo H, Ristic H, Lambert MP, et al. 2002. *Soluble oligomers of beta amyloid (1-42) inhibit long-term potentiation but not long-term depression in rat dentate gyrus*. Brain Res 924: 133-40. 10.1016/s0006-8993(01)03058-x

285. Kessels HW, Nabavi S, Malinow R. 2013. *Metabotropic NMDA receptor function is required for β-amyloid-induced synaptic depression*. Proc Natl Acad Sci U S A 110: 4033-8. 10.1073/pnas.1219605110

286. Li S, Hong S, Shepardson NE, Walsh DM, Shankar GM, Selkoe D. 2009. *Soluble oligomers of amyloid Beta protein facilitate hippocampal long-term depression by disrupting neuronal glutamate uptake*. Neuron 62: 788-801. 10.1016/j.neuron.2009.05.012

287. Heise C, Gardoni F, Culotta L, di Luca M, Verpelli C, Sala C. 2014. *Elongation factor-2 phosphorylation in dendrites and the regulation of dendritic mRNA translation in neurons*. Front Cell Neurosci 8: 35. 10.3389/fncel.2014.00035

288. Sakamoto S, Ishii K, Sasaki M, Hosaka K, Mori T, et al. 2002. *Differences in cerebral metabolic impairment between early and late onset types of Alzheimer's disease*. J Neurol Sci 200: 27-32. 10.1016/s0022-510x(02)00114-4

289. Ma T, Chen Y, Vingtdeux V, Zhao H, Viollet B, et al. 2014. *Inhibition of AMP-activated protein kinase signaling alleviates impairments in hippocampal synaptic plasticity induced by amyloid β*. J Neurosci 34: 12230-8. 10.1523/jneurosci.1694-14.2014

290. Li X, Alafuzoff I, Soininen H, Winblad B, Pei JJ. 2005. *Levels of mTOR and its downstream targets 4E-BP1, eEF2, and eEF2 kinase in relationships with tau in Alzheimer's disease brain*. Febs j 272: 4211-20. 10.1111/j.1742-4658.2005.04833.x

291. Um JW, Kaufman AC, Kostylev M, Heiss JK, Stagi M, et al. 2013. *Metabotropic glutamate receptor 5 is a coreceptor for Alzheimer aβ oligomer bound to cellular prion protein*. Neuron 79: 887-902. 10.1016/j.neuron.2013.06.036

292. Jan A, Jansonius B, Delaidelli A, Somasekharan SP, Bhanshali F, et al. 2017. *eEF2K inhibition blocks Aβ42 neurotoxicity by promoting an NRF2 antioxidant response*. Acta Neuropathol 133: 101-19. 10.1007/s00401-016-1634-1

293. Keith D, El-Husseini A. 2008. *Excitation Control: Balancing PSD-95 Function at the Synapse*. Front Mol Neurosci 1: 4. 10.3389/neuro.02.004.2008

294. Chen DS, Mellman I. 2017. *Elements of cancer immunity and the cancer-immune set point*. Nature 541: 321-30. 10.1038/nature21349

295. Graham S, Levin ML, Lilienfeld AM, Schuman LM, Gibson R, et al. 1966. *Preconception, intrauterine, and postnatal irradiation as related to leukemia*. Natl Cancer Inst Monogr 19: 347-71.

296. Topalian SL, Drake CG, Pardoll DM. 2015. *Immune checkpoint blockade: a common denominator approach to cancer therapy*. Cancer Cell 27: 450-61. 10.1016/j.ccell.2015.03.001

297. Leach DR, Krummel MF, Allison JP. 1996. *Enhancement of antitumor immunity by CTLA-4 blockade*. Science 271: 1734-6. 10.1126/science.271.5256.1734

298. Dong H, Strome SE, Salomao DR, Tamura H, Hirano F, et al. 2002. *Tumor-associated B7-H1 promotes T-cell apoptosis: a potential mechanism of immune evasion*. Nat Med 8: 793-800. 10.1038/nm730

299. Iwai Y, Ishida M, Tanaka Y, Okazaki T, Honjo T, Minato N. 2002. *Involvement of PD-L1 on tumor cells in the escape from host immune system and tumor immunotherapy by PD-L1 blockade*. Proc Natl Acad Sci U S A 99: 12293-7. 10.1073/pnas.192461099

300. Blank C, Brown I, Peterson AC, Spiotto M, Iwai Y, et al. 2004. *PD-L1/B7H-1 inhibits the effector phase of tumor rejection by T cell receptor (TCR) transgenic CD8+ T cells*. Cancer Res 64: 1140-5. 10.1158/0008-5472.can-03-3259

301. Zou W, Wolchok JD, Chen L. 2016. *PD-L1 (B7-H1) and PD-1 pathway blockade for cancer therapy: Mechanisms, response biomarkers, and combinations*. Sci Transl Med 8: 328rv4. 10.1126/scitranslmed.aad7118

302. Chen J, Jiang CC, Jin L, Zhang XD. 2016. *Regulation of PD-L1: a novel role of pro-survival signalling in cancer*. Ann Oncol 27: 409-16. 10.1093/annonc/mdv615

303. Shaw LM. 2011. *The insulin receptor substrate (IRS) proteins: at the intersection of metabolism and cancer*. Cell Cycle 10: 1750-6. 10.4161/cc.10.11.15824

304. Copps KD, White MF. 2012. *Regulation of insulin sensitivity by serine/threonine phosphorylation of insulin receptor substrate proteins IRS1 and IRS2*. Diabetologia 55: 2565-82. 10.1007/s00125-012-2644-8

305. Pijuan J, Barceló C, Moreno DF, Maiques O, Sisó P, et al. 2019. *In vitro Cell Migration, Invasion, and Adhesion Assays: From Cell Imaging to Data Analysis*. Front Cell Dev Biol 7: 107. 10.3389/fcell.2019.00107

306. Abcam. *Flow cytometry intracellular staining protocol*. Retrieved from https://docs.abcam.com/pdf/protocols/Flow_cytometry_intracellular-staining_protocol.pdf

307. Winograd-Katz SE, Fässler R, Geiger B, Legate KR. 2014. *The integrin adhesome: from genes and proteins to human disease*. Nat Rev Mol Cell Biol 15: 273-88. 10.1038/nrm3769

308. Branchini BR, Magyar RA, Murtiashaw MH, Portier NC. 2001. *The role of active site residue arginine 218 in firefly luciferase bioluminescence*. Biochemistry 40: 2410-8. 10.1021/bi002246m

309. Rakwalska M, Rospert S. 2004. *The ribosome-bound chaperones RAC and Ssb1/2p are required for accurate translation in Saccharomyces cerevisiae*. Mol Cell Biol 24: 9186-97. 10.1128/mcb.24.20.9186-9197.2004

310. Chu D, Kazana E, Bellanger N, Singh T, Tuite MF, von der Haar T. 2014. *Translation elongation can control translation initiation on eukaryotic mRNAs*. Embo j 33: 21-34. 10.1002/embj.201385651

311. Stewart JD, Cowan JL, Perry LS, Coldwell MJ, Proud CG. 2015. *ABC50 mutants modify translation start codon selection*. Biochem J 467: 217-29. 10.1042/bj20141453

312. McKeown SR. 2014. *Defining normoxia, physoxia and hypoxia in tumours-implications for treatment response*. Br J Radiol 87: 20130676. 10.1259/bjr.20130676

313. Cui W, Bai Y, Luo P, Miao L, Cai L. 2013. *Preventive and therapeutic effects of MG132 by activating Nrf2-ARE signaling pathway on oxidative stress-induced*

cardiovascular and renal injury. Oxid Med Cell Longev 2013: 306073. 10.1155/2013/306073

314. Balasubramanian S, Kanade S, Han B, Eckert RL. 2012. *A proteasome inhibitor-stimulated Nrf1 protein-dependent compensatory increase in proteasome subunit gene expression reduces polycomb group protein level*. J Biol Chem 287: 36179-89. 10.1074/jbc.M112.359281

315. Back SH, Scheuner D, Han J, Song B, Ribick M, et al. 2009. *Translation attenuation through eIF2alpha phosphorylation prevents oxidative stress and maintains the differentiated state in beta cells*. Cell Metab 10: 13-26. 10.1016/j.cmet.2009.06.002

316. Mandai M, Hamanishi J, Abiko K, Matsumura N, Baba T, Konishi I. 2016. *Dual Faces of IFNγ in Cancer Progression: A Role of PD-L1 Induction in the Determination of Pro- and Antitumor Immunity*. Clin Cancer Res 22: 2329-34. 10.1158/1078-0432.Ccr-16-0224

317. Abiko K, Mandai M, Hamanishi J, Yoshioka Y, Matsumura N, et al. 2013. *PD-L1 on tumor cells is induced in ascites and promotes peritoneal dissemination of ovarian cancer through CTL dysfunction*. Clin Cancer Res 19: 1363-74. 10.1158/1078-0432.Ccr-12-2199

318. Qian J, Wang C, Wang B, Yang J, Wang Y, et al. 2018. *The IFN-γ/PD-L1 axis between T cells and tumor microenvironment: hints for glioma anti-PD-1/PD-L1 therapy*. J Neuroinflammation 15: 290. 10.1186/s12974-018-1330-2

319. Permata TBM, Hagiwara Y, Sato H, Yasuhara T, Oike T, et al. 2019. *Base excision repair regulates PD-L1 expression in cancer cells*. Oncogene 38: 4452-66. 10.1038/s41388-019-0733-6

320. Truitt ML, Ruggero D. 2017. *New frontiers in translational control of the cancer genome*. Nat Rev Cancer 17: 332. 10.1038/nrc.2017.30

321. Khunger M, Jain P, Rakshit S, Pasupuleti V, Hernandez AV, et al. 2018. *Safety and Efficacy of PD-1/PD-L1 Inhibitors in Treatment-Naive and Chemotherapy-Refractory Patients With Non-Small-Cell Lung Cancer: A Systematic Review and Meta-Analysis*. Clin Lung Cancer 19: e335-e48. 10.1016/j.cllc.2018.01.002

322. Niu C, Jin H, Li M, Xu J, Xu D, et al. 2015. *In vitro analysis of the proliferative capacity and cytotoxic effects of ex vivo induced natural killer cells, cytokine-induced killer cells, and gamma-delta T cells*. BMC Immunol 16: 61. 10.1186/s12865-015-0124-x

323. Grasso CS, Wu Y-M, Robinson DR, Cao X, Dhanasekaran SM, et al. *The mutational landscape of lethal castration-resistant prostate cancer.*

324. Taylor BS, Schultz N, Hieronymus H, Gopalan A, Xiao Y, et al. 2010. *Integrative genomic profiling of human prostate cancer*. Cancer Cell 18: 11-22. 10.1016/j.ccr.2010.05.026

325. Yoshimura Y, Araki A, Maruta H, Takahashi Y, Yamashita H. 2017. *Molecular cloning of rat acss3 and characterization of mammalian propionyl-CoA synthetase in the liver mitochondrial matrix*. J Biochem 161: 279-89. 10.1093/jb/mvw067

326. Kohn AD, Kovacina KS, Roth RA. 1995. *Insulin stimulates the kinase activity of RAC-PK, a pleckstrin homology domain containing ser/thr kinase*. Embo j 14: 4288-95.

327. Lee AV, Gooch JL, Oesterreich S, Guler RL, Yee D. 2000. *Insulin-like growth factor I-induced degradation of insulin receptor substrate 1 is mediated by the 26S proteasome and blocked by phosphatidylinositol 3'-kinase inhibition*. Mol Cell Biol 20: 1489-96. 10.1128/mcb.20.5.1489-1496.2000

328. Rice KM, Turnbow MA, Garner CW. 1993. *Insulin stimulates the degradation of IRS-1 in 3T3-L1 adipocytes*. Biochem Biophys Res Commun 190: 961-7. 10.1006/bbrc.1993.1143

329. Garrido P, Osorio FG, Morán J, Cabello E, Alonso A, et al. 2015. *Loss of GLUT4 induces metabolic reprogramming and impairs viability of breast cancer cells*. J Cell Physiol 230: 191-8. 10.1002/jcp.24698

330. Barron C, Tsiani E, Tsakiridis T. *Expression of the glucose transporters GLUT1, GLUT3, GLUT4 and GLUT12 in human cancer cells*.

331. Mi YJ, Geng GJ, Zou ZZ, Gao J, Luo XY, et al. 2015. *Dihydroartemisinin inhibits glucose uptake and cooperates with glycolysis inhibitor to induce apoptosis in non-small cell lung carcinoma cells*. PLoS One 10: e0120426. 10.1371/journal.pone.0120426

332. Gonzalez-Menendez P, Hevia D, Alonso-Arias R, Alvarez-Artime A, Rodriguez-Garcia A, et al. 2018. *GLUT1 protects prostate cancer cells from glucose deprivation-induced oxidative stress*. Redox Biol 17: 112-27. 10.1016/j.redox.2018.03.017

333. Barbosa AM, Martel F. 2020. *Targeting Glucose Transporters for Breast Cancer Therapy: The Effect of Natural and Synthetic Compounds*. Cancers (Basel) 1210.3390/cancers12010154

334. Lin C, Blessing AM, Pulliam TL, Shi Y, Wilkenfeld SR, et al. 2021. *Inhibition of CAMKK2 impairs autophagy and castration-resistant prostate cancer via suppression of AMPK-ULK1 signaling*. Oncogene 40: 1690-705. 10.1038/s41388-021-01658-z

335. Mansoori B, Mohammadi A, Davudian S, Shirjang S, Baradaran B. 2017. *The Different Mechanisms of Cancer Drug Resistance: A Brief Review*. Adv Pharm Bull 7: 339-48. 10.15171/apb.2017.041